

博士學位論文

비선형 감쇠장치가 설치된 건축구조물의
내진 및 내풍 성능 평가를 위한
하이브리드 실험기법 및 가진시스템 설계

Hybrid Testing Method and Excitation System for Seismic
and Wind-resistance Performance Evaluation of Building
Structures with Nonlinear Dampers

提出者 : 朴恩泉
指導教授 : 閔慶元

2017

建築工學科
建築構造專攻
檀國大學校 大學院

비선형 감쇠장치가 설치된 건축구조물의
내진 및 내풍 성능 평가를 위한
하이브리드 실험기법 및 가진시스템 설계

Hybrid Testing Method and Excitation System for Seismic
and Wind-resistance Performance Evaluation of Building
Structures with Nonlinear Dampers

이 論文을 博士學位論文으로 提出함

檀國大學校 大學院
建築工學科
建築構造專攻

朴 恩 泉

朴恩泉의 博士學位 論文을
合格으로 判定함

審查日: 2017. 6. 16.

審查委員長 印

審查委員 印

審查委員 印

審查委員 印

審查委員 印

檀國大學校 大學院

Contents

1	Introduction	5
1.1	General	5
1.2	Objectives and Contents	6
1.3	Literature Review	9
1.3.1	Hybrid testing method	9
1.3.2	Design of Excitation System for Simulating Dynamic Loads	11
1.3.3	Hybrid Testing Method on a Semi-actively Controlled Building Structure Equipped with Full-scale MR Dampers	13
2	Hybrid Testing Method	14
2.1	Substructuring technique	14
2.1.1	Formulation and Implementation Methodology	16
2.1.2	Numerical Substructure	21
2.2	Hybrid Testing Method for the Performance Evaluation of a Tuned Liquid Damper	23
2.2.1	Hybrid Testing Method with TLD	24
2.3	Hybrid testing method for the Performance Evaluation of a Tuned Liquid Column Damper	26
2.3.1	RHybrid Testing Method with TLCD	27
2.4	Hybrid Testing Method for the Performance Evaluation of a Tuned Liquid Mass Damper	28
2.4.1	Developed TLMD Model	29
2.5	Design of Experimental Controller	32
2.5.1	Experimental System for Substructurubg Technique .	32
2.5.2	Shaking table controller	33
2.5.3	Experimental System for Hybrid Testing of Building with TLD	35
2.5.4	Experimental System for Hybrid Testing of Building with TLCD	37
2.5.5	Experimental System for Hybrid Testing of Building with TLMD	40
2.6	Experimental Verification	43
2.6.1	Experimental result of Substructuring technique . . .	43
2.6.2	Hybrid Testing Method of a Single Story Strcuture with a TLD	53
2.6.3	Hybrid Testing Method of Three Story Structure with a TLD	60

2.6.4	Hybrid Testing Method of a Single Story Structure with a TLCD	61
2.6.5	Conventional Experiment of a Building Controlled by TLMD	64
2.6.6	Experimental results	66
2.6.7	Hybrid Testing Method of a Single Story Building Controlled by TLMD	66
2.7	Summary	75
3	Design of Excitation System for Simulating Dynamic Loads	77
3.1	Design of an Actuator for Simulating Wind Response	77
3.1.1	Force of actuator	77
3.1.2	Numerical Example	79
3.1.3	Summary	89
3.2	Forced vibration test of full-scaled five-story building structure simulating eqearthquake responses	92
3.2.1	Overview	92
3.2.2	Experimental Real-Scale Building Model	93
3.2.3	Field measurement and experimental system	93
3.2.4	System Identification	95
3.2.5	Design of an Excitation System for Simulating Earthquake Response	99
3.2.6	Exoperimental Result	102
3.2.7	Error Analysis	106
3.2.8	Summary	107
3.3	Forced vibration test of MR Damper-based Semiactive Control Algorithms for Full-scaled Building	109
3.3.1	Overview	109
3.3.2	Full scaled MR Damper	110
3.3.3	Semi-active control algorithms	110
3.3.4	External excitation loads	111
3.3.5	Measurement Devices and Feedback Control System .	112
3.3.6	Testing building model	115
3.3.7	Experimental results	116
3.3.8	Summary	119
4	Hybrid Testing Method on a Semi-actively Controlled Building Structure Equipped with Full-scale MR Dampers	122
4.1	Outline of Methodology	122
4.2	Controller Strategied for Hybrid Testing Method	126
4.2.1	Experimental Set-up	126
4.2.2	Controller Design of UTM	126
4.3	Experimental Implementation	129

TABLE OF CONTENTS

4.3.1	Integrated Controller of the Numerical Substructure and UTM	129
4.3.2	Experimental Verification for Simple Bouc-Wen Model	130
4.3.3	Applied Semi-active Control Algorithms	136
4.4	Testing Result	140
4.4.1	Passive Control Performance	140
4.4.2	Semi-active Control Performance	143
4.5	Summary	146
5	Conclusions	148
5.1	Concluding Remarks	148
5.2	Future Study	149
Curriculum Vitæ		156

List of Figures

1.1	Contents of chapters and their relations	9
2.1	Conceptual illustrations of the substructuring methods	15
2.2	Schematic diagram of the proposed method	16
2.3	Concept of the proposed method	19
2.4	Dynamic equilibrium in experimental substructure	20
2.5	Comparison of experimental and approximated transfer functions.	22
2.6	Block diagram of the integrated controller for the substructuring testing system.	23
2.7	Conceptual view of the hybrid shaking table test	25
2.8	Concept of the hybrid testing method (TLCD)	27
2.9	Concept of a TLMD	30
2.10	Overall view of experimental system	32
2.11	Schematic diagram of experimental system	33
2.12	Inverse transfer function of shaking table	34
2.13	Definition of the transfer function of shaking table	34
2.14	Compensation using the inverse transfer function of shaking table	35
2.15	Flow chart of the experimental system controller	35
2.16	Compensation result for the dynamic characteristic of shaking table	36
2.17	Schematic diagram of experimental set-up	36
2.18	Block diagram of the integrated controller for the hybrid testing system.	37
2.19	Controller for implementing the hybrid testing method	38
2.20	Experimental view of a building with a TLCD	39
2.21	Conceptual view of the hybrid testing method of building with TLMD	40
2.22	Design of the controller for the hybrid testing method	42
2.23	Photograph of the hybrid testing	42
2.24	Design of the MATLAB Simulink window Target	42
2.25	Comparisons of results measured from the experiment without feedback and those calculated from numerical analysis.	45
2.26	Spectrograms and contour plots of the 3rd story acceleration measured from the experiment without feedback and that calculated from the numerical analysis.	46
2.27	Spectrograms and contour plots of the 4th story acceleration measured from the experiment without feedback and that calculated from the numerical analysis.	47

TABLE OF CONTENTS

2.28 Spectrograms and contour plots of the 5th story acceleration measured from the experiment without feedback and that calculated from the numerical analysis.	48
2.29 Comparisons between results from the experiment with feedback and those from analysis.	49
2.30 Spectrograms and contour plots of the 3rd story acceleration measured from the experiment with feedback and that calculated from the numerical analysis.	50
2.31 Spectrograms and contour plots of the 4th story acceleration measured from the experiment with feedback and that calculated from the numerical analysis.	51
2.32 Spectrograms and contour plots of the 5th story acceleration measured from the experiment with feedback and that calculated from the numerical analysis.	52
2.33 TLD-structure interaction experimental system.	54
2.34 TLD transfer function from the table acceleration to the base shear force	55
2.35 Structural acceleration in the time domain measured from the conventional shaking table test of TLD-structure interaction system (dotted line : without control, solid line : with control)	56
2.36 Structural acceleration in the frequency domain measured from the conventional shaking table test of TLD-structure interaction system (dotted line : without control, solid line : with control)	57
2.37 Comparisons of controlled structural accelerations in the time domain (dotted line : conventional shaking table test, solid line : hybrid shaking table test)	58
2.38 Comparisons of controlled structural accelerations in the frequency domain (dotted line : conventional shaking table test, solid line : hybrid shaking table test)	59
2.39 Absolute accelerations in the time domain, measured from the top story of MDOF structure with a TLD by the hybrid testing method (dotted line : without control, solid line : with control))	61
2.40 Absolute accelerations in the frequency domain, measured from the top story of MDOF structure with a TLD by the hybrid testing method (dotted line : without control, solid line : with control)	62
2.41 Behaviors of a TLD under the earthquake motion	62
2.42 Comparisons between the results from the conventional testing method(dotted line) and those from the hybrid testing method(solid line) for the controlled response	63
2.43 Photograph of the manufactured TLMD	64
2.44 Experimental TLMD-building model	65

TABLE OF CONTENTS

2.45	Conceptual view of experimental set-up	65
2.46	Free-body diagram of a building model.	65
2.47	Displacement in the frequency domain (TMD direction)	67
2.48	Acceleration in the frequency domain (TMD direction)	68
2.49	Displacement in the time domain (TMD direction, 0.82 Hz)	68
2.50	Displacement in the frequency domain (TLCD direction)	69
2.51	Acceleration in the frequency domain (TLCD direction)	70
2.52	Displacement in the time domain (TMD direction, 0 · 73 Hz)	70
2.53	Displacement in the frequency domain by the hybrid test (TMD direction)	71
2.54	Acceleration in the frequency domain by the hybrid test (TMD direction)	71
2.55	Displacement in the time domain by the hybrid test (TMD direction, 0.83 Hz)	72
2.56	Displacement in the frequency domain by the hybrid test (TLCD direction)	72
2.57	Acceleration in the frequency domain by the hybrid test (TLCD direction)	73
2.58	Displacement in the time domain by the hybrid test (TLCD direction, 0.73 Hz)	73
2.59	Uncontrolled displacement comparison in the time domain between the real-structure test and hybrid testing method (TMD direction)	74
3.1	Scheme of simulation of wind induced responses using LMS and ATMD	78
3.2	Exciter gain shape of the band-stop filter and the envelop function.	80
3.3	76th story benchmark model.	81
3.4	Transfer function of 75th story responses to LMS.	82
3.5	LMS force (unfiltered).	83
3.6	Frequency response of 75th floor with LMD force targeting displacement response.	84
3.7	Error distribution according to the filter usage and floor of target response.	85
3.8	Wind and LMS induced acceleration responses (when the target is 75th floor acceleration).	86
3.9	Wind and LMS induced acceleration responses (when the target is 30th floor acceleration).	87
3.10	ATMD Excitation.	88
3.11	Wind and ATMD induced acceleration responses (when the target is 75th floor acceleration).	89
3.12	Frequency response of wind and ATMD induced 75th floor accelerations	90

TABLE OF CONTENTS

3.13	Error Distribution with ATMD excitation.	90
3.14	Comparison between actuator forces in LMS and ATMD	91
3.15	Stroke Comparison.	92
3.16	Elevation view of the target structure.	94
3.17	Photograph and transfer function of the target building structure.	95
3.18	Schematic diagram of the field measurement, data acquisition and excitation system.	96
3.19	Installation pictures of the measurement, data acquisition and excitation system.	96
3.20	The transfer function from the absolute acceleration of the HMD to those of the structure.	97
3.21	The mode shape comparison of initial, the measured and the updated FE models.	99
3.22	The transfer function comparison of the initial, measured, updated FE model.	100
3.23	Photograph of the HMD installed in 5th floor.	102
3.24	Schematic diagram of the HMD controller.	102
3.25	Comparison of the measured and the approximated inverse transfer function of the HMD.	103
3.26	Comparison of the reference and measured acceleration time histories when the signals were generated by El Centro and Hachinohe earthquake.	104
3.27	Time history comparison of El Centro earthquake response in the analysis and experimental models. (when the target response is the 5th floor acceleration).	104
3.28	Comparison in frequency domain of El Centro earthquake response of the analysis and experimental models. (when the target response is the 5th floor acceleration).	105
3.29	Time history comparison of Hachinohe earthquake response in the analysis and experimental models. (when the target response is the 5th floor acceleration).	106
3.30	Comparison in frequency domain of Hachinohe earthquake response in the analysis and experimental models. (when the target response is the 5th floor acceleration).	107
3.31	Normalized RMS error floor distribution of the analysis FE model corresponding the distributed floor acceleration response.	108
3.32	Normalized RMS error floor distribution of the experimental results corresponding the distributed floor acceleration response.	109
3.33	Manufactured MR damper and test result.	111
3.34	Acceleration of HMD and PSD used as external excitation load.	113
3.35	Acceleration of HMD and PSD used as external excitation load.	114
3.36	MR damper-based semi-active feed back control system.	115

TABLE OF CONTENTS

3.37	Normalized maximum displacement of passive control cases (first floor).	117
3.38	Normalized maximum acceleration of passive control cases. .	117
3.39	Normalized maximum displacement comparison of MR damper-based control systems.	119
3.40	Normalized maximum acceleration comparison of MR damper-based control systems.	119
3.41	Time history responses of displacement at the first floor under the El Centro earthquake.	120
3.42	Time history responses of acceleration at the second floor under the Kobe earthquake.	120
4.1	Conceptual view of hybrid testing method for a building with an MR damper.	124
4.2	Schematic view of experimental set-up: (a) building model installed with an MR damper, (b) UTM installed MR damper, and (c) experimental instrumentation.	125
4.3	Configuration of experimental system.	127
4.4	Measured and approximated ITRFs from the displacement of UTM to the command signal.	129
4.5	Integrated controller for implementing RTHTM.	130
4.6	Comparison between calculated and experimentally measured responses for the Bouc-Wen model.	132
4.7	Comparison between calculated and experimentally measured responses under El Centro earthquake excitation.	133
4.8	Comparison between calculated and experimentally measured responses under Northridge earthquake excitation.	135
4.9	Comparison between calculated and experimentally measured hysteresis under El Centro earthquake excitation.	136
4.10	Comparison between calculated and experimentally measured hysteresis under Northridge earthquake excitation.	136
4.11	Identified Bouc-Wen parameters and the numerical model of an MR damper.	137
4.12	Clipped-optimal and hybrid testing method integrated controller.	139
4.13	MHF and hybrid testing method integrated controller.	140
4.14	Experimental results, in the time domain under El Centro earthquake excitation at different applied currents.	141
4.15	Experimental results, in the time domain under Northridge earthquake excitation at different applied currents.	142
4.16	First-story displacements in the frequency domain at different applied currents.	143
4.17	Comparison of numerical and experimental results under El Centro earthquake excitation.	144

LIST OF FIGURES

4.18 Passive and semi-active hybrid testing method experimental results(time domain)	145
4.19 Passive and semi-active hybrid testing method experimental results(frequency domain).	146

List of Tables

2.1	Frequencies observed in the time records of the experimental substructure from the test without feedback and the natural frequencies of the assumed whole structure	22
2.2	Similitude law applied to TLMD model	29
2.3	Design parameters of the building model	31
2.4	Design parameters of a TLMD model	31
2.5	Uncontrolled and controlled responses of a combined TLD–MDOF structure system	60
2.6	Control performance of real-structure test	70
2.7	Control performance of hybrid testing method	71
3.1	Cutoff frequency for filter design	84
3.2	Comparison between LMS and ATMD	91
3.3	Member list of the model structure	95
3.4	Identified natural frequencies and damping ratios	97
3.5	Natural frequencies (Hz) for the modal testing tower	99
3.6	Results obtained from the magnetic analysis.	110

ABSTRACT

Hybrid Testing Method and Excitation System for Seismic and Wind-resistance Performance Evaluation of Building Structures with Nonlinear Dampers

Park, Eunchurn
Department of Architectural
Engineering Graduate School
Dankook University

Advisor: Professor Min, Kyung-Won

Abstract: This paper proposes a real-time hybrid testing method and the controller design of actuators to simulate the responses of a building structure subjected to such dynamic excitations as earthquakes and wind loads. Firstly, The real-time hybrid testing method is a technique to experiment with a non-linear part in an entire structural system as an experimental model and a part that is expected to behave linearly as an analytical model. In this method, the interface between the experimental model and the analytical model should be selected, and an experimental system should be constructed in which the interface of the analytical model is designed to act as the excitation force of the experimental model. In this paper, a substructure test as part of real-time hybrid testing method by separating the structural system into the experimental structure and the analytical structure through the shaking table, and the hybrid test of nonlinear vibration control devices, the tuned liquid damper, the tuned liquid column damper and the tuned liquid mass damper as experimental models and building structures as analytical models were designed and implemented to evaluate the performance. Furthermore, seismic performance evaluation of a building with magneto-rheological (MR) damper installed by installing an MR damper, which is a 1-ton inter-story damper with high nonlinearity, on UTM, and the semi-active algorithm applied to the MR damper were experimentally evaluated. This method can provide the possibility and quantitative basis for experimentally finding and applying the optimum algorithm of the control device with unspecific nonlinearity or the performance of the device itself. Secondary, the controller system design that implements the dynamic response is a system that installs a linear mass shaker or an active mass damper on a specific floor and implements a pseudo-seismic or pseudo wind load response in a full-scale building. In this paper, in order to simulate of wind-induced responses, a 76-story benchmark building which has an analytical model and wind load data were numerically analyzed, and in order to realize the seismic responses, the pseudo-earthquake excitation is implemented by the hybrid mass damper with the real-scaled 5-story building. In addition, an MR damper with the capacity of 1-ton was installed to evaluate the semi-active control performance of MR damper under earthquakes load in a real scale building. These techniques can be used to evaluate the

ABSTRACT

seismic and wind resistance performance of real-scaled building structures and to evaluate the seismic and wind resistance performance of buildings with nonlinear control devices.

Firstly, in Chapter 2, a real-time hybrid testing method is proposed. First, a substructuring test of a building structure using the real-time hybrid testing method was performed by using a shaking table. Selecting a particular story of a shear-type building structure as an interface, the upper part of the target structure is divided into experimental substructure and the lower part is divided into numerical analytic substructure. The boundary load at the interface separated by the substructure is calculated in real time of the absolute acceleration response of the experimental model. The acceleration of the interface between two substructures is calculated by time history analysis of the numerical substructure and used as command signal of the shaking table controller. At this time, the shaking table controller that generates the command signal minimizes the error between the generated command signal and the shaking table motion for the excitation of the experimental substructure. The validity and accuracy of the shaking table substructure test of real-time hybrid testing method were confirmed by the experimental results and the numerical analysis results. Secondly, a real-time hybrid testing method for evaluating the control performance of a building structure subjected to earthquake excitation of a tuned liquid type damper (TLD, TLCD, and TLMD), which is a nonlinear control device, was experimentally performed. This experiment is performed by using only control devices (TLD, TLCD, and TLMD), load cell and shaking table without physical building structure because this experiment performs divided into nonlinear control device as an experimental model and building model as an analytical model. The structural responses of the interaction system are calculated numerically in real time using an analytical building model, a given earthquake record, and a shear force generated by the TLD, TLCD, and TLMD, and the shaking table reproduces both the controlled and uncontrolled absolute acceleration of the TLD, TLCD, and TLMD installed floor by modulating the feedback gain of the shear force signal measured by the load cell positioned between the TLD/TLCD/TLMD and the shaking table. In this paper, the results of the real-time hybrid test with those of the existing full-scale structural test are compared, and it is present that accurate results of the seismic performance of buildings with nonlinear vibration control system can be obtained by using real-time hybrid test without a physical model. In this paper, through not only TLD and TLCD which is verified through previous studies but also TLMD which is newly proposed to reduce bidirectional responses of building structures is evaluated by using real-time hybrid testing method, a real-time hybrid testing method is very useful for that the recently proposed control device can be assessed experimentally in design stage.

In Chapter 3, firstly, a design of an actuator for simulating the wind-

ABSTRACT

induced responses of a building structure is presented. The actuator force is calculated by using the inverse transfer function of a target structural responses to the actuator. Filter and envelope function are used such that the error between wind and actuator induced responses is minimized by preventing the actuator from the exciting unexpected modal responses and initial transient responses. The analyses result from a 76-story benchmark building problem in which wind load obtained by wind tunnel test is given, indicate that the actuator installed at a specific floor can approximately embody the structural responses induced by the wind load applied to each floor of the structure. The actuator designed by the proposed method can be effectively used for evaluating the wind response characteristics of a practical building structure and for obtaining an accurate analytical model of the building under wind load. Secondly, a full scale forced vibration test simulating earthquake response is implemented by using a hybrid mass damper. The finite element(FE) model of the structure was analytically constructed using ANSYS and the model was updated using the results experimentally measured by the forced vibration test. Pseudo-earthquake excitation tests showed that HMD (hybrid mass damper) induced floor responses coincided with the earthquake induced ones which were numerically calculated based on the updated FE model. Real-scaled MR damper was installed to verify the effectiveness of the pseudo-earthquake experiment in a real scale building. The MR damper-based control systems are realized when an MR damper is designed by deriving a suboptimal design procedure considering optimization problem and magnetic analysis, and then a damper with the capacity of 1.0 ton is manufactured. In the experiments, a linear active mass driver and the linear shaker seismic simulation testing method are used to excite the building structure to match the full-scale building vibrate as if the building undergoes an earthquake. Under the four historical earthquakes and one filtered artificial earthquake, the performance of the semi-active control algorithms including the passive optimal case is experimentally evaluated. From the experimental results, one can conclude that the Lyapunov and semi-active neuro-control algorithms are appropriate in reducing accelerations of the structural system, and the passive optimal case and the maximum energy dissipation algorithm show the excellent performance in reducing the first-floor displacement.

In chapter 4, The MR damper with the capacity of 1-ton was used from chapter 3.1, hybrid testing method of the real-scaled building with semi-active controlling MR damper implemented in the chapter 2 was applied by hybrid testing method technique. This study presents the quantitative evaluation of the seismic performance of a building structure installed with a MR damper using hybrid testing method as described in chapter 2. A building model is identified from the forced vibration testing results of a full-scale five-story building in Chapter 3 and is used as the numerical substructure, and an MR damper corresponding to an experimental substruc-

ABSTRACT

ture is physically tested using a universal testing machine (UTM). First, the force required to drive the displacement of the story, at which the MR damper is located, is measured from the load cell attached to the UTM. The measured force is then returned to a control computer to calculate the response of the numerical substructure. Finally, the experimental substructure is excited by the UTM with the calculated response of the numerical substructure. The hybrid testing method implemented in this study is validated because the real-time hybrid testing results obtained by application of sinusoidal and earthquake excitations and the corresponding analytical results obtained using the Bouc-Wen model as the control force of the MR damper with respect to input currents are in good agreement. Also, the results from hybrid testing method for the passive -on and -off control show that the structural responses did not decrease further by the excessive control force, but decreased due to the increase of the current applied to the MR damper. Also, two semi-active control algorithms (modulated homogeneous friction and the clipped-optimal control algorithms) are applied to the MR damper in order to optimally control the structural responses. To compare the hybrid testing method and numerical results, Bouc-Wen model parameters are identified for each input current. The results of the comparison of experimental and numerical responses show that it is more practical to use hybrid testing method in semi-active devices such as MR dampers. The test results show that a control algorithm can be experimentally applied to the MR damper using hybrid testing method. This study also provides a discussion on each algorithm with respect to the seismic performances.

Keywords: real-time hybrid testing method, substructuring technique, tuned liquid type damper, control-structure interaction, inverse transfer function, active tuned mass damper, hybrid mass damper, design of an actuator, 76-story benchmark problem building, force vibration testing, real-scale building, system identification, finite element model updating, magneto-rheological damper, semi-active control algorithms.

Student Number : 72070621

CHAPTER 1

Introduction

1.1 General

Accurate identification of the dynamic response characteristics of building structures excited by external loads such as earthquakes and wind loads is essential not only for the safety and serviceability evaluation of building structures but for the validation of analytical models used for seismic or wind design(Ljung, 1987). In the System Identification (SI) field, which constructs a system matrix that describes precise input and output relationships to build an analytical model of an architectural structure, it is critical that input should have sufficient energy to excite fundamental structural modes and a high quality of output containing structural information should be measured(Alvin and Park, 1994; Madenci and Barut, 1994). However, full-scale dynamic testing is difficult due to size and weight limitations in most large civil engineering structures. Also, in most cases, it is very difficult or impossible to extrapolate the results of small-scale model tests as a result of a full-scale structure that operates non-linearly in most cases. Therefore, it is used as a means to evaluate the dynamic performance of a building or to implement the system identification process by installing an excitation system such as an eccentric exciter or a linear mass shaker which excite the fundamental modes, in the building. However, to evaluate the seismic and the wind resist performance accurately, it is necessary to fully reflect the characteristics of the seismic load and the wind load.

One method to overcome these limitations is to use the hybrid testing method. This technique for the dynamic testing of large-scale structures, typically involving nonlinearities, does not test the entire structure as a whole. Instead, it often happens that nonlinearity or unpredictable behavior is concentrated in a limited number of local parts of the overall structure. Those important local parts are experimentally tested, while the rest of the structure, which is assumed to behave linearly, in essence, is modeled numerically. Numerical and experimental parts are allowed to interact with each other to produce the response of the entire system. The advantage of the hybrid testing technique over the reduced-scale model testing is that the experimental substructure is tested at full size and the scaling effect can be eliminated.

Another method to overcome above limitations is to design controller of actuators to simulate earthquake and wind-induced responses. This is a

forced vibration testing method to implement seismic or wind responses of a building structure by using a vibration control device already installed in a real building such as ATMD or installing additional exciter in specific story of the building. For the successful application of this method, several issues should be considered. First, interaction effects between the actuators and building structure and dynamic characteristics of the actuator itself should be compensated. Second, because this method uses inverse transfer function method, unexpected modal responses and transient responses should be reduced. This method may evaluate the seismic and wind performance not only of the existing building but for of the real scale building equipped with the nonlinear vibration control device.

1.2 Objectives and Contents

Figure 1.2 shows the contents of chapters and their relations in this paper. It can be classified into a hybrid testing method and a pseudo-excitation system for simulating a dynamic load of building structures. Verification methods can be summarized as numerical analysis, shaking table experiment, UTM experiment, and experiment with full-size building with HMD. The objective of this study is to design a hybrid testing method and a controller of an exciter to perform an experimental evaluation of seismic and wind resistance performance of building structures equipped with nonlinear vibration control devices. The contents for these objectives are as follows;

First, in chapter 2, the hybrid testing method is proposed. To be implemented by the hybrid testing technique and accurately represent the whole building structure, the experimental and numerical substructures must operate in parallel with minimal errors at the interface between them. Three factors are essential in the implementation issues of the hybrid testing method. Those issues are the measurement of the interface force between two substructures, the calculation of the numerical substructure, and the loading operation of the experimental substructure with an actuator. The responses of the shared degrees-of-freedom (DOF) are calculated using the numerical model and passed to the controller of actuators or a shaking table. The controller generates signals driving the actuators in order to impose these responses on the experimental substructure. To be replicated by the behavior of the whole structure by the hybrid testing method, it is important to design the controller of the actuators or the shaking table, so that difference between the expected and actual measured behavior at the interface of the two substructures is minimized. The vibration control effect of a tuned liquid type damper (TLD/TLCD) for a building structure excited by earthquake load is experimentally evaluated through the hybrid testing method. The hybrid testing method doesn't require a physical building structural model in performing the experiment of a TLD/TLCD-structure interaction system

and it only uses a TLD/TLCD which is known to have strong nonlinearity dependent on response amplitude, excitation frequency, and depth to length ratio (Yalla, 2001). A new control device, which is called tuned liquid mass damper (TLMD), is discussed in this chapter. The functional characteristic of a TLMD used in this study is that its mass is composed of both a mass of TLCD tank itself and that of liquid within a tank. Natural rubbers were also used to substitute the stiffness of a TMD. Therefore, a TLMD employed in this study operates as a TLCD in one direction and behaves as a TMD in the other orthogonal direction. Regarding the field of structural testing, hybrid testing method also implemented in this study. As mentioned in the previous sentence, TLD and TLCD has been subjected to many researches and experiments and has been verified by the RH-HYTEM technique in this study. Therefore, as hybrid testing method of building controlled by TLMD, it is significant to use the hybrid testing method technique by validating the control performance of the newly proposed control device by comparison between the SDOF-actuator experiment method and the hybrid testing method method. The structural responses of the interaction system are calculated numerically in real-time using the analytical structural model with the excitations of measured control force, user-defined base earthquake loads, and its state space realization incorporated in the integrated controller of an actuator. Also, in order to minimize the distortion of the acceleration of the shaking table or an actuator's displacement, the inverse transfer function of the shaking table or the actuator is identified and its state space realization is implemented in the hybrid testing method controller.

Secondly, in chapter 3.1, simulation of dynamic responses of a building structure using a linear mass shaker is conducted. In order for the linear shaker to keep the structure in the target response trajectory, an inverse transfer function of a structural response to the shaker force is obtained using a state space form governing equation of the structure and the discrete Fourier transform of structural response is performed. Filter and envelope function are used such that the error between wind and actuator induced responses is minimized by preventing the shaker from the exciting unexpected modal response and initial transient response. The effectiveness of the proposed method is verified through a numerical example of a 76 story-benchmark building excited by wind load of which deterministic time history is given. The effect of the type of the target structural response on a convergence of the shaker force signal and the error magnitude is investigated. Moreover, in this chapter, forced vibration pseudo-earthquake tests using an HMD(hybrid mass damper) installed on the 4th floor of the real-scale five-story modal testing tower were performed. To experimentally evaluate the seismic performance of a building structure with accuracy, shaking table test should be conducted. However, it is practically impossible and very expensive to excite a real scale structure using the shaking table. Yu presented a linear shaker system to simulate structural seismic response by using inverse

transfer function of the structural response induced by the linear shaker (Yu et al., 2005) is of the structure excited by earthquake load. Real-scaled MR damper was installed to verify the effectiveness of the pseudo-earthquake experiment in a real scale building. Under the four historical earthquakes and one filtered artificial earthquake, the performance of the semi-active control algorithms including the passive optimal case is experimentally evaluated by the pseudo-earthquake test method.

Finally, in chapter 4 shows the experimental verification of hybrid testing method applied to UTM with an MR damper. The MR damper with the capacity of 1-ton was used from chapter 3.1, hybrid testing method of the real-scaled building with semi-active controlling MR damper implemented in the chapter 2 was applied by hybrid testing method technique. This study presents the quantitative evaluation of the seismic performance of a building structure installed with a magnetorheological (MR) damper using hybrid testing method. A building model is identified from the forced vibration testing results of a full-scale five-story building and is used as the numerical substructure, and an MR damper corresponding to an experimental substructure is physically tested using a universal testing machine (UTM). First, the force required to drive the displacement of the story, at which the MR damper is located, is measured from the load cell attached to the UTM. The measured force is then returned to a control computer to calculate the response of the numerical substructure. Finally, the experimental substructure is excited by the UTM with the calculated response of the numerical substructure. The hybrid testing method implemented in this study is validated because the hybrid testing results obtained by application of sinusoidal and earthquake excitations and the corresponding analytical results obtained using the Bouc-Wen model as the control force of the MR damper with input currents are in good agreement. Also, the results from hybrid testing method for the passive -on and -off control show that the structural responses did not decrease further by the excessive control force, but decreased due to the increase of the current applied to the MR damper. Also, two semi-active control algorithms (modulated homogeneous friction and the clipped-optimal control algorithms) are applied to the MR damper in order to optimally control the structural responses. To be compared with the hybrid testing method and numerical results, Bouc-Wen model parameters should be identified for each input current. The results of the comparison of experimental and numerical responses show that it is more practical to use hybrid testing method in semi-active devices such as MR dampers. The test results indicate that a control algorithm can be experimentally applied to the MR damper using hybrid testing method. This study also provides a discussion on each algorithm with respect to the seismic performances.

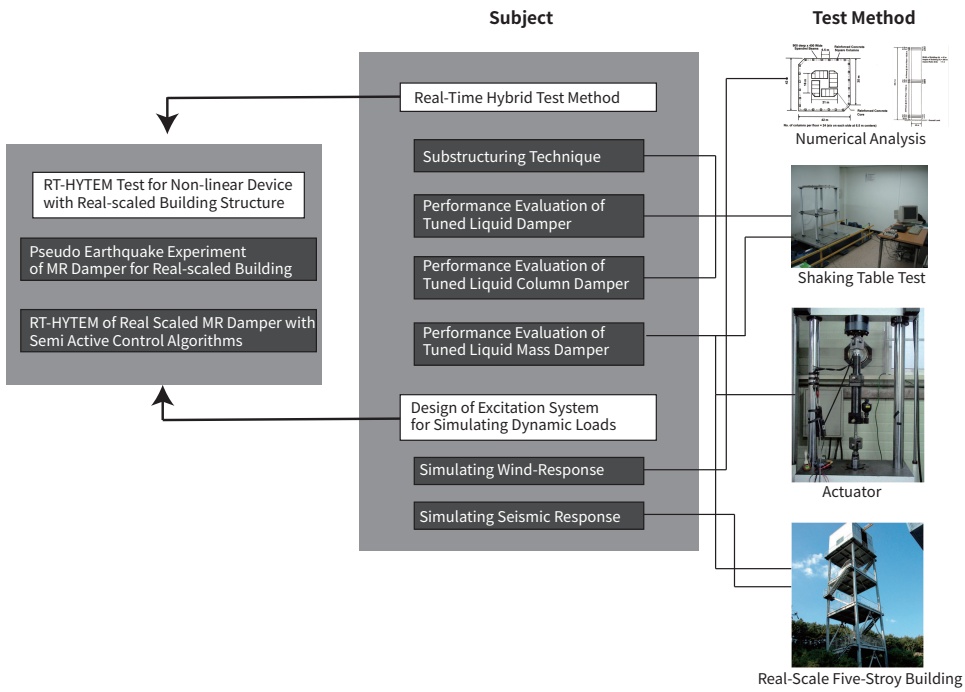


Figure 1.1: Contents of chapters and their relations

1.3 Literature Review

1.3.1 Hybrid testing method

Since the substructuring technique is first developed for large-scale structures by Nakashima et al. (1992), several pieces of research have been performed on the substructuring technique both experimentally and analytically to overcome difficulties in the test of large-scale structures. Blakeborough et al. (2001); Darby et al. (2001) focused on the control algorithm for operating hydraulic actuators and conducted experiments for a one-story frame with horizontal and rotational DOF and its corresponding numerical substructure, which shows the linear or nonlinear behavior (Darby et al., 2002). Neild et al. (2005) separated a large structural mass of the single DOF system into two parts and selected the smaller one as the experimental substructure and the larger one with attached spring and dashpot as the numerical substructure to conduct a shaking table test(Neild et al., 2005). Nakashima and Pan applied the method to a base-isolated structure consisting of the base-isolation layer as an experimental substructure and the rest of the upper structural model as a numerical substructure(Nakashima and Masaoka, 1999). Besides, they developed a mixed control algorithm using both displacement and force for its implementation(Pan et al., 2005).

Takanashi et al. (1975, 1980) have firstly developed the pseudo-dynamic testing method, in which only a part of the whole structure, mainly being expected to show nonlinearity, is manufactured and tested while the remainder showing linearity is numerically calculated(Takanashi et al., 1975, 1980). Because there exists propagation of experimental errors in pseudo-dynamic testing methods, the stability, and accuracy of the numerical integration methods were investigated(Shing and Mahin, 1983, 1984). In these pseudo-dynamic testing methods, as implied in the name, the experimental part is not “**dynamically**” but “**statically**” excited under the loading condition which makes the testing part represent identical displacement response to that of the part in whole structure excited by considered dynamic load such as ground acceleration.

Horiuchi et al. (1999) compensated the time-delay effect caused mainly by analytical procedure in the RHTM(Horiuchi et al., 1999). For its experimental verification, a small portion of mass was separated from a mass-spring-dashpot system, and only the small part of the mass was tested considering the effects of the other parts analytically. Iemura et al. (1999); Igarashi et al. (2000) verified the effect of vibration control devices such as a tuned mass damper and an active mass damper installed in a structure excited by ground acceleration, using the real-time hybrid shaking table testing method in which the control devices were experimental parts and the remaining structural model was a numerical part. The acceleration signal of the moving mass of the devices was measured and used as input to the numerical modelIemura et al. (1999); Igarashi et al. (2000).

Tuned liquid damper (TLD) dissipates structural vibratory energy by tuning the frequency of the liquid sloshing to one of the structure(Soong and Dargush, 1997). TLD has generally been applied to the control of wind-induced acceleration response(Chang and Qu, 1998), and recently, some investigations on the seismic control performance of the TLD have been made(Banerji et al., 2000). In order to describe the behavior of the TLD, linear model based on tuned mass damper analogy(Sun et al., 1995) and linear wave theory, nonlinear stiffness and damping model(Yu et al., 1999), and sloshing-slamping analogy(Yalla, 2001) can be used. However, because any model has the error in capturing the real dynamic characteristics of the control force generated by the TLD and furthermore the error increases for the case of non-stationary excitation such as the earthquake, evaluation of the seismic control performance of the TLD only numerically has the accuracy problem.

Recently, the tuned liquid column damper (TLCD) has received the attention of researchers as a type of auxiliary mass system(Samali et al., 1998). TLCD has the control characteristics similar to that of tuned mass damper (TMD), which is one of most frequently used dampers for vibration control. Since the viscosity term in the governing equation of motion of TLCD is a function of the absolute value of liquid velocity, the equation is non-

linear and the dynamic characteristics of TLCD depend on the magnitude and the characteristics of excitation forces and the corresponding structural responses of the floor at which TLCD is installed(Yalla, 2001).

Two or more TMDs and TLCDs have been installed in a building to control bidirectional responses(Xu and Igusa, 1992; Fujino and Sun, 1993; Yamaguchi and Harnpornchai, 1993; Igusa and Xu, 1994; Jangid and Datta, 1997; Li, 2000; LI et al., 2000; Singh et al., 2002) . Since multi-tuned mass dampers (MTLDs) had been proposed by Xu and Igusa (1992); Igusa and Xu (1994), many researchers have devoted their efforts to improve the control performance of MTLDs(Fujino and Sun, 1993; Yamaguchi and Harnpornchai, 1993; Jangid and Datta, 1997; Li, 2000; LI et al., 2000; Singh et al., 2002; ZHANG and ZHONG, 2004). Especially, Jangid and Datta (1997); Singh et al. (2002) have studied the MTMDs by which the torsional response of building structures subjected to bidirectional vibrations can be reduced. They also proposed the optimum parameters such as mass, frequency and damping ratios, in addition to the installation locations of MTMDs, to control the torsional response. Fujino and Sun (1993) have studied about the optimal frequency ratio and optimal number of MTLDs. However, for applying these multi dampers to building structures, there have been shortcomings such as high installation cost, hard maintenance and additional retrofitting of the story at which they are installed. Additionally, applying the pendulum type TMD used in Taipei 101 building has a limitation that the structural plan should be the similar shape in both weak and strong axes. Also, this type of TMD needs a large installation space(Haskett et al., 2004).

1.3.2 Design of Excitation System for Simulating Dynamic Loads

In the field of earthquake engineering, forced vibration tests for evaluating the dynamic characteristics of structures and evaluating seismic performance have been widely carried out from shaking table, eccentric exciter, and reaction wall to shrinking and real scale structures. Several studies on the system identification to establish the analytical structural model by using the modal characteristics, which are obtained by forced vibration tests, have also been carried out(Halling et al., 2001; Min et al., 2004). The primary purpose of system identification is to construct an analytical model that can simulate the relationship between the excitation load and the measurement response obtained in the forced excitation experiment.

Juang (1994) proposed the system identification method in the frequency domain by using matrix decomposition and that in the time domain by employing Markov parameters and Observer/Kalman filter(Juang, 1994). Dyke et al. (1994) obtained the system matrix of a structure by applying model reduction technique after exciting a 3-story small scale structural model with the shaking table and the active mass driver, and then performing the sys-

tem identification for the respective excitation loads. However, the analytical model that is identified by adopting their methods only describes its input and output relations and does not represent physical information such as the mass, viscosity, and stiffness(Dyke et al., 1994). Alvin and Park (1994) extracted the finite element model that has its physical meaning by using common based-normalized system identification (CBSI) technique(Alvin and Park, 1994).

The shaking table test, in which the loads similar to real earthquakes can be easily simulated, is frequently taken to experimentally assess the seismic performance of a structure with high accuracy. It is usually applied to tests on small-scale structure, however, since it is very difficult to excite real-scaled structures with a shaking table. Yu et al. (2005) designed the linear shaker system to simulate earthquake response of a structure by employing the methods both minimizing the error in time histories between the earthquake-induced structural responses and the linear shaker-induced ones and using the inverse transfer function of the responses of a structure loaded by a linear shaker(Yu et al., 2005). However, their study is based on numerical verification, and also has several limitations for being applied to real-scaled structures. First, forced vibration tests are not appropriate for utilizing the vibration source with large amplitude in the experimental structure. Especially, the structure can not be excited to its nonlinear range, since safety may not be ensured during the test and the linear structural model is used for the numerical simulation. Secondly, it is inappropriate for using the vibration source with full bandwidth. Thirdly, sensors may not be sufficiently deployed in field test due to expenses and their installations so that the structural members, in which critical behaviors are expected, are detected. Finally, the process of obtaining the system matrix of a structure by using the system identification technique should be additionally included in the entire research work, since the structure is based on an analytical model. Accordingly, the validity of the proposed pseudo-earthquake excitation test needs to be experimentally investigated under these constraints.

Dyke et al. (1994) obtained controller canonical form state space realization for a small scale three-story building by using both active mass driver and shaking table and measuring the absolute floor acceleration. Juang (1994) proposed Observer/Kalman filter identification using system Markov parameters in time-domain. These studies present the mathematical models which accurately describe input/output relationship but do not provide physical mass, stiffness, and damping matrices, finite element model based SI techniques are developed in the field of health monitoring or damage detection(Van der Auweraer and Peeters, 2003). Yu et al. (2005) performed a series of ambient vibration measurement and force vibration tests on four-story reinforced concrete building by using linear and eccentric mass shakers and updated the analytical finite element (FE) model based on the collected dynamic data. Also, Yu et al. (2005) presented a linear shaker system to

simulate linear elastic structural seismic response. However, because it is practically very difficult to excite large-scale civil structures by using artificial actuator-type devices, SI techniques using natural excitation such as the wind, vehicle, and human are investigated. In the most earthquake engineering, forced vibration testing has been implemented for many years to assess dynamic characteristics of a building structure. It is based on the fact that dynamic response is sensitive to changes in mass, damping, or stiffness of a structure. These changes would lead to shifts in the modal parameters, such as natural frequencies and mode shape. The dynamic characteristics in the system to identify the integrity of a structure have also been investigated(Dyke et al., 1994). The primary objective in system identification is to find the relationship between the experimental response data and the analytical model by adjusting the structural parameters in the model.

1.3.3 Hybrid Testing Method on a Semi-actively Controlled Building Structure Equipped with Full-scale MR Dampers

A wide variety of structural control strategies for civil engineering structures such as bridges and buildings have been proposed by structural engineers(Adeli, 1999). Various types of active and semi-active or hybrid control dampers have also been developed to enhance the performance of passive control devices(Kim and Adeli, 2005b,a). Analytical and experimental studies on these control devices when applied to MR dampers have been performed in an effort to reduce the structural responses, mainly due to their intrinsic stability and low power consumption. Semi-active and adaptive control strategies using the MR damper have also been extensively compared and analyzed(Jansen and Dyke, 2000; Kim et al., 2009; Bitaraf et al., 2010). In analytical studies, the Bingham, Bouc-Wen, and phenomenological models were proposed as analytical models for describing the hysteretic behavior of the MR damper(Spencer et al., 1997; Yang et al., 2004a). Although these models are useful in the design of the MR damper, they are inappropriate for characterizing the behavior of the MR damper under the excitation of irregular loads such as earthquakes and winds because of the strong nonlinearities of the MR damper due to its dependency on the loading rate and the amplitude of excitations. Also, the performance of the MR damper is not guaranteed in accordance with its current providing devices. Moreover, when the MR damper behaves as a semiactive control device, the hysteretic model is unreliable when it varies with the applied current(Lee et al., 2006). For these reasons, there may be disagreement between the corresponding analytical results and the actual responses of a building installed with an MR damper when the semi-active control strategy is applied.

CHAPTER 2

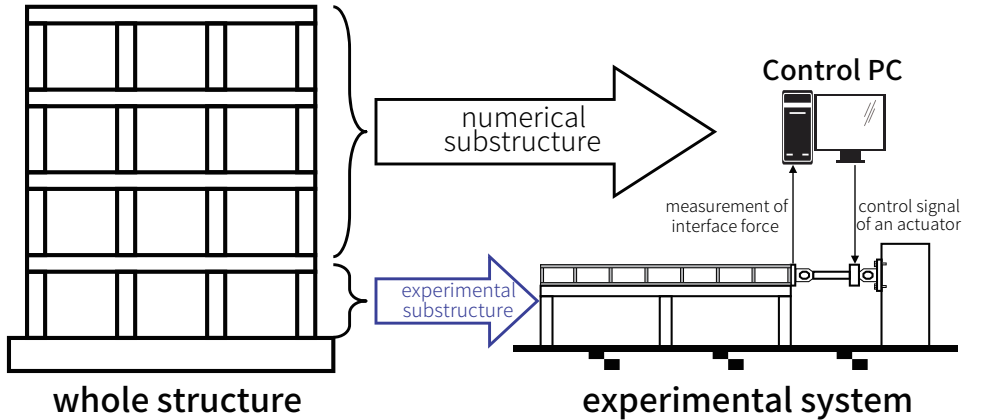
Hybrid Testing Method

In this chapter, the hybrid testing method is introduced as a classification according to equipment type. The hybrid testing method is largely divided into shaking table experiment and UTM experiment by its equipment type. First, the hybrid testing method using the shaking table is divided into the substructuring test method which tests the partial structural system separately, and the hybrid shaking table testing method by installing building structure with nonlinear mass typed vibration control devices such as TLD, TLCD, and TLMD. Secondly, in the case of MR damper which is a type of semi-active friction damper, it is very difficult to implement hybrid shaking table testing installed in an actual building. Therefore, the MR damper is installed in a universal testing machine (UTM), and a hybrid testing method is implemented by simulating the MR damper behavior mounted in a real scaled building. This subject will consider with chapter 4.

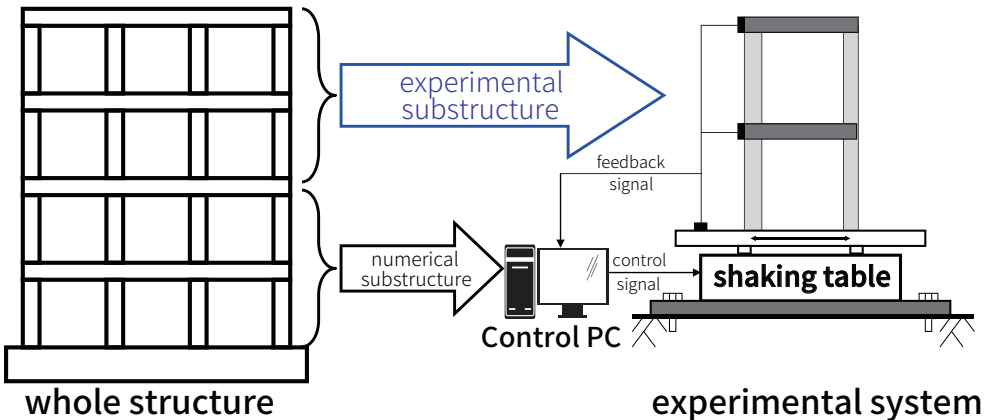
2.1 Substructuring technique

The most substructuring techniques focus on the nonlinear behavior of the lower stories, which are selected as the experimental substructure. Accordingly, the upper stories are considered as the numerical substructure in those conventional substructuring techniques. Differently, from those researches, these studies address the substructuring technique for the shaking table test of a building structure adopting the upper stories as the experimental substructure and the lower stories as the analytical substructure. Figure 2.1 shows the conceptual difference between the conventional and the proposed substructuring techniques as part of hybrid testing method. The necessity of testing the upper substructure is found in diverse structures. For example, the wind-induced acceleration response of slender building structures is usually very large in the top story, and detailed experiment for this upper part of the building structure may be required, since excessive acceleration response may be harmful to human comfort or high precision equipment. Also, in some cases, a light appendage, for example, a penthouse, a small housing for mechanical equipment and an advertising billboard, may vibrate excessively rather than the primary structure. Besides, to suppress excessive vibration induced by winds and earthquakes, a tuned mass damper or tuned liquid damper is employed on the top story of the high-rise building, and

its performance should be verified in the laboratory before installation. Finally, the base isolation system to protect expensive machinery housed in a building structure needs experimental verification for a certain level of earthquake.



(a) conventional method



(b) proposed method

Figure 2.1: Conceptual illustrations of the substructuring methods

On these backgrounds, this subsection proposes a shaking table testing method using the upper part of a building structure as the experimental substructure based on the acceleration feedback from the experimental substructure. Also, the proposed method is verified experimentally through real-time implementation. Figure 2.1 illustrates the schematic diagram of the proposed testing method in this study. At first, the interface force acting between the upper experimental and lower numerical substructures is calculated based on the acceleration feedback of the experimental substructure which is mounted on shaking table. Then the interface acceleration

required to replicate the dynamic behavior of the whole structure is calculated from the numerical substructure subjected to the interface force and assumed base motion for the entire structure. Finally, shaking table excites the upper experimental substructure according to the command signal from the shaking table controller. The series of above processes are performed during a single time interval and repeated over the entire duration of the experiment.

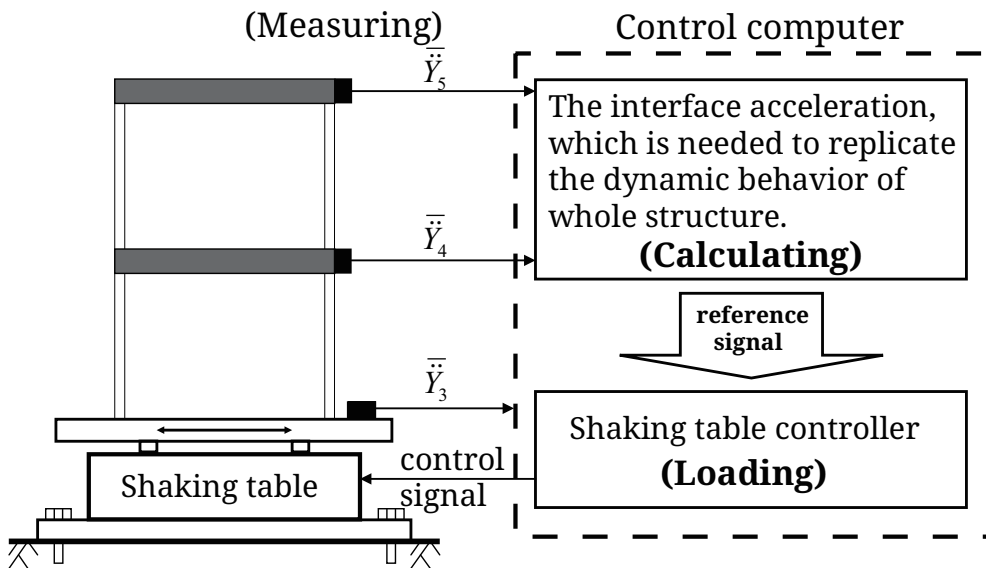


Figure 2.2: Schematic diagram of the proposed method

2.1.1 Formulation and Implementation Methodology

Experimental and Numerical Substructures

This subsection addresses physical interpretation and formulation of splitting the whole structure into the experimental and numerical substructures. A two-step process is carried out to formulate the equations of motion for those two substructures; separating the experimental substructure from the whole structure and constructing experimental substructure mounted on the shaking table and numerical substructures with external loads on the cutting plane, as shown in Figure 2.3.

The equation of motion of the whole shear-type building structure subjected to the ground acceleration, $\ddot{Y}_g(t)$, is represented in Figure 2.3(a) and expressed as

$$\mathbf{M}\ddot{\mathbf{Y}}(t) + \mathbf{C}\dot{\mathbf{Y}}(t) + \mathbf{K}\mathbf{Y}(t) = \mathbf{p}(t) \quad (2.1)$$

where, $\mathbf{Y}(t)$ is the $n \times 1$ vector of the absolute floor displacements given by $\{Y_1, Y_2, \dots, Y_n\}^\top$, and $\mathbf{p}(t)$ is the $n \times 1$ vector of the external force given by $\{0, \dots, 0, c_1 \dot{Y}_g(t) + k_1 Y_g(t)\}^\top$, \mathbf{M} , \mathbf{C} and \mathbf{K} are the structural mass, damping and stiffness matrices, respectively, and expressed as follows.

$$\begin{aligned}\mathbf{M} &= \begin{bmatrix} m_n & m_{n-1} \\ & \ddots \\ & & m_m & m_{m-1} \\ & & & \ddots \\ & & & & m_1 \end{bmatrix}, \\ \mathbf{C} &= \begin{bmatrix} c_n & -c_n & & & \\ -c_n & c_n + c_{n-1} & -c_{n-1} & & \\ & \ddots & \ddots & \ddots & \\ & & -c_{m+1} & c_{m+1} + c_m & -c_m \\ & & & -c_m & c_m + c_{m-1} & -c_{m-1} \\ & & & & \ddots & \ddots & \ddots \\ & & & & & -c_2 & c_2 + c_1 \end{bmatrix}, \\ \mathbf{K} &= \begin{bmatrix} k_n & -k_n & & & \\ -k_n & k_n + k_{n-1} & -k_{n-1} & & \\ & \ddots & \ddots & \ddots & \\ & & -k_{m+1} & k_{m+1} + k_m & -k_m \\ & & & -k_m & k_m + k_{m-1} & -k_{m-1} \\ & & & & \ddots & \ddots & \ddots \\ & & & & & -k_2 & k_2 + k_1 \end{bmatrix},\end{aligned}\tag{2.2}$$

The experimental and numerical substructures are separated from the whole structure by cutting at their interface, as shown in Figure 2.3(b). Mathematically, this operation means separating the equations included in Eq. (2.1) into two groups of which one corresponds to the upper part DOF, and the other corresponds to the lower part DOF. The dotted line in Eq. (2.2) divides those two groups, and the resulting two equations of motions are written as

$$\mathbf{M}_E \ddot{\mathbf{Y}}_E(t) + \mathbf{C}_E(t) \dot{\mathbf{Y}}_E(t) + \mathbf{K}_E \mathbf{Y}_E(t) = \mathbf{p}_E(t)\tag{2.3}$$

$$\mathbf{M}_N \ddot{\mathbf{Y}}_N(t) + \mathbf{C}_N(t) \dot{\mathbf{Y}}_N(t) + \mathbf{K}_N \mathbf{Y}_N(t) = \mathbf{p}_N(t)\tag{2.4}$$

where, subscripts E and N denote the experimental and numerical substructures, respectively. \mathbf{Y}_E and \mathbf{Y}_N are an $l \times 1$ vector given by $\{Y_{E(1)}, Y_{E(2)}, \dots, Y_{E(l)}\}^\top$ and an $m \times 1$ vector given by $\{Y_{N(1)}, Y_{N(2)}, \dots, Y_{N(m)}\}^\top$, respectively. Accordingly, n , the length of the displacement vector, shown in Eq. (2.1) equals to $m + l$. Also, $Y_{E(1)}$, $Y_{E(l)}$, $Y_{N(1)}$ and $Y_{N(m)}$ in Eq.'s (2.3) and (2.4) correspond to Y_{m+1} , Y_n , Y_1 and Y_m in Eq. (2.1), respectively. The mass, damping and stiffness matrices and the external force vectors in Eq. (2.3) and (2.4)

are expressed as follows.

$$\mathbf{M}_E = \begin{bmatrix} m_{E(l)} & & & \\ & m_{E(l-1)} & & \\ & & \ddots & \\ & & & m_{E(2)} & m_{E(1)} \end{bmatrix},$$

$$\mathbf{C}_E = \begin{bmatrix} c_{E(l)} & -c_{E(l)} & & \\ -c_{E(l)} & c_{E(l)} + c_{E(l-1)} & -c_{E(l-1)} & \\ & \ddots & \ddots & \ddots \\ & & -c_{E(3)} & c_{E(3)} + c_{E(2)} & -c_{E(2)} \\ & & & -c_{E(2)} & c_{E(2)} + c_{E(1)} \end{bmatrix}, \quad (2.5)$$

$$\mathbf{K}_E = \begin{bmatrix} k_{E(l)} & -k_{E(l)} & & \\ -k_{E(l)} & k_{E(l)} + k_{E(l-1)} & -k_{E(l-1)} & \\ & \ddots & \ddots & \ddots \\ & & -k_{E(3)} & k_{E(3)} + k_{E(2)} & -k_{E(2)} \\ & & & -k_{E(2)} & k_{E(2)} + k_{E(1)} \end{bmatrix}$$

$$\mathbf{M}_N = \begin{bmatrix} m_{N(m)} & & & \\ & m_{N(m-1)} & & \\ & & \ddots & \\ & & & m_{N(2)} & m_{N(1)} \end{bmatrix},$$

$$\mathbf{C}_N = \begin{bmatrix} c_{N(m)} & -c_{N(m)} & & \\ -c_{N(m)} & c_{N(m)} + c_{N(m-1)} & -c_{N(m-1)} & \\ & \ddots & \ddots & \ddots \\ & & -c_{N(3)} & c_{N(3)} + c_{N(2)} & -c_{N(2)} \\ & & & -c_{N(2)} & c_{N(2)} + c_{N(1)} \end{bmatrix}, \quad (2.6)$$

$$\mathbf{K}_N = \begin{bmatrix} k_{N(m)} & -k_{N(m)} & & \\ -k_{N(m)} & k_{N(m)} + k_{N(m-1)} & -k_{N(m-1)} & \\ & \ddots & \ddots & \ddots \\ & & -k_{N(3)} & k_{N(3)} + k_{N(2)} & -k_{N(2)} \\ & & & -k_{N(2)} & k_{N(2)} + k_{N(1)} \end{bmatrix}$$

$$\mathbf{p}_E(t) = \left\{ 0, \dots, 0, c_{E(1)} \dot{Y}_{N(m)} + k_{E(1)} Y_{N(m)} \right\}^\top \quad (2.7)$$

$$\mathbf{p}_N(t) = \left\{ c_{E(1)} (\dot{Y}_{E(1)} - \dot{Y}_{N(m)}) + k_{E(1)} (Y_{E(1)} - Y_{N(m)}), 0, \dots, 0, c_1 \dot{Y}_g(t) + k_1 Y_g(t) \right\}^\top \quad (2.8)$$

It is obvious from Eq. (2.7) that the absolute acceleration of the top story of the numerical substructure acts as the ground acceleration of the experimental substructure given by Eq. (2.3). This condition is physically realized by synchronizing the shaking table motion with the absolute acceleration of the top story of the numerical substructure. Besides, the first element of the external force vector in Eq. (2.8) means the interface force acting on the top

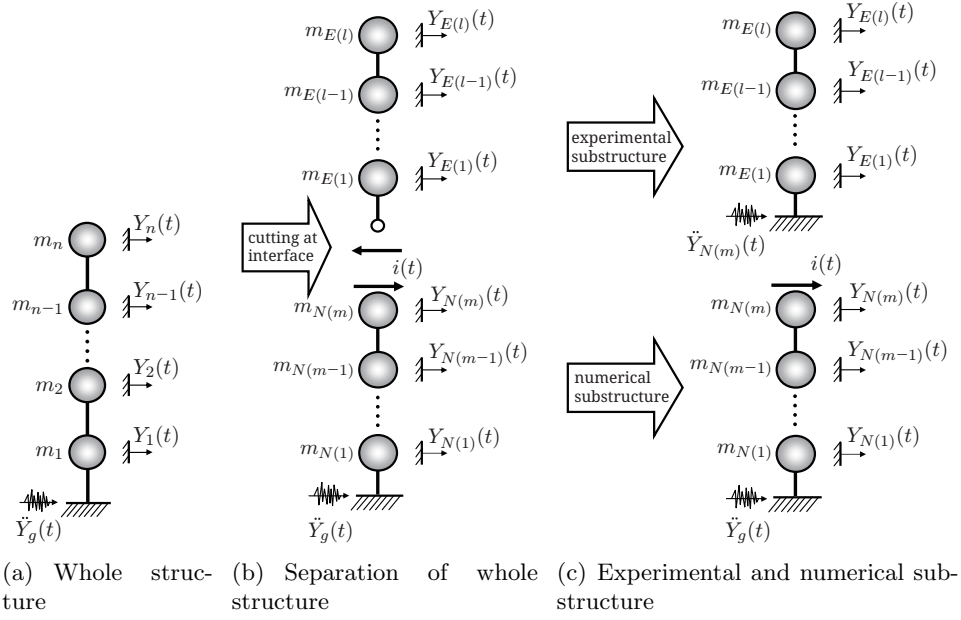


Figure 2.3: Concept of the proposed method

story of the numerical substructure. This interface force, which is denoted by $i(t)$ from now on, is produced by the damping and restoring forces of the first story in the upper experimental substructure and rewritten as follows.

$$i(t) = c_{E(1)} (\dot{Y}_{E(1)} - \dot{Y}_{N(m)}) + k_{E(1)} (Y_{E(1)} - Y_{N(m)}) \quad (2.9)$$

As a result, the numerical substructure, of which equation of motion is given by Eq. (2.4), is subjected to both the interface force at the top story and the ground motion at the base. The boundary condition and external load of each substructure are illustrated in Figure 2.3(c).

Measurement of the interface force

In this section, the interface force, $i(t)$, which should be fed-back to the numerical substructure for calculating the interface acceleration, is indirectly measured by the accelerometers attached on the experimental substructure, as shown in Figure 2.1. Dynamic equilibrium in the experimental substructure is applied to derive the interface force using acceleration response measurement of the experimental substructure. As shown in Figure 2.4, dynamic equilibrium in the experimental substructure is established between the interface force acting at its base and the resultant of its inertial forces, because internal forces between each story are canceled with each other. This relation can be derived in another way. First, the dotted parts are shown in Eq. (2.5) are moved to the right side of Eq. (2.3). Then the relation of Eq. (2.9) is

applied to the right side. Finally, the summation of l simultaneous equations for each side gives following expression of the interface force, $i(t)$.

$$i(t) = - \sum_{i=1}^l m_{E(i)} \ddot{Y}_{E(i)} \quad (2.10)$$

Eq. (2.10) physically implies that the interface force, which is required as an input data of the numerical substructure, can be calculated using the measured acceleration responses of the experimental substructure.

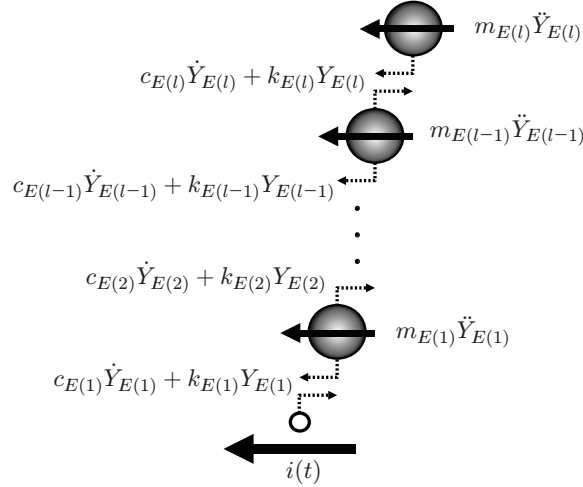


Figure 2.4: Dynamic equilibrium in experimental substructure

Calculation of the numerical substructure

The calculation of the numerical substructure shown in Figure 2.1 means on-line time history analysis of the Eq. (2.4) that represents the dynamic equilibrium of the numerical substructure shown in Figure 2.3(c). To integrate this analysis procedure with shaking table control process implemented on a digital computer, Eq. (2.4) is transformed into state-space equations. The state-space equations, of which the output is the absolute accelerations of the numerical substructure, are given by the following equations in the continuous time domain.

$$\begin{aligned} \dot{\mathbf{z}}(t) &= \mathbf{A}\mathbf{z}(t) + \mathbf{B}\mathbf{u}(t) \\ \mathbf{O}(t) &= \mathbf{C}\mathbf{z}(t) + \mathbf{D}\mathbf{u}(t) \end{aligned} \quad (2.11)$$

where, $\mathbf{z}(t)$ is the $2m \times 1$ vector of state variables composed of the relative displacement and velocity of the numerical substructure. $\mathbf{u}(t)$ is the 2×1 vector of input variables given by $\{i(t), \ddot{Y}_g(t)\}^\top$, in which the interface force, $i(t)$, is fed-back from the experimental substructure using Eq. (2.10). $\mathbf{O}(t)$

is the $m \times 1$ vector of the output composed of the absolute accelerations of the numerical substructure. The system matrices \mathbf{A} , \mathbf{B} , \mathbf{C} and \mathbf{D} have the dimension of $2m \times 2m$, $2m \times 2$, $m \times 2m$ and $m \times 2$, respectively, and are expressed as

$$\mathbf{A} = \begin{bmatrix} \mathbf{0}_{m \times m} & \mathbf{I}_{m \times m} \\ -\mathbf{M}_N^{-1}\mathbf{K}_N & -\mathbf{M}_N^{-1}\mathbf{C}_N \end{bmatrix} \quad (2.12)$$

$$\mathbf{B} = \begin{bmatrix} \mathbf{0} & \mathbf{0} \\ \mathbf{M}_N^{-1}\mathbf{b} & -\mathbf{1} \end{bmatrix} \quad (2.13)$$

$$\mathbf{C} = [-\mathbf{M}_N^{-1}\mathbf{K}_N \quad -\mathbf{M}_N^{-1}\mathbf{C}_N] \quad (2.14)$$

$$\mathbf{D} = [\mathbf{M}_N^{-1}\mathbf{b} \quad \mathbf{0}] \quad (2.15)$$

where, $\mathbf{0}$ and \mathbf{I} are $m \times m$ zero and unit matrices, respectively, and $\mathbf{0}$ and $-\mathbf{1}$ are an $m \times 1$ vector of 0 and an $m \times 1$ vector of -1 , respectively. \mathbf{b} is an $m \times 1$ vector given by $\{1, 0, \dots, 0\}^\top$. Eq. (2.11) with the inputs of the interface force and ground motion is incorporated in the ‘Calculating’ part shown in Figure 2.1, and produces the absolute acceleration responses of the numerical substructure on-line. Among those acceleration responses, the one corresponding to the top story is utilized as the reference signal to operate shaking table.

2.1.2 Numerical Substructure

For the verification experiment of the proposed methodology, the object structure is assumed to be a five-story shear type building structure, of which two upper stories are assumed to be the experimental substructure as shown in Figure 2.15. As a result, the numerical substructure is the three lower stories of the whole structure. For the construction of the finite element model of the numerical substructure, the inter-story damping and stiffness coefficients of the shear-type experimental substructure are identified based on the measured acceleration responses, and the mass of the two floors are measured directly. The system identification of the experimental substructure is conducted using the command `fmincon` in MATLAB(Coleman et al., 1999), which uses the interior-reflective Newton method to solve the constrained nonlinear minimization problem (Coleman, 1994; Coleman and Li, 1996). Resulting identified parameters can be summarized as follow.

$$\begin{aligned} m_{E(1)} &= m_4 = 2.04(kg), \quad m_{E(2)} = m_5 = 5.10(kg) \\ k_{E(1)} &= k_4 = 45.3(N/m), \quad k_{E(2)} = k_5 = 48.5(N/m) \\ c_{E(1)} &= c_4 = 0.023(N \cdot s/m), \quad c_{E(2)} = c_5 = 0.015(N \cdot s/m) \end{aligned} \quad (2.16)$$

which correspond to the first and second natural frequencies of 2.5 and $8.6Hz$, respectively, as given in Table 2.1. Figure 2.5 compares the exper-

imentally obtained transfer functions with numerically computed ones. As shown in Figure 2.5, measured transfer functions agree well with those of the corresponding numerical model.

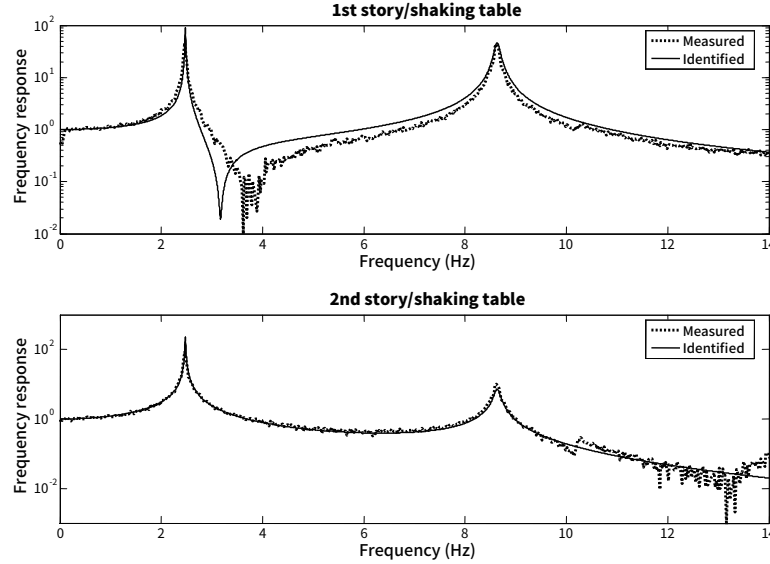


Figure 2.5: Comparison of experimental and approximated transfer functions.

Table 2.1: Frequencies observed in the time records of the experimental substructure from the test without feedback and the natural frequencies of the assumed whole structure

Mode	Frequency components(Hz) observed in the experimental substructure with 2 DOFs	Natural frequencies (Hz) of the whole structure with 5 DOFs
1	1.3	1.3
2	2.5	4.2
3	4.2	7.1
4	7.1	9.4
5	8.6	10.8

The structural parameters for the first story of the experimental structure given in Eq. (2.16) are applied to all stories of the numerical substructure and summarized as the following:

$$i(t) = -m_{E(1)}\ddot{Y}_{E(1)}(t) - m_{E(2)}\ddot{Y}_{E(2)}(t) \quad (2.17)$$

$$\ddot{Y}_{N(3)}(t) = -c_{N(3)}(\dot{Y}_{N(3)} - \dot{Y}_{N(2)}) - k_{N(3)}(Y_{N(3)} - Y_{N(2)}) + i(t) \quad (2.18)$$

Eq. (2.18) means that the interface force, which is produced by the shaking table, is calculated using the two measured absolute accelerations of the experimental substructure. Then, the interface acceleration is calculated from the numerical substructure expressed by Eq. (2.11). Figure 2.6 represents the block diagram of the entire substructuring testing system including the numerical substructure marked by the shaded area. In Figure 2.6, the ground acceleration, \ddot{Y}_g , is not a measured signal but an input data prescribed by a user. Finally, the shaking table motion is controlled using the inverse transfer function of Eq. (2.36) to minimize the errors between the interface acceleration computed as the third story absolute acceleration of the numerical substructure, $\ddot{Y}_{N(3)}$, and the actual shaking table acceleration. Therefore, the shaking table itself works as the interface node of Figure 2.3(b) and excites the upper experimental substructure. In the actual implementation of the shaking table test, the continuous filters included in Figure 2.6 are converted into discrete filters with a time step of 0.01 sec.

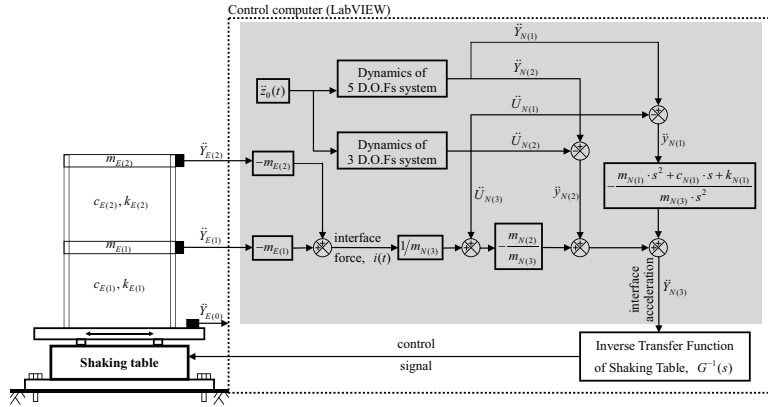


Figure 2.6: Block diagram of the integrated controller for the substructuring testing system.

2.2 Hybrid Testing Method for the Performance Evaluation of a Tuned Liquid Damper

In this section, the vibration control effect of a TLD for a building structure excited by earthquake load is experimentally evaluated through the hybrid testing method. The hybrid testing method does not require a physical

building structural model in performing the experiment of a TLD-structure interaction system, and it only uses a TLD which is known to have strong nonlinearity dependent on response amplitude, excitation frequency, and depth to length ratio(Yu et al., 1999). The structural responses of the interaction system are calculated numerically in real time using the analytical structural model with the excitations of measured control force, user-defined base earthquake loads, and its state space realization incorporated in the integrated controller of the shaking table. Also, in order to minimize the distortion of the acceleration of the shaking table, the inverse transfer function of the shaking table is identified and its state space realization is implemented in the shaking table controller. The motion of shaking table behaves both the controlled and uncontrolled absolute acceleration of the TLD mounted floor by modulating the feedback gain of the shear force measured by the load cell installed between the TLD and the shaking table. Comparison between the structural responses obtained by the hybrid testing method and the conventional shaking table test of a single story steel frame with TLD is made in order to verify the accuracy of the hybrid testing method and the uncontrolled and TLD-controlled structural responses of a three-story structure are obtained by the hybrid testing method in both time and frequency domains.

2.2.1 Hybrid Testing Method with TLD

Figure 2.7 depicts the conceptual illustrations of the hybrid testing method for an n-degrees-of-freedom structural model which is excited by base acceleration and has a tuned liquid damper at its top story. First, the whole control system is separated into the lower part structure, and the upper part TLD and the interaction force between the structure and TLD are considered. The TLD with the interacting force at its bottom is physically tested, and the response of the structure with interacting force at the top floor and the base acceleration is numerically calculated by using the computer controlling the motion of the shaking table. Measurement of interacting force is easily accomplished by installing a shear-type load-cell at the bottom of the TLD, as shown in Figure 2.7. TLD-generated shear force is fed back to the control computer. With this fed-back interacting force, the structural response of the story, where a TLD is installed, is calculated using the numerical part. The shaking table excites the upper TLD according to this calculated response. This process is carried out on real-time.

The numerical part with n -DOFs, which is subjected to the excitations of the measured control force, $i_e(t)$, and the input acceleration, $\ddot{z}_0(t)$, at its top and bottom, respectively, as enclosed in dotted line in Figure 2.7, is calculated by

$$\mathbf{M}\ddot{\mathbf{Y}}_i(t) + \mathbf{C}\dot{\mathbf{Y}}_i(t) + \mathbf{K}\mathbf{Y}_i(t) = \mathbf{p}(t) \quad (2.19)$$

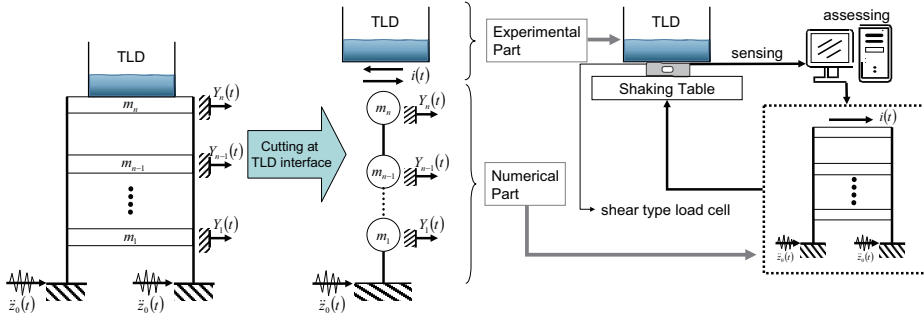


Figure 2.7: Conceptual view of the hybrid shaking table test

where, $\mathbf{Y}_i(t)$ is the absolute displacement at the i th ($i = 1 \rightarrow n$) story, and the location vector of external forces with the length of n , $\mathbf{p}(t)$ equals to $\{-i_e(t), 0, \dots, 0, c_1\dot{z}_0(t) + k_1z_0(t)\}^\top$, in which subscript “*e*” denotes the “*experimentally*” measured interacting force. Also, the structural mass, damping and stiffness matrices are represented by

$$\mathbf{M} = \begin{bmatrix} m_n & m_{n-1} & & \\ & \ddots & \ddots & \\ & & \ddots & m_1 \end{bmatrix}, \quad \mathbf{C} = \begin{bmatrix} c_n & -c_n & & \\ -c_n & c_n + c_{n-1} & -c_{n-1} & \\ \ddots & \ddots & \ddots & \ddots \\ & -c_2 & c_2 + c_1 & \end{bmatrix},$$

$$\mathbf{K} = \begin{bmatrix} k_n & -k_n & & \\ -k_n & k_n + k_{n-1} & -k_{n-1} & \\ \ddots & \ddots & \ddots & \ddots \\ & -k_2 & k_2 + k_1 & \end{bmatrix} \quad (2.20)$$

To calculate the numerical part such as Eq. (2.20) by a control computer on real-time, it is transformed into the state-space representation given by

$$\begin{aligned} \dot{\mathbf{z}}(t) &= \mathbf{A}_c \mathbf{z}(t) + \mathbf{B}_c \mathbf{u}(t) \\ \mathbf{O}(t) &= \mathbf{C}_c \mathbf{z}(t) + \mathbf{D}_c \mathbf{u}(t) \end{aligned} \quad (2.21)$$

where, the state variable vector, $\mathbf{z}(t)$, with the length of $2n$ comprises the state variables, $\{\mathbf{y}_i(t), \dot{\mathbf{y}}_i(t)\}^\top$, in which the structural relative displacement, $\mathbf{y}_i(t)$, equals to $\mathbf{Y}_i(t) - z_0(t)$. The input vector, $\mathbf{u}(t)$, with the length of 2 consists of $\{-i_e(t), \ddot{z}_0\}^\top$. The output vector, $\mathbf{O}(t)$, with the length of n corresponds to the structural absolute acceleration, $\ddot{\mathbf{Y}}_i(t)$, itself. The matrices \mathbf{A}_c , \mathbf{B}_c , \mathbf{C}_c and \mathbf{D}_c with the sizes of $2n \times 2n$, $2n \times 2$, $n \times 2n$ and $n \times 2$, respectively, are expressed as the following Eqs. (2.22)-(2.25).

$$\mathbf{A}_c = \begin{bmatrix} \mathbf{0}_{m \times n} & \mathbf{I}_{m \times n} \\ -\mathbf{M}^{-1}\mathbf{K} & -\mathbf{M}^{-1}\mathbf{C} \end{bmatrix} \quad (2.22)$$

$$\mathbf{B}_c = \begin{bmatrix} \mathbf{0}_{n \times 1} & \mathbf{0}_{n \times 1} \\ \mathbf{M}^{-1}\mathbf{b} & -\mathbf{1} \end{bmatrix} \quad (2.23)$$

$$\mathbf{C}_c = [-\mathbf{M}^{-1}\mathbf{K} \quad -\mathbf{M}^{-1}\mathbf{C}] \quad (2.24)$$

$$\mathbf{D}_c = [\mathbf{M}^{-1}\mathbf{b} \quad \mathbf{0}_{m \times 1}] \quad (2.25)$$

2.3 Hybrid testing method for the Performance Evaluation of a Tuned Liquid Column Damper

The tuned liquid column damper has received the attention of researchers as a type of auxiliary mass system(Samali et al., 1998). TLCD has the control characteristics similar to that of tuned mass damper , which is one of most frequently used dampers for vibration control. Since the viscosity term in the governing equation of motion of TLCD is a function of the absolute value of liquid velocity, the equation is nonlinear, and the dynamic characteristics of TLCD depend on the magnitude and the characteristics of excitation forces and the corresponding structural responses of the floor at which TLCD is installed(Yalla, 2001). In this section, the vibration control effect of a TLCD for a building structure excited by earthquake load is experimentally evaluated through the hybrid testing method. The hybrid testing method does not require a physical building structural model in performing the experiment of a TLCD-structure interaction system, and it only uses a TLCD. The structural responses of the interaction system are calculated numerically in real time using the analytical structural model with the excitations of measured control force, user-defined base earthquake loads, and its state space realization incorporated in the integrated controller of the shaking table. Also, in order to minimize the distortion of the acceleration of the shaking table, the inverse transfer function of the shaking table is identified, and its state space realization is implemented in the shaking table controller. The shaking table behaves as the absolute acceleration of the TLCD mounted floor by calculating the fed back signal of the shear force signal measured by the load cell positioned between the TLCD and plate of the shaking table. Comparison results between the structural responses obtained by the hybrid testing method and the conventional shaking table test of a single story steel frame with TLCD are made in order to verify the accuracy of the hybrid testing method in both time and frequency domains.

2.3.1 RHybrid Testing Method with TLCD

Figure 2.8 shows the conceptual view of the experiment. The whole structural control system, which a TLCD was installed onto the structural model with n -degrees-of-freedom at its top story, is separated, and as the result of that, the force interacts at their interface. The upper part of TLCD with the interacting force at its bottom is physically tested and the lower part of the structural model with the interacting force and the input motion at its top story and base, respectively, is numerically calculated within the computer to control the motion of shaking table. For the experimental implementation, interacting or control force generated by a TLCD, which is observed from a load-cell, is fed back to the control computer. With the fed-back interacting force, the structural response of the story, where a TLCD is incorporated, is calculated from the numerical part. The shaking table excites the upper TLCD with this calculated response. These processes are carried out on real-time.

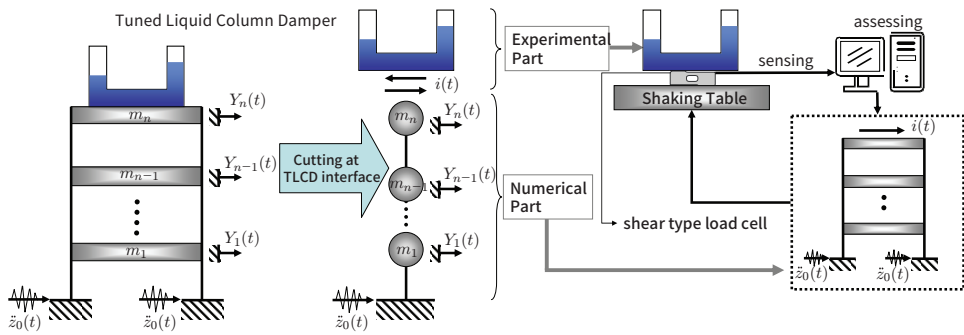


Figure 2.8: Concept of the hybrid testing method (TLCD)

Of these procedures, the numerical part with n -DOFs, which is subjected to the excitations of the experimentally measured control force, $i_e(t)$, and the input acceleration, $\ddot{z}_0(t)$, at its top and bottom, respectively, as enclosed in dotted line in Figure 2.8, is calculated by

$$\mathbf{M}\ddot{\mathbf{Y}}_i(t) + \mathbf{C}\dot{\mathbf{Y}}_i(t) + \mathbf{K}\mathbf{Y}_i(t) = \mathbf{p}(t) \quad (2.26)$$

where, $\mathbf{Y}_i(t)$ is the absolute displacement at the i th ($i = 1 \rightarrow n$) story, and the location vector of external forces with the length of n , $\mathbf{p}(t)$ equals to $\{-i_e(t), 0, \dots, 0, c_1\ddot{z}_0(t) + k_1z_0(t)\}^\top$, in which subscript “ e ” denotes the “experimentally” measured interacting force. Also, the structural mass, damp-

ing and stiffness matrices are represented by

$$\mathbf{M} = \begin{bmatrix} m_n & m_{n-1} & & \\ & \ddots & m_1 & \\ & & & \ddots \end{bmatrix}, \quad \mathbf{C} = \begin{bmatrix} c_n & -c_n & & \\ -c_n & c_n + c_{n-1} & -c_{n-1} & \\ & \ddots & \ddots & \ddots \\ & & -c_2 & c_2 + c_1 \end{bmatrix}, \quad (2.27)$$

$$\mathbf{K} = \begin{bmatrix} k_n & -k_n & & \\ -k_n & k_n + k_{n-1} & -k_{n-1} & \\ & \ddots & \ddots & \ddots \\ & & -k_2 & k_2 + k_1 \end{bmatrix}$$

To calculate the numerical part such as Eq. (2.20) by a control computer on real-time, it is transformed into the state-space representation given by

$$\begin{aligned} \dot{\mathbf{z}}(t) &= \mathbf{A}_c \mathbf{z}(t) + \mathbf{B}_c \mathbf{u}(t) \\ \mathbf{O}(t) &= \mathbf{C}_c \mathbf{z}(t) + \mathbf{D}_c \mathbf{u}(t) \end{aligned} \quad (2.28)$$

where, the state variable vector, $\mathbf{z}(t)$, with the length of $2n$ comprises the state variables, $\{\mathbf{y}_i(t), \dot{\mathbf{y}}_i(t)\}^\top$, in which the structural relative displacement, $\mathbf{y}_i(t)$, equals to $\mathbf{Y}_i(t) - z_0(t)$. The input vector, $\mathbf{u}(t)$, with the length of 2 consists of $\{-i_e(t), \ddot{z}_0\}^\top$. The output vector, $\mathbf{O}(t)$, with the length of n corresponds to the structural absolute acceleration, $\ddot{\mathbf{Y}}_i(t)$, itself. The matrices \mathbf{A}_c , \mathbf{B}_c , \mathbf{C}_c and \mathbf{D}_c with the sizes of $2n \times 2n$, $2n \times 2$, $n \times 2n$ and $n \times 2$, respectively, are expressed as the following Eqs. (2.29)-(2.32).

$$\mathbf{A}_c = \begin{bmatrix} \mathbf{0}_{m \times n} & \mathbf{I}_{m \times n} \\ -\mathbf{M}^{-1}\mathbf{K} & -\mathbf{M}^{-1}\mathbf{C} \end{bmatrix} \quad (2.29)$$

$$\mathbf{B}_c = \begin{bmatrix} \mathbf{0}_{n \times 1} & \mathbf{0}_{n \times 1} \\ \mathbf{M}^{-1}\mathbf{b} & -\mathbf{1} \end{bmatrix} \quad (2.30)$$

$$\mathbf{C}_c = [-\mathbf{M}^{-1}\mathbf{K} \quad -\mathbf{M}^{-1}\mathbf{C}] \quad (2.31)$$

$$\mathbf{D}_c = [\mathbf{M}^{-1}\mathbf{b} \quad \mathbf{0}_{m \times 1}] \quad (2.32)$$

where, $\mathbf{0}_{n \times n}$ and $\mathbf{I}_{n \times n}$ are the zero and unit matrices, respectively, with the size of $n \times n$. $\mathbf{0}_{n \times 1}$ and $-\mathbf{1}$ are the vector whose components are 0 and -1 , respectively, with the length of $n \times 1$. \mathbf{b} equal to $\{1, 0, \dots, 0\}^\top$ with the length of $n \times 1$.

2.4 Hybrid Testing Method for the Performance Evaluation of a Tuned Liquid Mass Damper

In previous study(Heo et al., 2009), a new control device, which is called tuned liquid mass damper (TLMD), was developed and discussed in this section. The dynamic characteristics of a TLMD used in this study are that its mass is composed of both a mass of TLCD frame itself and that of liquid

in a tank. Natural rubber columns were used to substitute the stiffness of a TMD. Therefore, a TLMD operates as a TLCD in one direction and behaves as a TMD in the other orthogonal direction.

In this section, the control performance of the proposed TLMD for reducing bidirectional responses of building structures is experimentally verified through both a conventional structural testing method and hybrid testing method. First, the control performance of a TLMD is evaluated by forced vibrating sinusoidal signal to an experimental prototype which is composed of both a TLMD and a building structure. Then, the hybrid testing method is performed to evaluate the performance of a TLMD, in which the building structural model is used as a numerical part, and the TLMD is experimentally tested.

2.4.1 Developed TLMD Model

Figure 2.9 shows the plan view of the TLMD used in this study. The bidirectional TLMD would be installed in the POSCO New Songdo City Tower 1A in Incheon, South Korea with 64 stories and 236 meters in height. An eigenvalue analysis of the tower resulted in 0.182 and 0.162Hz in the x , y -directions, respectively, for the first natural frequencies, and $34,000\text{tons}$ for the first modal mass. The total mass of the bidirectional TLMD is 600tons that results from the effective mass ratio of about 1.76% .

The experimental building and TLMD models were manufactured by applying the scaling factors given in Table 2.2 to the first modal properties of the prototype tower. The building model with the parameters shown in Table 2.3 was made by applying the scaling factors in Table 2.2 to the prototype building. Applying the scale $1/\sqrt{20}$ in frequency to the natural frequencies of a prototype model, 0.182 and 0.162Hz , gives 0.82 and 0.73Hz in the x - and y -directions, respectively. Also, the mass of a building structure is reduced by $4,250\text{kg}$. The stiffness of a building model is calculated to be $4250(\text{kg}) \times (2\pi \times 0.82(\text{Hz}))^2 \cong 110000(\text{N/m})$ in the x -direction and $4250(\text{kg}) \times (2\pi \times 0.73(\text{Hz}))^2 \cong 89,000(\text{N/m})$ in the y -direction, respectively.

Table 2.2: Similitude law applied to TLMD model

Quantity	Dimension	Scaling factor
Length	L	$1 : 20$
Mass	M	$1 : 20^3 = 1 : 8000$
Frequency (Hz)	T^{-1}	$1 : 1/\sqrt{20} = 1 : 0.223$
Acceleration	LT^{-2}	$1 : 1$

As shown in Table 2.4, it is obvious that the natural frequencies of a TLMD tune to those of a building structure in the TMD(x) and TLCD(y)-

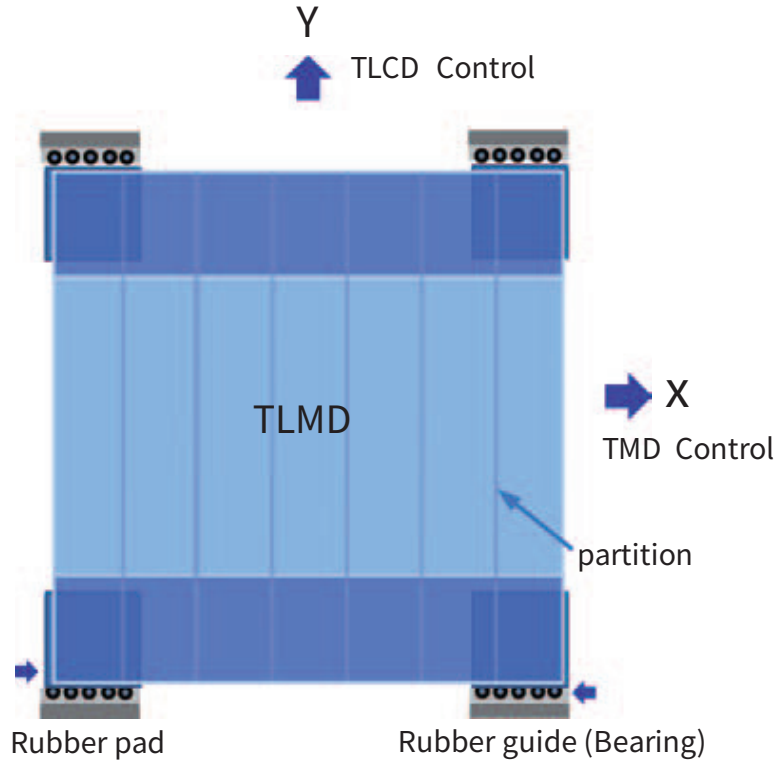


Figure 2.9: Concept of a TLMD

control directions, respectively. The masses of a TLMD with the ratios of 1.8 and 0.8% to the mass of a building model become 75kg in the TMD-control and 32kg in the TLCD-control directions, respectively. The stiffness of rubber columns used in a TMD, k , and the liquid length of a TLCD, L , are determined by

$$k = m (2\pi f_m)^2 \quad (2.33)$$

$$L = \frac{2g}{(2\pi f_L)^2} \quad (2.34)$$

where m and f_m are the mass and the tuned frequency of a TLCD, respectively, in the TMD-control direction. g and f_L are the gravity acceleration and the tuned frequency of the TLCD, respectively, in the TLCD-control direction. With these relations, the final parameters of a TLMD are shown in Table 2.4.

Table 2.3: Design parameters of the building model

Design parameter	<i>y</i> -direction	<i>x</i> -direction
Siffness (N/m)	88,000	110,000
Frequency (Hz)	0.73	0.82
Mass (kg)	4,250	4,250

Table 2.4: Design parameters of a TLMD model

Design parameters	TLCD control direction	TMD control direction
Siffness or liquid length	$0.98m$ (liquid length)	$1990N/m$ (stiffness)
Frequency (Hz)	0.73	0.82
Mass (kg)	35	75

2.5 Design of Experimental Controller

2.5.1 Experimental System for Substructurubg Technique

The experimental system is shown in Figure 2.10 and 2.11 was equipped in Seismic Retrofitting & Remodeling Research Center at the Dankook University, Seoul, Korea. The test structure (the experimental substructure) used in this experiment is a two-story steel frame with a single bay. The height and width of the experimental substructure are 1.0 and 0.6 m, respectively. The first floor mass, $m_{E(1)}$, and the second floor mass, $m_{E(2)}$, are 2.04 and 5.10 kg, respectively. The experimental substructure is excited by a uni-axial shaking table. The accelerometers are attached to each floor of the experimental substructure to measure its absolute floor acceleration responses. Additionally, an accelerometer is placed on the shaking table to monitor its motion. The data acquisition and implementation of the digital shaking table controller are performed using a real-time digital signal processor (DSP). The major task of the data acquisition board is to carry out the analog-to-digital (A/D) conversion of the measured acceleration data and the digital-to-analog (D/A) conversion of the reference signal computed by the shaking table controller, which is programmed using LabVIEW (Bishop, 2007). An 8-channel data acquisition system was employed using an NI PCI-6052E board and an NI SC-2345 BNC cable connector as a signal conditioner.



Figure 2.10: Overall view of experimental system

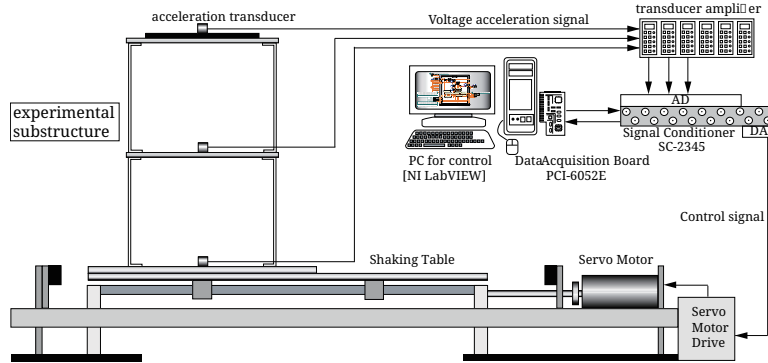


Figure 2.11: Schematic diagram of experimental system

2.5.2 Shaking table controller

The composition of the experimental system is illustrated in Figure 2.11. The shaking table shown in Figure 2.11 moves in accordance with the control signal, which is generated by the control computer and sent through D/A conversion board. In almost every case, the target acceleration signal and actual acceleration produced by the shaking table are different in their amplitudes and phases due to the shaking table dynamics. Therefore, in order to compensate the distortion of the actual shaking table acceleration against the shaking table dynamics existing between the reference signal and the actual measured acceleration of the shaking table, the inverse transfer function of the actual acceleration of shaking table with respect to the command signal generated by the control computer is constructed and implemented in the shaking table control computer as shown in Figure 2.15. First, the inverse transfer function, of which amplitude and phase are represented in Figure 2.12 by the dashed line, is obtained experimentally. Then, the experimental inverse transfer function is approximated by a rational function for its implementation in the control computer. In this verification experiment, the inverse transfer function of the shaking table is approximated using the command `invfreqs` in MATLAB (Little and Shure, 1992), which adopts the damped Gauss-Newton method for the iterative search to minimize the sum of the squared error between the measured and the desired frequency response points(Dennis Jr and Schnabel, 1983). The approximation result is given by the following 5-th order linear filter and compared with the experimental one in Figure 2.12.

Inverse transfer function, Eq. (2.35), corresponds to the shaking table controller of Figure 2.1.

$$G^{-1}(s) = \frac{0.6s^5 + 94s^4 + 10746s^3 + 498200s^2 + 167124s + 108216}{s^5 + 204s^4 + 15900s^3 + 8252s^2 + 4676s + 405} \quad (2.35)$$

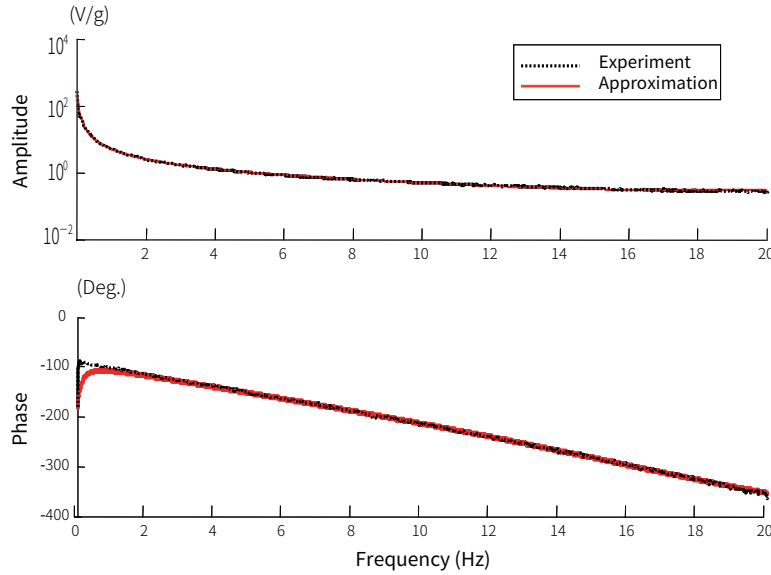


Figure 2.12: Inverse transfer function of shaking table

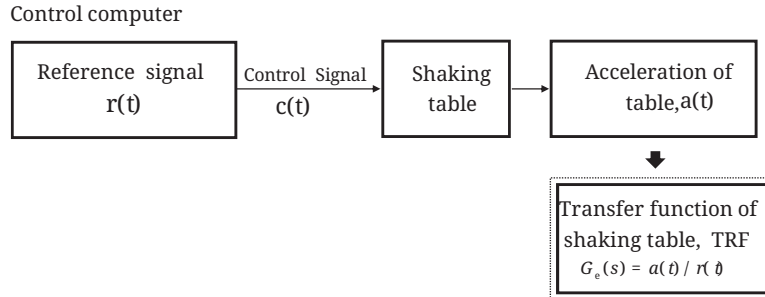


Figure 2.13: Definition of the transfer function of shaking table

For the implementation in the digital computer, Eq. (2.35) is realized into the following state equation.

$$\begin{aligned}\dot{\mathbf{x}}_c &= \mathbf{A}_c \mathbf{x}_c + \mathbf{B}_c r_c \\ y_c &= \mathbf{C}_c \mathbf{x}_c + D_c r_c\end{aligned}\quad (2.36)$$

where, \mathbf{x}_c , r_c and y_c is the state vector, the reference signal, the control signal of the shaking table controller, respectively. \mathbf{A}_c , \mathbf{B}_c , \mathbf{C}_c and D_c is the 5×5 state matrix, the 5×1 reference signal influence matrix, the 1×5 output matrix and the coupling coefficient between the reference and control signal.

In order to verify the performance of the shaking table controller, a down-scaled El Centro earthquake is input to the inverse transfer function of the shaking table. Then, the corresponding acceleration of the shaking table is measured. Figure 2.16 compares the reference acceleration with the

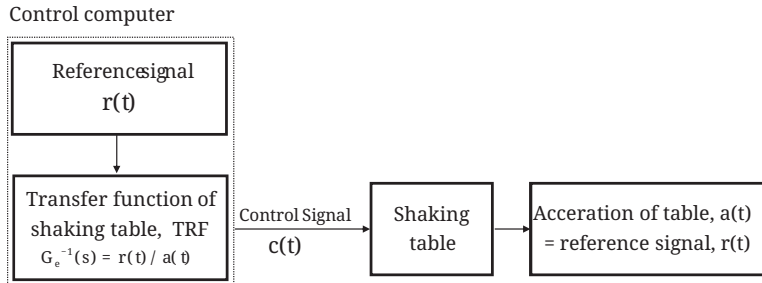


Figure 2.14: Compensation using the inverse transfer function of shaking table

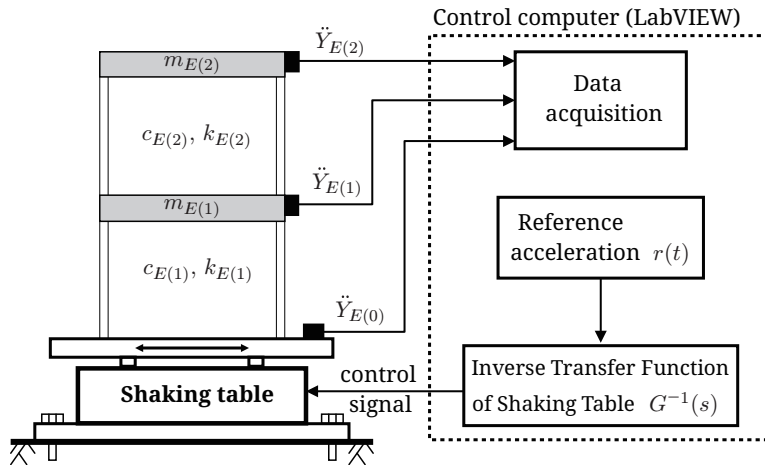


Figure 2.15: Flow chart of the experimental system controller

corresponding measured acceleration of the shaking table. It is observed that they agree well with each other.

2.5.3 Experimental System for Hybrid Testing of Building with TLD

Experimental setup

In order to experimentally verify the hybrid testing method, an experimental system shown in Figure 2.17 was set up in Seismic Retrofitting & Remodeling Research Center at the Dankook University, Seoul, Korea. The TLD was uniaxially excited by the shaking table on which it was mounted. The shear-type load-cell was inserted between the TLD and the shaking table to measure the base shear force yielded by the horizontal motion of the TLD during the test. Also, an accelerometer was attached to the shaking table to monitor its motion.

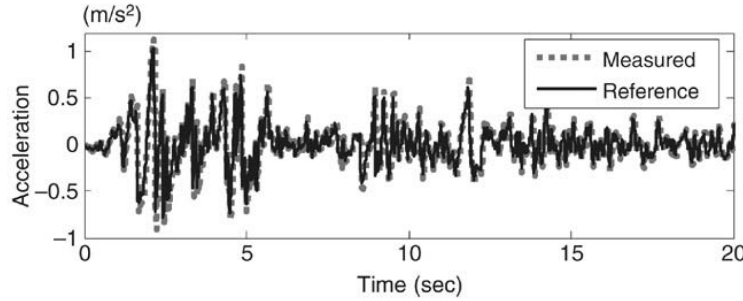


Figure 2.16: Compensation result for the dynamic characteristic of shaking table

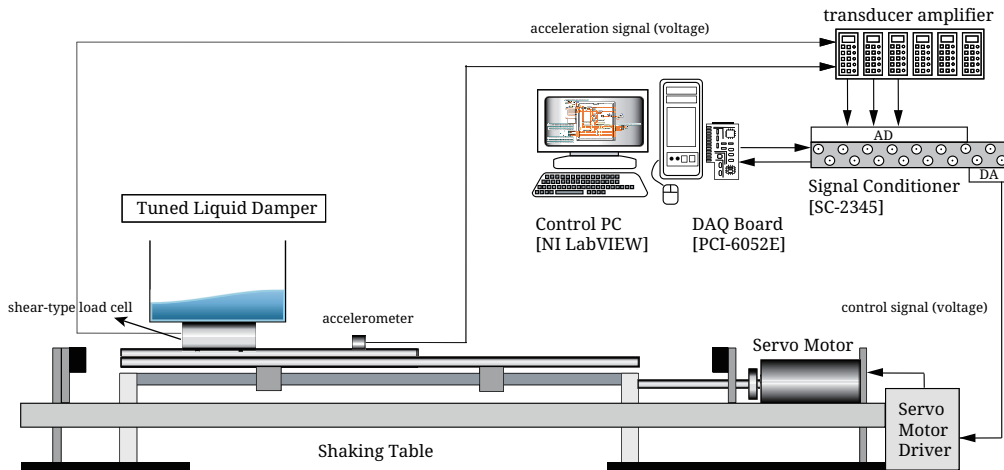


Figure 2.17: Schematic diagram of experimental set-up

Integrated Controller of the Numerical Structural Model and the Shaking Table

The numerical structural model and the shaking table dynamics discussed in the previous subsections are integrated into the controller to implement the hybrid testing method. Figure 2.18 illustrates the block diagram for the hybrid testing method. In the figure, the absolute acceleration is produced by the numerical structural model of Eq. (2.21) with two inputs of the measured interacting force, $i_e(t)$, and not the measured but the prescribed earthquake record signal, $\ddot{z}_0(t)$, as marked by the shaded area. The motion of the shaking table is driven by the controller using the inverse transfer function to minimize the error between the absolute acceleration, $\ddot{Y}_n(t)$, calculated as the top story response of the structure and the actual shaking table acceleration, $\ddot{Y}_e(t)$. Accordingly, the shaking table itself behaves as the top story of the structure, at which a TLD is installed, and excites the upper TLD that should be physically tested.

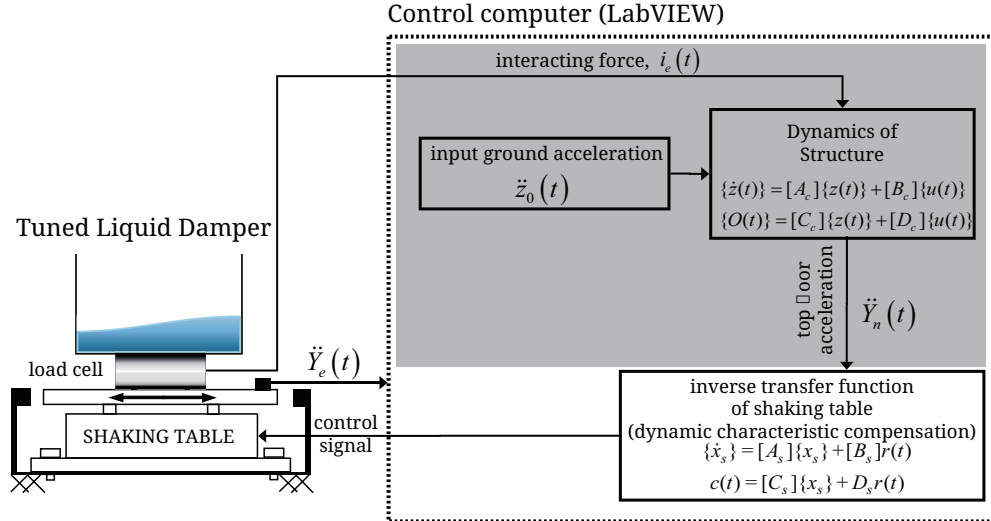


Figure 2.18: Block diagram of the integrated controller for the hybrid testing system.

2.5.4 Experimental System for Hybrid Testing of Building with TLCD

The numerical part and the shaking table controller discussed in previous subsections should be integrated into the controller to implement the hybrid testing shown in Figure 2.8. Figure 2.19 illustrates the block diagram for experimentally implementing the testing method. In the figure, the absolute acceleration is produced by the numerical part such as Eq. (2.28) with two inputs of the measured interacting force, $i_e(t)$, and not the measured but the prescribed earthquake record signal, $\ddot{z}_0(t)$, by a user in the control computer, as marked by the shaded area. The motion of shaking table is driven by the controller using the inverse transfer function to minimize the error between the controlled absolute acceleration, $\ddot{Y}_n(t)$, calculated as the top story response of structure and the actual shaking table acceleration, $\ddot{Y}_e(t)$. Accordingly, the shaking table itself behaves as the top story of structure, at which a TLCD is installed, and excites the upper TLCD that should be physically tested. To verify the hybrid testing method, firstly the conventional TLCD-structure interaction model shown in Figure 2.20(a) is experimentally implemented. Then, the hybrid test is shown in Figure 2.20(b), which the structural model in Figure 2.20(a) is incorporated in the numerical calculation of its identified damping and stiffness coefficients and measured mass, is performed for the controlled case. Finally, two results from controlled cases are compared for the experimental verification of the hybrid testing method.

The only shear-type structural model without the upper TLCD shown in Figure 2.20(a) has the 0.6m and 1.0m of width and height and 169.7kg of measured floor mass. Two records of El Centro and Kobe earthquake waves

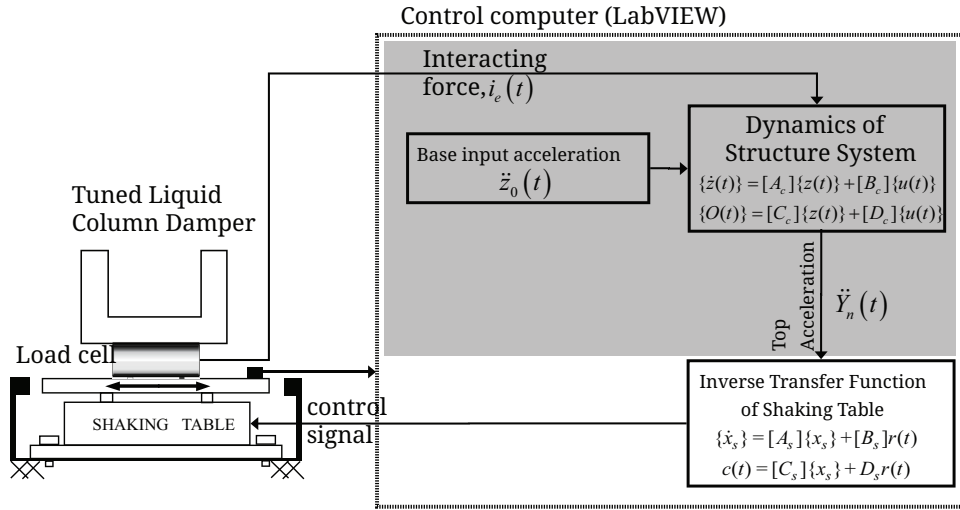
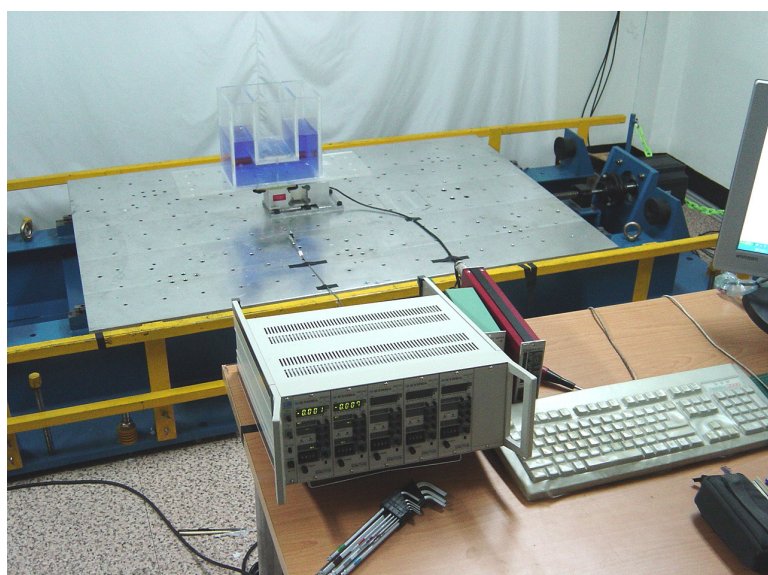


Figure 2.19: Controller for implementing the hybrid testing method

were excited by the shaking table to measure the absolute structural acceleration. The identification was conducted with measured accelerations of the structure model and the shaking table. The identified parameters have slight differences according to input earthquake waves. The averaged damping, and stiffness coefficients were determined by $14.6\text{N}\cdot\text{s}/\text{m}$ and $9914.3\text{N}/\text{m}$, respectively, which correspond to 1.23Hz of structural natural frequency. The level of water in a TLCD tank was adjusted to sympathize the TLCD frequency to this identified structural one.



(a) conventional testing method



(b) hybrid testing method

Figure 2.20: Experimental view of a building with a TLCD

2.5.5 Experimental System for Hybrid Testing of Building with TLMD

The difference between the conventional test method and hybrid testing method is that the upper TLMD is adopted as the experimental part, while the structural model is numerically calculated by a computer in the hybrid testing method, as shown in Figure 2.21. The control force acting between their interfaces is measured with a shear-type load cell which is mounted on the shaking table. Then, the measured force is fed-back to the numerical analysis part. Finally, the shaking table vibrates the upper experimental part with the responses calculated from the numerical analysis part.

In this case, the shaking table is moved by the control signal sent from the control computer through DA channel of DAQ board. The amplitude and phase of the signal values measured at the shaking table, however, are different from the control signal sent from the control computer. In this paper, the inverse transfer function of a shaking table was designed through the definition of the transfer function of a shaking table, as shown in Figure 2.13. Then, a white-noise excitation test of the shaking table is carried out to compensate the dynamic characteristics between the shaking table and control signals, as shown in Figure 2.14.

Figure 2.12 shows the inverse transfer function of the shaking table which was measured by the acceleration signal as an input data and the command signal as an output data. The measured inverse transfer function of the shaking table could be approximated by using a fifth-order linear filter represented by

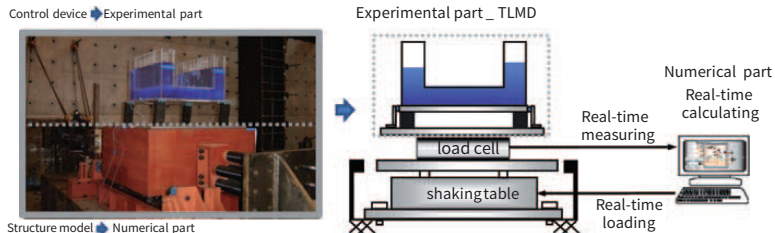


Figure 2.21: Conceptual view of the hybrid testing method of building with TLMD

Experimental setup

The SDOF structure subjected to both the external and control forces is given by

$$m\ddot{x} + c\dot{x} + kx = F(t) - i(t) \quad (2.37)$$

where m , c and k are the mass, damping coefficient and stiffness of the

SDOF structure, respectively. $F(t)$ and $i(t)$ are the excitation force and TLMD control force measured at the load cell, respectively.

The state-space equation and the output equation for the absolute acceleration of the SDOF structural model such as Eq. (2.37) are represented by

$$\dot{\mathbf{z}} = \mathbf{Az} + \mathbf{Bu} \quad (2.38)$$

$$\bar{y}_1 = \mathbf{Cz} + \mathbf{Du} \quad (2.39)$$

where z and u are state variable and input vector, and can be expressed as $\mathbf{z} = [x, \dot{x}]^\top$ and $\mathbf{u} = [i(t), F(t)]^\top$, respectively. \bar{y}_1 is the absolute acceleration of the SDOF structural model, and the matrices \mathbf{A} , \mathbf{B} , \mathbf{C} and \mathbf{D} are follow-up as Eqs. (2.40)-(2.43), respectively.

$$\mathbf{A} = \begin{bmatrix} 0 & 1 \\ -k/m & -c/m \end{bmatrix} \quad (2.40)$$

$$\mathbf{B} = \begin{bmatrix} 0 & 0 \\ -1/m & 1/m \end{bmatrix} \quad (2.41)$$

$$\mathbf{C} = [-k/m \quad -c/m] \quad (2.42)$$

$$\mathbf{D} = [-1/m \quad 1/m] \quad (2.43)$$

Finally, the controller both considering the numerical part of the SDOF structural model and the inverse transfer function of a shaking table is constructed to implement the hybrid testing method as shown in Figure 2.22. Figure 2.23 shows the experimental configuration of the test. The hybrid testing method is fatal to the noise and phase error because the shaking table is vibrated by the numerical part which is calculated in real-time. Accordingly, the hybrid test using the Real-Time Window Target of the MATLAB Simulink with the sampling rate of 1000 Hz was implemented to minimize the calculation and phase error in the actual test. Figure 2.24 is an excitation model of the Real-Time Window Target of the MATLAB Simulink, and it includes the inverse transfer function of the shaking table and numerical analysis of the SDOF structure.

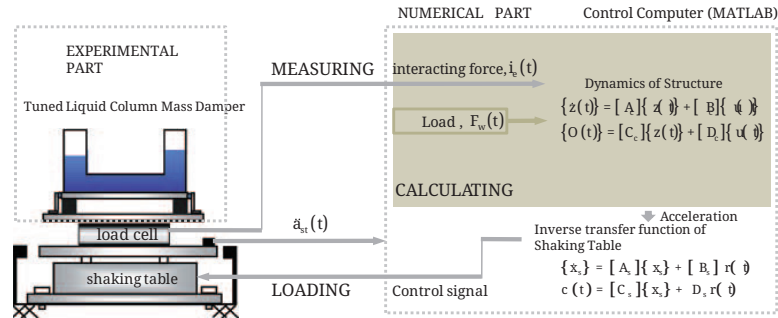


Figure 2.22: Design of the controller for the hybrid testing method

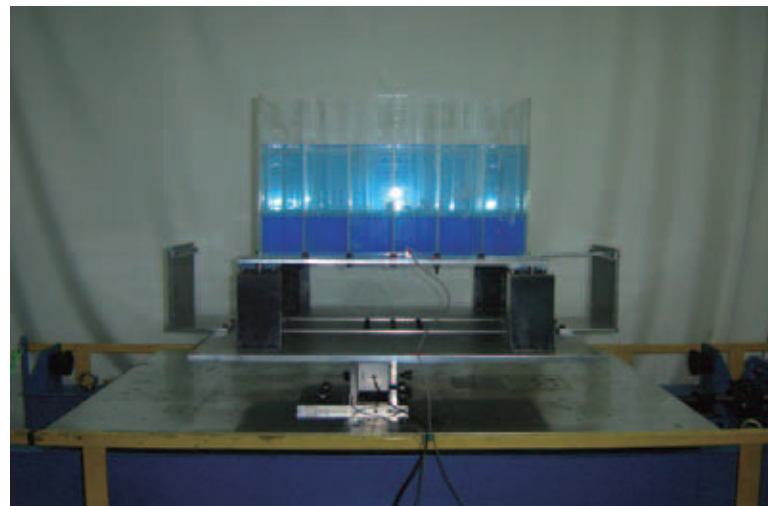


Figure 2.23: Photograph of the hybrid testing

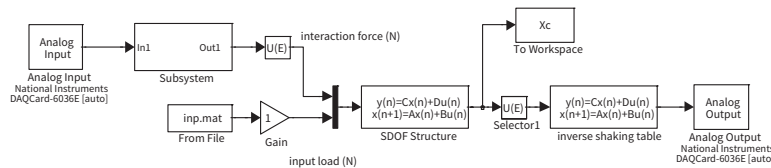


Figure 2.24: Design of the MATLAB Simulink window Target

2.6 Experimental Verification

2.6.1 Experimental result of Substructuring technique

The validity of the proposed substructuring technique as part of hybrid testing method is verified for the experimental setting described in the previous sections. First, the shaking table test without feedback loop of accelerations measured from the experimental substructure into the shaking table controller in Figure 2.6 is performed to experimentally confirm the validity of the proposed method. In this case, the third story acceleration of responses pre-calculated from the assumed whole building with structural parameters such as Eqs. (2.16) and (2.17) is used as a reference signal in Figure 2.15. Figure 2.25 compares the time histories and Fourier transform of the acceleration responses, which are measured from the experimental substructure and shaking table, with those calculated from the numerical analysis of the whole assumed structure. In other words, the responses corresponding to the 3rd, 4th and 5th story accelerations are compared. Also, Figures 2.26-2.28 showing the variation of frequency components according to time lapse illustrate the spectrogram and contour plots of experimental and numerical accelerations of the 3rd, 4th and 5th story, respectively. As can be confirmed from Figure 2.25, the experimental accelerations obtained from the shaking table test without their feedback agree well with those obtained from the analysis of the whole assumed structure in both time and frequency domains. However, it can be observed that the small discrepancies are shown in the time histories of 4th and 5th story accelerations as shown from Figure 2.25, while the 3rd story acceleration is identical to the numerical one over the entire time history as known from Figures 2.25-2.26. These differences are caused by the inherent modes of experimental substructure; the frequency components of 2.5 and 8.6 Hz corresponding to the first and second modes of the experimental substructure, respectively, are observed in the measured acceleration of 4th story as known from Figure 2.27, and also the component of 2.5 Hz is expressed in the 5th story experimental acceleration as like Figure 2.28. It is considered that this tendency is especially conspicuous in the case of utilizing a lightly-damped testing model as an experimental substructure. Table 1 shows the frequency components observed in the time records of an experimental substructure from the test without its acceleration feedback and the natural frequencies calculated from the whole assumed structure with five stories. From Table 2.1, it can be noted that the first natural frequency of the experimental substructure is shifted from 2.5 Hz to 1.3 Hz by the dynamics of the three-story numerical substructure added to its base. Then, the substructuring testing expressed as Figure 2.6 was carried out based on the acceleration feedback of the experimental substructure. Figure 2.29 compares the responses measured by the test with the acceleration feedback of the experimental substructure with those cal-

culated from the numerical analysis of the whole assumed structure with 5 DOFs. Also, Figures 2.30-2.32 express the frequency components according to time lapse, which are observed in the measured responses from the test with feedback and the calculated ones of the 3rd, fourth and fifth story, respectively. As known from Figure 2.29, the inclination in entire time history responses measured from the proposed testing method agrees well with that calculated from the whole assumed structure. These are why the first mode responses of substructured system coincide well with those of the whole assumed system over the entire time range, as shown in Figures 2.30-2.32. However, as can be confirmed from Figures 2.30-2.32, instead of the second and third mode responses of substructured system, those of the experimental substructure are observed from the testing results in the vicinity of 2.5 and 8.6 Hz. It is considered that in the process of the acceleration feedback of the experimental substructure, its fundamental modes affect to the numerical substructure and then the numerical error occurs in calculating the numerical substructure.

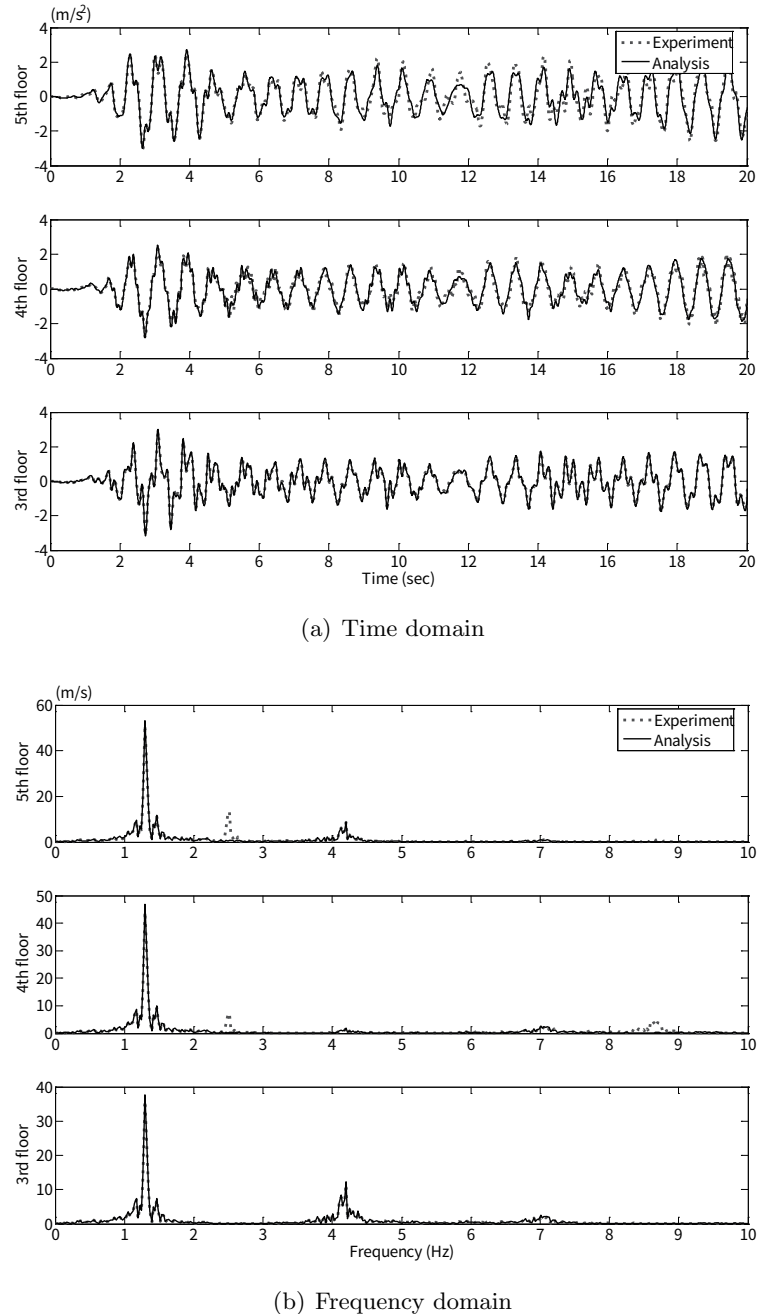


Figure 2.25: Comparisons of results measured from the experiment without feedback and those calculated from numerical analysis.

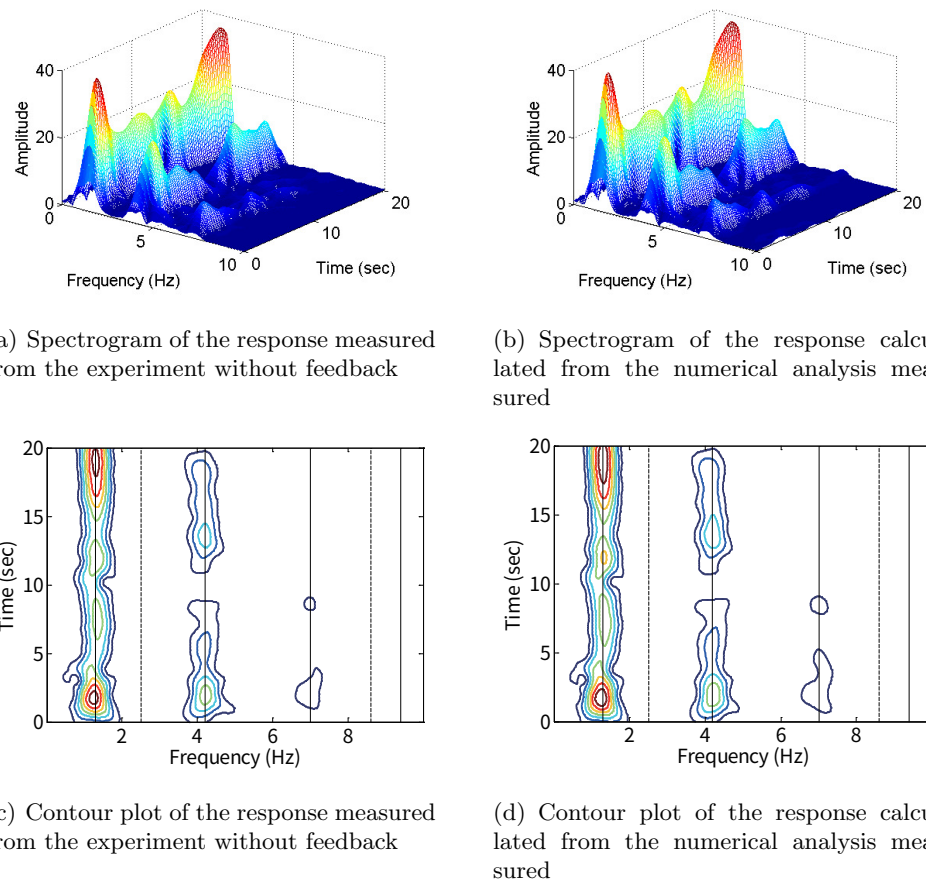


Figure 2.26: Spectrograms and contour plots of the 3rd story acceleration measured from the experiment without feedback and that calculated from the numerical analysis.

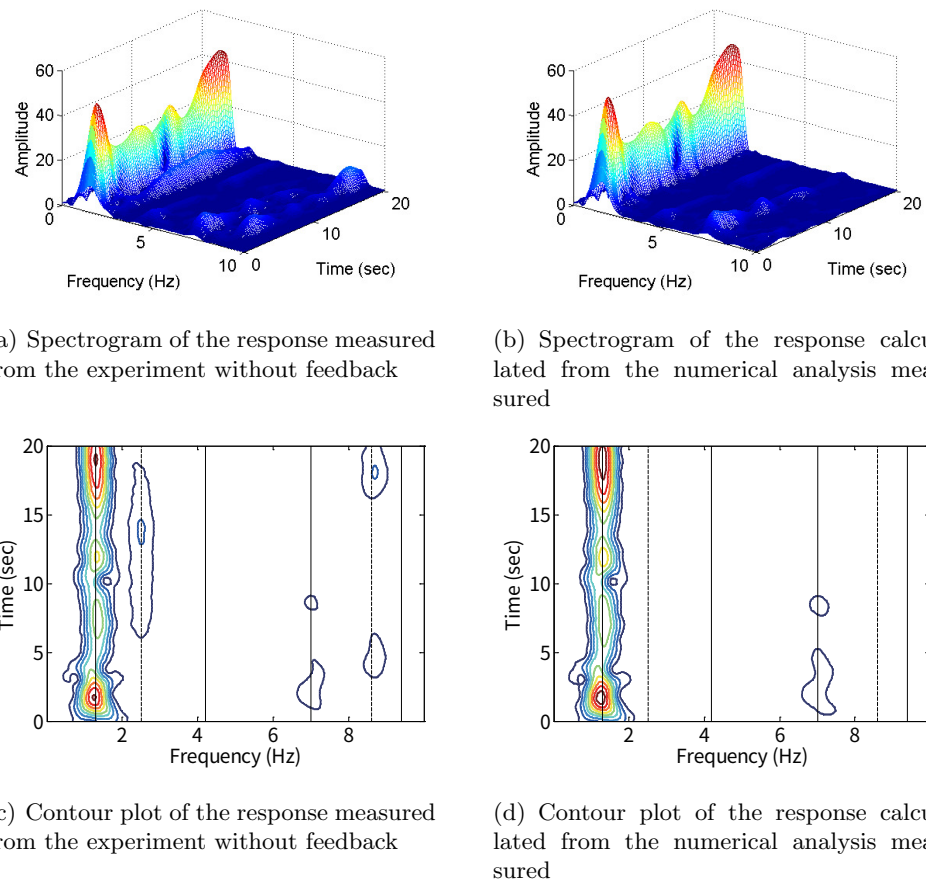


Figure 2.27: Spectrograms and contour plots of the 4th story acceleration measured from the experiment without feedback and that calculated from the numerical analysis.

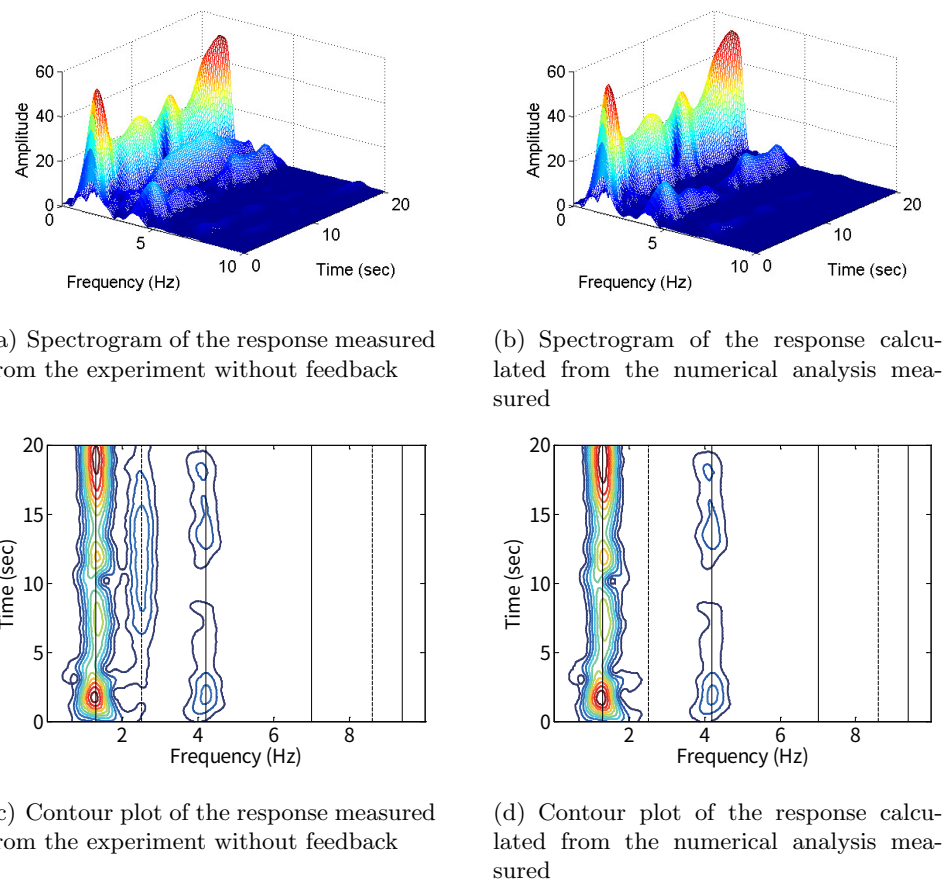


Figure 2.28: Spectrograms and contour plots of the 5th story acceleration measured from the experiment without feedback and that calculated from the numerical analysis.

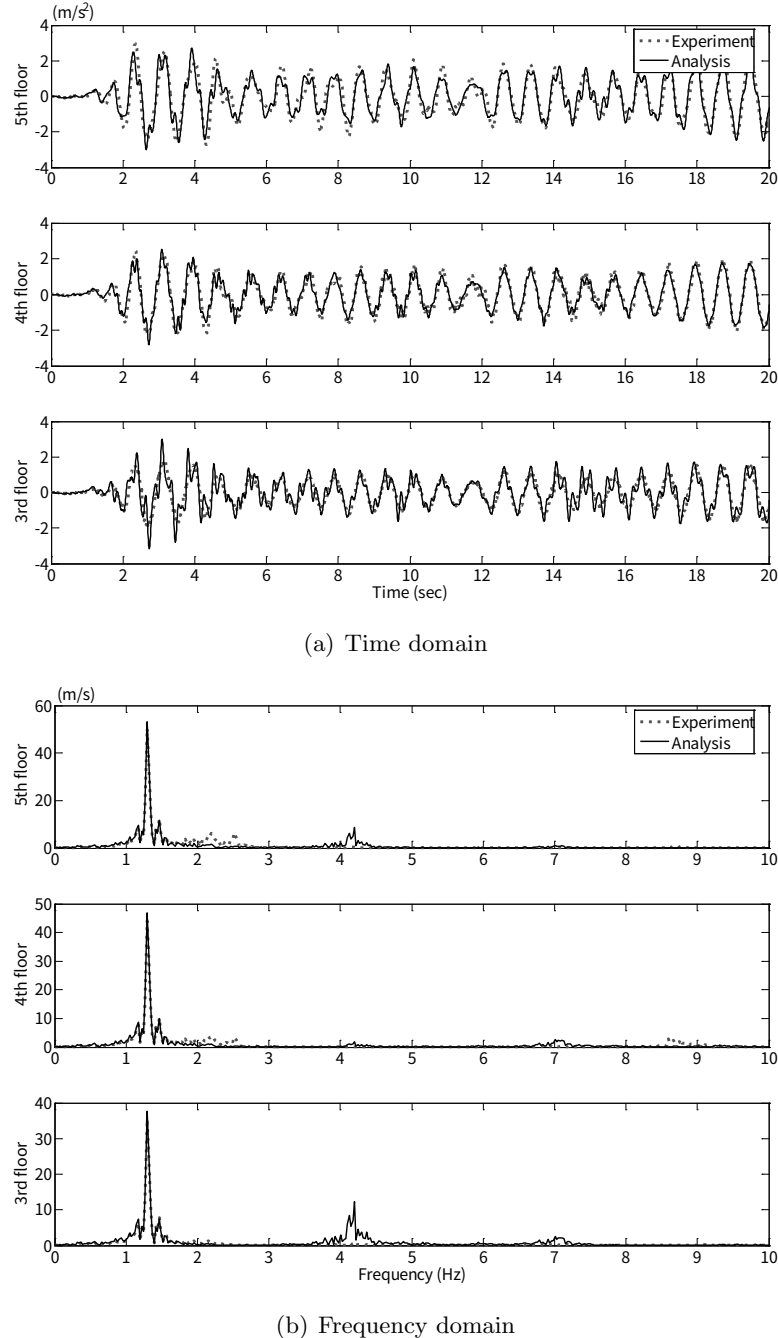


Figure 2.29: Comparisons between results from the experiment with feedback and those from analysis.

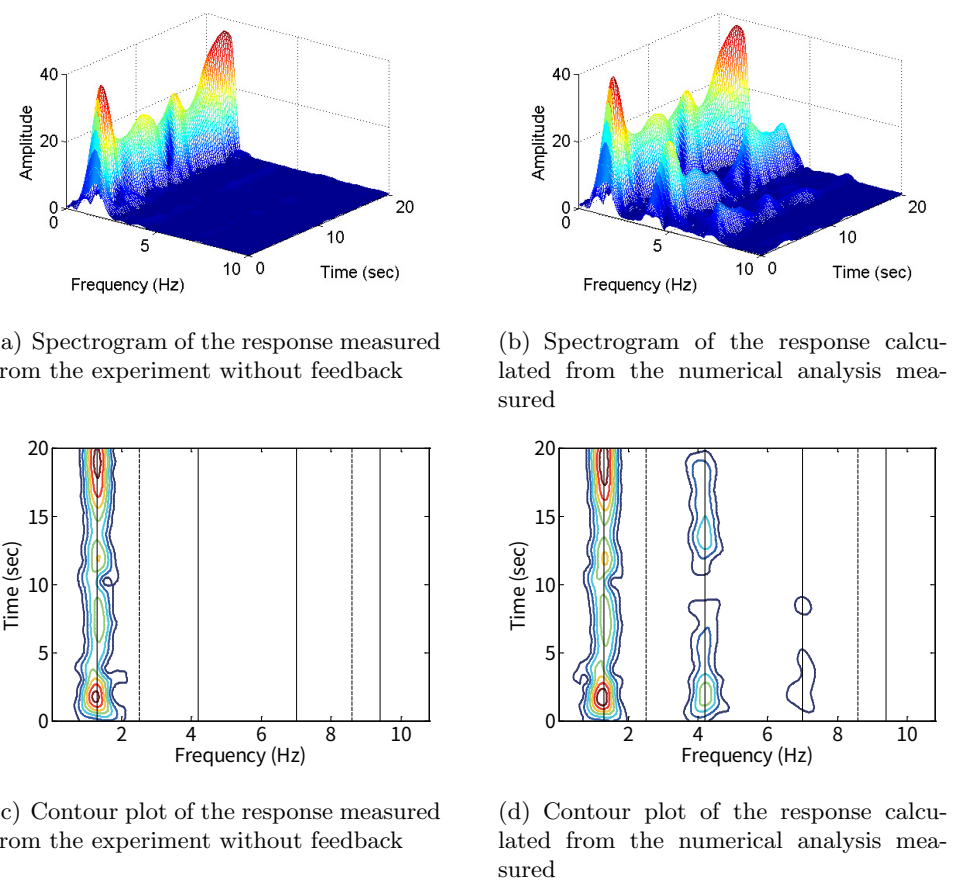


Figure 2.30: Spectrograms and contour plots of the 3rd story acceleration measured from the experiment with feedback and that calculated from the numerical analysis.

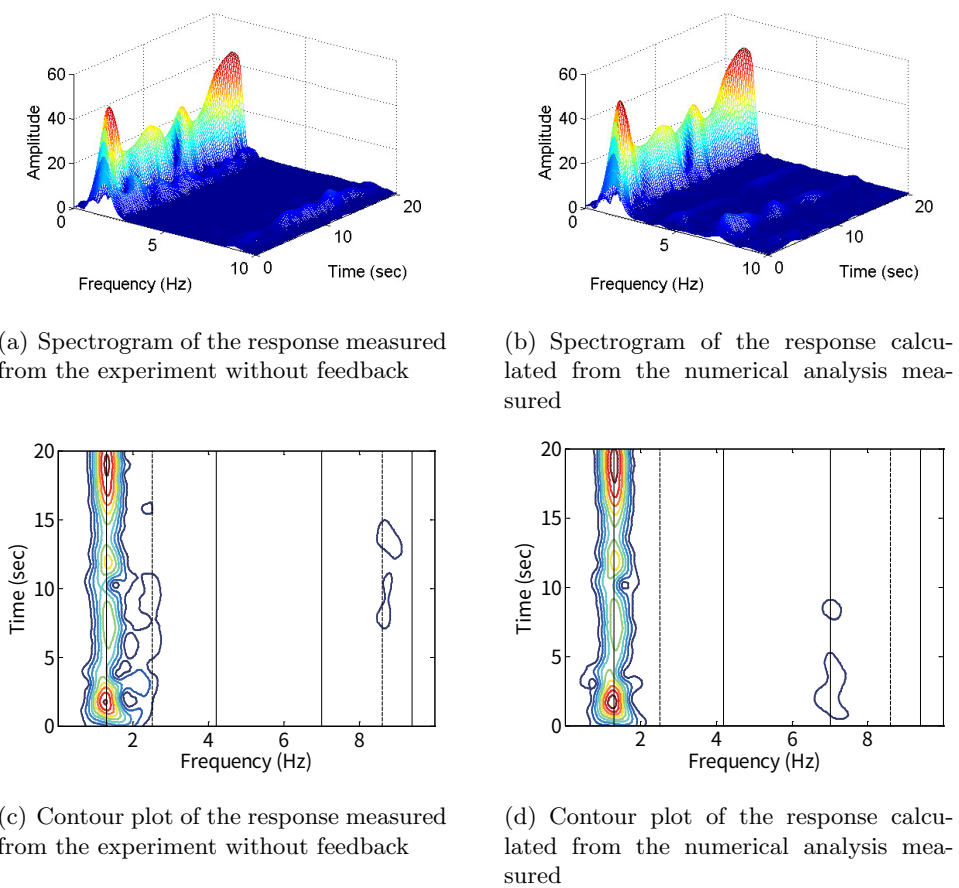


Figure 2.31: Spectrograms and contour plots of the 4th story acceleration measured from the experiment with feedback and that calculated from the numerical analysis.

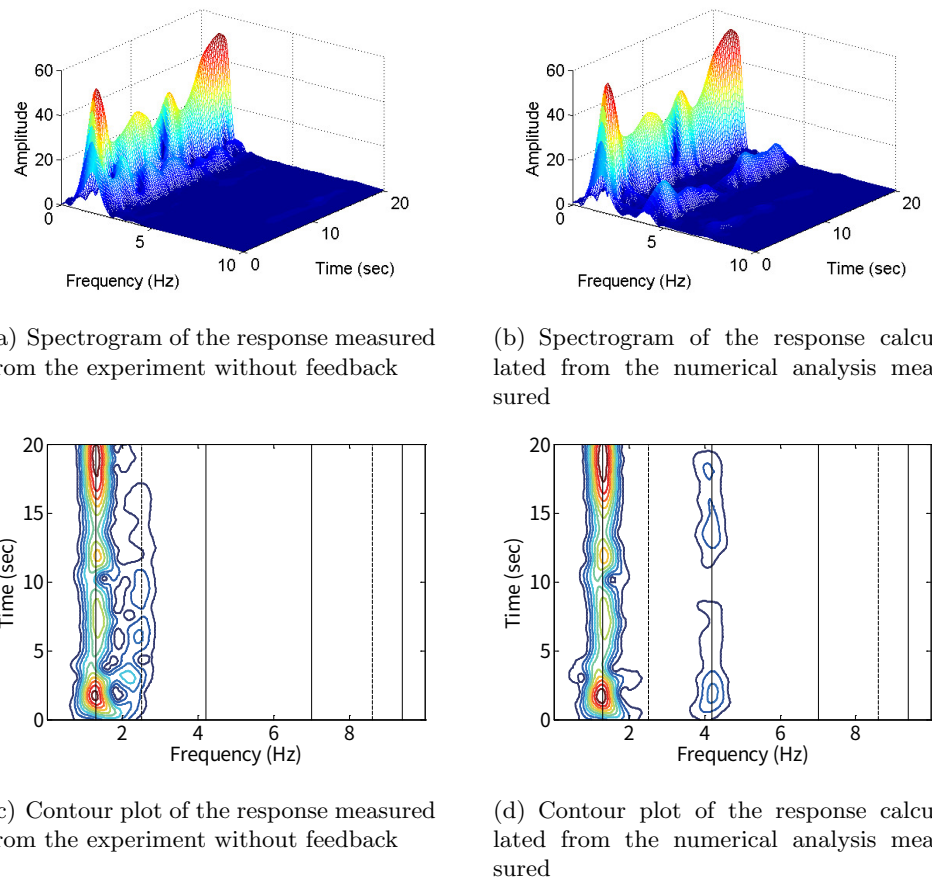
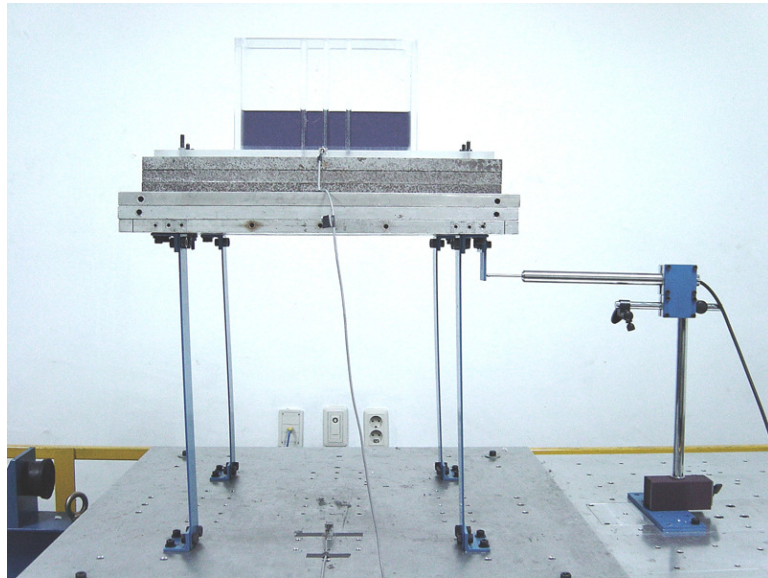


Figure 2.32: Spectrograms and contour plots of the 5th story acceleration measured from the experiment with feedback and that calculated from the numerical analysis.

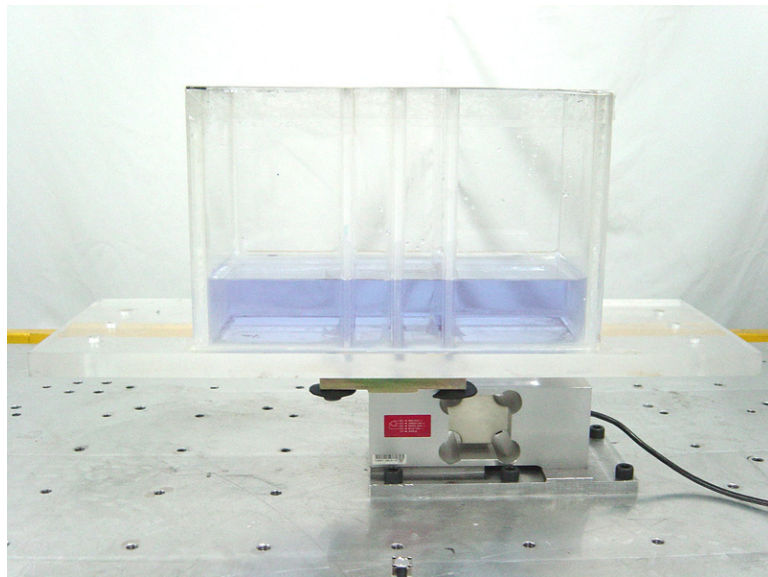
2.6.2 Hybrid Testing Method of a Single Story Structure with a TLD

In this section, experimental verification of the hybrid testing method is conducted for a single story steel frame with a TLD. First, the conventional TLD-structure interaction model shown in Figure 2.33(a) is tested. Then, the hybrid testing method shown in Figure 2.33(b), which incorporates the single story steel frame in the numerical calculation, is performed and the results from the two testing methods are compared to each other. For the numerical structural model used in hybrid testing method, the single story steel frame is assumed to be an SDOF mass-damping-spring system. The structure has $0.6m$ of width, $1.0m$ of height and $169.7kg$ of measured floor mass. El Centro, Hachinohe, Mexico City, and Northridge earthquake waves were realized by the shaking table, and the resulting absolute accelerations of the floor and the shaking table were measured. The system identification was conducted using the measured absolute accelerations. The identified parameters slightly vary according to input earthquake waves. The averaged damping and stiffness coefficients are $14.6N \cdot s/m$ and $9914.3N/m$, respectively, which correspond to $1.23Hz$ of structural natural frequency. The TLD shown in Figure 2.33 has the size of $31(cm) \times 14(cm) \times 20(cm)$. The level of water in the TLD was adjusted to have $3.4cm$ that is theoretically calculated based on the linear wave theory(Soong and Dargush, 1997) for the TLD to have fundamental sloshing frequency tuned to the identified structural natural frequency. As a result, the mass ratio of the TLD to the structure is about 1.3%. To confirm whether the numerically calculated frequency of the TLD is modulated to the structural one, the transfer function is shown in Figure 2.34, from the shaking table acceleration to the shear force by the TLD, was obtained by using the white noise excitation. It is observed in Figure 2.34 that the TLD has the sloshing frequency of $1.25Hz$ which is very close to the structural natural frequency of $1.23Hz$.

At first, the conventional shaking table test is shown in Figure 2.33(a) is performed to investigate the seismic response control performance of the TLD. Previously mentioned four earthquake records are scaled to have the peak acceleration of 100 gals and used to excite the TLD-structure system. Figures 2.35 and 2.36 show the measured structural acceleration responses in the time and frequency domains, respectively. It is observed from Figure 2.35 that acceleration in the latter part of the total response history is significantly reduced. This is a common tendency in the structural response controlled by a tuned mass-type control device since it makes an effect when the structural response is governed by the fundamental mode after initial strong impulse like component has passed. In response to Mexico-city earthquake excitation, as shown in Figure 2.36(c), the first peak corresponding to the major frequency component of the earthquake itself is not controlled, but the response in the region of the TLD modulation frequency is reduced



(a) Conventional shaking table test



(b) Hybrid shaking table test

Figure 2.33: TLD-structure interaction experimental system.

to nearly zero.

Then, the hybrid testing method is applied with the experimental set-up shown in Figure 2.33(b). For its implementation for the controlled case, the identified structural parameters are reflected in the numerical part expressed by the shaded region in the integrated controller shown in Figure 2.18. The

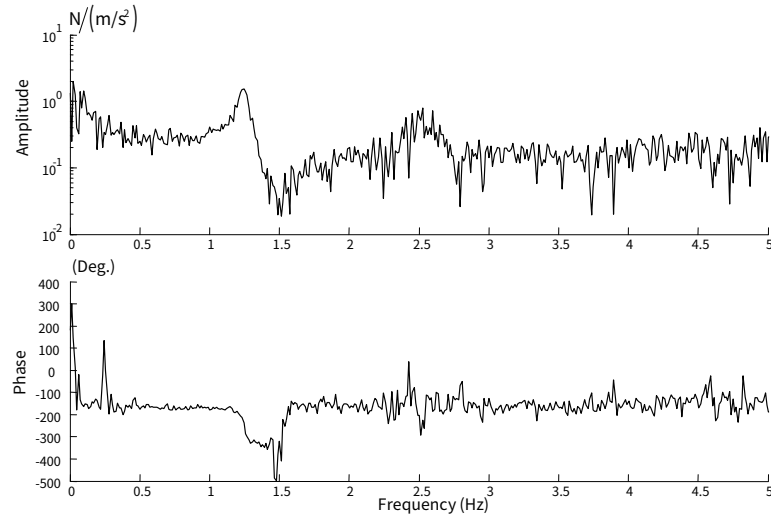


Figure 2.34: TLD transfer function from the table acceleration to the base shear force

continuous filters are converted into discrete ones with a time interval of 0.01 second. Figures 2.37 and 2.38 compare the controlled accelerations obtained by performing the conventional and the hybrid testing method in time and frequency domains, respectively. The effectiveness of the hybrid testing method is verified from the fact that the experimental results from two methods coincide well with each other on the whole. The small discrepancies existing in the controlled responses subjected to El Centro and Hachinohe earthquakes are considered to result from the underestimation of damping coefficients in the numerical structural model since averaged parameters for the four earthquake data were used.

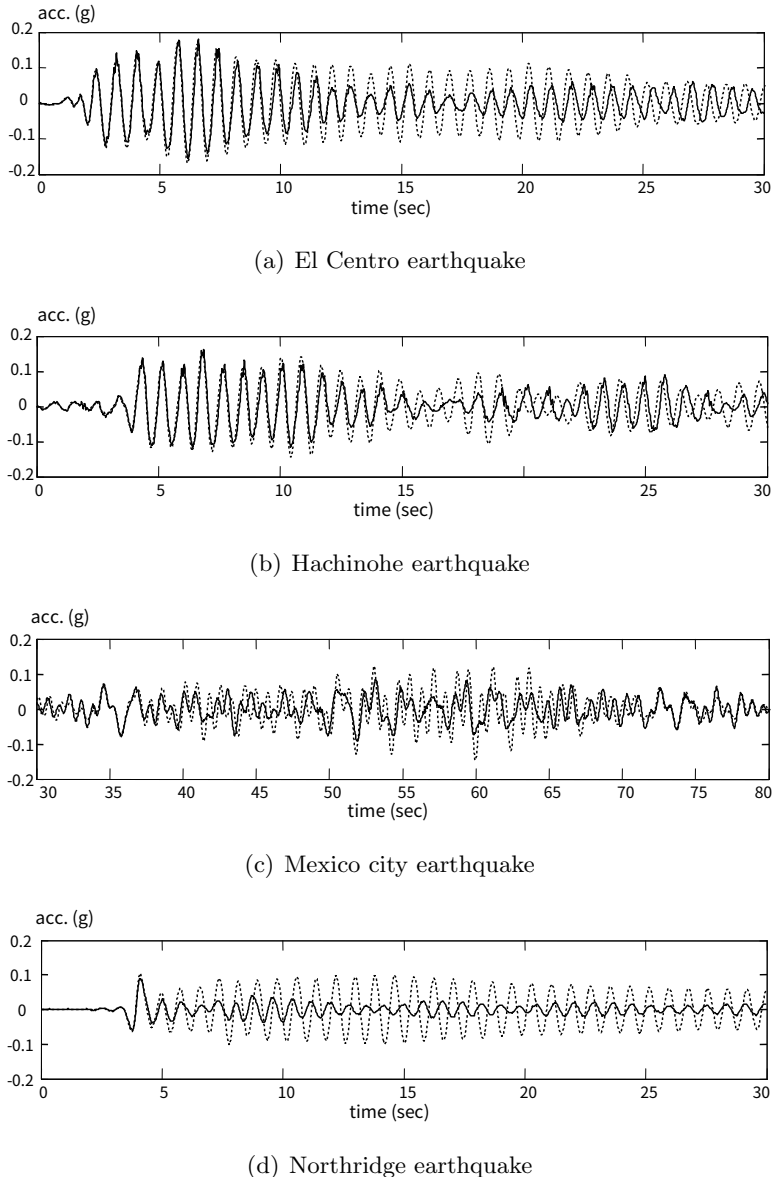


Figure 2.35: Structural acceleration in the time domain measured from the conventional shaking table test of TLD-structure interaction system (dotted line : without control, solid line : with control)

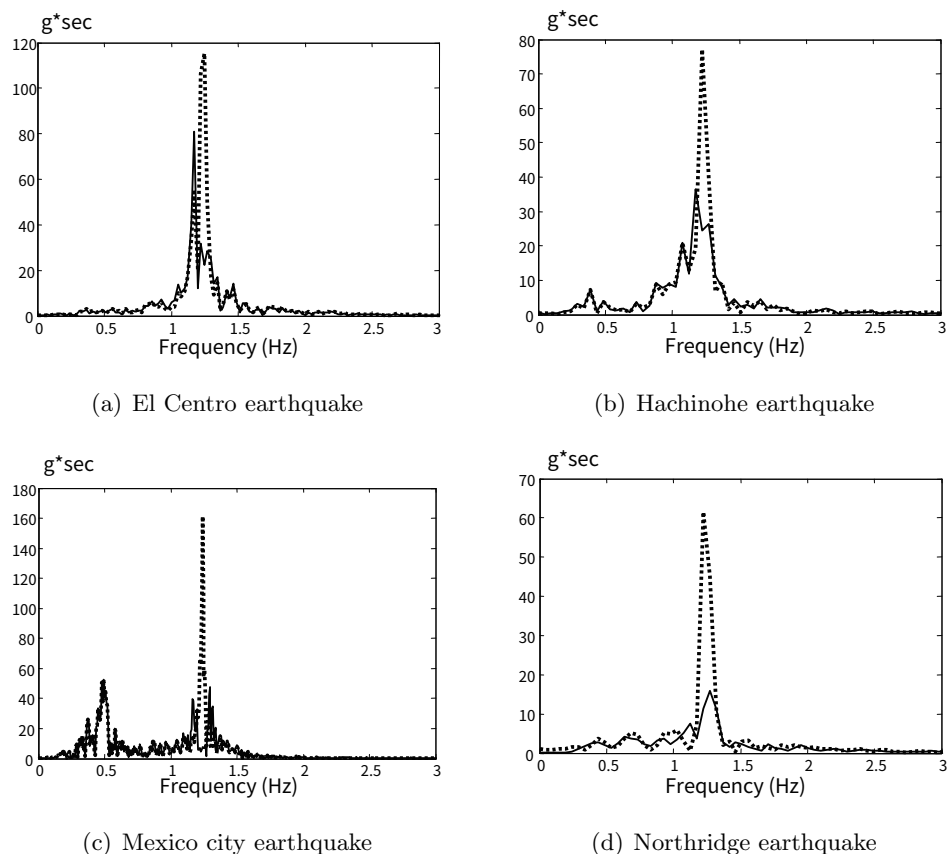


Figure 2.36: Structural acceleration in the frequency domain measured from the conventional shaking table test of TLD-structure interaction system (dotted line : without control, solid line : with control)

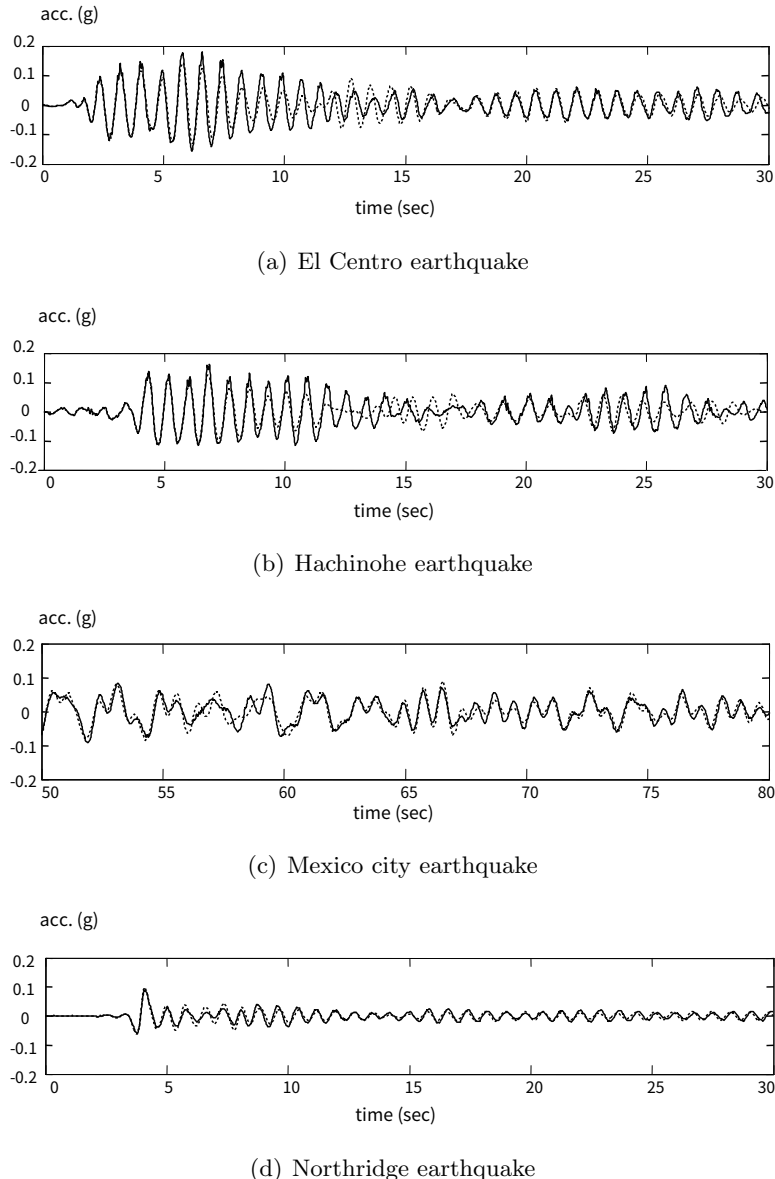


Figure 2.37: Comparisons of controlled structural accelerations in the time domain (dotted line : conventional shaking table test, solid line : hybrid shaking table test)

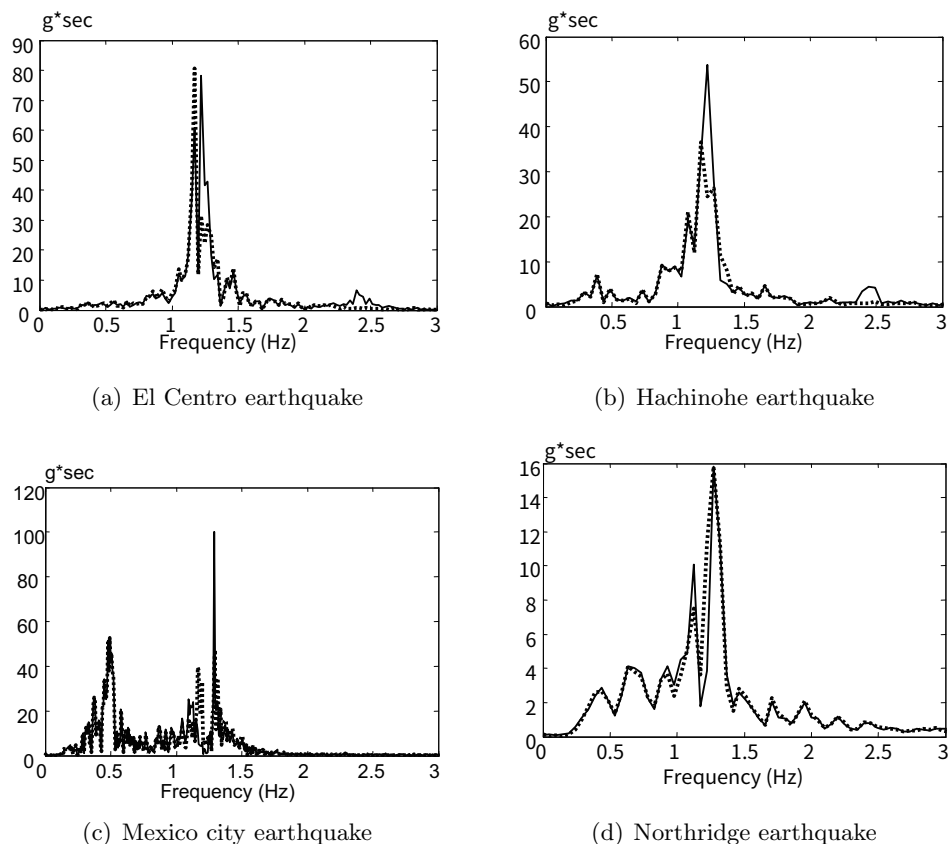


Figure 2.38: Comparisons of controlled structural accelerations in the frequency domain (dotted line : conventional shaking table test, solid line : hybrid shaking table test)

2.6.3 Hybrid Testing Method of Three Story Structure with a TLD

The control performance of a TLD installed in a three-story structure is investigated by using the hybrid testing method. The structure is assumed to be a three story shear-type model, which has identical story properties as follows; $m_i = 128.8kg$, $c_i = 13.52N \cdot s/m$, $k_i = 33908N/m$ for $i = 1, 2, 3$. The structure has natural frequencies of $1.15Hz$, $3.22Hz$ and $4.65Hz$. The TLD discussed in the previous section is used, and its water level is modulated to $4.6cm$ for the TLD to have sloshing frequency of $1.15Hz$. As a result, the mass ratio of the TLD to the structure is about 2% . The four earthquake waves used for the excitation of the single story steel frame were scaled to have peak acceleration of $40gal$. The uncontrolled structural responses were obtained by removing the feedback loop of the TLD-generated interacting force, which causes the numerical structural model to be excited only by the base earthquake motion. Figures 2.39 and 2.40 compare the uncontrolled and controlled accelerations of the third story in time and frequency domains, respectively, which is realized by the shaking table through the hybrid testing method. It is observed that the structural accelerations are significantly reduced by the TLD, especially in the region of the fundamental frequency. Table 2.5 indicates that the acceleration is reduced by $4 - 30\%$ in peak and by $18 - 60\%$ in RMS responses. It is also identified in Figure 2.40(d) that the TLD lessens the additional second mode response of the structure. Figure 2.41 shows the typical sloshing and slamming behaviors of the water in the TLD tanks during the experiment, which occur in the small and large amplitude of the water motion, respectively(Yalla, 2001).

Table 2.5: Uncontrolled and controlled responses of a combined TLD–MDOF structure system

Responses(g)	El Centro	Hachinohe	Mexico City	Northridge
<i>Peak acceleration</i>				
Uncontrolled	3.85	2.71	2.63	1.34
Controlled	2.69	2.19	252	1.34
<i>RMS acceleration</i>				
Uncontrolled	1.91	1.36	0.54	0.33
Controlled	0.74	0.66	0.45	0.27

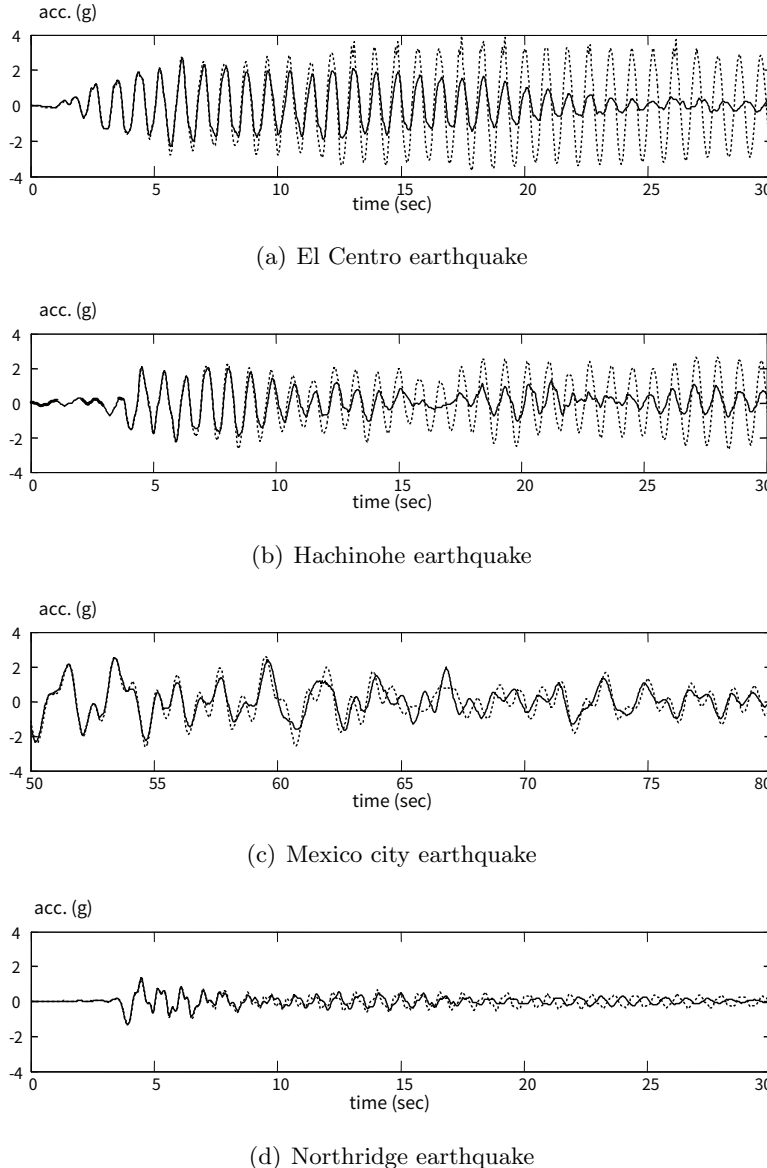


Figure 2.39: Absolute accelerations in the time domain, measured from the top story of MDOF structure with a TLD by the hybrid testing method (dotted line : without control, solid line : with control))

2.6.4 Hybrid Testing Method of a Single Story Structure with a TLCD

At first, the conventional shaking table test with this TLCD shown in Figure 2.20(a) is performed to reduce the structural response. Two earthquake records with the maximum acceleration of 100gal due to the shaking table

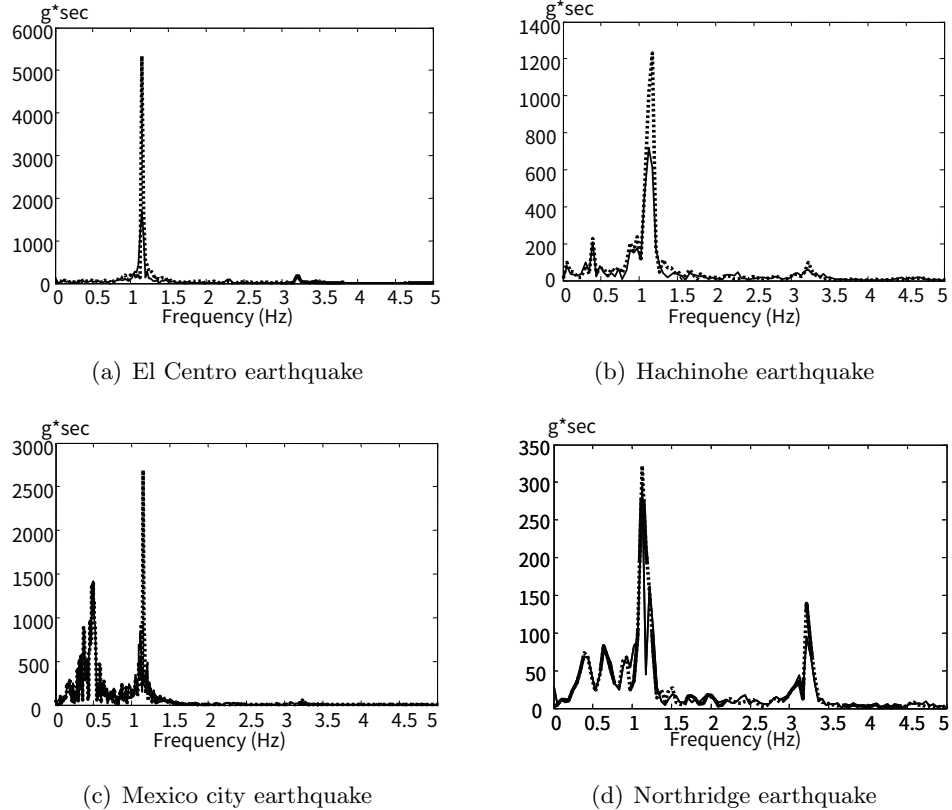


Figure 2.40: Absolute accelerations in the frequency domain, measured from the top story of MDOF structure with a TLD by the hybrid testing method (dotted line : without control, solid line : with control)

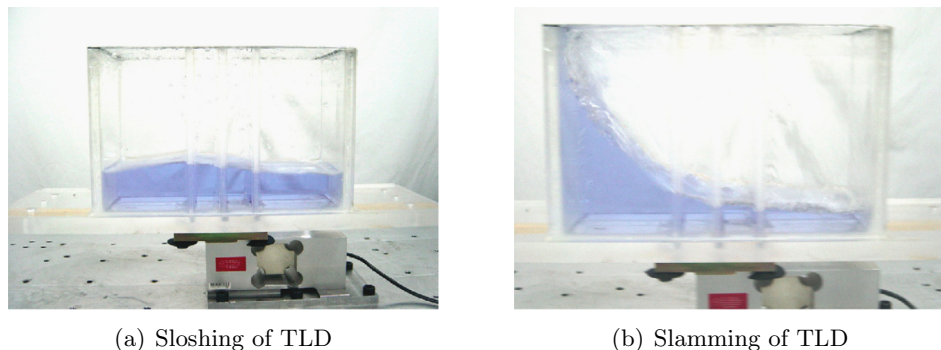


Figure 2.41: Behaviors of a TLD under the earthquake motion

performance are used to excite the TLCD-structure system with control case. Then, the hybrid shaking table test is conducted with the experimental set-up shown in Figure 2.20(b). For its experimental implementation, the iden-

tified structural parameters are reflected in the numerical part expressed by the shaded region in the integrated controller shown in Figure 2.19. The continuous filters in the figure are converted into discrete ones with a time step of 0.01 sec in the actual implementation of the experiment. Figure 2.42 compare the controlled accelerations experimentally measured by implementing the conventional and the hybrid testing method in both time and frequency domain, respectively. The validity of the hybrid testing method performed in this paper is verified from the fact that the experimental results from two methods well coincide with each other on the whole.

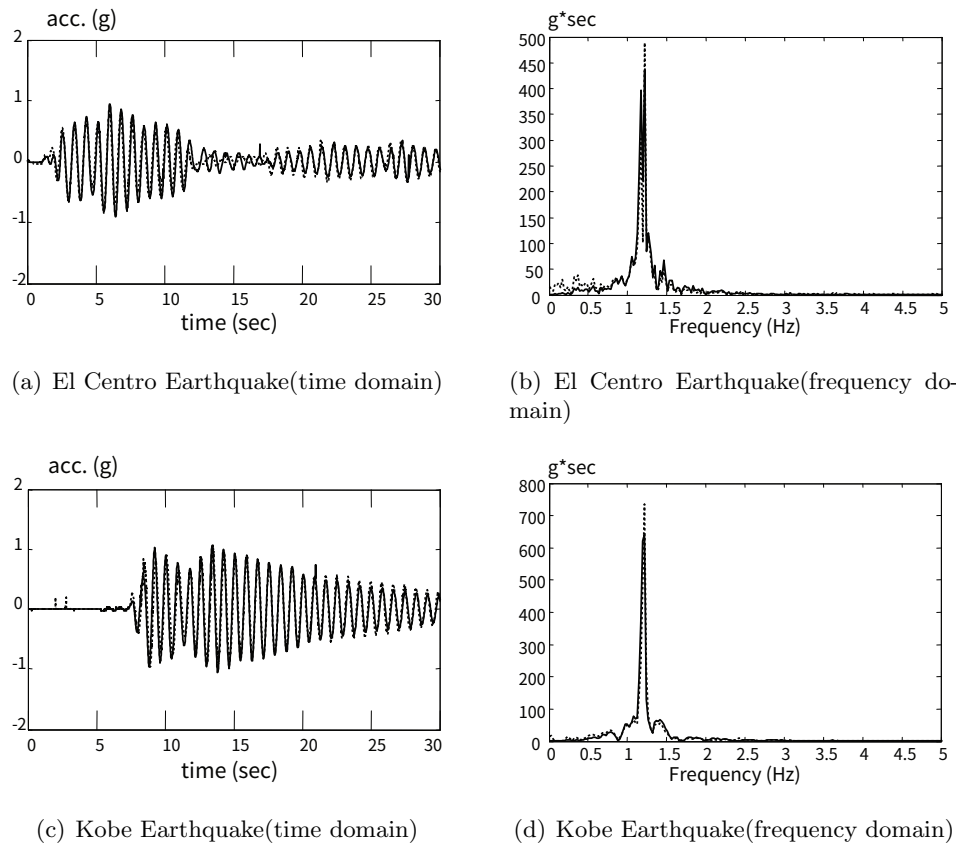


Figure 2.42: Comparisons between the results from the conventional testing method(dotted line) and those from the hybrid testing method(solid line) for the controlled response

2.6.5 Conventional Experiment of a Building Controlled by TLMD

Experimental installation

The test on a scaled-down TLMD building model shown in Figure 2.44 was performed to experimentally verify the control performance of a proposed TLMD.

In order to experimentally describe the dynamic behavior of a building model, the moving mass of 4250kg was mounted on guide rails. Also, the springs that connect the moving mass to both the actuator and the retaining block were devised to characterize the behavior of the stiffness of a building model, as shown in Figure 2.45. In the figure, m_s , c_s and $k_1 + k_2 = k_s$ represent the mass, damping coefficient and stiffness of a building model, respectively. x_1 , x_2 and x_3 denote the displacement and acceleration of a building model, dynamic actuator and TLMD, respectively. Ten springs with the stiffness of $11,000\text{N/m}$ for each one were used for the case of a test in the TMD control direction, and eight springs with 8800N/m for each one for the case of a test in the TLCD control direction.

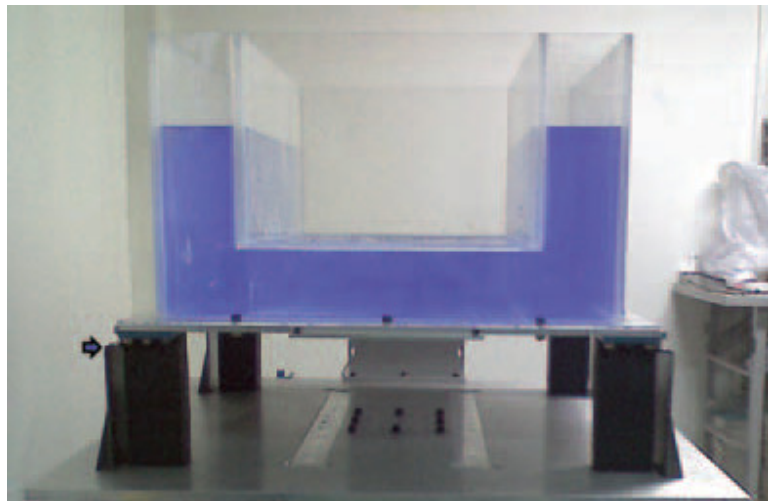


Figure 2.43: Photograph of the manufactured TLMD

It is noted from Figure 2.46 that the mass of a building model is excited by the force transmitted by the spring, k_2 , through the displacement of an actuator, x_2 . Accordingly, the motion of a building model is expressed by

$$m_s \ddot{x}_1 + c_s \dot{x}_1 + k_1 x_1 - k_2 (x_2 - x_1) = 0 \quad (2.44)$$

In this case, the displacement of an actuator, x_2 , is given by

$$x_2 = A \sin (2\pi f_e t) \quad (2.45)$$

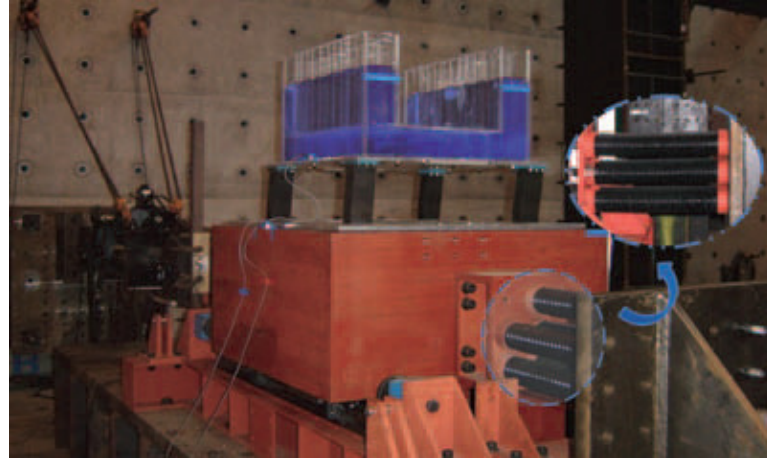


Figure 2.44: Experimental TLMD-building model

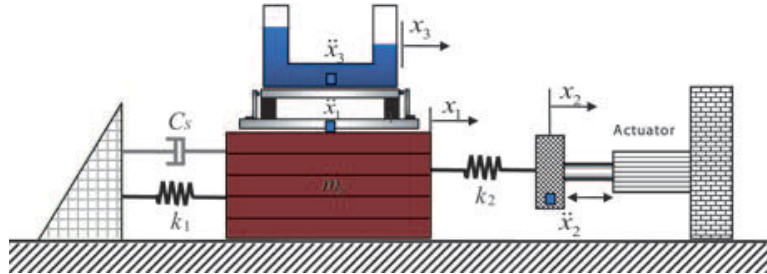


Figure 2.45: Conceptual view of experimental set-up

where A and f_e are the excitation amplitude and frequency of an actuator, respectively.

Finally, the equation of motion of a building model is obtained by substituting Eq. (2.45) into Eq. (2.44).

$$m_s \ddot{x}_1 + c_s \dot{x}_1 + k_s x_1 = k_2 A \sin(2\pi f_e t) \quad (2.46)$$

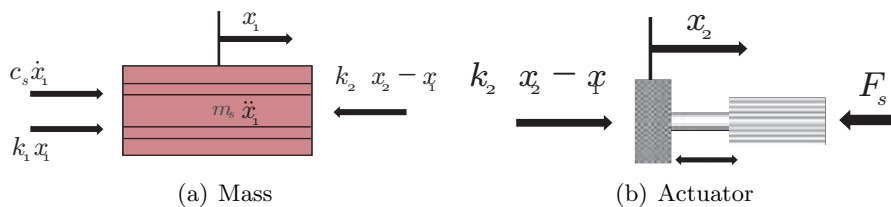


Figure 2.46: Free-body diagram of a building model.

2.6.6 Experimental results

In this test, the building model was excited by a dynamic actuator installed on the strong wall. Maximum excitation displacement of the dynamic actuator was set to be 4 mm. Harmonic waves with the frequency interval of 0.05 Hz from 0.1 to 3.0 Hz were imposed on the moving mass of a building model by the actuator. Especially, harmonic waves with the frequency interval of 0.01 Hz were excited to the moving mass in the vicinity of its natural frequencies during 200s. Then, the steady-state response of the moving mass was obtained in each excitation frequency.

First, the test was performed in the TMD control direction. In this case, the frequency of structural model was set to 0.82 Hz by connecting springs with the stiffness of 110,000 N/m to the structural model with the mass of 4,250 kg. Figures 2.47 and 2.48 show the displacement and acceleration response of the SDOF structure in the frequency domain, respectively. It is verified that the displacement response of the SDOF structure was reduced by 82% for the case in the TMD control direction. The displacement control performance index of a TMD is 0.18, as shown in Figure 2.47. Also, the acceleration response of the SDOF structure was reduced by 80%, and the acceleration control performance index of a TMD is 0.20, as shown in Figure 2.48. Figures 2.47 and 2.50 show the displacement and acceleration response of the SDOF structure in the time domain, respectively. Also, the response of the SDOF structure tuned by the TMD is considerably reduced at a resonance frequency of 0.82 Hz, as shown in Figure 2.49.

Then, the test was carried out in the TLCD control direction. In this case, the frequency of structural model was tuned to 0.73 Hz by connecting springs with the stiffness of 88,000 N/m to the moving mass of 4,250 kg. Figures 2.50 and 2.51 show the displacement and acceleration response of the SDOF structure in the frequency domain, respectively. It is observed that the displacement response of the SDOF structure was reduced by 71% for the case in the TLCD control direction. The displacement control performance index of a TLCD is 0.29, as shown in Figure 2.50. Also, the acceleration response of the SDOF structure was reduced by 70%, and the acceleration control performance index of a TLCD is 0.30, as shown in Figure 2.51. Also, the displacement response of the SDOF structure tuned by TLCD is considerably reduced at a resonance frequency of 0.73 Hz, respectively, as shown in Figure 2.52.

2.6.7 Hybrid Testing Method of a Single Story Building Controlled by TLMD

A TLMD is excited by uniaxial shaking table. Shear type load cell and acceleration sensors are attached on the shaking table to monitor the dynamic characteristic of the shaking table. The vibration control and data

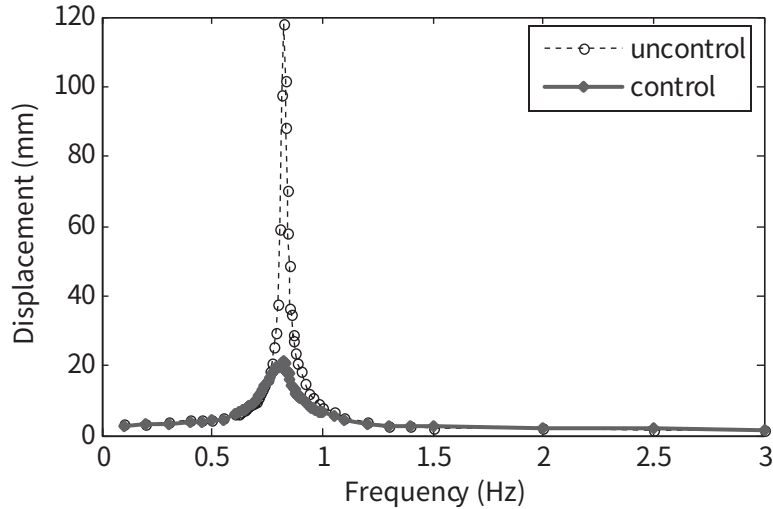


Figure 2.47: Displacement in the frequency domain (TMD direction)

acquisition are conducted using a real-time digital signal processor. The main task of the data acquisition board is data conversion; it converts the measured shear force and acceleration to the digital data and converts the reference signal computed by the control program MATLAB to the analog data. An eight-channel data acquisition system was adopted which uses an NI DAQcard-6036E board and a BNC-2110 BNC cable connector. At the hybrid testing method, the control performance results of the TLMD were evaluated. In this test, the checking point is whether the natural frequencies of the TLMD in the TMD and TLCD control direction were seen at 0.82 and 0.73 Hz, respectively. Then, control performance of the bidirectional TLMD will be evaluated.

First, the test was performed in the TMD control direction. Figures 2.53 and 2.54 show the displacement and acceleration response in the frequency domain, respectively. It is observed that the displacement response of the shaking table was reduced by 78% for the case in the TMD control direction. The displacement control performance index of a TMD is 0.22, as shown in Figure 2.53. Also, the acceleration response of the shaking table was reduced by 78%, as shown in Figure 2.54. Figure 2.55 shows the displacement in the time domain. The response of the shaking table is considerably reduced by 78% at a resonance frequency of 0.82 Hz.

Then, the test was performed in the TLCD control direction. Figures 2.56 and 2.57 show the displacement and acceleration response of the shaking table in the frequency domain, respectively. It is observed that the displacement response was reduced by 71% for the case in the TLCD control direction, and the acceleration response reduced by 70%. Also, the displacement and acceleration response of the shaking table are considerably reduced at

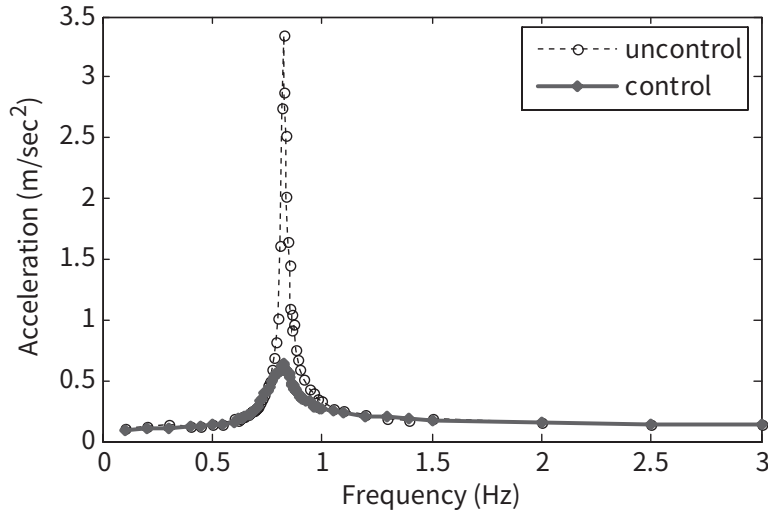


Figure 2.48: Acceleration in the frequency domain (TMD direction)

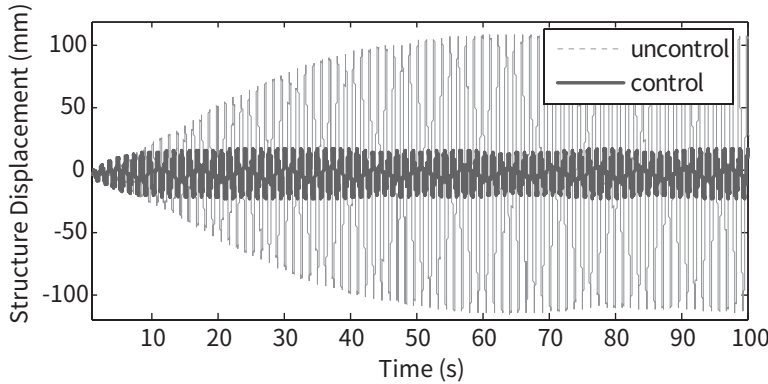


Figure 2.49: Displacement in the time domain (TMD direction, 0.82 Hz)

a resonance frequency of 0.73 Hz, respectively, as shown in Figure 2.58.

Comparisons of conventional experiment and hybrid testing method results

In order to compare the control performances of the TLMD at the hybrid testing method and conventional method, J_1 , J_2 , J_3 , J_4 , are represented by

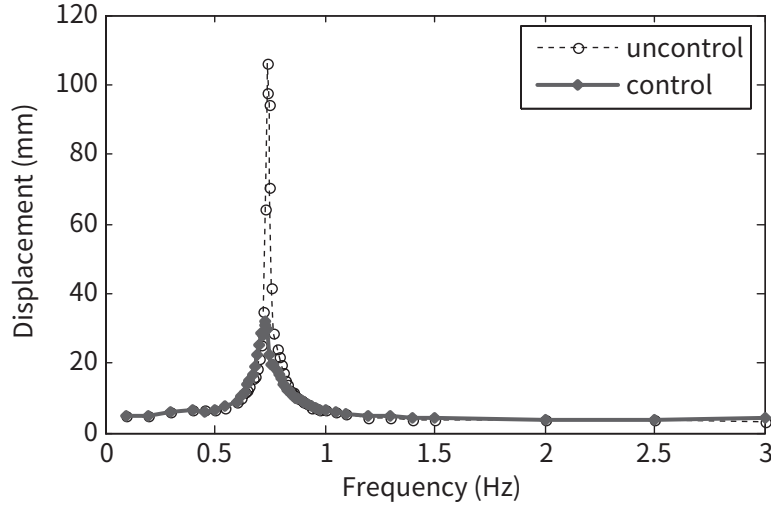


Figure 2.50: Displacement in the frequency domain (TLCD direction)

$$J_1 = \frac{\max [x_c(t)]}{\max [x_u(t)]} \quad (2.47)$$

$$J_2 = \frac{\max [\ddot{x}_c(t)]}{\max [\ddot{x}_u(t)]} \quad (2.48)$$

$$J_3 = \frac{\text{rms} [x_c(t)]}{\text{rms} [x_u(t)]} \quad (2.49)$$

$$J_4 = \frac{\text{rms} [\ddot{x}_c(t)]}{\text{rms} [\ddot{x}_u(t)]} \quad (2.50)$$

where x_u and x_c are uncontrolled displacement and controlled displacement, respectively. \ddot{x}_u and \ddot{x}_c are uncontrolled acceleration and controlled acceleration, respectively.

Tables 2.6 and 2.7 show the control performance of the TLMD through the conventional test and hybrid test, respectively. According to the test result in the TLCD control direction, the errors of J_1 or J_2 between the results of the conventional test and hybrid test were all 0.01, but the errors of J_3 or J_4 between the conventional test and hybrid test were 0.03 and 0.04, respectively. In the TMD control direction, the errors of J_1 , J_2 , J_3 , J_4 between the conventional test and hybrid test were 0.04, 0.02, 0.06, 0.06, respectively.

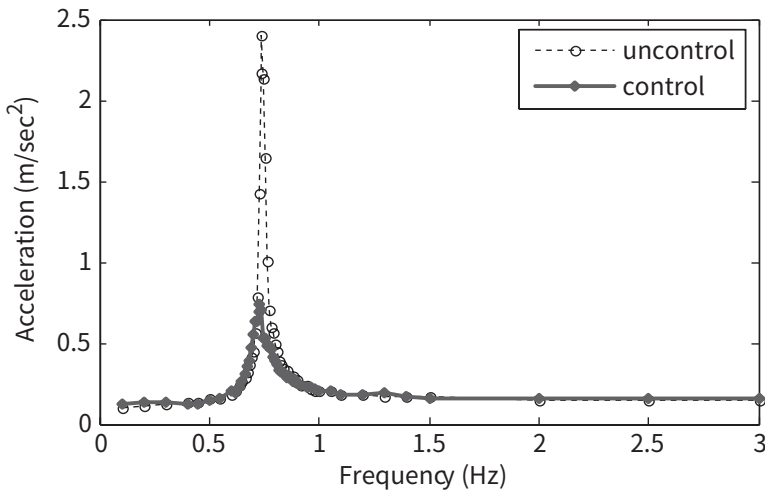


Figure 2.51: Acceleration in the frequency domain (TLCD direction)

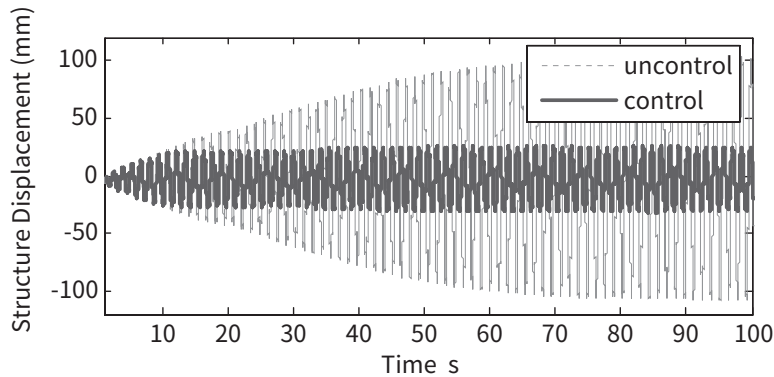


Figure 2.52: Displacement in the time domain (TMD direction, 0 - 73 Hz)

Table 2.6: Control performance of real-structure test

		TMD	TLCD
Effective mass		1.8%	0.8%
Peak value	J_1	0.18	0.29
	J_2	0.20	0.30
RMS value	J_3	0.17	0.28
	J_4	0.17	0.27

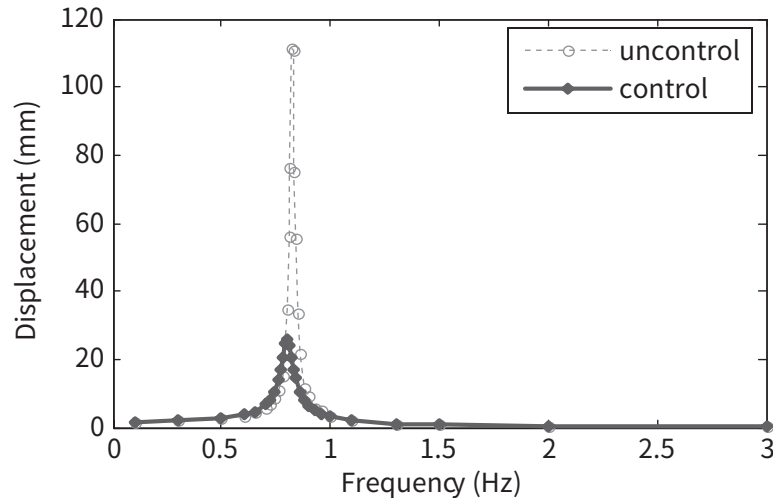


Figure 2.53: Displacement in the frequency domain by the hybrid test (TMD direction)

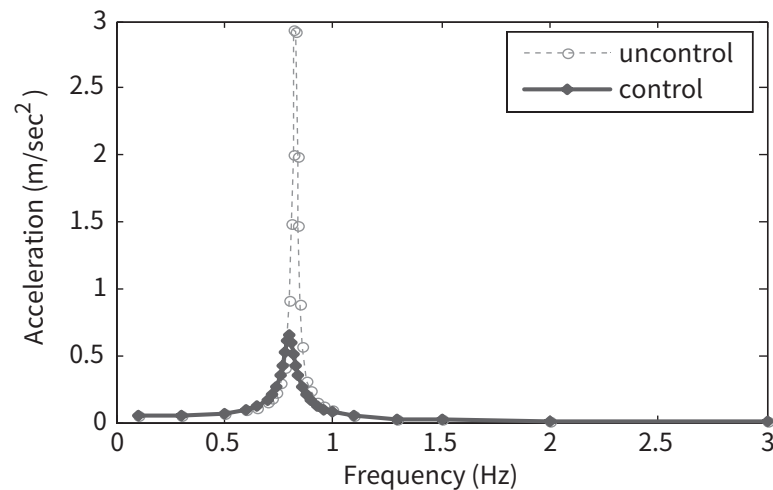


Figure 2.54: Acceleration in the frequency domain by the hybrid test (TMD direction)

Table 2.7: Control performance of hybrid testing method

		TMD	TLCD
Effective mass		1.8%	0.8%
Peak value	J_1	0.22	0.30
	J_2	0.22	0.29
RMS value	J_3	0.23	0.31
	J_4	0.23	0.31

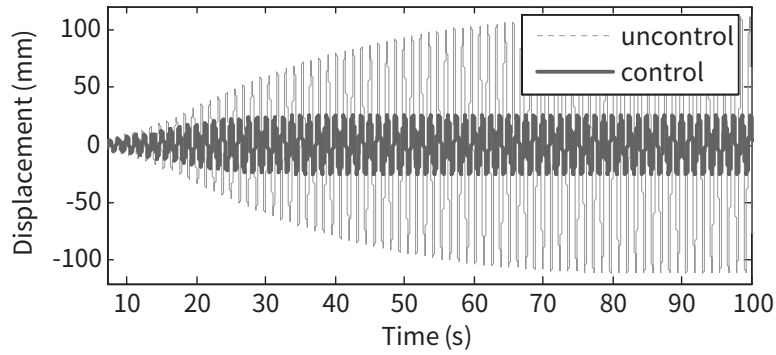


Figure 2.55: Displacement in the time domain by the hybrid test (TMD direction, 0.83 Hz)

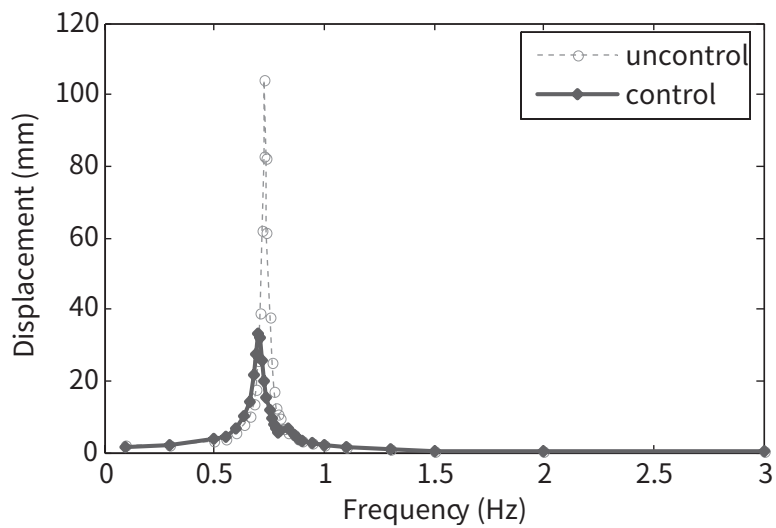


Figure 2.56: Displacement in the frequency domain by the hybrid test (TLCD direction)

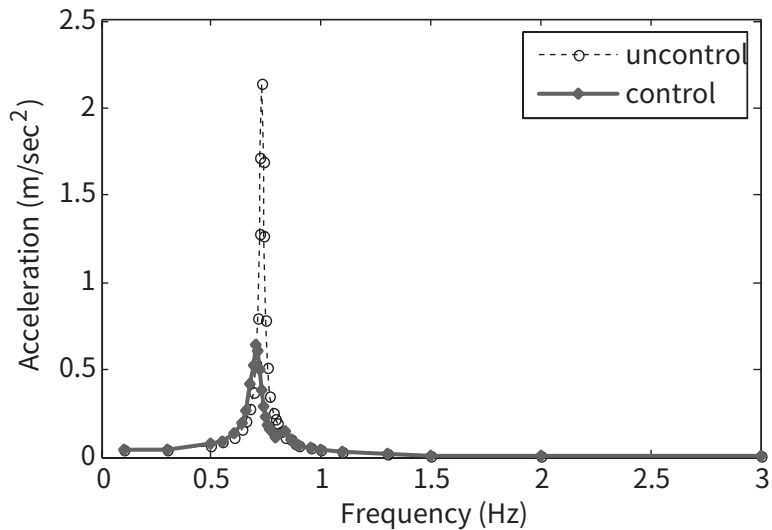


Figure 2.57: Acceleration in the frequency domain by the hybrid test (TLCD direction)

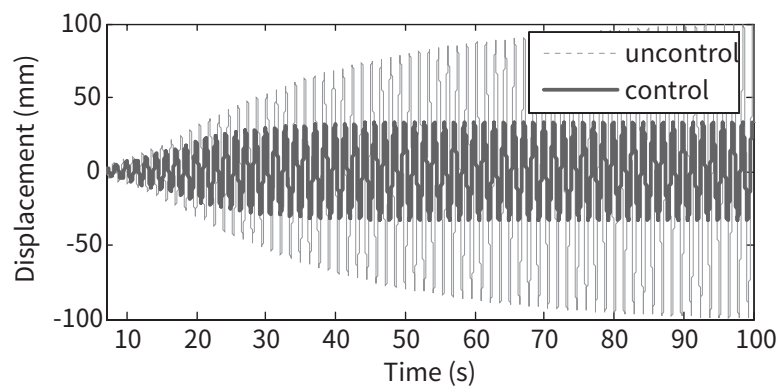


Figure 2.58: Displacement in the time domain by the hybrid test (TLCD direction, 0.73 Hz)

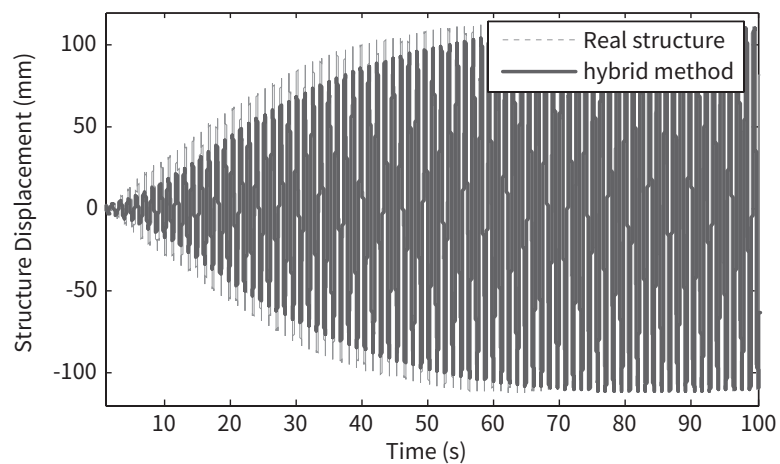


Figure 2.59: Uncontrolled displacement comparison in the time domain between the real-structure test and hybrid testing method (TMD direction)

2.7 Summary

In this chapter, a substructuring technique as part of hybrid testing method for the shaking table test was proposed. The proposed substructuring technique adopts the upper part of the whole structure as the experimental substructure, which corresponds to a physical test model. The lower part is modeled numerically. In order to verify the validity and accuracy of the proposed technique, a shaking table test was conducted. The result of the study can be summarized as follows.

1. To reduce the distortion of the interface acceleration, the inverse transfer function of the shaking table was identified and its state space realization was implemented in the shaking table controller.
2. In this paper, the linear transfer function approach for controlling the motion of a shaking table was considered to experimentally verify the proposed method for a linear experimental part. However, this approach would be inappropriate for a coupled non-linear system leading to experimental instability. Therefore, in such case the controller using the inverse transfer function of shaking table, shown in Figure 2.6, would be modified to compensate an experimental instability.
3. The interface force between the experimental and numerical substructures was obtained using only acceleration measurement and mass information, so that high-capacity loads cell and installation jigs are not required in the experiment.
4. The proposed method basing the interface force measurement on acceleration measurements from an experimental substructure is partially available only when the mass distribution is discrete - for example this would be applicable to the TMD as an experimental part. Also, the interface force measurement using force transducers is required to perform the proposed method when wind forces are applied to the experimental substructure.
5. Experimental results demonstrate that the proposed substructuring technique can reproduce the dynamic behavior of the assumed whole structure.
6. Unexpected vibration of the experimental substructure can be induced by the feedback of responses including its inherent natural modes and then by the error occurred in calculating the numerical substructure.
7. It is considered that to minimize the effect of natural modes of an experimental substructure on the substructured system, the structural model as heavily-damped as possible would be used as an experimental part.

8. The proposed technique can be extended to the substructuring technique with the middle part of a whole structure in combination with the conventional substructuring technique employing lower part as the experimental substructure.

The TLD installed at the top floor of the structure is physically tested, and simultaneously numerical calculation is carried out for the assumed analytical structural model. Comparison between the structural responses obtained by the hybrid testing method and the conventional shaking table test of a single story steel frame with TLD and TLCD indicates that the performance of the TLD and TLCD can be accurately evaluated using the hybrid testing method without the physical structural model. Finally, the uncontrolled and TLD-controlled structural responses of a three story structure are obtained by the hybrid testing method in both time and frequency domains, showing that TLD can effectively mitigate the seismic responses of building structures and the hybrid testing method can reproduce the dynamic behavior of TLD–structure interaction systems for both the uncontrolled and controlled case. The hybrid testing method can be also applied to the performance evaluation of tuned liquid column damper which has strong inherent nonlinearity.

The bi-directional control performance of the TLMD was confirmed through the conventional and hybrid testing method. First, resonance frequencies in the TMD and TLCD control direction were confirmed at $0 \cdot 82$ and $0 \cdot 73$ Hz. In the TMD control direction (x-direction), 80% of the uncontrolled peak response of the target structure was removed by a TLMD. Also, in the TLCD control direction (y-direction), 70% was removed by a TLMD. The control performances of the TLMD were checked and compared through the two testing methods. In the TLCD and TMD control direction, the errors of the peak values between the conventional and hybrid testing method were $0 \cdot 01$ and $0 \cdot 02\sim0 \cdot 04$, respectively. Also, the errors of RMS values between the conventional testing method and hybrid testing method were up to $0 \cdot 06$. However, tuning error and outside environment are thought as the causes of the differences. The error of the convergence times reaching to the peak value as shown in Figure 2.59. This is caused by the minute error of the mass, stiffness and damping ratio at the numerical analysis, which was thought as either reason. As showing the similar results of the two kind of testing methods, the hybrid testing method, which does not require the physical structural model but with simple installation, as well as the conventional testing method, can accurately evaluate the control performance of a control device.

CHAPTER 3

Design of Excitation System for Simulating Dynamic Loads

3.1 Design of an Actuator for Simulating Wind Response

In this section, simulation of wind induced responses of a building structure using linear mass shaker (LMS) and active tuned mass damper (ATMD) as actuator is conducted as shown in Figure 3.1. In order for the linear actuator to keep the structure in the target response trajectory, an inverse transfer function of a structural response to the shaker force is obtained using a state space form governing equation of the structure and the discrete Fourier transform of structural response is performed. Filter and envelop function are used such that the error between wind and actuator induced responses is minimized by preventing the shaker from actuating unexpected modal responses and initial transient responses. The effectiveness of the proposed method is verified through a numerical example of a 76 story-benchmark building excited by wind load of which deterministic time history is given. The effect of the type of the target structural response on convergence of the actuator force signal and the error magnitude is investigated.

3.1.1 Force of actuator

The state space form equation of a structure excited by wind load f and the shaker generated force u of size r is as follows.

$$\begin{aligned}\dot{\mathbf{z}} &= \mathbf{Az} + \mathbf{B}_f f + \mathbf{B}_u u \\ y &= \mathbf{Cz} + \mathbf{D}_f f + \mathbf{D}_u u\end{aligned}\tag{3.1}$$

where, z is the state vector and y is the output vector of size m . The output transfer function to f or u is given by

$$\begin{aligned}\mathbf{T}_{yf} &= \mathbf{Y}_f(s)\mathbf{F}(s)^{-1} = \mathbf{C}(s\mathbf{I} - \mathbf{A})^{-1}\mathbf{B}_f \\ \mathbf{T}_{yu} &= \mathbf{Y}_u(s)\mathbf{U}(s)^{-1} = \mathbf{C}(s\mathbf{I} - \mathbf{A})^{-1}\mathbf{B}_u\end{aligned}\tag{3.2}$$

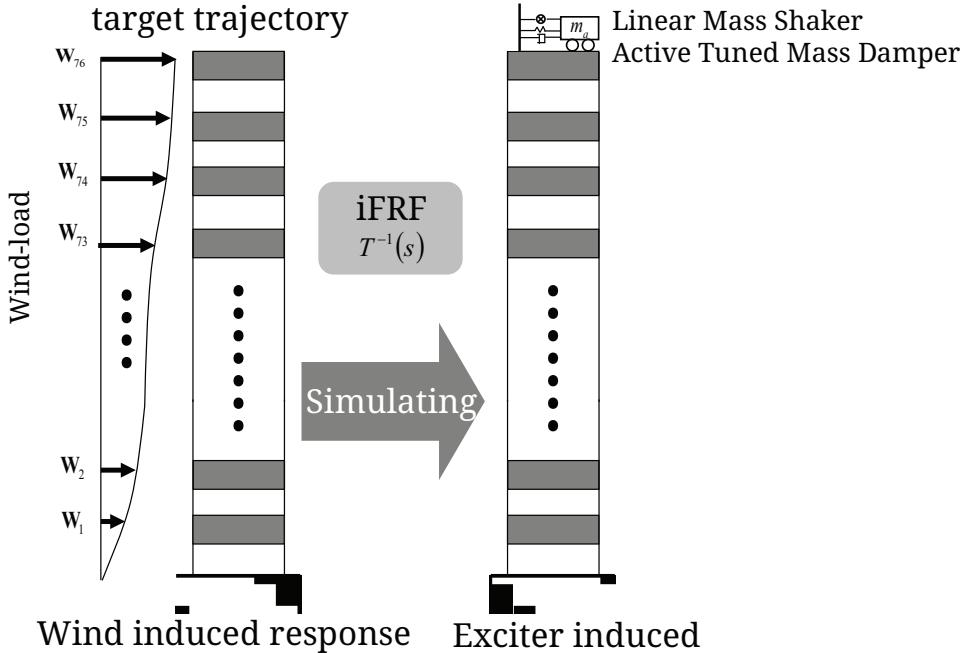


Figure 3.1: Scheme of simulation of wind induced responses using LMS and ATMD

where the scalar s is a complex variable $j\omega$. The inverse of \mathbf{T}_{yu} exists only if r equals to m and the Laplace transform of u providing the identical output to wind load induced one is determined as

$$\begin{aligned}\mathbf{U}(s) &= \mathbf{T}_{yu}^{-1} \mathbf{Y}_u(s) \\ &= \mathbf{T}_{yu}^{-1} \mathbf{T}_{yf} \mathbf{F}(s)\end{aligned}\quad (3.3)$$

when r is smaller than m , the number of structural responses which can be modulated by u is restricted to r and target structural response should be selected. The Laplace transform of input realizing the target response \bar{y} of size r is

$$\begin{aligned}\hat{\mathbf{U}}(s) &= \hat{\mathbf{T}}_{yu}^{-1} \hat{\mathbf{Y}}_u(s) \\ &= \hat{\mathbf{T}}_{yu}^{-1} \hat{\mathbf{Y}}_f(s) \\ &= \hat{\mathbf{T}}_{yu}^{-1} \hat{\mathbf{T}}_{yf} \mathbf{F}(s)\end{aligned}\quad (3.4)$$

where, $\hat{\mathbf{T}}_{yu}^{-1}$ is a sub-matrices of \mathbf{T}_{yu}^{-1} is constructed by extracting the columns in \mathbf{T}_{yu}^{-1} corresponding to the target response.

Filter and envelop function

The transfer function of structural response may have frequency intervals in which the magnitude is as small as zero, and in those intervals the magni-

tude of the inverse transfer function increases infinitely. Because the input force is calculated by the product of the inverse transfer function and the output signal, significant input force may be calculated in order to realize the small magnitude of output components corresponding to the intervals. This implies that the shaking system becomes very sensitive to the slight frequency variation of output signal resulting from measurement noise and spectral leakage which is inevitable in signal processing using discrete Fourier transform, and then unnecessarily large input energy excites unexpected frequency response such that target response may not be induced. Particularly, low frequency component leads to large stroke of the shaker. In this study, following band-stop filter (BSF) using cosine function is used to prevent the unexpected frequency response from occurring.

$$\hat{\mathbf{U}}_p(\omega) = G(\omega)\hat{\mathbf{U}}(s) \quad (3.5)$$

where,

$$G(\omega) = \frac{1 - a_{co}}{2} \cos\left(\frac{2\pi}{\omega_2 - \omega_1}\omega\right) + \frac{1 + a_{co}}{2} \quad (3.6)$$

$$a_{co} = \begin{cases} \omega < \omega_1 & : 1 \\ \omega_1 \leq \omega \leq \omega_2 & : 0 \\ \omega > \omega_2 & : 1 \end{cases} \quad (3.7)$$

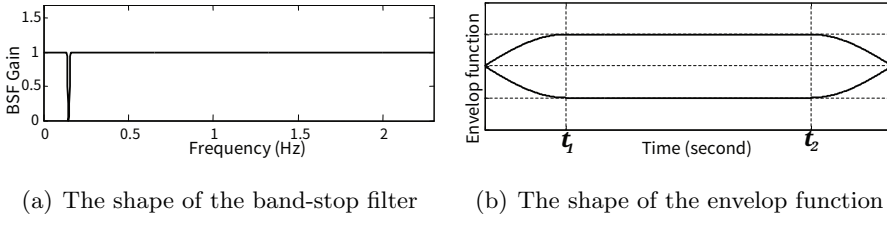
where, ω_1 and ω_2 are frequencies defining the cut-off frequency interval, and a_{co} is gain value of the cut-off frequency. Figure 3.2(a) shows the shape of the band-stop filter

In discrete Fourier transform dealing with the finite duration discrete signal as an infinite one multiplied by a rectangular window, the original signal in time domain is distorted especially in initial and final time intervals. This distortion can be reduced by using an envelop function such that the given deterministic wind load has ascending and descending time intervals. Although the envelope function changes the deterministic wind load, the effect of this another distortion would be trivial in evaluating the characteristics of wind load induced response because grave concern is generally in the intermediate time of the total loading duration when the peak response is expected to occur. Figure 3.2(b) shows the shape of the envelope function used in this study.

3.1.2 Numerical Example

76 story wind-induced benchmark buildings

The wind-induced response simulating actuator is applied to a 76-story 306 meters office tower benchmark building which is slender with a height to width ratio of $306.1/42 = 7.3$. Because the deterministic across-wind load



(a) The shape of the band-stop filter (b) The shape of the envelop function

Figure 3.2: Exciter gain shape of the band-stop filter and the envelop function.

data is given through wind tunnel tests for this benchmark building, the force of the actuator force realizing target across-wind induced structural response can be calculated using Eq. (3.4). In order to reduce numerical computation time, a 23 degree of freedom (DOF) state reduced-order system model proposed by Yang et al. (2004b). is used in this study. The wind load vector is modeled physically by lumping wind forces on adjacent floors at the locations that correspond to the 23 DOF model. Figures 3.3(a), 3.3(b) shows the plan view and elevation view of the 76th benchmark building and Figures 3.3(c), 3.3(d) show the mode shape of first three mode of the structure and time history of wind-load.

Error evaluation criteria

In order to verify the effectiveness of proposed method through the comparison between the wind and actuator induced structural responses, two error criteria are considered in time and frequency domains, respectively. In time domain, the normalized tracking error is defined as

$$e_t = \frac{1}{n} \sum_{i=0}^{n-1} \sqrt{\{z_a(i\Delta t) - z_f(i\Delta t)\}^2} \Bigg/ \max \left[\sqrt{z_f(i\Delta t)^2} \right] \quad (3.8)$$

where, Δt denotes time interval, n denotes the data number. $x_a(i\Delta t)$ and $x_f(i\Delta t)$ are, respectively, actuator and wind induced structural response at the i th time step.

In frequency domain, the normalized tracking error is defined as

$$e_f = \frac{1}{N} \sum_{i=1}^N \sqrt{|Z_a(\omega_i) - Z_f(\omega_i)|^2} \Bigg/ \max \left[\sqrt{|Z_f(\omega_i)|^2} \right] \quad (3.9)$$

where N is the number of frequency response data, and $X_f(\omega)$ and $X_t(\omega)$ are discrete-Fourier transformation of $\ddot{x}_f(t)$ and $\ddot{x}_t(t)$, which $E[\epsilon_f(\omega)]$ is normalized mean tracking error in frequency domain.

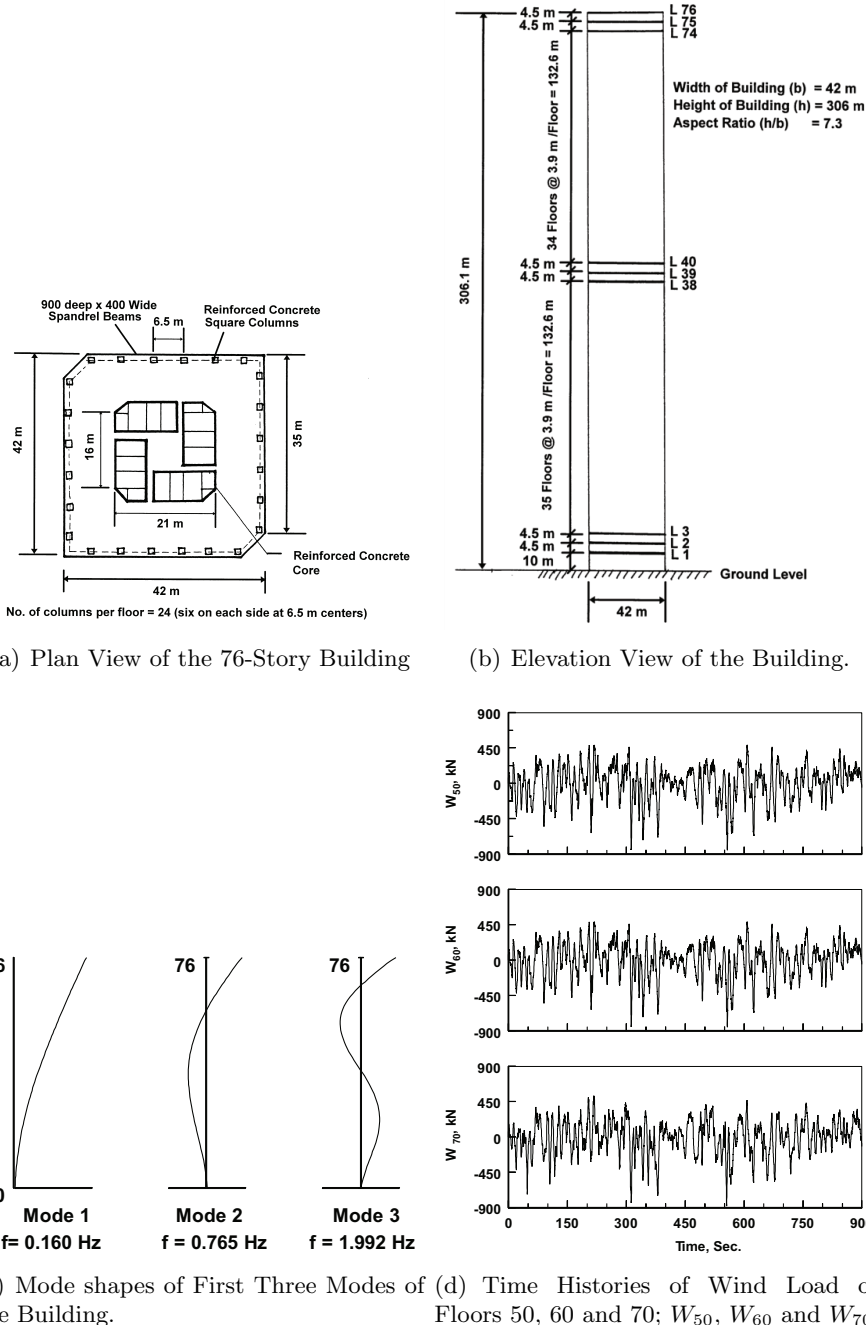


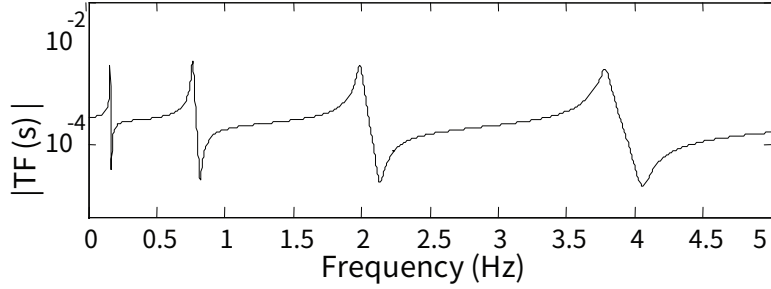
Figure 3.3: 76th story benchmark model.

LMS excitation

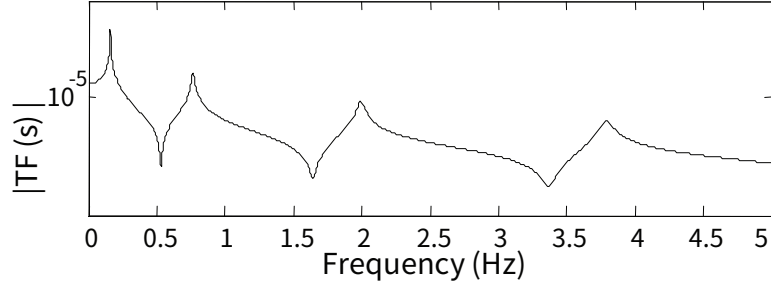
In this subsection, a LMS which can produce arbitrary desired force is used as an actuator. LMS is assumed to have mass of 500 metric ton and be

installed at 76th floor. The mass is identical to that of an ATMD used as a vibration dissipation device for the benchmark problem. The mass is about 45% of the top floor mass, which is 0.327% of the total mass of the building.

Figures 3.4(a) and 3.4(b) show the transfer function of the 75th floor acceleration and displacement responses. It is observed that acceleration transfer function in Figure 3.4(a) has zero near the each modal natural frequency with slightly larger value than the corresponding natural frequency. Especially the zero exists near the first modal frequency which is expected to dominate the overall wind induced structural responses.



(a) 75th story acceleration transfer function.

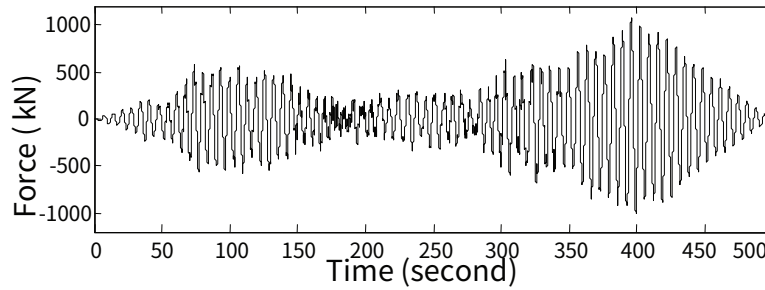


(b) 75th story displacement transfer function.

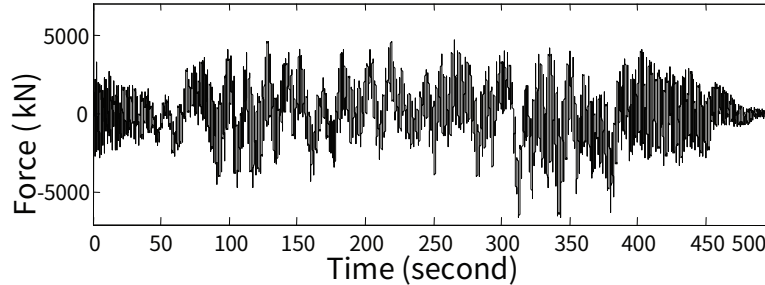
Figure 3.4: Transfer function of 75th story responses to LMS.

Figure 3.5 shows the frequency response function and the time history of the actuator force obtained without using filter when the target response is acceleration or displacement of 75th floor. It is known from Figure 3.5 that much larger force are required for the shaker to achieve the target displacement than acceleration response, and furthermore there exist high frequency components in Figure 3.4(b), which result in high speed-switching of control force as shown in Figure 3.5(b). In practice, hydraulic actuators popular in civil engineering structures is not suitable for this undesirable chattering problem which cause spillover instability in higher modes, and acceleration response concerned with serviceability criteria is more critical for such high-rise building excited by wind load as this benchmark building

than displacement. Figure 3.6 shows the comparison between the frequency responses of wind and LMS induced 75th floor acceleration and displacement when the target response is 75th displacement. It is obviously shown that wind and LMD induced displacement coincide well with each other while acceleration responses are very different. Based upon the observation in Figure 3.5 and 3.6, only acceleration response is considered as target response for calculating LMD force reproducing wind induced displacement as well as acceleration in this study.



(a) LMS force targeting on 75th floor acceleration.

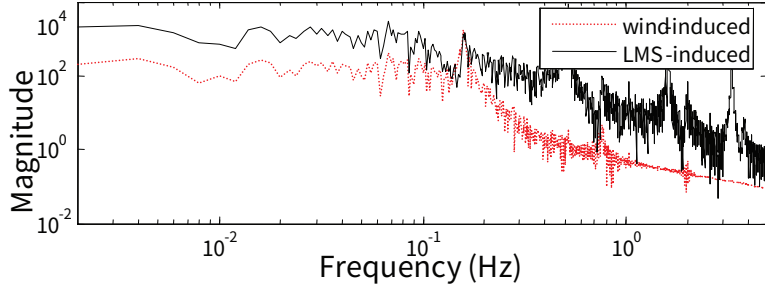


(b) LMS force targeting on 75th floor displacement.

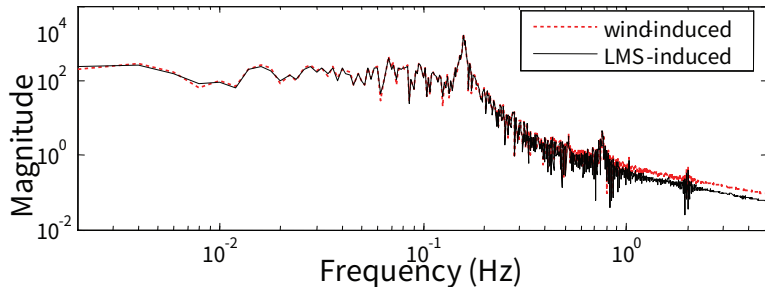
Figure 3.5: LMS force (unfiltered).

Numerical analyses are conducted with/without using the filter and envelop function for different target responses. Table 3.1 lists the cut-off frequencies used for cancelling previously mentioned undesirable amplification effect by the zero in the inverse transfer function of each target response. Envelop function with $t_1 = 100$ second and $t_2 = 100$ second is applied.

Figure 3.7 shows the floor distribution of the time and frequency domain errors defined in previous subsection, which are obtained with/without using the filter for different target responses. Processed signal denotes one yielded by using filter. It is identified from Figure 3.7 that the processed signal using filter significantly reduce the magnitude of the tracking error when the target response is 75-floor acceleration of which transfer function has band-stop frequency near the first modal frequency (as observed in Figure 3.4(a)) while



(a) Acceleration response.



(b) Displacement response.

Figure 3.6: Frequency response of 75th floor with LMD force targeting displacement response.

Table 3.1: Cutoff frequency for filter design

Target response	ω_1 (rad/sec)	ω_2 (rad/sec)
75th floor acceleration	1.01	1.13
50th floor acceleration	8.17	8.80
30th floor acceleration	17.59	20.73

the processing effect is trivial when the target response is 30th or 50th floor acceleration of which transfer function has zero away from the first modal one. Also, it is known from observing the error distribution that the targeted responses are almost identical to wind-induced ones with small magnitude of error while the other non-targeted responses are slightly different with increasing error. Targeting 30th or 50th floor acceleration provides greater discrepancy between the wind and LMS induced 75-floor accelerations which are critical in evaluating serviceability. The comparison between the results in Figure 3.7(a) and 3.7(b) indicates that the distribution tendency of e_t and e_f is quite different and the magnitude of e_t is much larger than that of e_f . When targeting response is 75th floor acceleration, both values of e_t and e_f are smallest for the targeted 75th floor acceleration, but the value of e_f

becomes larger for the other story responses while the value of e_f generally keeps the smallest except for 30th story acceleration. The larger value of e_t results from the phase difference between wind and LMS induced responses since e_t is obtained based on the response difference at the same time step. The phase of the wind induced response is not important parameter in evaluating the wind resistance performance of a building structure, e_f can be said to be more appropriate index for evaluating the wind response reproducing performance of LMS.

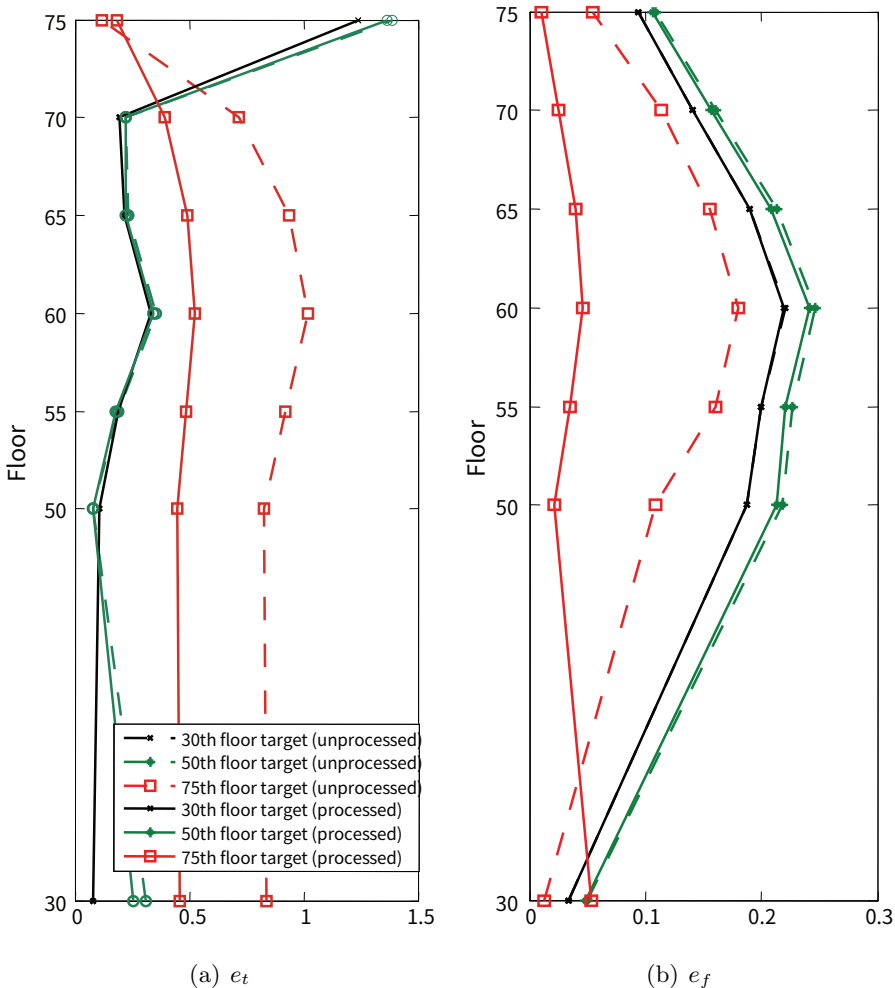


Figure 3.7: Error distribution according to the filter usage and floor of target response.

Figures 3.8 and 3.9 compare the time histories of the wind and LMS induced structural responses for the cases that the target responses are, respectively, 75th and 30th floor accelerations and filter is applied for the design of LMS. Figure 3.8 shows that the LMS induced acceleration response

including targeted 75th floor acceleration agree well with wind-induced ones while displacement responses at all floors are underestimated by LMS. It is observed in Figure 3.9 that the shaker simulated targeted 30th floor acceleration as well as displacement responses but overestimates 75th floor acceleration.

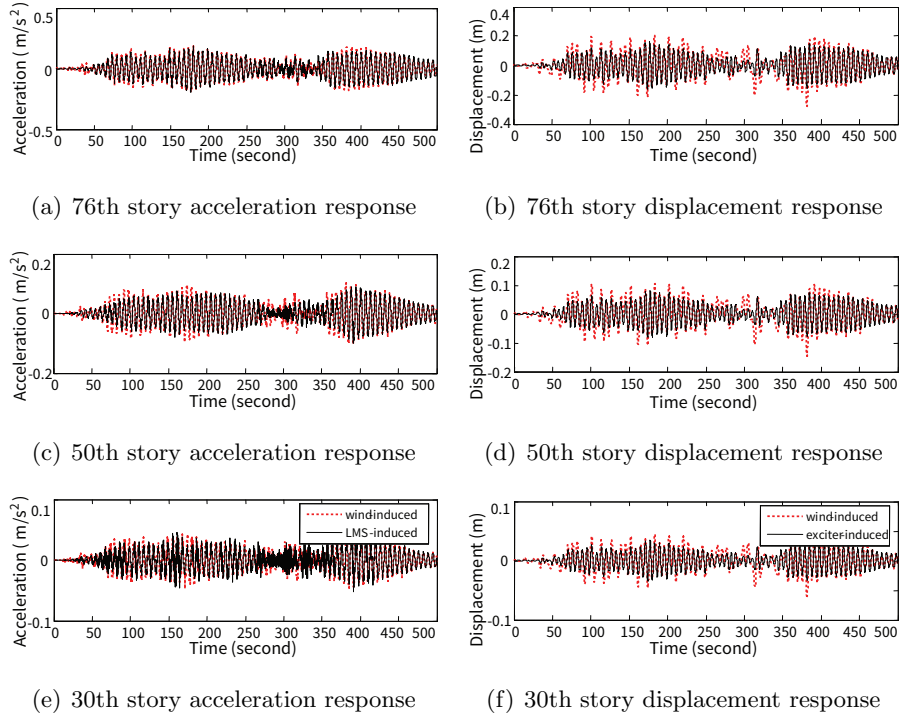


Figure 3.8: Wind and LMS induced acceleration responses (when the target is 75th floor acceleration).

ATMD excitation

In the 76th story building benchmark problem, ATMD is used as an example controller, which is composed of spring and viscous damper in addition to the mass and actuator of the LMS. In this subsection, the ATMD is considered as another exciter. The mass of the ATMD is 500 metric ton and the undamped natural frequency and damping ratio are, respectively, 0.16Hz and 20% (Yang et al., 2004b). Simplification for the control environments have been made, in particular, the actuator dynamics and controller-structure interaction are not considered in the benchmark problem. The equation of motion of the building equipped with an ATMD on the top floor can be expressed as

$$\mathbf{M}\ddot{\mathbf{x}} + \mathbf{C}\dot{\mathbf{x}} + \mathbf{K}\mathbf{x} + \mathbf{H}u = \eta\mathbf{W} \quad (3.10)$$

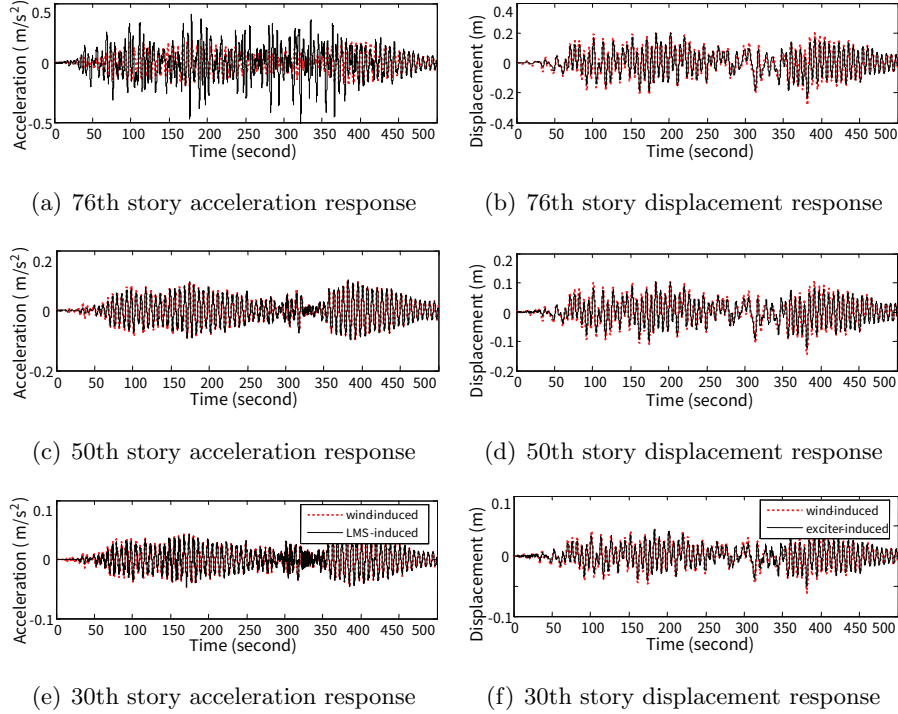


Figure 3.9: Wind and LMS induced acceleration responses (when the target is 30th floor acceleration).

and considering no wind-load input, the equation of motion of the building can be expressed as

$$\begin{bmatrix} \mathbf{M}_s & 0 \\ \mathbf{0} & m_t \end{bmatrix} \begin{Bmatrix} \ddot{\mathbf{x}}_s \\ \ddot{x}_t \end{Bmatrix} + \begin{bmatrix} \mathbf{C}_s + c_t \mathbf{B}_t \mathbf{B}_t^\top & -c_t \mathbf{B}_t \\ -c_t \mathbf{B}_t^\top & c_t \end{bmatrix} \begin{Bmatrix} \dot{\mathbf{x}}_s \\ \dot{x}_t \end{Bmatrix} + \begin{bmatrix} \mathbf{K}_s + k_t \mathbf{B}_t \mathbf{B}_t^\top & -k_t \mathbf{B}_t \\ -k_t \mathbf{B}_t^\top & k_t \end{bmatrix} \begin{Bmatrix} \mathbf{x}_s \\ x_t \end{Bmatrix} = \begin{bmatrix} -\mathbf{B}_t \\ 1 \end{bmatrix} u \quad (3.11)$$

where \mathbf{B}_t is position vector of floor installed ATMD, \mathbf{M}_s , \mathbf{C}_s and \mathbf{K}_s is the mass, damping coefficient and stiffness matrix of the structure and m_t , c_t and k_t is the mass, damping coefficient and stiffness of the ATMD.

Figure 3.10(a) shows the transfer function of the 75th floor acceleration to the absolute acceleration the ATMD. No zero point is observed in the vicinity of the first modal frequency unlike the case for LMS, which indicates that band-stop filter is not required for preventing the ATMD to excite the unexpected frequency response. Figure 3.10(b) shows the frequency response of the actuator force of the ATMD and Figure 3.10(c) and 3.10(d) show the frequency and time responses of the effective force applied to the structure by the ATMD.

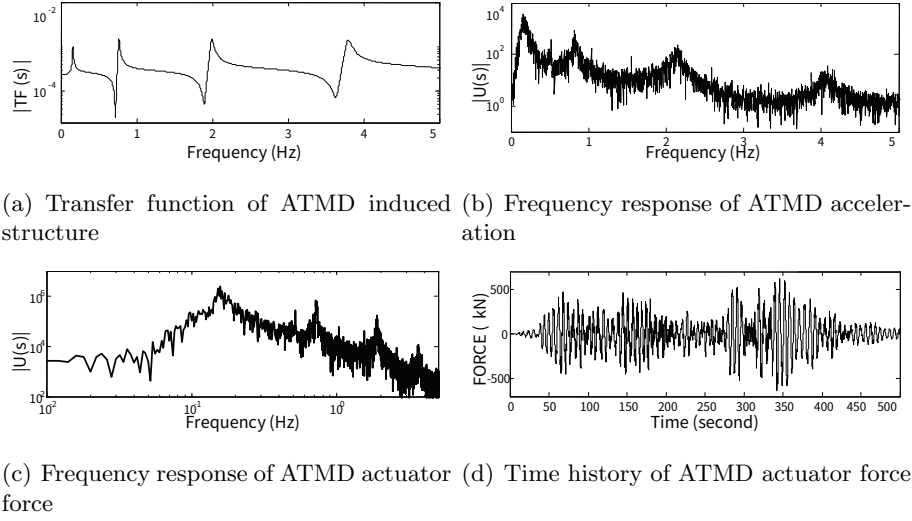


Figure 3.10: ATMD Excitation.

Figure 3.11 shows the time history comparison between wind induced acceleration and ATMD induced one targeting on 75th story acceleration response.

All acceleration responses coincide well with each other, but in displacement response, there exists slight underestimation and overestimation according to the time ranges.

Figure 3.12 shows the comparison between the frequency responses of 75th floor acceleration and it is observed that wind and ATMD induced responses show good agreement over all frequency range.

Figure 3.13 shows the error distribution according to the floor of targeted acceleration response. From Figure 3.13(b) showing that e_f has the smallest value over floors when the target response is 75th floor acceleration and the corresponding value ranges only between 1% and 10%, ATMD targeting 75th floor acceleration can be said to provide best performance and it can exactly reproduce the wind-induced acceleration response of all floors including targeted 75th floor.

Comparison between LMS and ATMD

Figure 3.14 shows time history of the actuator forces in LMS and ATMD excitation systems. The peak actuator force required for ATMD is larger than that for LMS. Figure 3.15 compares the stroke of LMS with/without filter and ATMD. The stroke of LMS with filter is much smaller than those of LMS without filter and ATMD. This fact implies that ATMD requires large stroke in order to show good performance in wind-induced response realization and this stroke requirement should be checked in the design of

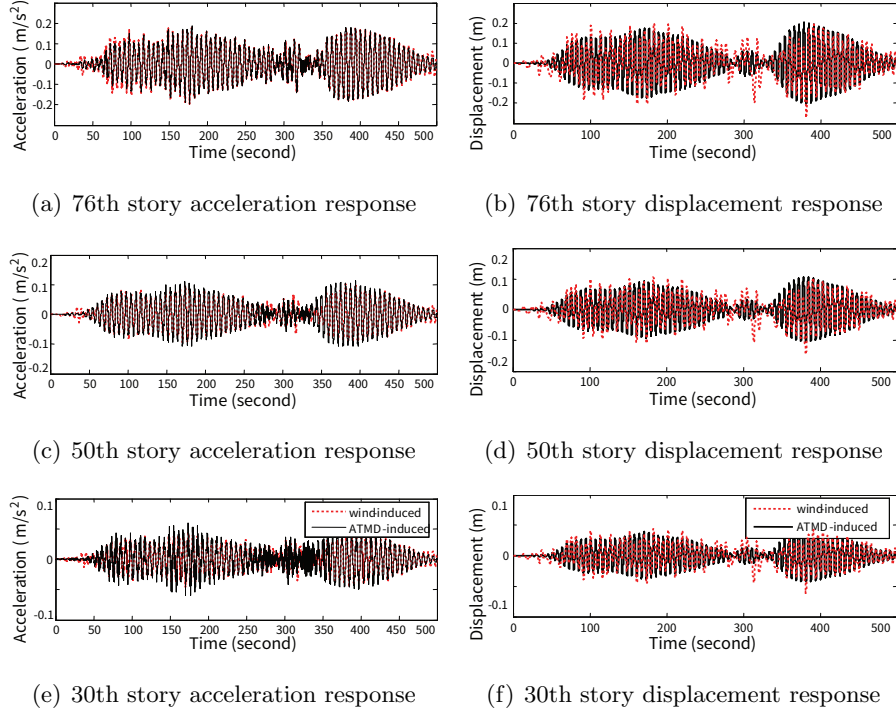


Figure 3.11: Wind and ATMD induced acceleration responses (when the target is 75th floor acceleration).

ATMD.

Table 3.2 shows the numerical values of the error, actuator force, and actuator stroke in LMS with/without filter, and ATMD systems. The errors are obtained when the target and evaluation responses are identical, and actuator force and stroke are obtained when the target response is 75th floor acceleration. The facts observed from Figures 3.14 and 3.15 that the performance of LMS can be enhanced using band-stop filter and ATMD reproduces wind-induced response better than LMS but ATMD requires larger actuator force and stroke can be identified once more.

3.1.3 Summary

Design of excitation systems for simulating wind induced responses of a building structure was presented as a preliminary study for evaluating wind-resistance characteristics of practical building structures. The actuator forces of the LMS and ATMD were obtained using the inverse transfer function of structural responses. Also, band stop filter was used in LMS to remove zero of the transfer function such that undesirable modal excitation is prevented, and envelop function was used to reduce the error occurring in transient initial states in both LMS and ATMD. The numerical analyses results from

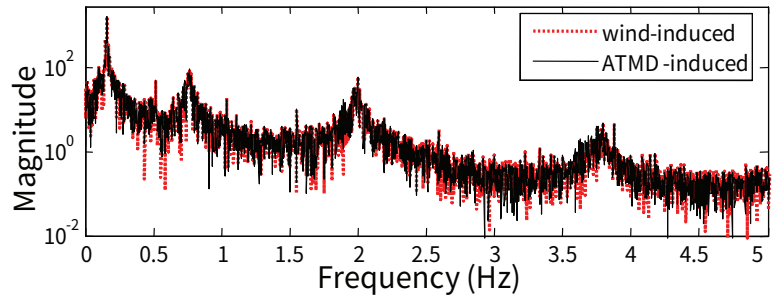


Figure 3.12: Frequency response of wind and ATMD induced 75th floor accelerations

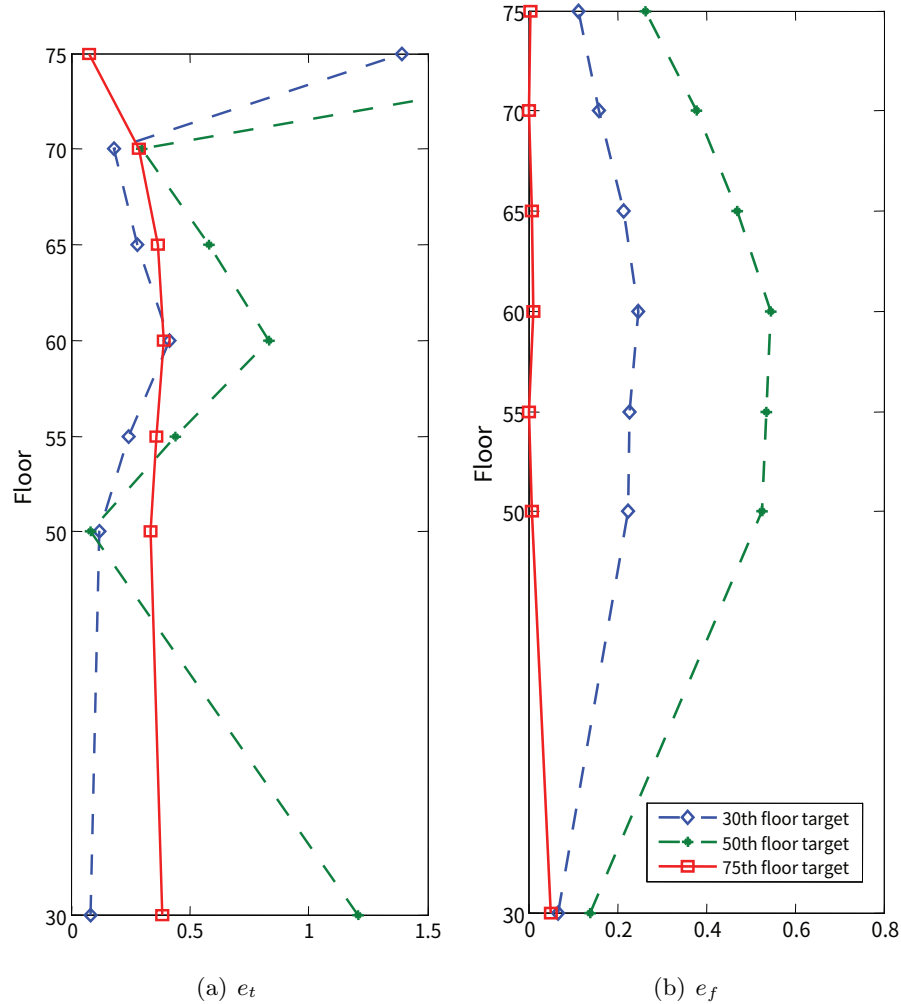


Figure 3.13: Error Distribution with ATMD excitation.

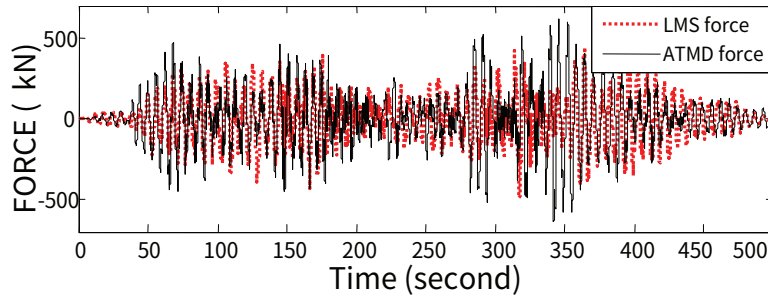


Figure 3.14: Comparison between actuator forces in LMS and ATMD

Table 3.2: Comparison between LMS and ATMD

		LMS (unfiltered)	LMS (filtered)	ATMD
75th floor acceleration	e_t	0.117	0.192	0.074
	e_f	0.054	0.011	0.003
50th floor acceleration	e_t	0.081	0.081	0.083
	e_f	0.219	0.213	0.525
30th floor acceleration	e_t	0.082	0.082	0.082
	e_f	0.034	0.033	0.065
Stroke	Peak (m)	1.402	0.519	1.265
	RMS (m)	0.436	0.183	0.333
Actuator force	Peak (kN)	1068.22	441.68	655.78
	RMS (kN)	323.92	136.44	170.39

a 76-story benchmark building confirmed that the structural responses of a building structure excited by wind loads acting at all floors could be reproduced by the proposed excitation systems installed at a specific floor. The performances of the excitation systems were dependent on type and position of the target structural response for which acceleration response was suitable because targeting displacement response required large and high-speed changing control force. In order to enhance practical applicability of the wind-response simulating excitation systems, finite element model updating based on measured data, and the scaling or restriction of the excitation force or stroke limit for avoiding damage of the practical building etc. should be considered in further study.

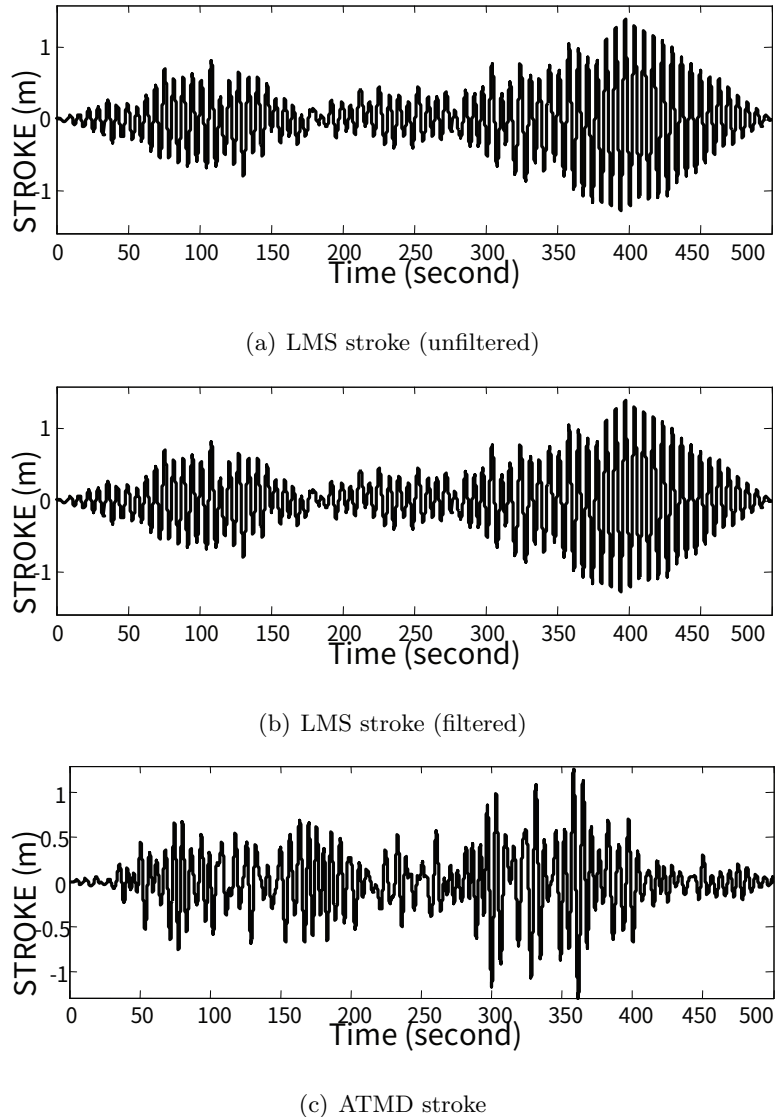


Figure 3.15: Stroke Comparison.

3.2 Forced vibration test of full-scaled five-story building structure simulating eqearthquake responses

3.2.1 Overview

In this section, the hybrid mass damper (HMD) controller for the pseudo-earthquake excitation test is designed by employing the method using the inverse transfer function of a structure, which is one of methodologies pro-

posed by previous section, and is verified for its experimental implementation. First, a real-scaled 5 story steel frame, in which a HMD installed, is shaken and then transfer functions from the HMD to structural responses of each story are obtained. Then, the FE model numerically calculated from the software for commercial use is renewed based on the modal information extracted from experimentally obtained transfer functions. Also, the earthquake responses based on the renewed structural model are numerically calculated, and the structure is excited by a HMD input signal which is produced to simulate a specific target response of a structure out of these numerically calculated earthquake responses. Finally, the effectiveness of pseudo-earthquake excitation presented in this study is verified by comparing numerically calculated seismic responses with experimentally measured ones.

The pseudo-earthquake excitation testing method presented in this study has several importance in an engineering aspect. First, the testing method that is performed for a real-scaled structure in field is free from lots of artificial constraints accompanied in laboratory test. Secondly, valuable data, which are available for the verification of structural seismic performance and the evaluation of the availability of vibration technique required in structural health monitoring, can be acquired from the test. Thirdly, large shaking table is not required to evaluate the seismic response of real-scaled building structures, since in this study the earthquake response is simulated by actuating a structure with a HMD installed at upper story.

3.2.2 Experimental Real-Scale Building Model

The experimental model, which is shown in Figure 3, is a full-scale five-story steel structure which has the story height of 6m, the plan of $6m \times 6m$, and the story mass of 20,000kg. Each floor is composed of four identical wide-flange type steel columns. A HMD using larger scale linear motor damper which was also designed as a passive damper has moving mass on the fifth floor excited the model structure. Because the columns consist of I-shaped steel, the HMD was installed in minor axis of the structure.

3.2.3 Field measurement and experimental system

Field measurement and experimental system is shown in Figs. 6.3 and 6.4. To minimize the latency between the excitation and the measurement, one lap-top PC in the experimental system was used for simultaneously implementing the excitation and the measurement. The measurement system has accelerometers, PCB Corp. 393B12 model was installed at the center of the 2nd 5th floor and KYOWA Corp. AS-2GB model was attached to the HMD. PCB Monitran and KYOWA DPM-711B was used to amplify their measured signals. The data cabling connection system has BNC cable with

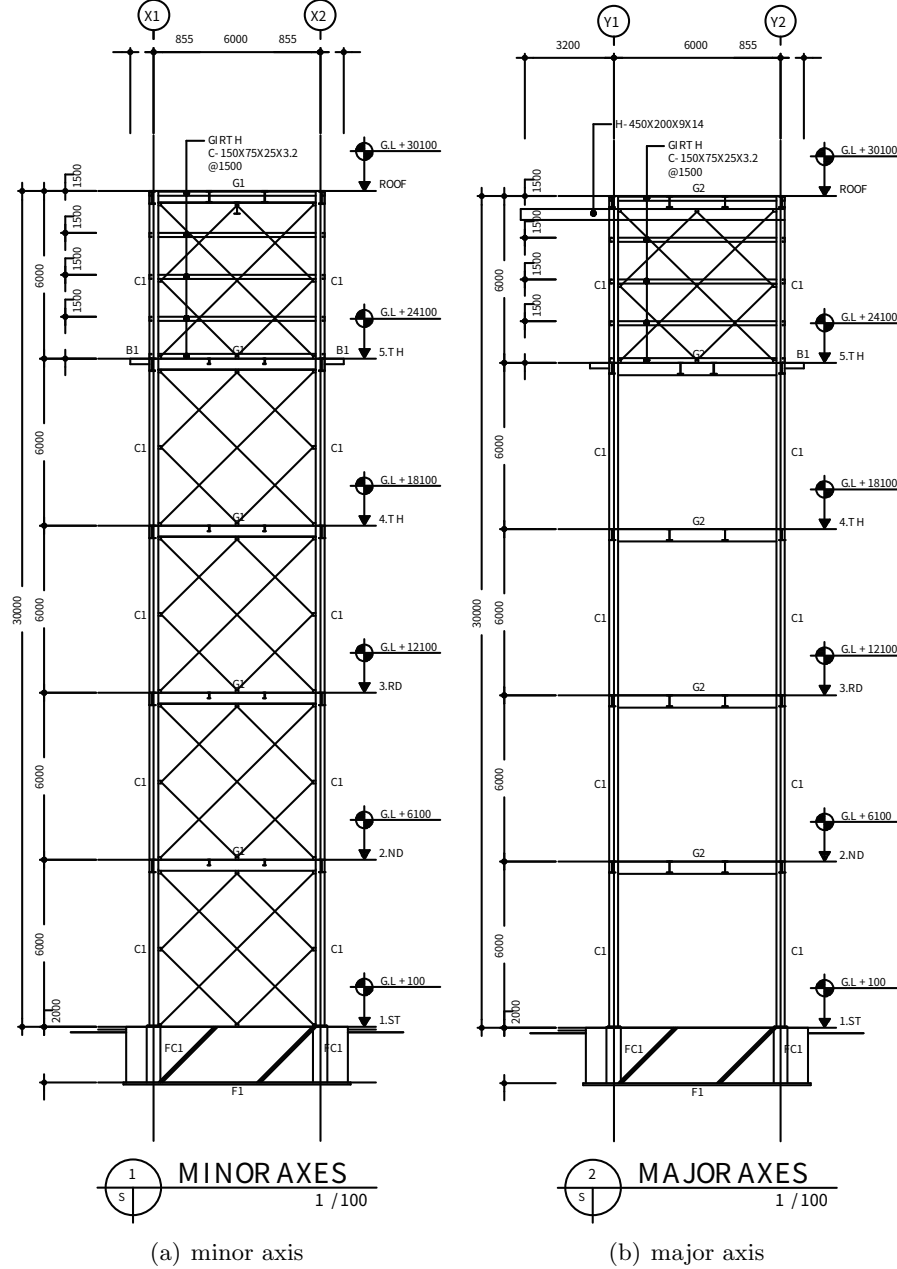
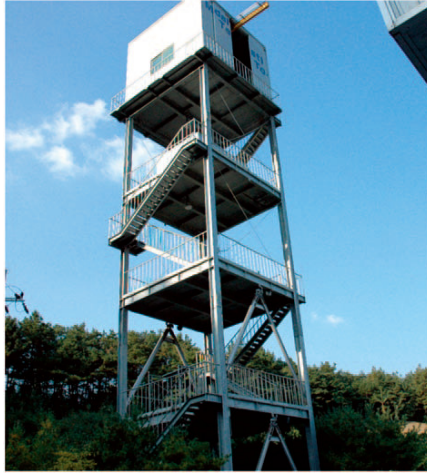
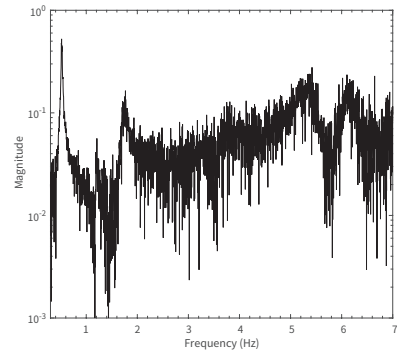


Figure 3.16: Elevation view of the target structure.

lengths of 25m and 50m. In the data acquisition system, the DAQ board of NI DAQCard-6036E with 16bit-range was used to perform the AD and DA conversion. Also, it was connected to the signal conditioner of NI SCC-2345 by using both the input modules and the output module. In this excitation system, both excitation and measurement signals are voltage signals, and



(a) Five-story building structure.



(b) Transfer function of target floor response to the HMD.

Figure 3.17: Photograph and transfer function of the target building structure.

Table 3.3: Member list of the model structure

MEMBER LIST	
C1	H-310×310×20×20
G1	H-400×200×8×13
G2	H-450×200×9×14
B1	H-200×100×5.5×8
B2	H-400×200×8×13
RB1	H-400×200×8×13
FC1	500×500

this excitation signal transfers equivalent thrust generated according to the input voltage signal through the inverter of HMD, to the mass of HMD. Accordingly, the excitation signal should be generated to move within safety range, because the excessive response of the HMD is prevented by its safety device.

3.2.4 System Identification

White-noise Test

White noise vibration test were carried out by using broad-band random signals during 410sec. Both the excitation and measurement ware performed by constructing a close-loop system to minimize the latency, by which time delay would be induced, and experimental data was acquired with a sampling

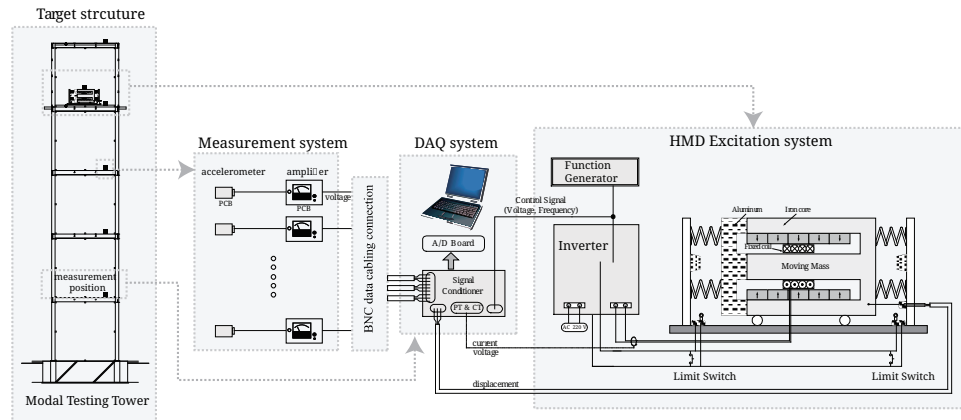


Figure 3.18: Schematic diagram of the field measurement, data acquisition and excitation system.



Figure 3.19: Installation pictures of the measurement, data acquisition and excitation system.

rate of 100Hz. In order to reduce the unexpected noise in the experiment, low-pass filter of 30Hz within the amplifier and 25Hz within the signal conditioner module was utilized and the acquisition system was insulated with the reference signal ended (RSE) method for its grounding. Fig.6.5 shows the transfer function from the absolute acceleration of the HMD to the building accelerations.. The lower fundamental modes of the structure are apparently shown

Finite Model Updating

It is difficult to establish the FE model because of limitations in the number of sensors that may be deployed and the difficulty of actuating a structure to higher modes. The process of developing a FE model of a structure relating

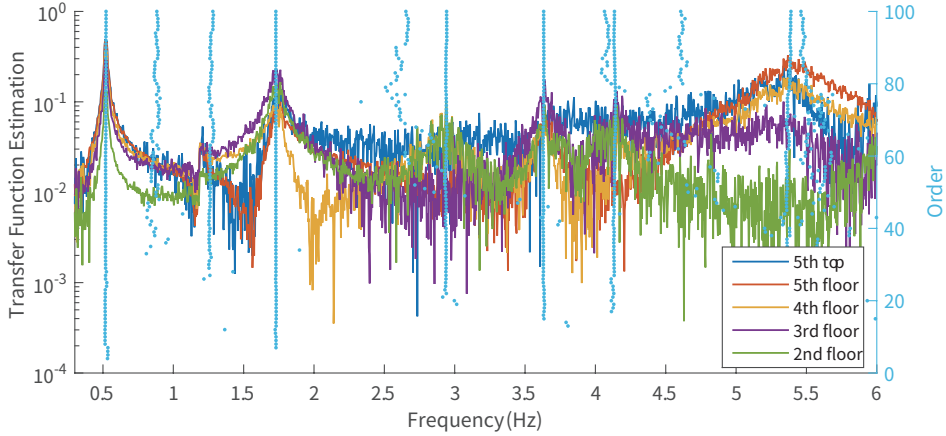


Figure 3.20: The transfer function from the absolute acceleration of the HMD to those of the structure.

Table 3.4: Identified natural frequencies and damping ratios

Modes	Frequency (Hz) & COV (%)	Damping ratio (%) & COV (%)
1	0.52(1.82)	1.46(14.42)
2	1.73(0.13)	2.71(9.40)
3	2.94(0.10)	3.54(1.93)
4	4.14(0.08)	1.72(1.70)
5	5.36(0.23)	3.84(3.56)

it to the experimental model is called FE model updating(Bagchi, 2005). In this paper, an analysis model was established by modeling using ANSYS and model updating was carried out by using the measured modal data.

In this study the optimal matrix update method was used which is based on a constraint optimization problem where the minimum changes in the mass matrix or the stiffness matrix are found subjected to constraints such as symmetry, connectivity and definiteness(Baruch, 1978; Baruch and Bar Itzhack, 1979). The mass matrix is assumed to be exact. There exists a constraint on the corrected stiffness matrix which should reproduce the measured modal data with symmetry. The two independent constraint equations are Eqs. (3.12) and (3.13). The function to be minimized must relate in some way to the difference between the corrected stiffness matrix, \mathbf{K} , and the analytically derived stiffness matrix, \mathbf{K}_a , which is shown in the form of norm in Eq. (3.14). The expression for the updated mode and stiffness matrix, which is obtained by minimizing Eq. (3.14) satisfying Eqs. (3.12) and (3.13), lead to Eqs. (3.15) and (3.16)(Baruch and Bar Itzhack, 1979;

Baruch, 1978).

$$\mathbf{K}\Phi = \mathbf{M}_a\Phi\Lambda, \Phi^\top\mathbf{M}_a\Phi = \mathbf{I} \quad (3.12)$$

$$\mathbf{K}^\top = \mathbf{K} \quad (3.13)$$

$$J = \frac{1}{2} \left\| \mathbf{N}^{-1} (\mathbf{K} - \mathbf{K}_a)^{-1} \right\| \quad (3.14)$$

$$\Phi = \Phi_m \left[\Phi_m^\top \mathbf{M}_a \Phi_m \right]^{-1/2} \quad (3.15)$$

$$\begin{aligned} \mathbf{K} = & \mathbf{K}_a - \mathbf{K}_a \Phi \Phi^\top \mathbf{M}_a - \mathbf{M}_a \Phi \Phi^\top \mathbf{K}_a \\ & + \mathbf{M}_a \Phi \Phi^\top \mathbf{K}_a \Phi \Phi^\top \mathbf{M}_a + \mathbf{M}_a \Phi \Lambda \Phi^\top \mathbf{M}_a \end{aligned} \quad (3.16)$$

where, \mathbf{M}_a and \mathbf{K}_a are the analytically derived mass matrix and stiffness matrix, respectively, Φ_m is the measured eigenvector matrix, Λ is a diagonal matrix of the measured eigenvalues and \mathbf{N} is the appearance of the square root of the mass matrix $\mathbf{N} = \mathbf{M}_a^{1/2}$.

In this study, as shown in Figure 3.20, the measured eigenvector is extracted from the measured modal data using respectively accurate the first and the second modal information. When the measured eigenvector matrix would be extracted, it could be extracted from the transfer function in case of modal resonance using Eq. (3.17) and the sign of the eigenvector is determined from the phase of the transfer function. Reinhorn et al. assumed that resonance responses of the each mode are dependent in case the modal frequencies are not adjacent each other and proposed equation of the transfer function, which is expressed as

$$T_{ai}(\omega_k) = \phi_{ik} H_{ik}(\omega_k) \Gamma_k \quad (3.17)$$

where, $T_{ai}(\omega_k)$, $H_{ik}(\omega_k)$ are the transfer functions to the i th floor and the k th mode of structures in case of resonance and not, Γ_k is the k th scalar value of $\Gamma = -\Phi^\top \mathbf{M}_a \mathbf{I}$ and \mathbf{I} is the influence vector of HMD load. The k th value of eigenvector by ratio of the i th floor over the j th floor can be calculated from amplitude ratio of the transfer function to absolute acceleration responses, which is expressed as

$$\phi_{ik}/\phi_{jk} = T_{ai}(\omega_k)/T_{aj}(\omega_k) \quad (3.18)$$

By updating the natural frequencies and modes, the exact results are obtained comparing to those of the initial analysis.

Table 3.5: Natural frequencies (Hz) for the modal testing tower

	1st mode	2nd mode	3rd mode	4th mode	5th mode
initial	0.5022	1.5623	2.74	3.91	4.83
measured	0.5249	1.7578	2.94	3.67	5.38
updated	0.5249	1.7578	2.95	3.67	5.38

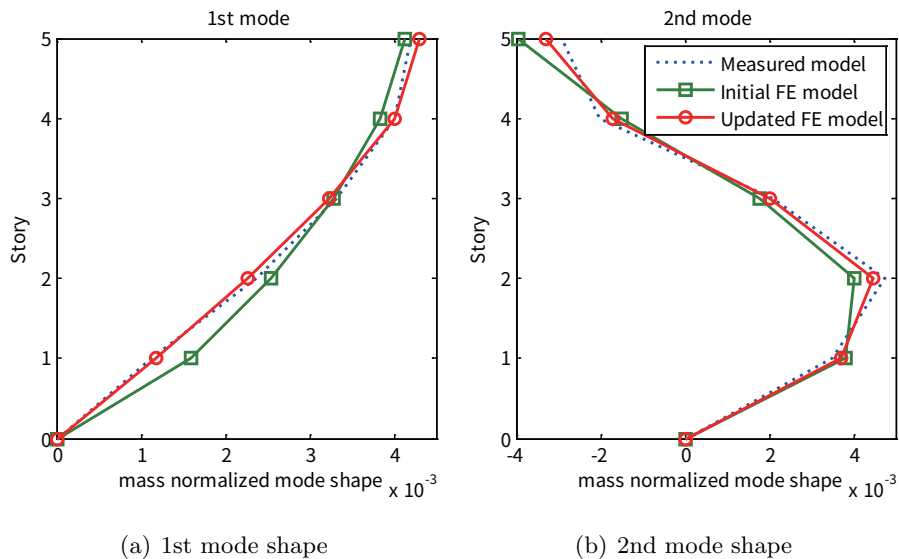


Figure 3.21: The mode shape comparison of initial, the measured and the updated FE models.

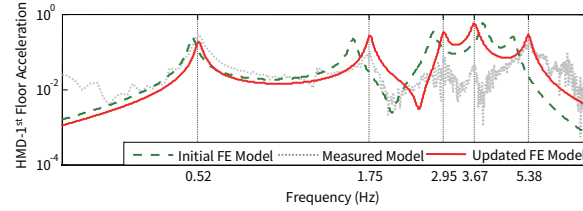
3.2.5 Design of an Excitation System for Simulating Earthquake Response

Generating Input Signal of HMD

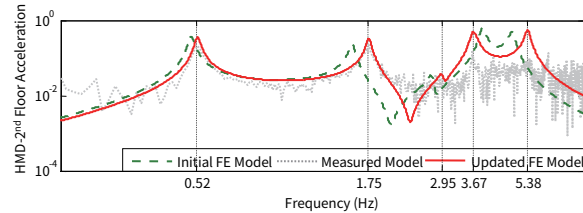
In this chapter, the process of generating the HMD input signal which is simulating earthquake response in the elastic range of model structure by HMD is introduced. The state-space form equation of a structure excited by the base acceleration \ddot{u}_b and HMD acceleration \ddot{u}_h with size of r is expressed as follows

$$\begin{aligned}\dot{\mathbf{z}} &= \mathbf{A}\mathbf{z} + \mathbf{B}_b\ddot{u}_b + \mathbf{B}_h\ddot{u}_h \\ \mathbf{y} &= \mathbf{C}\mathbf{z} + \mathbf{D}_b\ddot{u}_b + \mathbf{D}_h\ddot{u}_h\end{aligned}\quad (3.19)$$

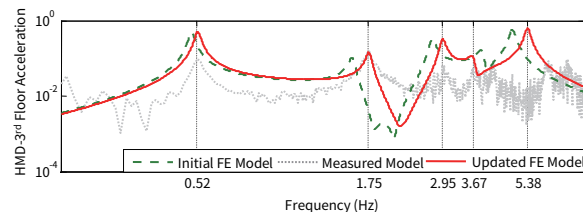
where \mathbf{z} is state variable vector size of $2n \times 1$ and \mathbf{y} is output vector with



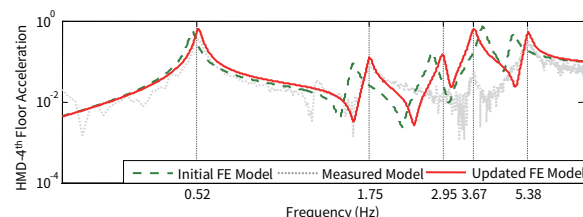
(a) Transfer function of HMD to 1st floor acceleration



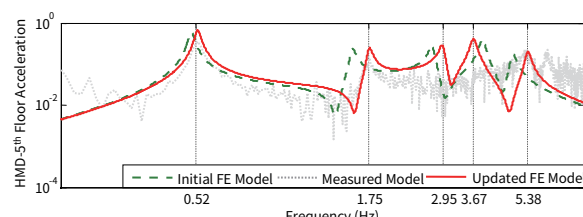
(b) Transfer function of HMD to 2nd floor acceleration



(c) Transfer function of HMD to 3rd floor acceleration



(d) Transfer function of HMD to 4th floor acceleration



(e) Transfer function of HMD to 5th floor acceleration

Figure 3.22: The transfer function comparison of the initial, measured, updated FE model.

size of m . The output transfer functions to \ddot{u}_b or \ddot{u}_h are given by

$$\begin{aligned}\mathbf{T}_h &= \mathbf{Y}_h(s)\mathbf{U}_h(s)^{-1} = \mathbf{C}(s\mathbf{I} - \mathbf{A})^{-1}\mathbf{B}_h + \mathbf{D}_h \\ \mathbf{T}_b &= \mathbf{Y}_b(s)\mathbf{U}_b(s)^{-1} = \mathbf{C}(s\mathbf{I} - \mathbf{A})^{-1}\mathbf{B}_b\end{aligned}\quad (3.20)$$

where the scalar s is a complex variable $j\omega$. The inverse of \mathbf{T}_h exists only if r equals to m and the Laplace transform of \ddot{u}_h providing the identical output to the base acceleration induced one is determined as

$$\mathbf{U}_h(s) = \mathbf{T}_h^{-1}\mathbf{Y}_h(s) = \mathbf{T}_h^{-1}\mathbf{Y}_b(s) = \mathbf{T}_h^{-1}\mathbf{T}_b\mathbf{U}_b(s) \quad (3.21)$$

when r is smaller than m , the number of structural responses which can be modulated by \ddot{u}_h is restricted to r and target structural response should be selected. The Laplace transform of input realizing the target response \bar{y} with size of r is

$$\hat{U}_h(s) = \hat{T}_h^{-1}\hat{Y}_h(s) = \hat{T}_h^{-1}\hat{Y}_b(s) = \hat{T}_h^{-1}\hat{T}_b\hat{U}_b(s) \quad (3.22)$$

where, \hat{T}_h^{-1} is a sub-matrices of \mathbf{T}_h^{-1} . \hat{T}_h^{-1} is constructed by extracting the columns in \mathbf{T}_h^{-1} corresponding to the target response.

Design of HMD controller

The excitation force is generated by the HMD to vibrate the structure in the elastic range. In order to control the HMD, the linear oscillating actuator (LOA) using electromagnetic force as an exciter was adopted. The mass of HMD is 1,500kg mass mounted in the 5th floor of the structure. The excitation force is generated by not the HMD acceleration of input voltage signal but 5th floor absolute acceleration. Therefore, in order to compensate the distortion of the actual HMD acceleration against the HMD dynamics existing between the reference signal and the actual measured acceleration of the HMD, the inverse transfer function of the actual acceleration of HMD with respect to the command signal generated from the control computer is constructed and implemented in the HMD control computer as shown in Figure 3.24. First, the inverse transfer function, of which amplitude and phase are represented in Figure 3.25 by the dashed line, is obtained experimentally. Then, the experimental inverse transfer function is approximated by a rational function for its implementation in the control computer. In this verification experiment, the inverse transfer function of the HMD is approximated using the command `invfreqs` in MATLAB(Coleman et al., 1999), which adopts the damped Gauss-Newton method for iterative search to minimize the sum of the squared error between the measured and the desired frequency response points(Dennis Jr and Schnabel, 1983). The approximation result is given by the following linear filter and compared with the experimental one in Figure 3.25.



Figure 3.23: Photograph of the HMD installed in 5th floor.

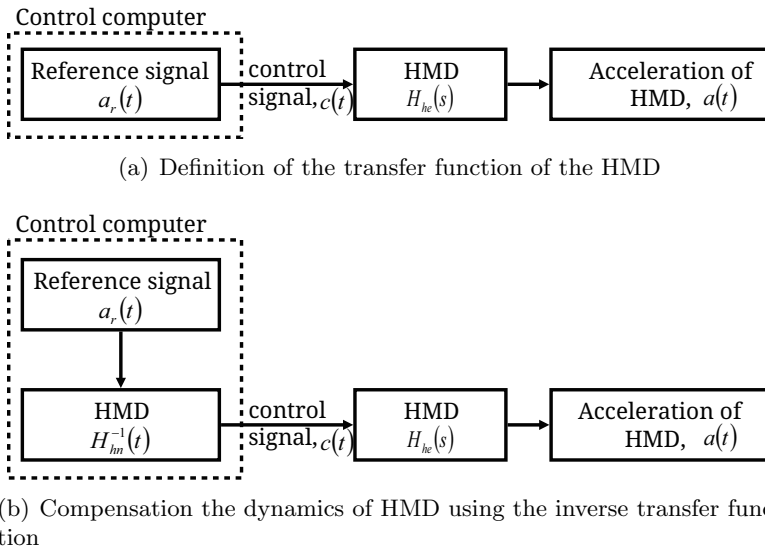


Figure 3.24: Schematic diagram of the HMD controller.

3.2.6 Experimental Result

Pseudo-earthquake excitation result

The pseudo-earthquake forced vibration testing is implemented. The earthquake El Centro(1940, NS) and Hachinohe(1968, NS) earthquake acceleration which PGAs were scaled down to 0.05g for the safety limit device were used in this study. The pseudo-earthquake excitation signal was generated by the inverse transfer function of structure introduced in the chapter 3.2.5 corresponding to the target responses and the excitation was implemented through the HMD controller introduced in the chapter 3.2.5.

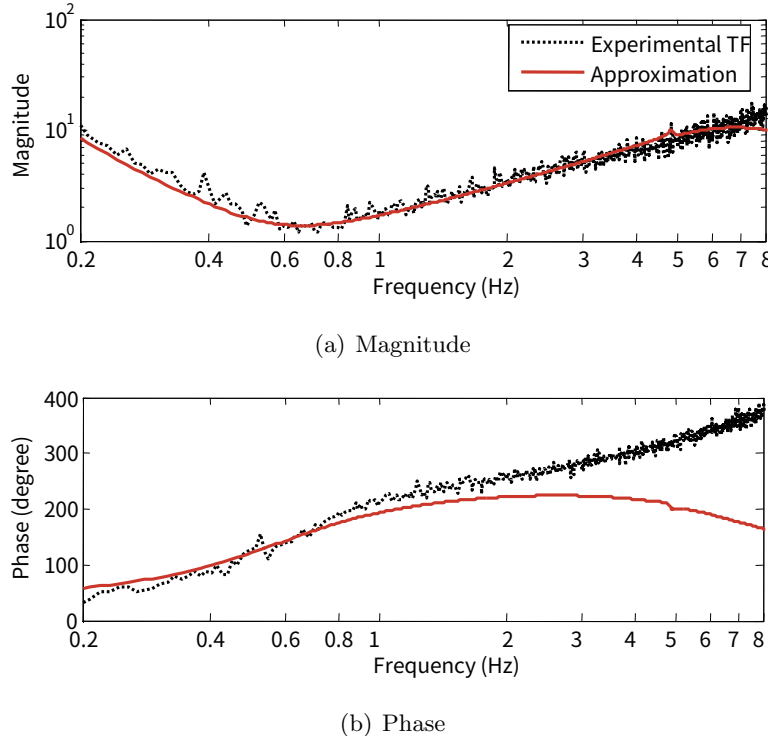
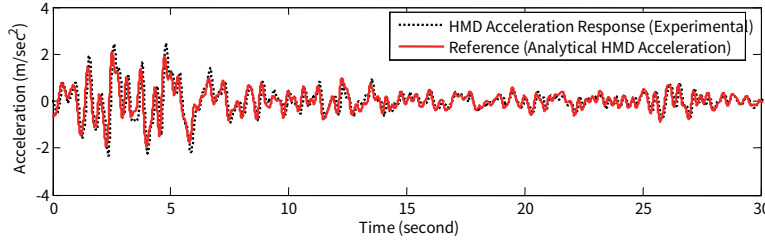


Figure 3.25: Comparison of the measured and the approximated inverse transfer function of the HMD.

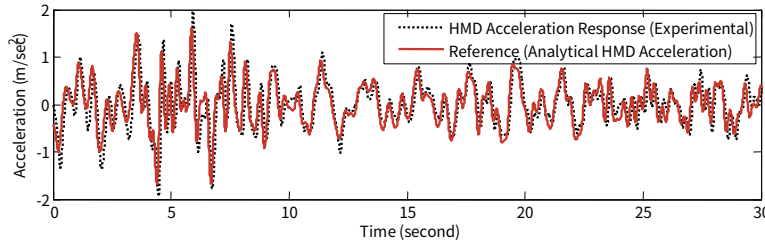
Figure 3.27 compares the result in time history of El Centro earthquake response in the analysis and experimental models. It is observed that both results from FE model and experimental one coincides well each other in initial time range, but the phase in post time range shows a tendency to be changed over 90 degrees. It is caused that the constraint in curve fitting the transfer function was considered weightily with the amplitude of the response not the phase, since in the seismic performance of the structure the amplitude was laid more weight on than the phase.

Figure 3.28 compares the result in frequency domain of El Centro earthquake response in analysis model and experimental one. It is observed that both of results from FE model and experimental one coincides well each other, respectively

Figure 3.29 compares the result in time domain of Hachinohe earthquake response in analysis model and experimental one. It is observed that both of results from FE model and experimental one are good agreement and demonstrate the effectiveness proposed pseudo-earthquake forced vibration testing method. The discrepancy in amplitude at the second mode frequency is caused by the difficulty of excitationa a structure to higher modes limit the modal testing method to capturing only a few lower modes. To improve

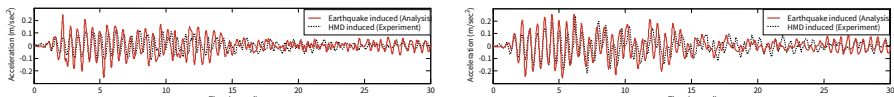


(a) Acceleration of HMD excited by El Centro earthquake

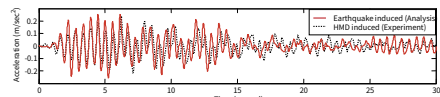


(b) Acceleration of HMD excited by Hachinohe earthquake

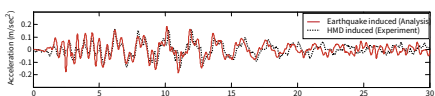
Figure 3.26: Comparison of the reference and measured acceleration time histories when the signals were generated by El Centro and Hachinohe earthquake.



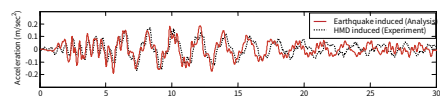
(a) 1st floor acceleration of El Centro earthquake excitation



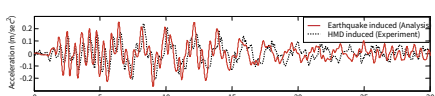
(b) 2nd floor acceleration of El Centro earthquake excitation



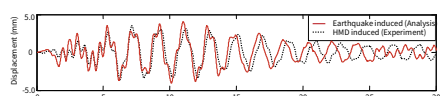
(c) 3rd floor acceleration of El Centro earthquake excitation



(d) 4th floor acceleration of El Centro earthquake excitation



(e) 5th floor acceleration of El Centro earthquake excitation



(f) 1st floor displacement of El Centro earthquake excitation

Figure 3.27: Time history comparison of El Centro earthquake response in the analysis and experimental models. (when the target response is the 5th floor acceleration).

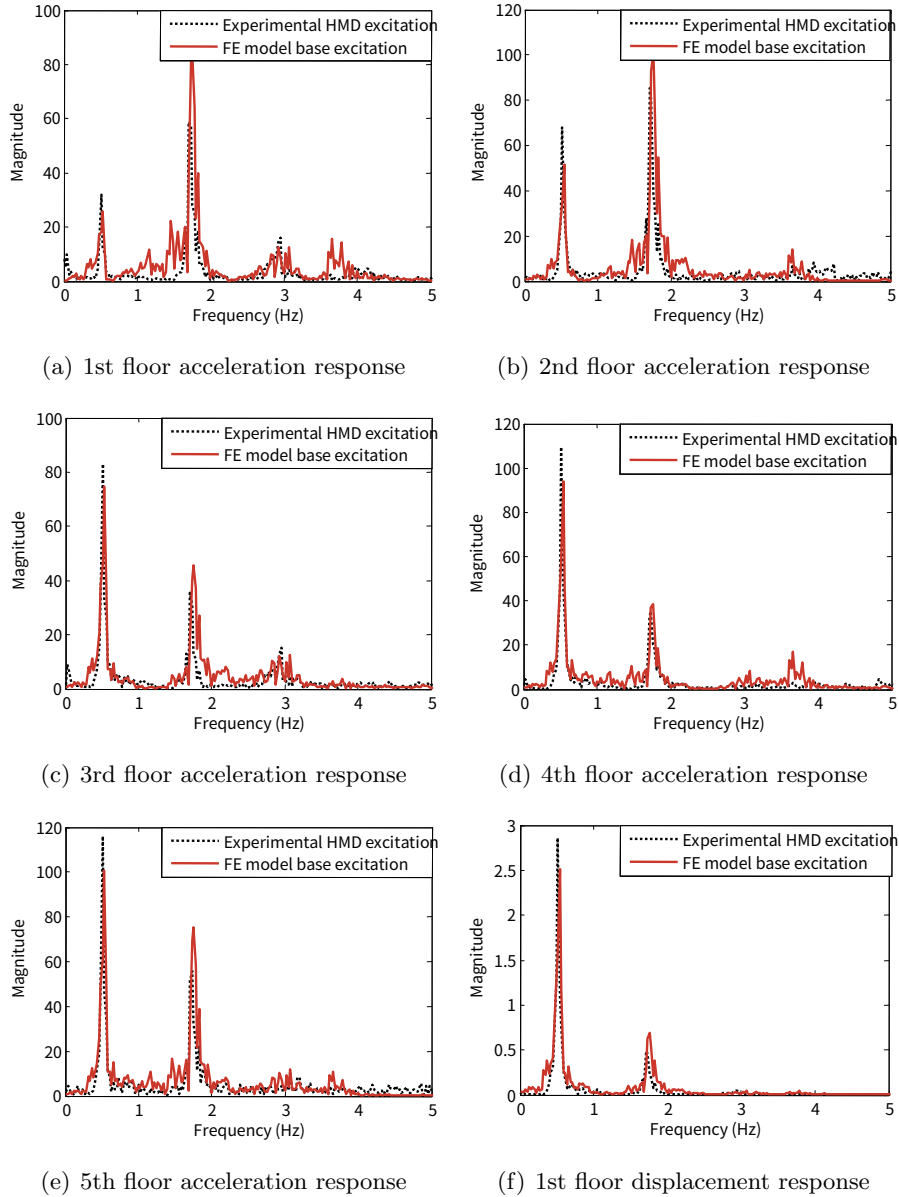


Figure 3.28: Comparison in frequency domain of El Centro earthquake response of the analysis and experimental models. (when the target response is the 5th floor acceleration).

this phenomenon, it should be designed to be able to excite higher mode which has fundamental frequencies of a structure.

Figure 3.30 compares the result in frequency domain of Hachinohe earthquake response in analysis model and experimental one. It is observed that the coincidence of the response at the first mode and second mode frequency

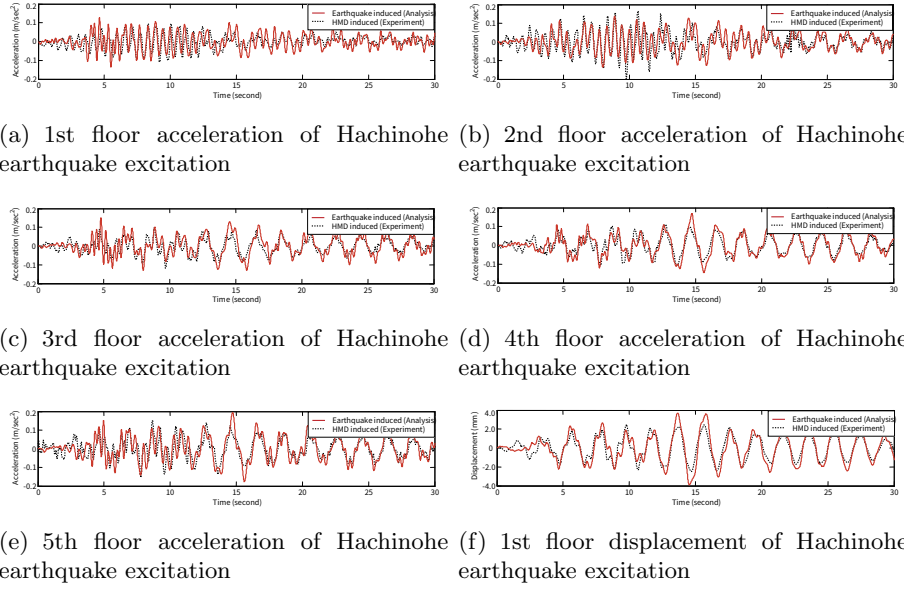


Figure 3.29: Time history comparison of Hachinohe earthquake response in the analysis and experimental models. (when the target response is the 5th floor acceleration).

was shown, but it would not reflect the responses at the third mode or higher mode frequency in Figures 3.30(a)-3.30(c).

3.2.7 Error Analysis

The normalized RMS error between the absolute acceleration induced by HMD and the base acceleration could be express as Eq. (3.23). Figure 3.31 is shown the floor distribute errors corresponding to the target responses of the analysis FE model. All responses are contained 10-20% error values and the minimal error value presented when the target response consider the 5th floor acceleration.

$$\text{Normalized RMS Error}(\%) \epsilon = \frac{\sum_{t=0}^T \left\{ \sqrt{\ddot{y}_g(t)^2} \right\} - \sum_{t=0}^T \left\{ \sqrt{\ddot{y}_h(t)^2} \right\}}{\sum_{t=0}^T \left\{ \sqrt{\ddot{y}_g(t)^2} \right\}} \quad (3.23)$$

where \ddot{y}_g , \ddot{y}_h are the structural acceleration responses which are the base acceleration and the HMD acceleration induced. T is total excitation time of the earthquakes.

Figure 3.32 shows the floor distribute errors of the experimental measured response corresponding to the target responses. All responses are contained 20-30% error values when the HMD induced.

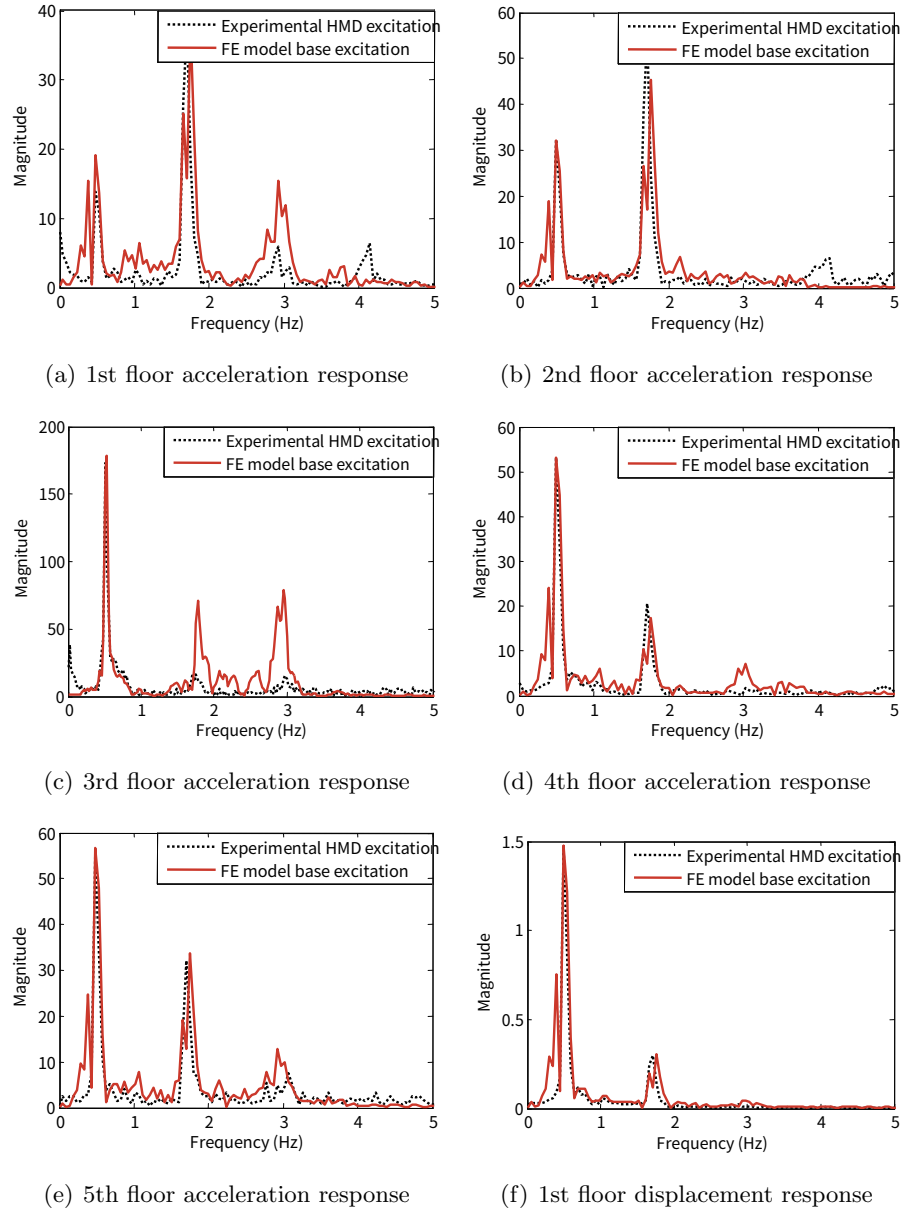


Figure 3.30: Comparison in frequency domain of Hachinohe earthquake response in the analysis and experimental models. (when the target response is the 5th floor acceleration).

3.2.8 Summary

In this section, filed measurement system of a full-scale structure and excitation system were established, and then forced vibration test was carried out using the Hybrid Mass Damper designed to simulate seismic load. System

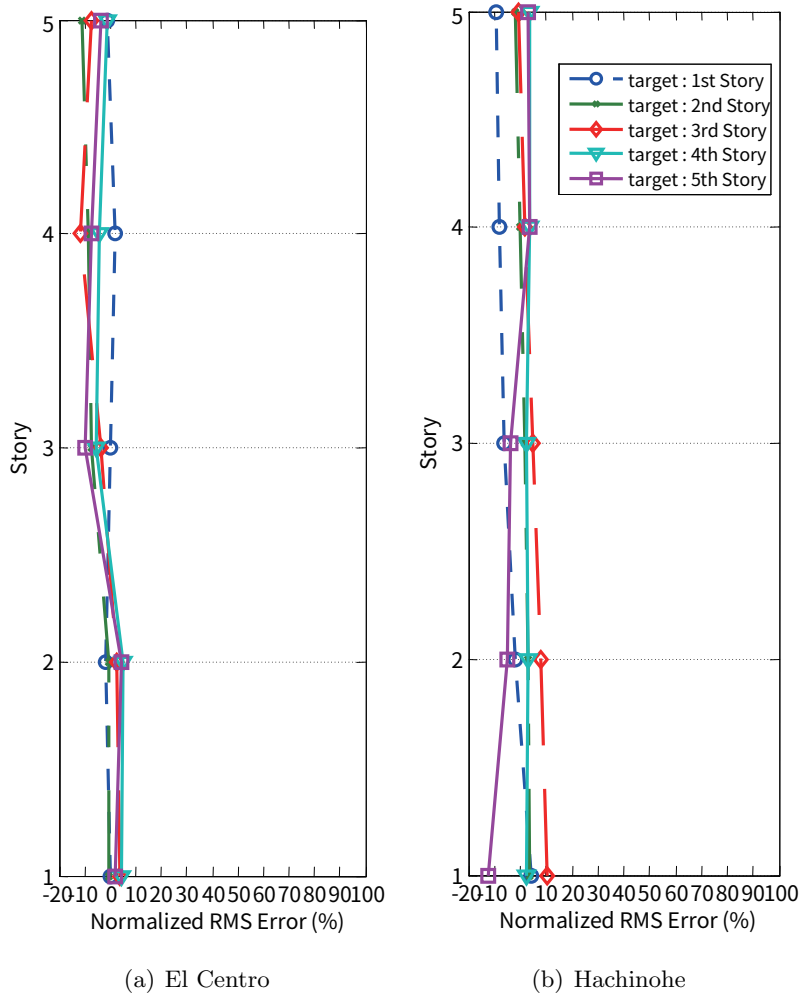


Figure 3.31: Normalized RMS error floor distribution of the analysis FE model corresponding the distributed floor acceleration response.

identification of the full-scale structure was carried out through white noise test and finite element model is updated. The seismic excitation system was accomplished through inverse transfer functions of structure and HMD by the system identifications. The propriety of seismic excitation system was verified by a comparison between the seismic numerical analysis results of finite element model and the experimental results of HMD excitation.

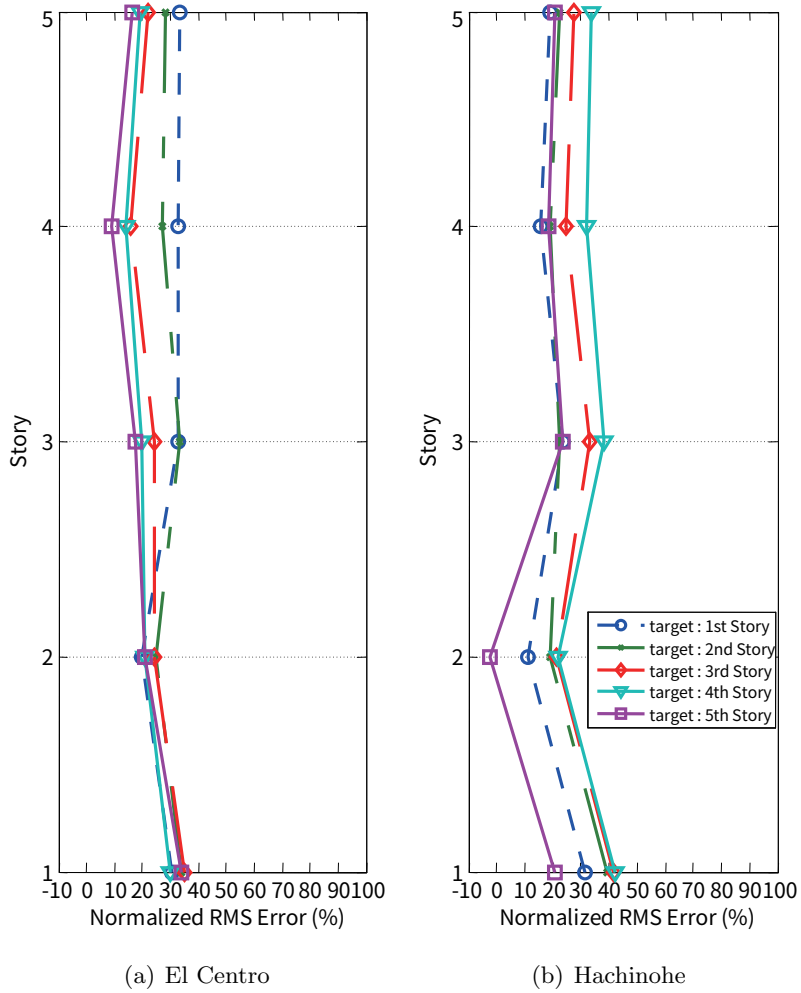


Figure 3.32: Normalized RMS error floor distribution of the experimental results corresponding the distributed floor acceleration response.

3.3 Forced vibration test of MR Damper-based Semiactive Control Algorithms for Full-scaled Building

3.3.1 Overview

In this section, the effectiveness of the MR damper-based semiactive control systems for seismic protection of a full-scale five-story steel frame building structure is experimentally verified, when some semi-active control algorithms such as the clipped-optimal control algorithm (CO), the maximum energy dissipation algorithm (MEDA), the Lyapunov stability theory based

control algorithm (LYAP) and the neuro-control algorithm are considered. This may be the first experimental investigation of several semiactive control algorithms using a full-scale test structure. In the experiment, two MR dampers are attached between the ground and the first floor. As described in previous section, the pseudo earthquake testing method are used to excite the building structure as if it is subjected to earthquake loading. This method uses filters that modify the displacement of the HMD using both transfer function in frequency domain and the least squares approximation in time domain. All the semiactive control algorithms are evaluated under four historical earthquakes (El Centro, Hachinohe, Kobe, and Northridge earthquakes) and one filtered artificial earthquake. The experimental results are compared with the passive optimal case which provides the specific constant voltage to the MR damper.

3.3.2 Full scaled MR Damper

Lee et al. (2010) had developed full-scaled MR damper, an MR damper is designed by deriving a suboptimal design procedure considering optimization problem and magnetic analysis, and a damper with the capacity of 1.0ton is manufactured.

Table 3.6: Results obtained from the magnetic analysis.

No. of stage	3	3	4
Flux density in steel	< 1.5T	> 1.5T	< 1.5T
Magnetic field intensity	< 150 kAmp/m	>150 kAmp/m	< 150 kAmp/m
Coil turns	20AWG/200 turns	20AWG/230 turns	21AWG/200 turns
Input current	3A	3A	3A

In order to use the designed MR dampers in the experiment, two MR dampers are manufactured as shown in Figure 3.33(a) and 3.33(b) and tested with harmonic dynamic displacements applied by a servo-hydraulic testing system. The result of variable current test is shown in Figure 3.33(c). As shown in Figure 3.33(c), the total damper force at design velocity (60mm/s) is about 10kN. Among the total force, the uncontrollable force is about 2kN or more and controllable force approximately 8kN or less.

3.3.3 Semi-active control algorithms

Semiactive control algorithms determine the most appropriate voltage in order to change viscous characteristics of the MR damper from the structural

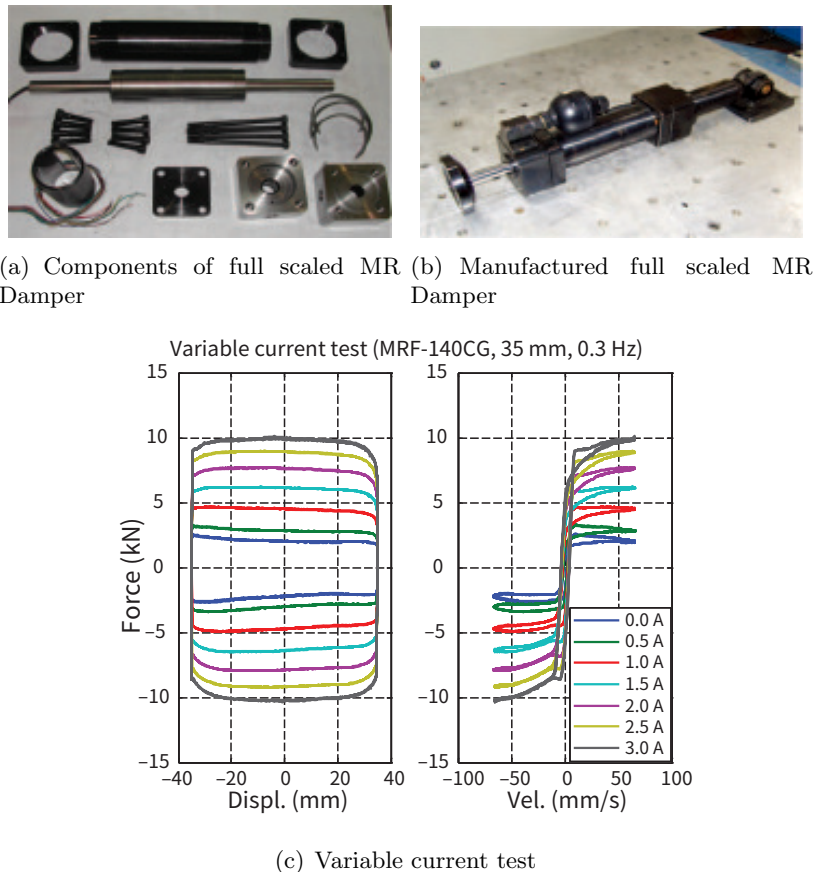


Figure 3.33: Manufactured MR damper and test result.

response measurements. Since the MR damper force is related with not only command voltage but also the relative velocity and displacement between both ends of the damper, the MR dampers cannot be directly controlled by the command voltage. So far various semiactive control algorithms have been proposed for control of MR dampers (Jansen and Dyke, 2000). In this section, four different control algorithms are considered; CO, LYAP, MEDA, and cost function-based SNC.

3.3.4 External excitation loads

In order to evaluate the performance of the MR damper-based semiactive control algorithms and passive control system, a suite of historical ground motions that are intended to encompass both moderate events and severe events is considered as external excitation load. Moreover, a filtered artificial earthquake (Kanai-Tajimi filter) is also adopted to verify the effectiveness of the control algorithms. Each historical ground motion and the artificial earthquake are scaled down in order to bound HMD by limited maximum

displacement for safety. Each ground motions used in this investigation are as follows and the acceleration of HMD and its power spectral density are shown in Figure 3.34 and 3.35.

Moderate events

- El Centro : N-S component of the 1940 Imperial valley, California earthquake (magnitude 7.1) recorded at Imperial Valley Irrigation District substation in El Centro, California, USA (scaled down to 0.303g);
- Hachinohe : N-S component of the 1968 Takochioki(Hachinohe) earthquake (magnitude 7.9) recorded at Hachinohe, Japan (scaled down to 0.265g);

Severe events

- Kobe : N-S component of the 1995 Hyogo-ken Nanbu(Kobe) earthquake (magnitude 7.2) recorded at Kobe Japanese Meteorological Agency (JMA), Kobe, Japan (scaled down to 0.318g);
- Northridge : N-S component of the 1994 Northridge earthquake (magnitude 6.8) recorded at the Sylmarcounty Hospital parking lot in Sylmar, California, USA (scaled down to 0.227g);

Artificial eartuquake

- Kanai-Tajimi filtered artificial earthquake (PGA:0.105g)

3.3.5 Measurement Devices and Feedback Control System

Measurement devices used in this experiment are displacement sensors, accelerometers, load cells, and current probe. The displacement sensors are used in measuring the relative displacement between ground and the first floor, which is the displacement of MR damper's both ends. When the MR dampers are installed, two LVDT type potentiometers (Midori America LP-19FB) are used. To the contrary, two laser displacement sensors (Optex CD4-350D) are used, when the MR dampers are not installed. Each floor's acceleration is measured by five accelerometers (PCB 393A03) and that of LAMD by Kyowa AS-2GB accelerometer. The load cells (CAS load cell LS-2T) measuring the MR damper control force are installed between the MR damper and the first floor. The current probes (Tektronix A622) measuring the current into each MR damper are also installed along the MR damper's power cable.

The measured data from the above measurement devices are collected and digitalized through a data acquisition system (NI DAQ-card 6062E).

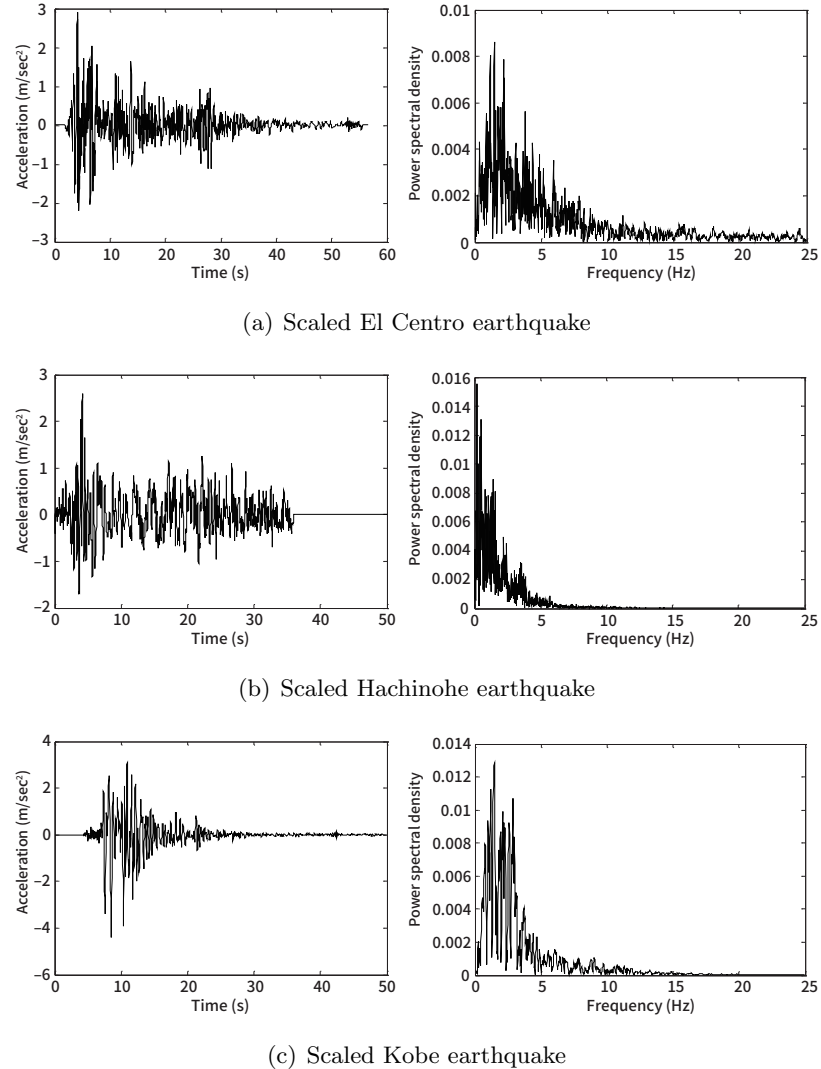


Figure 3.34: Acceleration of HMD and PSD used as external excitation load.

The collected data is selected for each semiactive control algorithm, and finally determined command voltage is sent to a current generator, which converts voltage to corresponding current. Then the MR damper is able to control the building structure with the generated current.

Finally, the MR damper-based semiactive feedback control system, which has 12 inputs and two outputs, can be formed as shown in Figure 3.3.5.

The CO as well as the cost function-based SNC algorithm needs full state or specific state of the structural system in order to calculate the appropriate desired control force. Actually, the control implementation requires a large amount of sensors and that would be even impossible. Therefore the Kalman filters as an observer for state estimation is desirable. Consider a

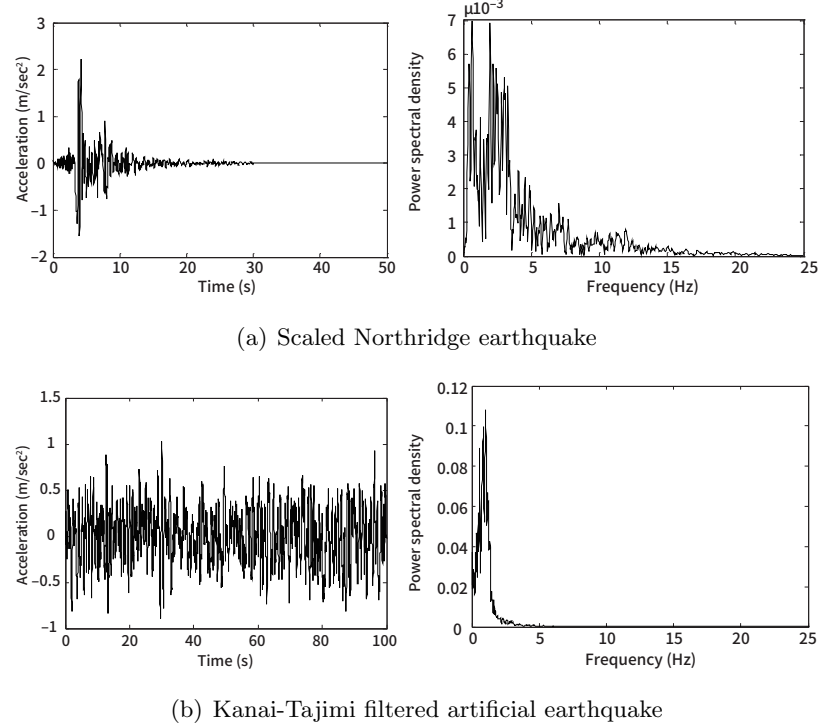


Figure 3.35: Acceleration of HMD and PSD used as external excitation load.

controllable and observable system and assume that full state estimation is required. Then the main purpose of the general Kalman filter is constructing a state estimate $\hat{\mathbf{x}}(t)$ that minimizes the steady-state error covariance which is defined by:

$$P = \lim_{t \rightarrow \infty} E \left([\mathbf{x} - \hat{\mathbf{x}}] [\mathbf{x} - \hat{\mathbf{x}}]^T \right) \quad (3.24)$$

The optimal estimator for the state of interest is the Kalman filter which can be expressed as:

$$\begin{aligned} \hat{\mathbf{x}} &= (\mathbf{A} - \mathbf{LC}) \hat{\mathbf{x}} + [\mathbf{L} \quad \mathbf{B} - \mathbf{LD}] \begin{Bmatrix} \mathbf{y} \\ \mathbf{u} \end{Bmatrix} \\ \begin{Bmatrix} \hat{\mathbf{y}} \\ \hat{\mathbf{x}} \end{Bmatrix} &= \begin{bmatrix} \mathbf{C} \\ \mathbf{I} \end{bmatrix} \hat{\mathbf{x}} + \begin{bmatrix} \mathbf{0} & \mathbf{D} \\ \mathbf{0} & \mathbf{0} \end{bmatrix} \begin{Bmatrix} \mathbf{y} \\ \mathbf{u} \end{Bmatrix} \end{aligned} \quad (3.25)$$

where filter gain \mathbf{L} is determined by solving an algebraic Riccati equation. The Kalman filter uses the known input \mathbf{u} and the measurements \mathbf{y} to generate the output and state estimates, that is, $\hat{\mathbf{y}}$ and $\hat{\mathbf{x}}$. Note that $\hat{\mathbf{y}}$ estimates the true system output without noises.

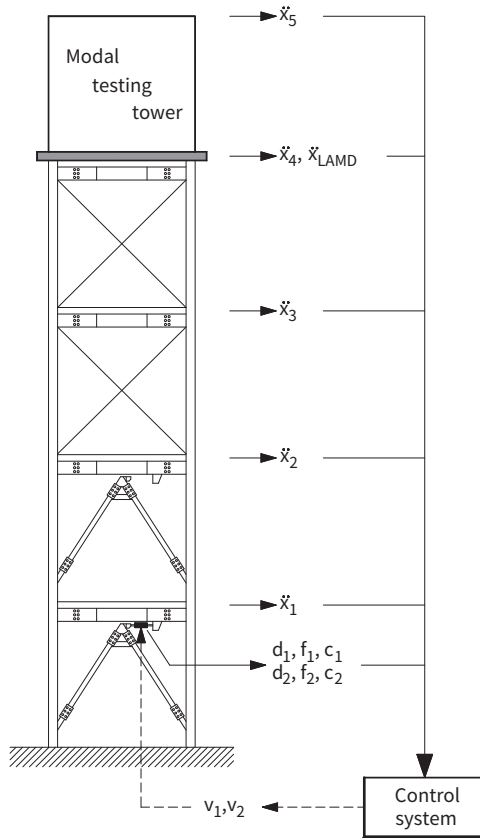


Figure 3.36: MR damper-based semi-active feed back control system.

3.3.6 Testing building model

All the stories in this building are 6m in height and are $6 \times 6m^2$ in plan. To investigate the modal characteristics of the building, a forced-vibration test is performed using a hybrid mass damper (HMD) located on the fourth floor in previous section. The building is excited by a white-noise signal with frequency components of 0-10 Hz, and the corresponding acceleration responses are then measured at each floor. Using these measured acceleration data, transfer functions in the frequency domain are obtained, as shown by the dotted lines in Figure 3.22. Finally, the structural damping and stiffness matrices are identified based on the experimentally obtained transfer functions, as shown by the solid lines in Figure 3.22. The estimated mass and the identified damping and stiffness matrices are given in Eqs. (3.26)-(3.28), respectively, with results of 0.52, 1.76, 2.95, 3.67, and 5.38 Hz for each mode.

$$\mathbf{M}_5 = \begin{bmatrix} 19365.5 & 0 & 0 & 0 & 0 \\ 0 & 19365.5 & 0 & 0 & 0 \\ 0 & 0 & 19365.5 & 0 & 0 \\ 0 & 0 & 0 & 19365.5 & 0 \\ 0 & 0 & 0 & 0 & 19365.5 \end{bmatrix} kg \quad (3.26)$$

$$\mathbf{C}_5 = \begin{bmatrix} 14.184 & -5.015 & 0.084 & -0.789 & 0.101 \\ -5.015 & 14.990 & -6.397 & 0.822 & -1.145 \\ 0.084 & -6.397 & 15.830 & -6.120 & -0.925 \\ -0.789 & 0.822 & -6.120 & 14.065 & -6.383 \\ 0.101 & -1.145 & -0.925 & -6.383 & 9.750 \end{bmatrix} kN \cdot s/m \quad (3.27)$$

$$\mathbf{K}_5 = \begin{bmatrix} 7473.953 & 4860.497 & 1295.606 & -908.262 & 432.162 \\ -4860.497 & 9640.722 & -6637.235 & 2446.225 & -926.951 \\ 1295.606 & -6637.235 & 10861.354 & -6005.863 & 748.607 \\ -908.262 & 2446.225 & -6005.863 & 9132.066 & -4852.783 \\ 432.162 & -926.951 & 748.607 & -4852.783 & 4543.854 \end{bmatrix} kNm \quad (3.28)$$

3.3.7 Experimental results

The passive control cases which provide specific constant voltage or current to the MR damper are the simplest means to operate the semiactive control using MR damper, because they need neither control algorithms nor measuring sensors. In this study, therefore, the passive optimal case is determined by a series of passively controlled experiments and compared with the performance of the other semiactive control algorithms.

Optimal Passive Case

As described above, passive control cases provide specific constant voltage or current to the MR damper. A passive-off case means a case of which voltage is always set to zero, and a passive-on case sets the voltage to maximum level. Since the maximum current level of the manufactured MR damper used in the experiments is 3.0A (Ampere), a series of passively controlled tests are conducted as increasing the current level from 0.0A to 3.0A by 0.5A to obtain the passive optimal case. Figures 3.37 and 3.38 show the normalized maximum displacement of the first floor and the normalized maximum acceleration among all the five floors.

It is demonstrated from Figure 3.37 that the performance in the maximum displacement gets better as the current input is increased. The passive-off case (i.e., 0.0A current input) shows the worst performance. In addition, the passive control cases with 1.0 or larger input current show the similar performance. As seen in Figure 3.38, however, there is no trend in the

performance of the normalized maximum acceleration. Under the moderate earthquakes and the artificial earthquake, most of the normalized values in maximum acceleration beneath 1.0 which means that the controlled seismic response might be reduced compared with that of the uncontrolled case. Nevertheless, most of the normalized values in acceleration are larger than 1.0 under the severe earthquake such as Kobe and Northridge earthquake. These results indicate that the MR damper-based passive control system is more suitable in moderate earthquake region than severe earthquake region for reducing the structural acceleration. From the abovementioned observation, the passive control case with 1.0A can be considered as the optimal passive case. The results in cases of the passive optimal (1.0A) and passive on (3.0A) cases are compared with those in the cases of the other semiactive control algorithms.

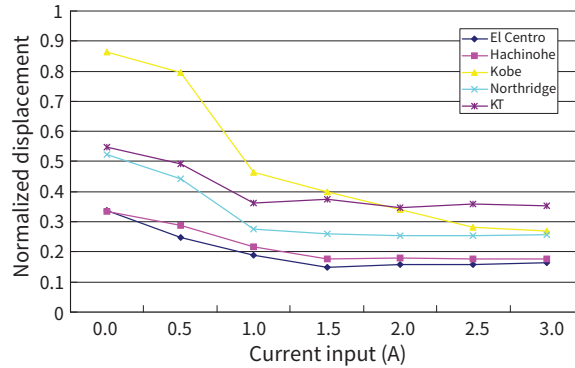


Figure 3.37: Normalized maximum displacement of passive control cases (first floor).

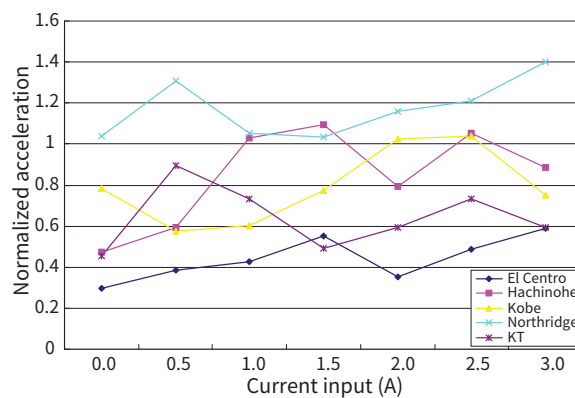


Figure 3.38: Normalized maximum acceleration of passive control cases.

Semiactive Control Cases

After the optimal passive case is determined, the full scale five-story steel frame building structure is excited with previously mentioned external excitation loads using LAMD and controlled with various semiactive control algorithms, such as the clipped optimal control algorithm (CO), the LYAP, the MEDA, and the SNC, using MR dampers. The responses of each control case are measured and summarized in Figures 3.39 and 3.40. Figure 3.39 shows the normalized maximum displacement of the first floor with various control algorithms and Figure 3.40 shows the normalized maximum acceleration among all the floors. From the experimental results, one can conclude as follows:

The CO shows good performance in reducing both displacement and acceleration. For severe earthquakes and artificial earthquake, however, the performance becomes slightly worse than that of moderate earthquakes. To obtain the better control performance from the CO, it should be designed more appropriately by altering the weighting parameters for the specific purpose of a designer. The Lyapunov algorithm and the SNC algorithm reduce the acceleration response well enough, but they cannot show the good performance in reducing displacement. In these cases, the MR dampers generate less control force than in the clipped optimal algorithm case. The Lyapunov algorithm shows the worst performance among five algorithms in reducing acceleration under the artificial earthquake, and the SNC has a drawback in reducing displacement under the severe earthquakes. Note that among all the semiactive control algorithms, the MEDA shows the best performance in reducing displacement and the worst performance in reducing acceleration. As the MEDA makes the MR dampers generate larger force, the first floor is almost locked with the ground. This causes a considerable increase of the acceleration response of the first floor. It is shown in some cases that maximum acceleration with controller is larger than that of the uncontrolled case. It is considered that in the experiments, the unexpected electrical and the external environmental noises are involved in the feedback of measured responses, which deteriorates the acceleration control performance that is sensitive to those noises. The passive optimal and passive on cases are one of the best control algorithms in reducing displacement of the structure except the performance in reducing acceleration. The inter-story drift between the first and second floors can be larger than the displacement of the first floor when the damper force is quite large. Owing to limitation in measuring displacements, inter-story drift of the second floor could not be measured. In order to verify the above observation, the inter-story drift of the second floor should be measured in the additional tests. The LYAP and SNC algorithms are appropriate in reducing accelerations of the structural system. On the other hand, the passive optimal and passive on cases and the MEDA show excellent performance in reducing the first floor displacement.

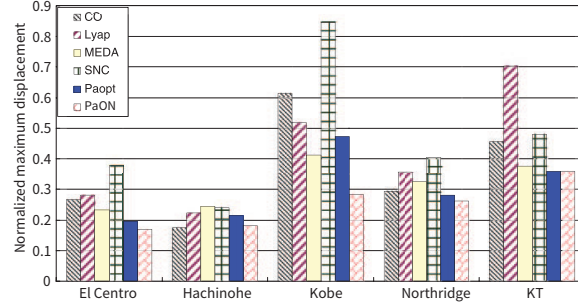


Figure 3.39: Normalized maximum displacement comparison of MR damper-based control systems.

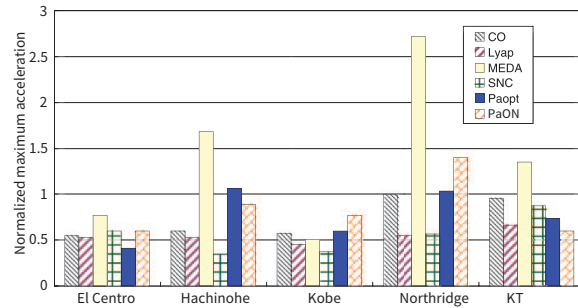


Figure 3.40: Normalized maximum acceleration comparison of MR damper-based control systems.

Figures 3.41 and 3.42 represent time history responses of displacement at first floor and acceleration at second floor, respectively. As shown in the figures, the structural responses in all the control cases are significantly reduced compared to the uncontrolled case results. Especially, some semiactive cases such as the neuro-control algorithm show the good performance in reduction of the acceleration at the second floor, while the passive cases show good performance in reduction of the displacement at the first floor.

3.3.8 Summary

The effectiveness of the MR damper-based control systems with various control algorithms for seismic protection of full-scale five-story steel frame building structure is experimentally verified in this investigation. An MR damper is designed by deriving a suboptimal design procedure considering optimization problem and magnetic analysis, and manufactured into 1.0ton MR damper in order to realize semiactive control systems. In the experiments, pseudo earthquake testing method are used to excite the building structure as if it is subjected to earthquake loading. Under the four historical earthquakes and one filtered artificial earthquake, various semiactive control

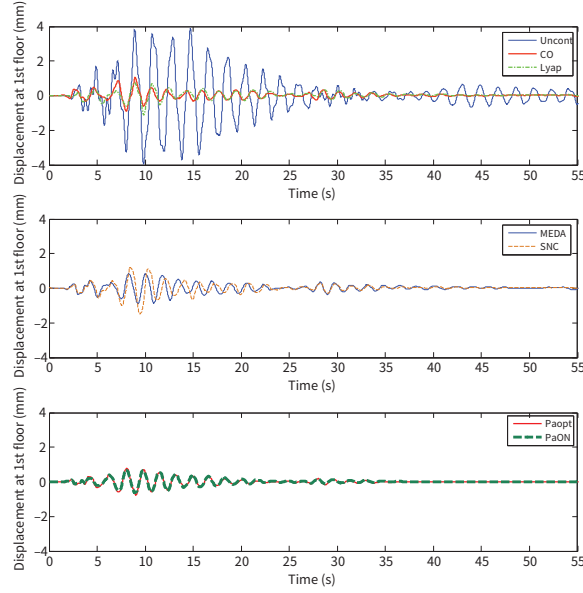


Figure 3.41: Time history responses of displacement at the first floor under the El Centro earthquake.

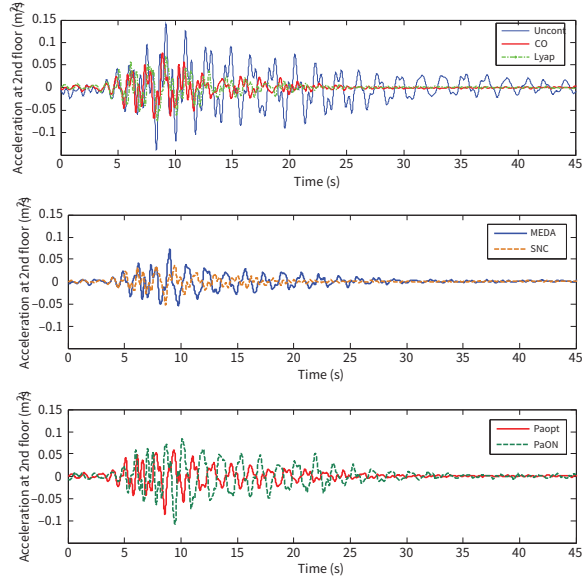


Figure 3.42: Time history responses of acceleration at the second floor under the Kobe earthquake.

algorithms including the passive optimal case are evaluated and compared with one another. From the series of passively controlled tests which are conducted as increasing the current level, the passive case with the input current

of 1.0A is chosen as the passive optimal system. From the experimental results, one can conclude that LYAP and SNC algorithms are appropriate in reducing accelerations of the structural system, and passive optimal case and MEDA shows excellent performance in reducing the first floor displacement.

CHAPTER 4

Hybrid Testing Method on a Semi-actively Controlled Building Structure Equipped with Full-scale MR Dampers

In this study, the investigation of the hysteretic behavior of an MR damper and the quantitative evaluation of the seismic performance of a building structure installed with an MR damper are carried out experimentally using the hybrid testing method. This component should be an electronic control unit or a real engine. The interface between simulated and physical components is achieved through the direct transfer of electrical signals, without actuation devices(Christenson et al., 2008). As described in chapter 2, hybrid testing method is a structural testing technique, in which the numerical integration of the equation of motion of a numerical substructure and the physical testing of an experimental substructure with severe non-linear characteristics are carried out simultaneously in real-time. In chapter 2, it has been performed both experimentally and analytically on the hybrid testing technique in order to overcome the difficulties in the testing of large-scale structures. This technique is especially useful for evaluating the performance of the nonlinear control device itself as well as that of the integrated system incorporated with the nonlinear control device such as MR damper.

4.1 Outline of Methodology

Figure 4.1 shows the concept of the hybrid testing method, which is experimentally implemented in this study. As shown in Figure 4.1(a), the structural response of a building model with n -degrees-of-freedom subjected to base input motion, $\ddot{x}_g(t)$, is controlled by an MR damper, which is typically located in the first story to reduce the maximum shear force of a bare structure. The whole system is divided into experimental and numerical substructures (Figure 4.1(b)). The MR damper is used as an experimental substructure because it is very difficult to numerically predict its exact dynamic behavior under seismic load, due to its strong non-linear characteristic of the dependency of the damper force on the loading rate and amplitude.

The remaining parts, that is, the structure without an MR damper, are analytically calculated. As shown in Figure 4.1(c), three procedures including the measurement of force, the numerical calculation of analytical parts, and the loading of the experimental substructure are used to implement hybrid testing method for the whole structural control system(Blakeborough et al., 2001). First, the force acting at the interface between experimental and numerical substructures (here, the control force generated by the MR damper), is measured by the load cell attached to an actuator. The value of this measured control force is then returned to the control computer for use in the calculation of the displacement constraint condition, which should be satisfied by both the experimental and numerical substructures. Finally, the MR damper physically tested in the laboratory is loaded by an actuator with respect to the displacement response of the story installed with the MR damper. The numerical substructure surrounded by the dotted line in Figure 4.1(c) is calculated based on the equation of motion for the building model equipped with an MR damper that is subjected to ground input acceleration, which is represented by:

$$\mathbf{M}\ddot{\mathbf{x}}(t) + \mathbf{C}\dot{\mathbf{x}}(t) + \mathbf{K}\mathbf{x}(t) = -\mathbf{M}\Gamma\ddot{x}_g(t) + \mathbf{H}f_e(t) \quad (4.1)$$

where, \mathbf{M} , \mathbf{C} , and \mathbf{K} represent the $n \times n$ structural mass, damping, and stiffness matrices, respectively; $\mathbf{x}(t)$ the $n \times 1$ vector of the relative structural displacement to the ground input motion; Γ the $n \times 1$ vector of the ground input motion influence coefficients; \mathbf{H} the $n \times 1$ vector that represents the location of the MR dampers; $\ddot{x}_g(t)$ the ground input acceleration; and $f_e(t)$ the control force exerted by the MR damper on the structure, in which subscript ‘e’ represent ‘experimentally’ measured control force.

To perform hybrid testing method, Eq. (4.1) is transformed into its state-space representation, which positively specifies the relationship between the input and output of the numerical substructure and can be written as:

$$\begin{aligned} \dot{\mathbf{z}}_s(t) &= \mathbf{A}_s \mathbf{z}(t) + \mathbf{B}_s \mathbf{u}(t) \\ \mathbf{Y}_s(t) &= \mathbf{C}_s \mathbf{z}(t) + \mathbf{D}_s \mathbf{u}(t) \end{aligned} \quad (4.2)$$

where $\mathbf{z}_s(t) = \{\mathbf{x}(t), \dot{\mathbf{x}}\}^\top$ is the $2n \times 1$ system state vector; $\mathbf{U}(t) = \{f_e(t), \ddot{x}_g(t)\}^\top$ the 2×1 system input vector; and $\mathbf{Y}_s(t) = \mathbf{x}(t)$ the $n \times 1$ system output vector. The $2n \times 2n$ system state matrix, \mathbf{A}_s , and the $2n \times 2$ location matrix of system input, \mathbf{B}_s , both associated with the system state variables, are represented by:

$$\begin{aligned} \mathbf{A}_s &= \begin{bmatrix} \mathbf{0}_{n \times n} & \mathbf{I} \\ -\mathbf{M}^{-1}\mathbf{K} & -\mathbf{M}^{-1}\mathbf{C} \end{bmatrix} \\ \mathbf{B}_s &= \begin{bmatrix} \mathbf{0}_{n \times 1} & \mathbf{0}_{n \times 1} \\ -\mathbf{M}^{-1}\mathbf{H} & -\Gamma \end{bmatrix} \end{aligned} \quad (4.3)$$

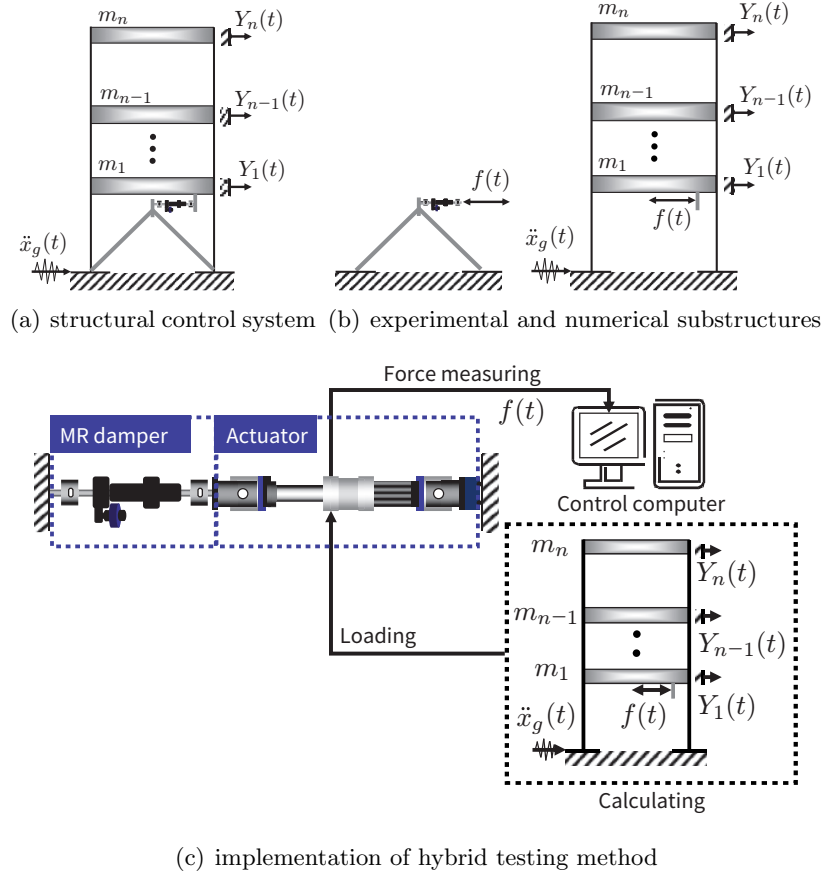


Figure 4.1: Conceptual view of hybrid testing method for a building with an MR damper.

and the $n \times n$ system out matrix, \mathbf{C}_s , and the $n \times 2$ direct transmission matrix, \mathbf{D}_s , both related to the system output variables, are given by:

$$\mathbf{C}_s = \mathbf{I}, \mathbf{D}_s = \mathbf{0}_{n \times 1} \quad (4.4)$$

In Eqs. (4.3) and (4.4), \mathbf{I} is the $n \times n$ unit matrix, while $\mathbf{0}_{n \times n}$ and $\mathbf{0}_{n \times 1}$ are the $n \times n$ and $n \times 1$ zero matrices, respectively. Note that, in the actual implementation of hybrid testing method, the system output vector, $\mathbf{Y}_s(t)$, in Eq. (4.2) should be designated as the story drifts where the MR dampers are installed and Eq. (4.4) should also be modified because these story drifts affect the system output vector.

A full-scale five-story steel frame building is considered as the model of the numerical substructure to use in the structural modal testing of this study, as shown in Figure 3.17.

When these identified structural properties are incorporated in the nu-

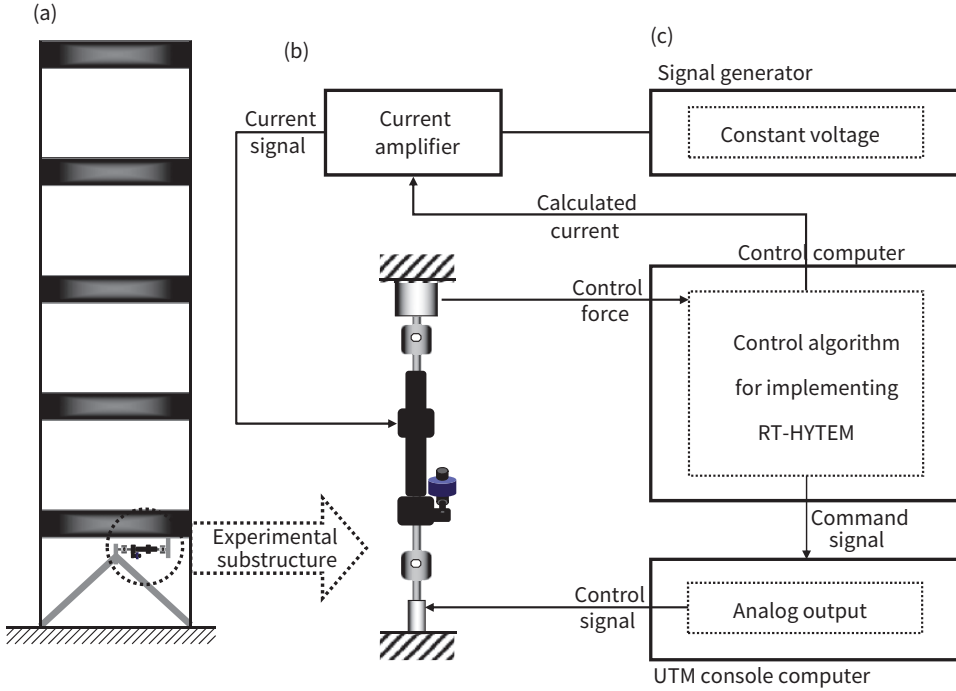


Figure 4.2: Schematic view of experimental set-up: (a) building model installed with an MR damper, (b) UTM installed MR damper, and (c) experimental instrumentation.

numerical substructure, Eqs. (4.2), (4.3) and (4.4) can be rewritten as Eqs. (4.5), (4.6) and (4.7), respectively.

$$\begin{aligned}\dot{\mathbf{z}}_n(t) &= \mathbf{A}_n \mathbf{z}_n(t) + \mathbf{B}_n \mathbf{u}(t) \\ \mathbf{Y}_n(t) &= \mathbf{C}_n \mathbf{z}_n(t) + \mathbf{D}_n \mathbf{u}(t)\end{aligned}\quad (4.5)$$

where, $\mathbf{Z}_n(t) = \{x_1(t), \dots, x_5(t), \dot{x}_1(t), \dots, \dot{x}_5(t)\}^\top$ is the 10×1 system state vector; $\mathbf{u}(t) = \{f_e(t), \ddot{x}_g(t)\}^\top$ the 2×1 system input vector; and $\mathbf{Y}_n(t) = \{x_1(t), \dots, x_5(t), \dot{x}_1(t), \dots, \dot{x}_5(t), \ddot{x}_1(t), \dots, \ddot{x}_5(t)\}^\top$ the 15×1 system output vector. The 10×10 system state matrix, \mathbf{A}_n , and the 10×2 location matrix of system input, \mathbf{B}_n , are represented by Eq. (4.6):

$$\begin{aligned}\mathbf{A}_n &= \begin{bmatrix} \mathbf{0}_{5 \times 5} & \mathbf{I} \\ -\mathbf{M}_5^{-1} \mathbf{K}_5 & -\mathbf{M}_5^{-1} \mathbf{C}_5 \end{bmatrix} \\ \mathbf{B}_n &= \begin{bmatrix} \mathbf{0}_{5 \times 1} & \mathbf{0}_{5 \times 1} \\ -\mathbf{M}_5^{-1} \mathbf{H}_5 & -\mathbf{\Gamma}_5 \end{bmatrix}\end{aligned}\quad (4.6)$$

and the 15×10 system out matrix, \mathbf{C}_5 , and the 15×2 direct transmission

matrix, \mathbf{D}_5 are given by Eq. (4.7)

$$\begin{aligned}\mathbf{C}_n &= \begin{bmatrix} \mathbf{I} & \mathbf{0}_{5 \times 5} \\ \mathbf{0}_{5 \times 5} & \mathbf{I} \\ -\mathbf{M}_5^{-1}\mathbf{K}_5 & -\mathbf{M}_5^{-1}\mathbf{C}_5 \end{bmatrix} \\ \mathbf{D}_n &= \begin{bmatrix} \mathbf{0}_{5 \times 1} & \mathbf{0}_{5 \times 1} \\ \mathbf{0}_{5 \times 1} & \mathbf{0}_{5 \times 1} \\ -\mathbf{M}_5^{-1}\mathbf{H}_5 & -\mathbf{\Gamma}_5 \end{bmatrix}\end{aligned}\quad (4.7)$$

In Eq. (4.6) and (4.7), \mathbf{I} is the 5×5 unit matrix, while $\mathbf{0}_{5 \times 5}$ and $\mathbf{0}_{5 \times 1}$ are the 5×5 and 5×1 zero matrices, respectively.

4.2 Controller Strategied for Hybrid Testing Method

4.2.1 Experimental Set-up

In general, the successful experimental implementation of hybrid testing method with high accuracy depends strongly on the dynamic performance of the actuators used to excite the experimental substructure in the test. Namely, the actuators used in the test should promptly react to applied command signals and load the experimental substructure. In this study, a universal testing machine (UTM), which is commonly used for the performance test of various structural materials, is utilized as an actuator to load the experimental part. Figure 4.3 shows the experimental set-up using UTM with the maximum loading capacity of 200kN and excitation frequency range of 0-10 Hz (Model name STL-HU10T). An MR damper, which can develop a control force ranging from 3 to 12 kN, is connected to this system. As shown in Figure 4.2, in order to perform RTHYTEM, three apparatuses with interconnected functions are equipped on the experimental set-up. The main task of the signal generator is to generate the current signal, by which an MR damper is operated and control force is exerted on the UTM. The control computer with a digital signal processing (DSP) board calculates the responses of the numerical substructure using the input (the control force measured from a load cell of the UTM), and sends the command signal to the UTM console computer. The primary task of the UTM console computer is to transfer the command signal generated by the control computer, according to the control algorithm for implementing hybrid testing method, to the UTM. Finally, the UTM excites the experimental part according to this control signal.

4.2.2 Controller Design of UTM

In order to accurately load the experimental substructure by an actuator and in accordance with the control algorithm of hybrid testing method,



Figure 4.3: Configuration of experimental system.

the dynamic property of the actuator itself between the command signal and the measured response should be appropriately compensated. Without this compensation, problems can occur with the experimental results such as chattering problems or the operating performance of the testing system can be degraded. In particular, during structural testing associated with vibration control issues, the control force often acts as an external load, and as a result, the experimental system can become unstable.

To experimentally measure the dynamics of UTM, white noise with a frequency ranging from 0 to 10Hz is used as the command signal, as shown in Figure 4.2, and the corresponding displacement of UTM that is driven by this signal is then measured. Using these input and output data sets in the time domain, the transfer function in the frequency domain, which corresponds to the dynamics of the UTM itself, is obtained.

The phase delay is compensated using the inverse transfer function (ITRF; Lee et al. (2007a,b)), in which the relationship between the input and output in the transfer function is reversed. Accordingly, the measured ITRF is obtained with the input of the measured displacement of the UTM and the output of the command signal, as shown by the dotted lines in Figure 4.4. This measured ITRF should be incorporated in the control computer as part of the control algorithm shown in Figure 4.2, in order to compensate the phase delay of the UTM and to correctly excite the experimental substructure. The measured ITRF is approximated using the `invfreqs` command in MATLAB(Coleman et al., 1999), which finds the real numerator and denominator coefficient vectors of the approximated transfer function in the form of a fractional expression by adopting the damped Gauss-Newton method for iterative search, which minimizes the sum of the squared error between the measured and the approximated frequency response points(Dennis Jr and Schnabel, 1983). The approximation result shown by the solid line in Figure 4.4 is given by the following second-order linear analog filter.

$$G^{-1}(s) = \frac{7.1945s^2 + 636.4862s + 27368.6533}{s^2 + 412.4726s + 27758.6756} \quad (4.8)$$

where the Laplace variable, s , equals $j\omega$ with the imaginary constant, j .

Figure 4.4 shows that, at 5 Hz, compensation on phase lag is attained only by 20° with the approximated ITRF, while the phase lag of 60° is observed in the measured ITRF. Further compensation would be possible with the use of other filters. However, further compensation is excluded here since it would have resulted in an unstable ITRF.

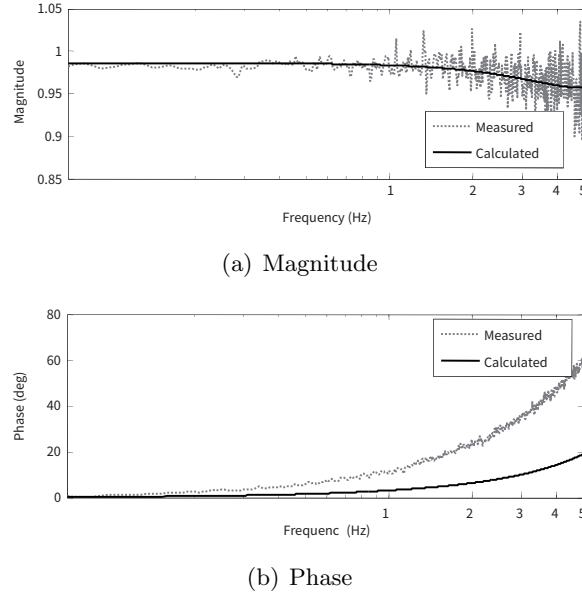


Figure 4.4: Measured and approximated ITRFs from the displacement of UTM to the command signal.

Eq.(4.8) is converted into the following statespace realization for implementation in the control computer.

$$\begin{aligned} \mathbf{y}_s &= \mathbf{A}_i \mathbf{y}_s(t) + \mathbf{B}_i r(t) \\ c(t) &= \mathbf{C}_i \mathbf{y}_s(t) + D_i r(t) \end{aligned} \quad (4.9)$$

where \mathbf{y}_s , $r(t)$ and $c(t)$ are the 2×1 state vector, the 1×1 reference signal, and the 1×1 command signal of the UTM, respectively; and \mathbf{A}_i , \mathbf{B}_i , \mathbf{C}_i and \mathbf{D}_i are the 2×2 , 2×1 , 1×2 and 1×1 system matrices, respectively.

4.3 Experimental Implementation

4.3.1 Integrated Controller of the Numerical Substructure and UTM

The numerical substructure and the approximated ITRF explained above are incorporated into the control computer as an integrated controller to implement hybrid testing method, as shown by the shaded area in Figure 4.5. First, when the constant current sent from the signal generator for the passive control test and the calculated current of semi-active control algorithms sent from the analog output for the semi-active control test are applied to the MR damper, the control force proportional to the magnitude of the current signal is developed and transferred to the UTM. The drift response, $x_1(t)$, of the first story where the MR damper is positioned is then calculated

from the numerical substructure, given by Eq. (4.5), with two inputs: the control force, $f_e(t)$, measured from the load cell attached to the UTM and the ground input acceleration, $\ddot{x}_g(t)$ given by the user. The motion of the UTM is driven by the controller using the ITRF, represented by Eq (4.9), so that the UTM itself operates as the first story where the MR damper is located, and excites the MR damper that should be physically tested. In the actual experimental implementation of hybrid testing method, the continuous filters shown in Figure 4.5 are converted into discrete filters with a time interval of 0.01s, while MATLAB *Simulink*(Simulink, 2009) and *Real-Time Windows Target*(Target, 2009) are used as the control system.

4.3.2 Experimental Verification for Simple Bouc-Wen Model

hybrid testing method with a sinusoidal wave excitation is carried out to investigate the hysteretic behavior of the MR damper and to verify the hybrid testing method experimentally implemented in this study. A current of 0 A is applied to the MR damper and a sine wave with a frequency of 0.52 Hz, which corresponds to the fundamental frequency of the numerical substructure, and with an amplitude of $5m/s^2$ is used as the ground input acceleration as shown in Figure 4.5.

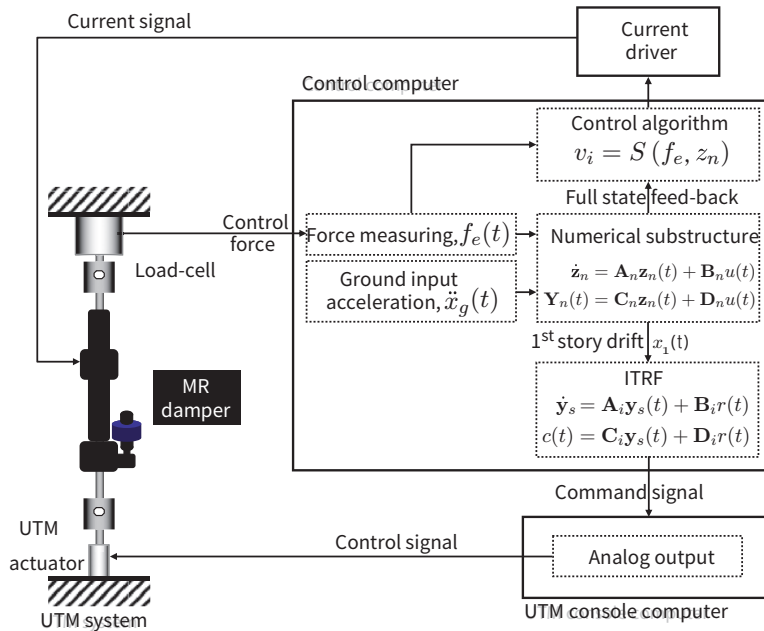


Figure 4.5: Integrated controller for implementing RTHTM.

Parametric identification is then performed to find the numerical model of the MR damper on the basis of the experimentally measured hysteretic loop. The Bouc-Wen model is widely used for modeling various hysteretic

loops(Wen, 1976). The control force by the MR damper can also be specified using this model. The force described by this model is represented by:

$$f_{MR}(t) = \alpha z(t) + c_{MR}\dot{x}_1(t) + k_{MR}x_1(t) + f_0 \quad (4.10)$$

where, k_{MR} and c_{MR} are the stiffness and viscosity of the MR damper; f_0 the initial friction force; z a dimensionless valuable introduced to describe the hysteresis; and α a variable that regulates the effect of z on $f_{MR}(t)$ which depends on the magnetic field; z is given by the following differential equation.

$$\dot{z}(t) = -\gamma|\dot{x}_1(t)|z(t)|z(t)|^{n-1} - \beta\dot{x}_1(t)|z(t)|^n + A\dot{x}_1(t) \quad (4.11)$$

where γ , β , A and the superscript n are the coefficients determining the shape of the hysteretic curve.

The eight parameters in Eqs. (4.10) and (4.11) (α , c_{MR} , k_{MR} , f_0 , γ , n , β and A) are identified using least-squares optimization to minimize the performance index defined as:

$$J(\mathbf{p}) = \sum_{k=1}^N [f_e(k \cdot \Delta t) - f_{MR}(\mathbf{p}, k \cdot \Delta t)]^2 \quad (4.12)$$

where $f_e(k \cdot \Delta t)$ represents the force data measured at the k -th sampling time; \mathbf{p} the 1×8 vector of the identification parameter, $\{\alpha, c_{MR}, k_{MR}, f_0, \gamma, n, \beta, A\}$; and $f_{MR}(\mathbf{p}, k \cdot \Delta t)$ the force obtained at the k -th calculating time from Eq. (4.10) and (4.11) using the parameter \mathbf{p} .

This procedure is carried out using MATLAB subroutines(Coleman et al., 1999), and the identified parameters are given by:

$$\begin{aligned} \alpha &= 13288.130(N/m), & c_{MR} &= 81418.582(N \cdot s/m), \\ k_{MR} &= 16647.456(N/m), & f_0 &= 6.10(N), \\ n &= 3.0581, & \gamma &= 471409.377(m^{-n}), \\ \beta &= 335518.804(m^{-n}), & A &= 497.295 \end{aligned} \quad (4.13)$$

A comparison between the calculated and experimental responses is provided in Figure 4.6. The displacement and velocity in Figures 4.6(b) and 4.6(c) correspond to the first-story drift and velocity responses, respectively. The Bouc-Wen model represents the force-displacement and the force-velocity hysteretic behaviors of the damper well.

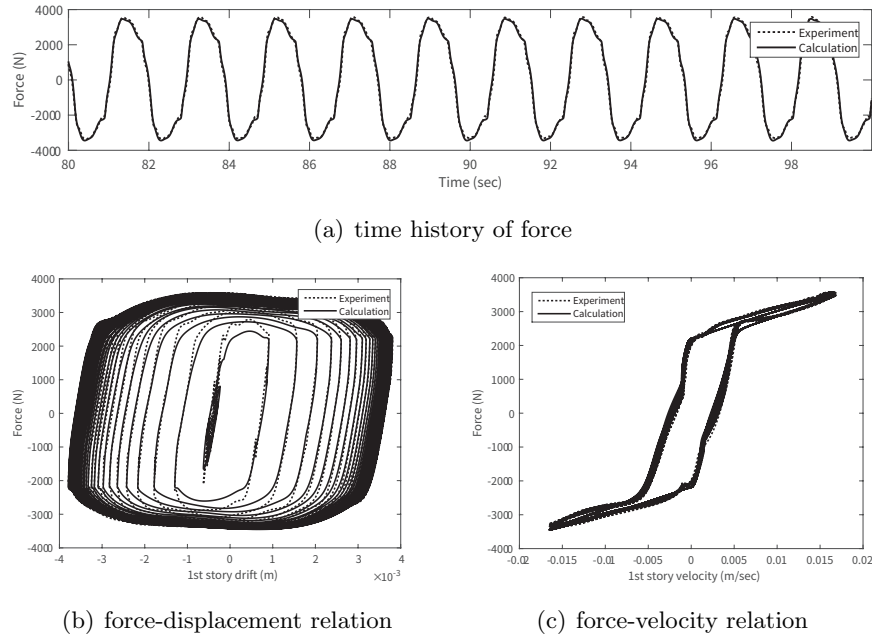


Figure 4.6: Comparison between calculated and experimentally measured responses for the Bouc-Wen model.

The hybrid testing method implemented in this study is verified by experiment using the excitation of historical seismic measurements. Four different records of earthquake acceleration measurements taken at El Centro, Hachinohe, Kobe, and Northridge are used as ground input acceleration in Figure 4.5 by multiplying them by 0.05. Also, the current of 0 [A] is applied to an MR damper in the same manner as the sinusoidal excitation test above. In addition to the measurement of the control force produced by an MR damper, given by Eqs. (4.5)-(4.7), the structural displacement, velocity, and absolute acceleration responses are obtained from hybrid testing method for earthquake excitations. Figures 4.7 and 4.8 show a comparison of the responses measured from hybrid testing method, as shown in Figure 4.5, with those calculated from the five-story building model installed with an MR damper with the identified parameters such as in Eq. (4.13), in order to compute the control force.

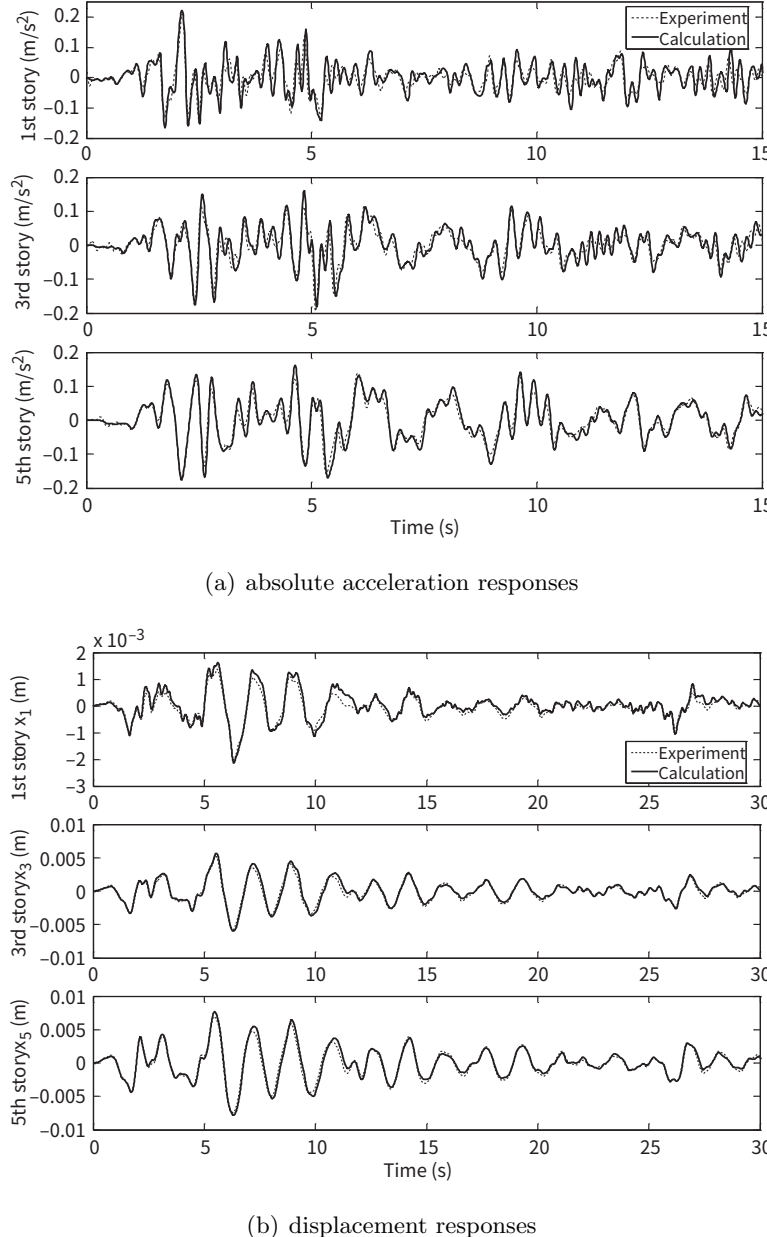


Figure 4.7: Comparison between calculated and experimentally measured responses under El Centro earthquake excitation.

In addition, the measured and calculated hysteretic behaviors, shown in Figures 4.9 and 4.10, are compared for different seismic excitations. Figures 4.7 and 4.8 show that the two results agree well with each other. Figures 4.9 and 4.10 show that the Bouc-Wen model successfully predicted the overall hysteretic behaviors. In particular, the Bouc-Wen model successfully predicted the hysteretic behavior of an MR damper under the excitation

of the seismic measurements of a narrow frequency band, such as those of the Kobe and Northridge earthquakes corresponding to the representative examples of near-fault source ground motion.

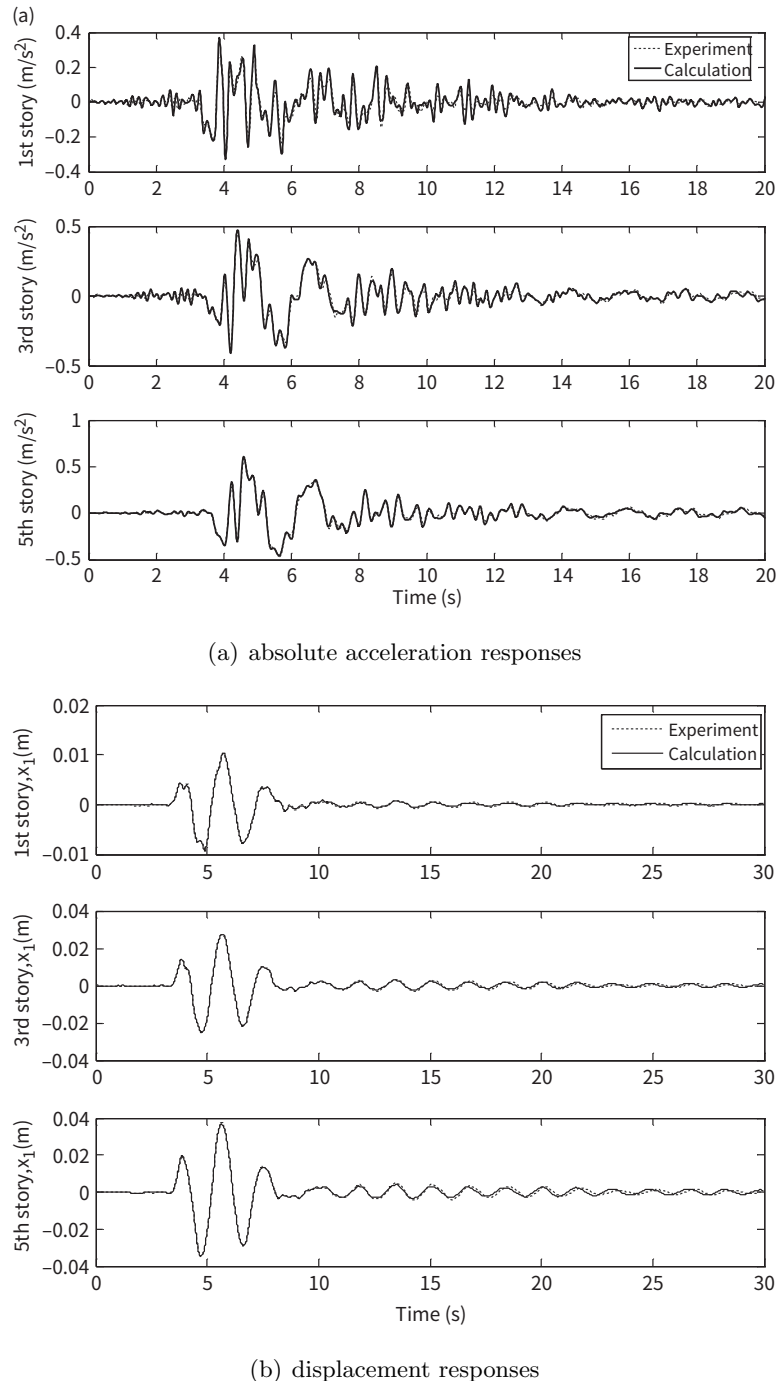


Figure 4.8: Comparison between calculated and experimentally measured responses under Northridge earthquake excitation.

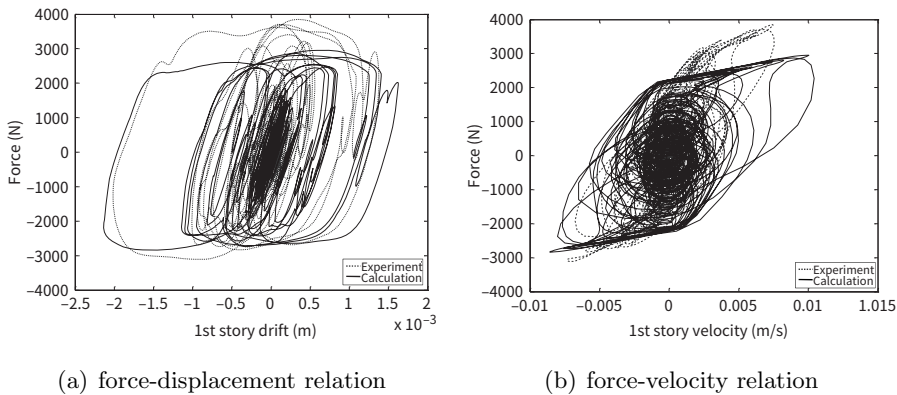


Figure 4.9: Comparison between calculated and experimentally measured hysteresis under El Centro earthquake excitation.

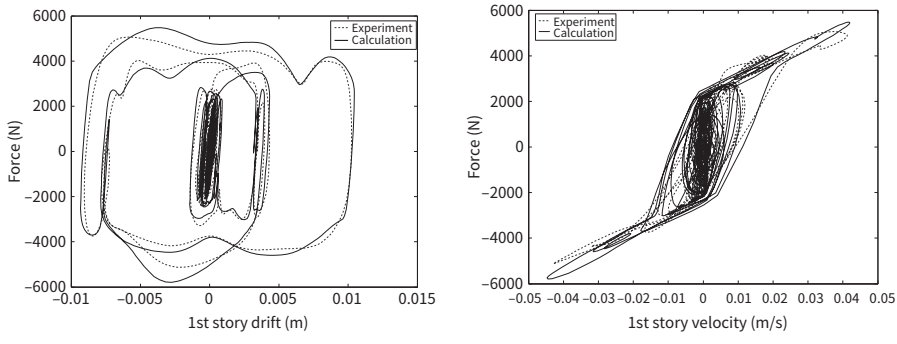


Figure 4.10: Comparison between calculated and experimentally measured hysteresis under Northridge earthquake excitation.

4.3.3 Applied Semi-active Control Algorithms

OPTIMIZATION OF BOUC-WEN PARAMETER BY INPUT CURRENTS

In order to compare the results of the numerical analysis with the results of the semi-active hybrid testing method, the identification of the Bouc-Wen parameter corresponding to input currents is required. In this study, a sinewave excitation test is implemented and Bouc-Wen parameters (α , A , c_{MB}) are identified.

Figure 4.11 shows a comparison between the test model and the identified Bouc-Wen model with respect to different input currents. The optimal parameter of the Bouc-Wen model is established by force-velocity and force-displacement relationships, as shown in Figure 4.11(a) and 4.11(b).

For implementing the semi-active control of an MR damper, three parameters which are assumed to be polynomial exponential functions of the input current are identified using the least square method. Figures 4.11(c)-4.11(e) show the results of each parameter identified and tested.

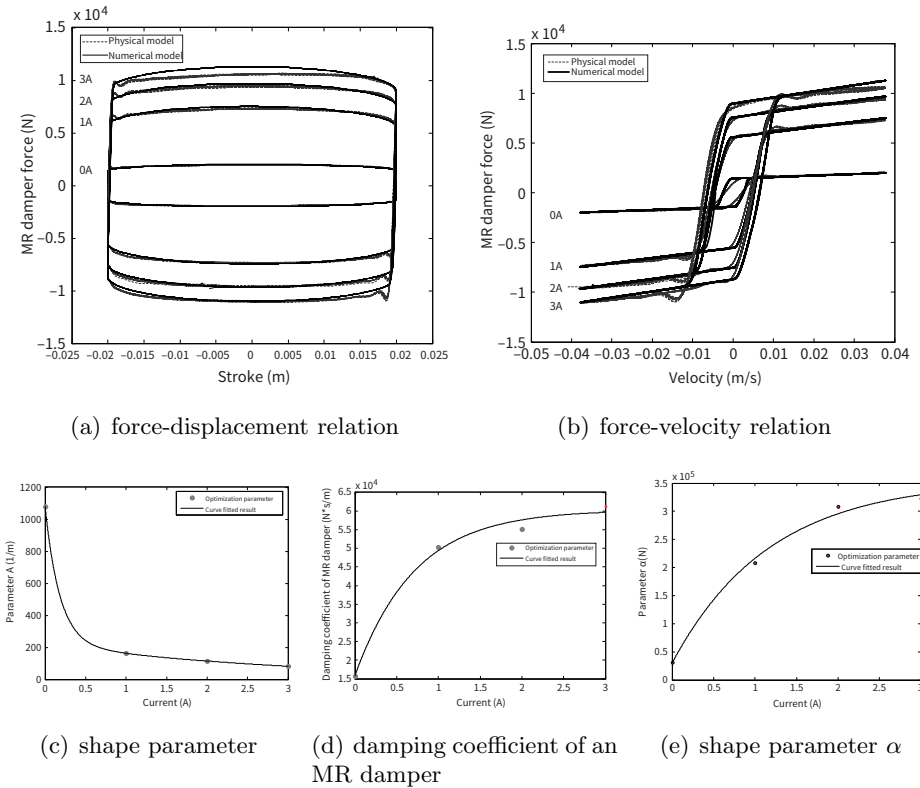


Figure 4.11: Identified Bouc-Wen parameters and the numerical model of an MR damper.

$$\alpha = -324576.03 \exp(-0.85x) + 354777.40 \quad (4.14)$$

$$c_{MR} = -44567.17 \exp(-1.4x) + 60330.96 \quad (4.15)$$

$$A = 854.7 \exp(-5.476x) + 222.5 \exp(-0.3321x) \quad (4.16)$$

where, x is input current (A)

Clipped-optimal Control Algorithm

In terms of implementation, this control strategy seems to be the most direct because it can take advantage of the significant number of experimental and practical studies that have been conducted on active control strategies. The clipped-optimal algorithm that has been shown to be effective for use with

the MR damper has been proposed by Dyke et al. (1996). The clipped-optimal control approach involves designing a linear optimal controller $\mathbf{K}_c(s)$ that calculates a vector of desired control forces $\mathbf{f}_c = \{f_{c_1}, f_{c_2}, \dots, f_{c_n}\}^\top$ based on the measured structural responses \mathbf{y} and the measured control force vector \mathbf{f} applied to the structure, that is,

$$\mathbf{f}_c = \mathcal{L}^{-1} \left\{ -\mathbf{K}_c(s) \mathcal{L} \{\mathbf{y}, \mathbf{f}\}^\top \right\} \quad (4.17)$$

where, $\mathcal{L} \{\cdot\}$ is the Laplace transform.

Because the force generated in the MR damper is dependent on the local responses of the structural system, the desired optimal control force f_{c_i} cannot always be produced by the MR damper. Only the control voltage v_i can be directly controlled to increase or decrease the force produced by the device. Thus, a force feedback loop is incorporated to induce the MR damper to approximately generate the desired optimal control force f_{c_i} .

To induce the MR damper to approximately generate the corresponding desired optimal control force f_{c_i} , the command signal v_i is selected as follows. When the i -th MR damper is providing the desired optimal force, the voltage applied to the damper should remain at the present level. If the magnitude of the force produced by the damper is smaller than the magnitude of the desired optimal force and the two forces have the same sign, the voltage applied to the current driver is increased to the maximum level so that the force produced by the damper is increased to match the desired control force. Otherwise, the commanded voltage is set to zero. The algorithm for selecting the command signal for the i -th MR damper is stated as Eq. (4.18) (Jansen and Dyke, 2000).

$$v_i = V_{\max} H(\{f_{c_i} - f_i\} f_i) \quad (4.18)$$

Although a variety of approaches may be used to design the optimal controller, linear quadratic regulator (LQR) methods are advocated because of their successful application. The optimal gain of a state vector based on the target building model with MR damper is used as follows:

$$\begin{aligned} \mathbf{K}_c = [& -98301479.1, 110902868.9, \\ & -36659599.6, 24569454.5, -12841877.0, \\ & -4926535.9, -3813412.5, -331115.5, \\ & -1239172.8, -1309155.8] \end{aligned}$$

For implementing the hybrid testing method experiment, the integrated MATLAB *Simulink* controller is designed as shown in Figure 4.12. In the field testing application of this control law, it is required that a full structural state vector be obtained using a filter estimation method such as Observer/Kalman. However, because hybrid testing method uses the structural

model as a numerical model, this method has the advantage that the structural state variable be easily used in the experiment.

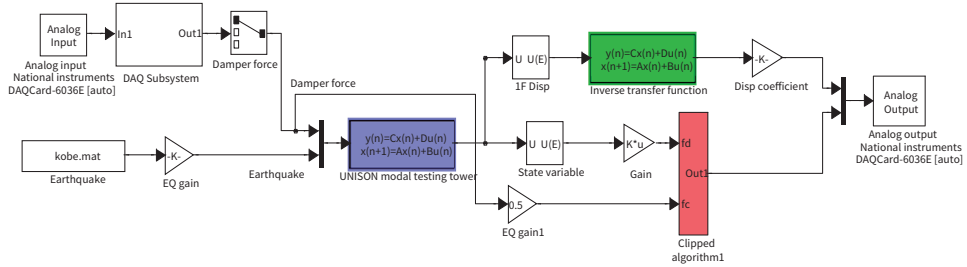


Figure 4.12: Clipped-optimal and hybrid testing method integrated controller.

MODULATED HOMOGENEOUS FRICTION ALGORITHM (MHF)

This control strategy is originally developed for a variable-friction damper. In this approach, at every occurrence of local extremes in the deformation of the device, the normal force applied to the frictional interface is updated to a new value. At each local minimum or maximum in the deformation, the normal force $N_i(t)$ is chosen to be proportional to the absolute value of the semi-active damper deformation. The control law is written as Eq. (4.19)(Inaudi, 1997):

$$N_i(t) = g_i |P[\Delta_i(t)]| \quad (4.19)$$

where g_i is a positive gain and the operator $P[\cdot]$ as the prior-local-peak operator is defined as $P[\Delta_i(t)] = \Delta_i(t-s)$, where $s = \left\{ \min x \geq 0 : \dot{\Delta}(t-x) = 0 \right\}$, defining $\Delta(t-s)$ as the most recent local extreme in the deformation. Because this algorithm was developed for variable friction devices, the following modifications are needed when applying it to MR dampers.

- (i) There is often no need to check if the force is greater than the static friction, because MR dampers have no static friction.
- (ii) A force feedback loop is used to induce the MR damper to produce approximately the frictional force corresponding to the required normal force.

Thus, the goal is to generate a required control force with a magnitude of:

$$f_{n_i} = \mu g_i |P[\Delta_i(t)]| = g_{n_i} |P[\Delta_i(t)]| \quad (4.20)$$

where the proportionality constant g_{n_i} has a unit of stiffness N/mm.

As with the clipped-optimal control law, because the force produced by the MR damper cannot be directly commanded, a force feedback loop is

used. The measured force is compared to the desired force determined by Eq. (4.20), and the resulting control law is:

$$v_i = V_{\max} H (f_{n_i} - |f_i|) \quad (4.21)$$

where V_{\max} is the maximum current value that can be offered for the MR damper.

An appropriate choice of g_{n_i} will maintain the force f_{n_i} within the operating envelope of each MR damper for the majority of the time, allowing the MR damper forces to closely approximate the desired force of each device. However, the optimal value of g_{n_i} is dependent on the amplitude of the ground acceleration. In this study, the g_{n_i} value is chosen as 150 kN/m based on the excitation of three earthquakes.

In addition, note that this control law is quite straightforward to implement because it only requires the measurement of the applied force and the relative displacements of the control device.

For applying the hybrid testing method experiment, the integrated MATLAB *Simulink* controller is designed as shown in Figure 4.13.

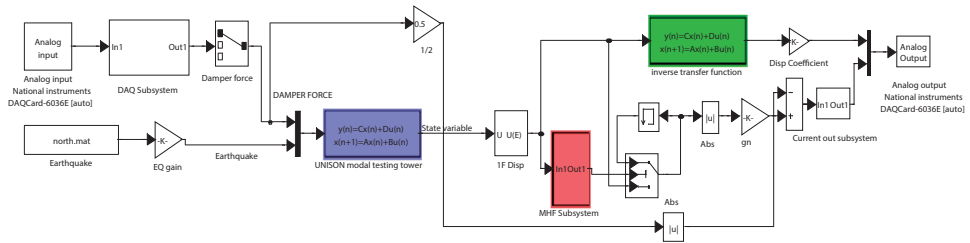


Figure 4.13: MHF and hybrid testing method integrated controller.

4.4 Testing Result

4.4.1 Passive Control Performance

The hybrid testing method illustrated in Figure 4.5 is implemented to evaluate the seismic performance of the passive-controlled MR damper used in this study. With the exception of the variation of the applied current to the MR damper (in the same manner as that above), four earthquake records are also given as the ground accelerations in Figure 4.5. The tests for the controlled case are carried out by increasing the current applied to the MR damper from 0 to 3 A. As shown in Figure 4.6, the test for the uncontrolled case is performed by removing the feedback loop of the control force generated by an MR damper into the control computer. Therefore, the numerical substructure is excited only by the ground input acceleration (even though a current of 0A was applied to the MR damper).

Figures 4.14 and 4.15 show comparisons for the selected floors of the time histories of experimentally measured structural displacement responses to the excitation of two earthquake excitations, as the current applied to the MR damper is varied. Significant control effects are observed between the uncontrolled and the passiveoff case, but are not observed in the other passive-on cases with the increase of the applied current.

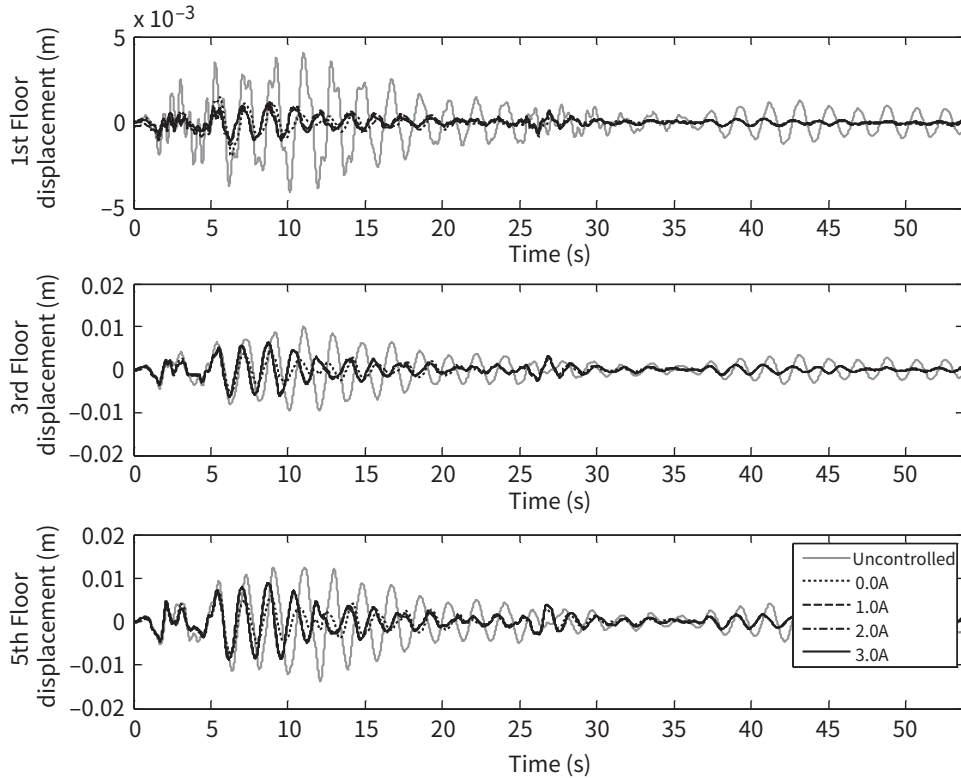


Figure 4.14: Experimental results, in the time domain under El Centro earthquake excitation at different applied currents.

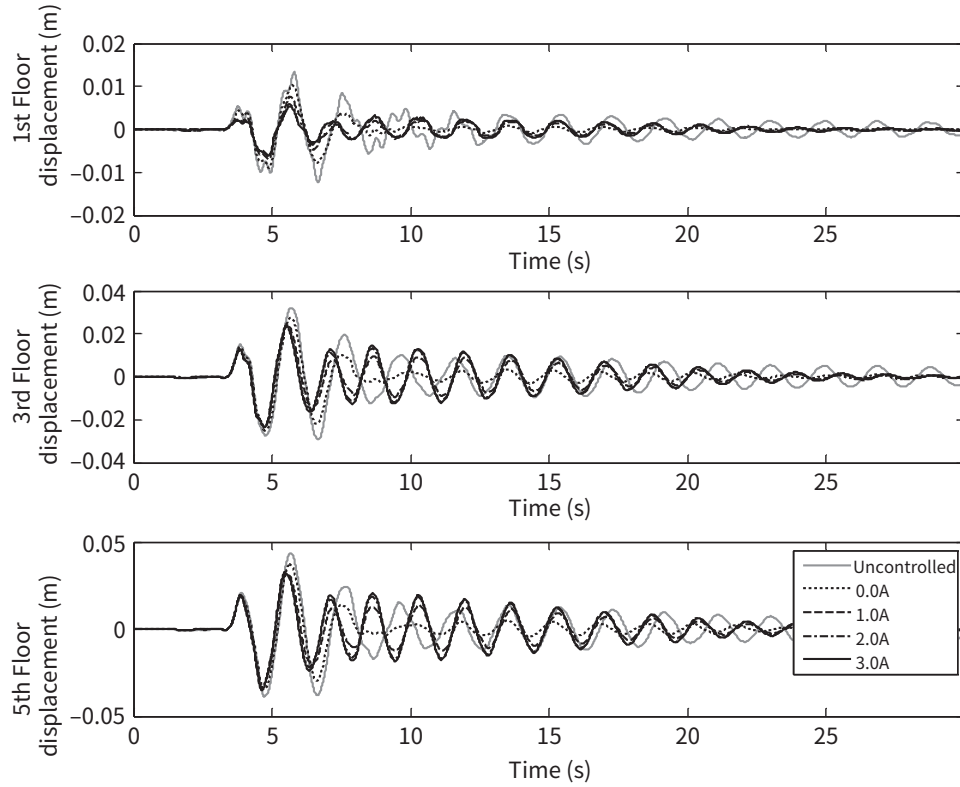


Figure 4.15: Experimental results, in the time domain under Northridge earthquake excitation at different applied currents.

In addition, the displacement responses in the frequency domain to four earthquake excitations at different applied currents are compared for the first floors, as shown in Figure 4.16. The figures show that the peak in the uncontrolled case appears at 0.52 Hz, corresponding to the fundamental frequency of the numerical substructure under consideration, but the peak is shifted to the vicinity of 0.62 Hz as the applied current increases. This small amount of frequency shifting is due to the stiffening effect of the MR damper used in this study as the applied current is increased.

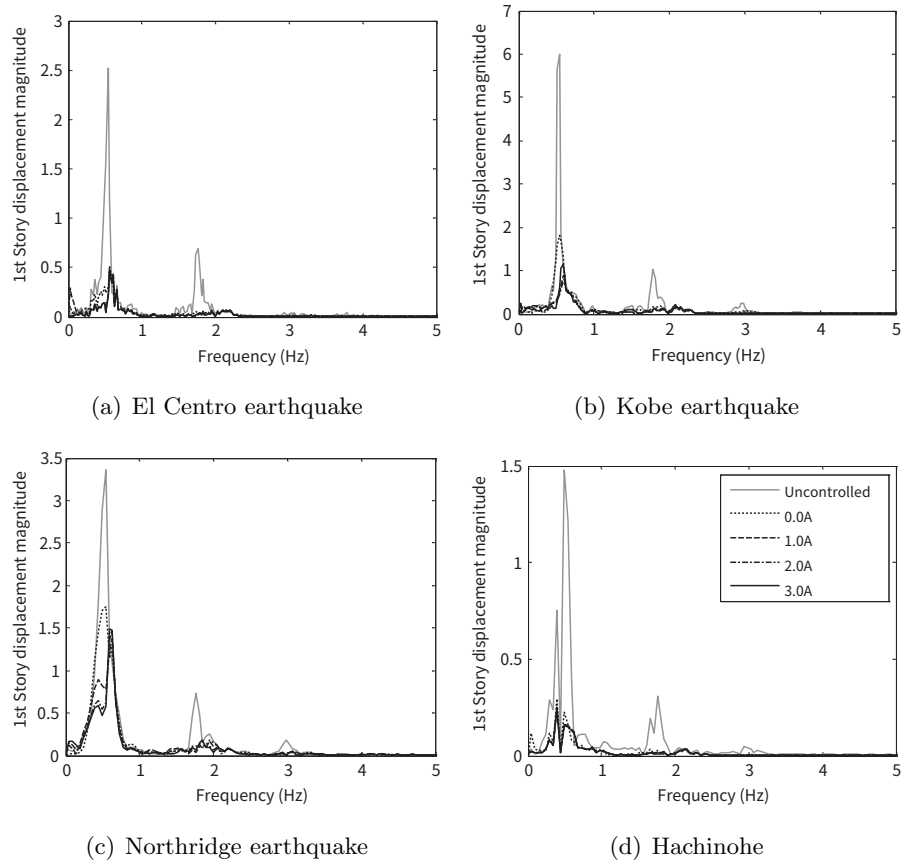


Figure 4.16: First-story displacements in the frequency domain at different applied currents.

4.4.2 Semi-active Control Performance

Figure 4.17 shows a comparison between numerical and experimental results for the clipped-optimal control under El Centro earthquake excitation based on identified Bouc-Wen parameters. As shown in Figure 4.17, the experimental and numerical results show different currencies. Moreover, because the peak responses are very important in evaluating seismic performance, it is critical to have large differences between the experimental and numerical results. These results are due to the nonlinearity of MR dampers which varies in the numerical model corresponding to frequencies of piston and nonlinear reaction velocity of input currents. Consequently, these results prove that using the hybrid testing method is more practical in non-linear damper models such as MR dampers.

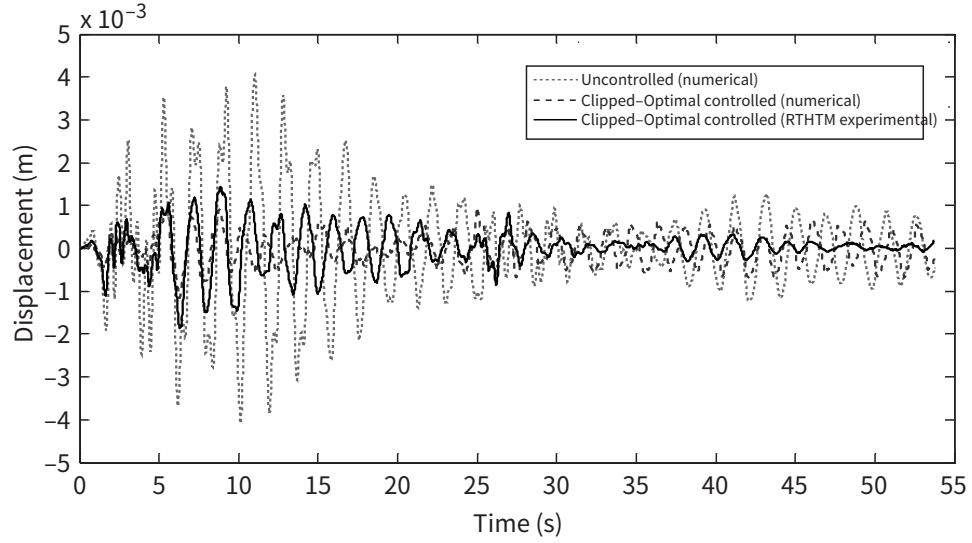


Figure 4.17: Comparison of numerical and experimental results under El Centro earthquake excitation.

Figure 4.18 shows a comparison between the first-floor displacements for the time histories of experimentally measured structural displacement responses to the excitation of three earthquake excitations, as the current applied to the MR damper is varied corresponding to each semi-active control algorithm. Significant control effects are observed between the uncontrolled and the passive control cases, but are not observed in each semi-active control case of El Centro, as shown in Figure 4.18(a). In Figure 4.18(c), the clipped optimal control algorithms show remarkable performances in controlling displacement response.

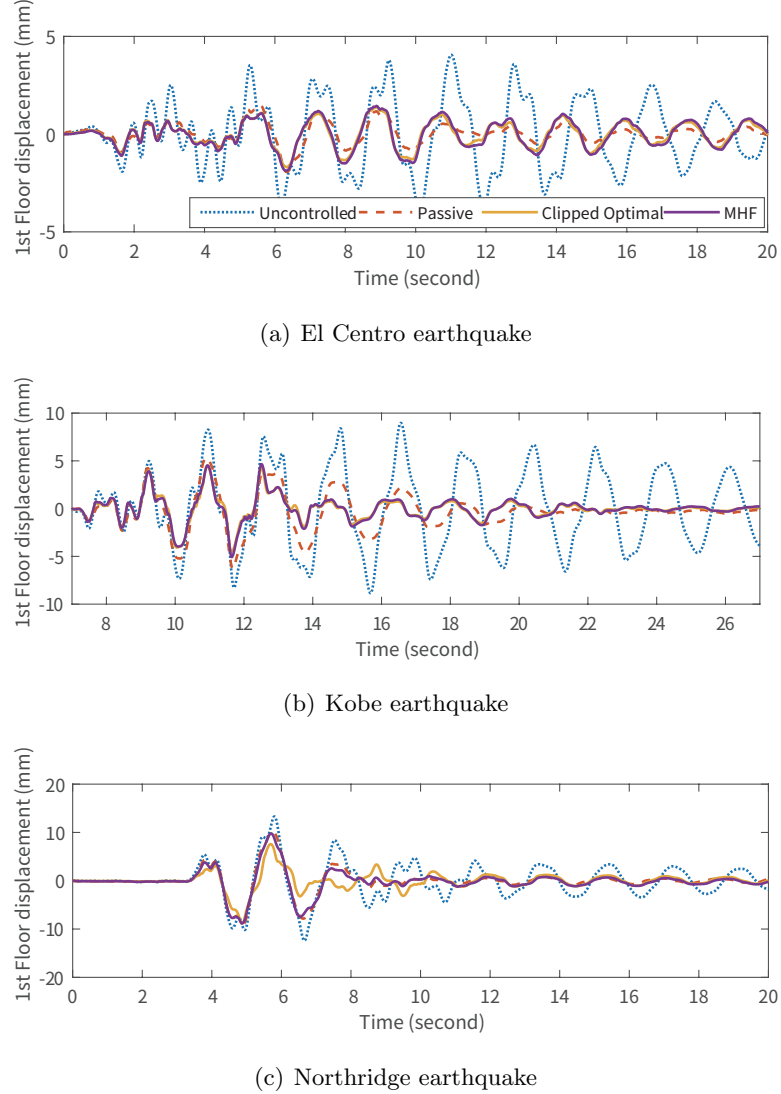


Figure 4.18: Passive and semi-active hybrid testing method experimental results(time domain).

Also, the displacement responses in the frequency domain to three earthquake excitations applied to uncontrolled, passive, and semi-active controlled hybrid testing method are compared for the first floor, as shown in Figure 4.19. The figures show that an overall best control performance is achieved when the clippedoptimal control algorithms are applied to the structure. However, all the results show insignificant control performance against the passive control. These results are influenced by the long-period model structure having 0.52 Hz and a scaled-down excitation load due to the UTM capacity. For the passive result, the peak response is shifted to the

vicinity of 0.62 Hz in a semi-active controlled result. This small amount of frequency shifting is due to the stiffening effect of the MR damper used in this study as the applied current is increased for the passive control results.

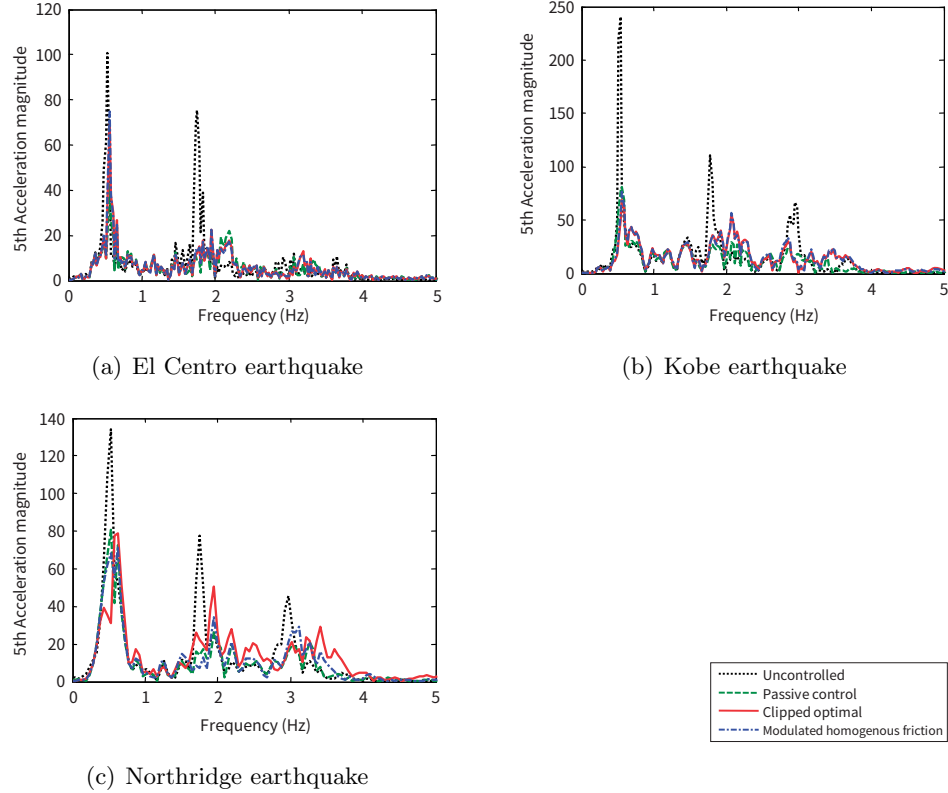


Figure 4.19: Passive and semi-active hybrid testing method experimental results(frequency domain).

4.5 Summary

In this chapter, the investigation of the hysteretic behavior of an MR damper and the seismic performance evaluation of a building structure, installed with an MR damper, are experimentally implemented using the hybrid testing method. In the tests, the building model that is identified from the force-vibration test results of a full-scale five-story building is adopted as a numerical substructure in this study. Also, an MR damper that corresponds to an experimental substructure is physically tested using a UTM. The Bouc-Wen model is used to calculate the control force of the MR damper used in this study, and its parameters are identified based on the experimental results from the hybrid testing method, which used a sinusoidal wave as the ground input acceleration. hybrid testing method is validated because the

hybrid testing results from the sinusoidal and earthquake excitations and the corresponding analytical results agreed well with each other. In particular, the hybrid testing method is highly reliable with the impulse-like seismic excitation such as that of the Northridge earthquake. To compare the results obtained from the hybrid testing method and the numerical analysis, Bouc-Wen model parameters are identified by each input current. The results of this comparison show that the hybrid testing method is more practical than the numerical analysis due to the non-linear variations of the reaction velocity and excitation frequency. The experimental results from the hybrid testing method for the passive control show that structural responses did not decrease further by the excessive control force, but they decreased with the increase of the current applied to the MR damper. In addition, the semi-active controlled result shows an insignificant control performance compared to the passive controlled result. It seems that the passive control forces of the MR damper already reached the optimal friction force by the proportional shear force of the first floor. To achieve a better performance for semi-active control algorithms, further loading capacity is required for the UTM, of which the optimal friction force of the structure can be laid in the maximum and minimum force of the MR damper. All results indicated that the seismic performance of a building structure installed with an MR damper can be indirectly evaluated by the hybrid testing method, in which only the MR dampers are physically tested. For further study, various applications of semi-active algorithms and a further minimizing technique for the time delay in hybrid testing method would be required.

CHAPTER 5

Conclusions

5.1 Concluding Remarks

This research focused on the design of exciting systems for simulating dynamic loads. The controller design of an actuator is presented to simulate the responses of a building structure subjected to such dynamic excitations as earthquakes and wind loads. Also, the real-time hybrid shaking table testing method (RHSTTM) and the real-time substructuring technique are proposed by using only the physical control device and upper substructure as an experimental part and considering control-structure interaction. All of testing results shows the good agreement between conventional testing method or numerical analysis and proposed testing method or experimental results. The result of the study can be summarized as follows. (1) The linear transfer function approach for controlling the motion of a shaking table was considered to experimentally verify the proposed method for a linear experimental part. However, this approach would be inappropriate for a coupled non-linear system leading to experimental instability. Therefore, in such case the controller using the inverse transfer function of shaking table would be modified to compensate an experimental instability. (2) It is considered that to minimize the effect of natural modes of an experimental substructure on the substructured system, the structural model as heavily-damped as possible would be used as an experimental part. (3) The proposed technique can be extended to the real-time substructuring technique with the middle part of a whole structure in combination with the conventional substructuring technique employing lower part as the experimental substructure. (4) Comparison between the structural responses obtained by the RHSTTM and the conventional shaking table test of a single story steel frame with TLD/TLCD indicates that the performance of the TLD/TLCD can be accurately evaluated using the RHSTTM without the physical structural model. (5) A design of a shaker for simulating wind induced responses of a building structure was presented as a preliminary study for evaluating wind-resistance characteristics of practical building structures. (6) The force of the shaker was obtained using the inverse transfer function of structural responses. Also, band stop filter was used to remove zero of the transfer function such that undesirable modal excitation is prevented, and envelop function was used to reduce the error occurring in transient initial states. The numerical analyses results from a 76-story benchmark building confirmed that the structural responses

of a building structure excited by wind loads acting at all floors could be reproduced by the proposed linear shaker installed at a specific floor. (7) The field measurement system of full-scale structure and excitation system were established, and then forced vibration test was carried out using the Hybrid Mass Damper designed to simulate seismic load. (8) System identification of full-scale structure was carried out through white noise test and Finite Element (FE) model is updated. The seismic excitation system was accomplished through inverse transfer functions of structure and HMD by the system identifications. (9) The normalized RMS error through the experimental results showed more increasing one than numerical analysis. This phenomenon is caused by the errors due to each system identification and curve fitting the inverse transfer function of HMD. (10) In simulating the pseudo-earthquake response, unexpected modal responses should be considered, when the excitation signal is generated through the inverse transfer function of structure, because it is measured non-existent errors such as noises of structural response.

Also, in further study, it needs to consider as follows, (1) The proposed technique can be extended to the real-time substructuring technique with the middle part of a whole structure in combination with the conventional substructuring technique employing lower part as the experimental substructure. (2) In order to enhance practical applicability of the wind-response simulating shaker, a FE modeling error, updating of the FE model based on measured data, dynamics of the shaker, and the scaling or restriction of the shaker force limit for avoiding damage of the practical building etc. should be considered in further study. (3) In order to minimize these excitation system errors of structure, accordingly, It essentially needs to prevent the unexpected modal responses from the inverse transfer functions of HMD and to identify the exact system. Accordingly the band-pass filter or band-stop filter should be designed in order to minimize the unexpected modal responses.

5.2 Future Study

Bibliography

- Adeli, H. (1999). *Control, optimization, and smart structures: high-performance bridges and buildings of the future*. John Wiley & Sons, Inc.
- Alvin, K. F. and Park, K. (1994). Second-order structural identification procedure via state-space-based system identification. *AIAA journal*, 32(2):397–406.
- Bagchi, A. (2005). Updating the mathematical model of a structure using vibration data. *Journal of Vibration and Control*, 11(12):1469–1486.
- Banerji, P., Murudi, M., Shah, A. H., and Popplewell, N. (2000). Tuned liquid dampers for controlling earthquake response of structures. *Earthquake engineering & structural dynamics*, 29(5):587–602.
- Baruch, M. (1978). Optimization procedure to correct stiffness and flexibility matrices using vibration tests. *AIAA journal*, 16(11):1208–1210.
- Baruch, M. and Bar Itzhack, I. (1979). Optimal weighted orthogonalization of measured modes. *AIAA Journal*, 17(8):927–928.
- Bishop, R. H. (2007). *LabVIEW 8 student edition*. Pearson Prentice Hall.
- Bitaraf, M., Barroso, L. R., and Hurlebaus, S. (2010). Adaptive control to mitigate damage impact on structural response. *Journal of Intelligent Material Systems and Structures*.
- Blakeborough, A., Williams, M., Darby, A., and Williams, D. (2001). The development of real-time substructure testing. *Philosophical Transactions of the Royal Society of London A: Mathematical, Physical and Engineering Sciences*, 359(1786):1869–1891.
- Chang, C. and Qu, W. (1998). Unified dynamic absorber design formulas for wind-induced vibration control of tall buildings. *The structural design of tall buildings*, 7(2):147–166.
- Christenson, R., Lin, Y. Z., Emmons, A., and Bass, B. (2008). Large-scale experimental verification of semiactive control through real-time hybrid simulation 1. *Journal of Structural Engineering*, 134(4):522–534.
- Coleman, T., Branch, M. A., and Grace, A. (1999). *Optimization toolbox user's guide*.

Bibliography

- Coleman, T. F. and Li, Y. (1996). An interior trust region approach for nonlinear minimization subject to bounds. *SIAM Journal on optimization*, 6(2):418–445.
- Coleman, Thomas F. and Li, Y. (1994). On the convergence of interior-reflective newton methods for nonlinear minimization subject to bounds. *Mathematical Programming*, 67(1):189–224.
- Darby, A., Blakeborough, A., and Williams, M. (2001). Improved control algorithm for real-time substructure testing. *Earthquake engineering & structural dynamics*, 30(3):431–448.
- Darby, A., Williams, M., and Blakeborough, A. (2002). Stability and delay compensation for real-time substructure testing. *Journal of Engineering Mechanics*, 128(12):1276–1284.
- Dennis Jr, J. E. and Schnabel, R. B. (1983). Numerical methods for unconstrained optimization and nonlinear equations. *Prentice-Hall Series in Computational Mathematics, Englewood Cliffs: Prentice-Hall, 1983, edited by Dennis, JE; Schnable, Robert B.*, 1.
- Dyke, S., Spencer Jr, B., Quast, P., Sain, M., Kaspari Jr, D., and Soong, T. (1994). Experimental verification of acceleration feedback control strategies for an active tendon system. *Nat. Center for Earthquake Engrg. Res., Tech. Report NCEER-94*, 24.
- Dyke, S., Spencer Jr, B., Sain, M., and Carlson, J. (1996). Modeling and control of magnetorheological dampers for seismic response reduction. *Smart materials and structures*, 5(5):565.
- Fujino, Y. and Sun, L. (1993). Vibration control by multiple tuned liquid dampers (mtlds). *Journal of Structural Engineering*, 119(12):3482–3502.
- Halling, M. W., Muhammad, I., and Womack, K. C. (2001). Dynamic field testing for condition assessment of bridge bents. *Journal of Structural Engineering*, 127(2):161–167.
- Haskett, T., Breukelman, B., Robinson, J., and Kottelenberg, J. (2004). Tuned mass dampers under excessive structural excitation. *Report of the Motioneering Inc., Guelph, Ontario, Canada*.
- Heo, J.-S., Lee, S.-K., Park, E., Lee, S.-H., Min, K.-W., Kim, H., Jo, J., and Cho, B.-H. (2009). Performance test of a tuned liquid mass damper for reducing bidirectional responses of building structures. *The Structural Design of Tall and Special Buildings*, 18(7):789–805.
- Horiuchi, T., Inoue, M., Konno, T., and Yamagishi, W. (1999). Development of a real-time hybrid experimental system using a shaking table.(proposal

Bibliography

- of experiment concept and feasibility study with rigid secondary system). *JSME International Journal Series C Mechanical Systems, Machine Elements and Manufacturing*, 42(2):255–264.
- Iemura, H., Igarashi, A., and Takahashi, Y. (1999). Substructured hybrid techniques for actuator loading and shaking table tests. In *Proceedings of the First International Conference on Advances in Structural Engineering and Mechanics*, pages 821–826.
- Igarashi, A., Iemura, H., and Suwa, T. (2000). Development of substructured shaking table test method. In *Proceedings of the 12th World Conference on Earthquake Engineering*.
- Igusa, T. and Xu, K. (1994). Vibration control using multiple tuned mass dampers. *Journal of sound and vibration*, 175(4):491–503.
- Inaudi, J. A. (1997). Modulated homogeneous friction: A semi-active damping strategy. *Earthquake engineering & structural dynamics*, 26(3):361–376.
- Jangid, R. and Datta, T. (1997). Performance of multiple tuned mass dampers for torsionally coupled system. *Earthquake engineering & structural dynamics*, 26(3):307–317.
- Jansen, L. M. and Dyke, S. J. (2000). Semiactive control strategies for mr dampers: comparative study. *Journal of Engineering Mechanics*, 126(8):795–803.
- Juang, J.-N. (1994). Applied system identification.
- Kim, H. and Adeli, H. (2005a). Hybrid control of irregular steel highrise building structures under seismic excitations. *International Journal for Numerical Methods in Engineering*, 63(12):1757–1774.
- Kim, H. and Adeli, H. (2005b). Hybrid control of smart structures using a novel wavelet-based algorithm. *Computer-Aided Civil and Infrastructure Engineering*, 20(1):7–22.
- Kim, Y., Langari, R., and Hurlebaus, S. (2009). Semiactive nonlinear control of a building with a magnetorheological damper system. *Mechanical Systems and Signal Processing*, 23(2):300–315.
- Lee, H.-J., Jung, H.-J., Moon, S.-J., Lee, S.-K., Park, E.-C., and Min, K.-W. (2010). Experimental investigation of mr damper-based semiactive control algorithms for full-scale five-story steel frame building. *Journal of Intelligent Material Systems and Structures*.

Bibliography

- Lee, H.-J., Yang, G., Jung, H.-J., Spencer, B. F., and Lee, I.-W. (2006). Semi-active neurocontrol of a base-isolated benchmark structure. *Structural Control and Health Monitoring*, 13(2-3):682–692.
- Lee, S.-K., Park, E. C., Min, K.-W., Lee, S.-H., Chung, L., and Park, J.-H. (2007a). Real-time hybrid shaking table testing method for the performance evaluation of a tuned liquid damper controlling seismic response of building structures. *Journal of Sound and Vibration*, 302(3):596–612.
- Lee, S.-K., Park, E. C., Min, K.-W., and Park, J.-H. (2007b). Real-time substructuring technique for the shaking table test of upper substructures. *Engineering Structures*, 29(9):2219–2232.
- Li, C. (2000). Performance of multiple tuned mass dampers for attenuating undesirable oscillations of structures under the ground acceleration. *Earthquake Engineering & Structural Dynamics*, 29(9):1405–1421.
- LI, C.-x., LIU, Y.-x., WANG, Z.-m., and HUANG, J.-z. (2000). The optimum design of mtld system for controlling the seismic responses of tall steel structures [j]. *Engineering Mechanics*, 2:016.
- Little, J. N. and Shure, L. (1992). *Signal Processing Toolbox User's Guide*.
- Ljung, L. (1987). *System Identification: Theory for the user*.
- Madenci, E. and Barut, A. (1994). A free-formulation-based flat shell element for non-linear analysis of thin composite structures. *International journal for numerical methods in engineering*, 37(22):3825–3842.
- Min, K.-W., Kim, J., and Lee, S.-H. (2004). Vibration tests of 5-storey steel frame with viscoelastic dampers. *Engineering Structures*, 26(6):831–839.
- Nakashima, M., Kato, H., and Takaoka, E. (1992). Development of real-time pseudo dynamic testing. *Earthquake Engineering & Structural Dynamics*, 21(1):79–92.
- Nakashima, M. and Masaoka, N. (1999). Real-time on-line test for mdof systems. *Earthquake engineering & structural dynamics*, 28(4):393–420.
- Neild, S., Stoten, D., Drury, D., and Wagg, D. (2005). Control issues relating to real-time substructuring experiments using a shaking table. *Earthquake engineering & structural dynamics*, 34(9):1171–1192.
- Pan, P., Nakashima, M., and Tomofuji, H. (2005). Online test using displacement–force mixed control. *Earthquake engineering & structural dynamics*, 34(8):869–888.

Bibliography

- Samali, B., Kwok, K., and Gao, H. (1998). Wind induced motion control of a 76 storey building by liquid dampers. In *Proceedings of second world conference on structural control*, volume 1, pages 1473–1480.
- Shing, P. and Mahin, S. A. (1983). Experimental error propagation in pseudodynamic testing. Technical report.
- Shing, P. and Mahin, S. A. (1984). Pseudodynamic test method for seismic performance evaluation: theory and implementation. Technical report.
- Simulink, U. G. (2009). Version 7. *The MathWorks Inc.*
- Singh, M. P., Singh, S., and Moreschi, L. M. (2002). Tuned mass dampers for response control of torsional buildings. *Earthquake engineering & structural dynamics*, 31(4):749–769.
- Soong, T. T. and Dargush, G. F. (1997). *Passive energy dissipation systems in structural engineering*. Wiley.
- Spencer, B., Dyke, S., Sain, M., and Carlson, J. (1997). Phenomenological model for magnetorheological dampers. *Journal of engineering mechanics*, 123(3):230–238.
- Sun, L., Fujino, Y., Chaiser, P., and Pacheco, B. (1995). The properties of tuned liquid dampers using a tmd analogy. *Earthquake engineering & structural dynamics*, 24(7):967–976.
- Takanashi, K., Taniguchi, H., and Tanaka, H. (1980). Inelastic response of h-shaped columns to two dimensional earthquake motions. *Bulletin of Earthquake Resistant Structure Research Center*, (13).
- Takanashi, K., Udagawa, K., Seki, M., Okada, T., and Tanaka, H. (1975). Nonlinear earthquake response analysis of structures by a computer-actuator on-line system. *Bulletin of Earthquake Resistant Structure Research Center*, 8:1–17.
- Target, R.-T. W. (2009). User's guide, r2007a.
- Van der Auweraer, H. and Peeters, B. (2003). Sensors and systems for structural health monitoring. *Journal of structural control*, 10(2):117–125.
- Wen, Y.-K. (1976). Method for random vibration of hysteretic systems. *Journal of the engineering mechanics division*, 102(2):249–263.
- Xu, K. and Igusa, T. (1992). Dynamic characteristics of multiple substructures with closely spaced frequencies. *Earthquake engineering & structural dynamics*, 21(12):1059–1070.

Bibliography

- Yalla, S. K. (2001). *Liquid dampers for mitigation of structural response: theoretical development and experimental validation.*
- Yamaguchi, H. and Harnpornchai, N. (1993). Fundamental characteristics of multiple tuned mass dampers for suppressing harmonically forced oscillations. *Earthquake engineering & structural dynamics*, 22(1):51–62.
- Yang, G., Spencer Jr, B. F., Jung, H.-J., and Carlson, J. D. (2004a). Dynamic modeling of large-scale magnetorheological damper systems for civil engineering applications. *Journal of Engineering Mechanics*, 130(9):1107–1114.
- Yang, J. N., Agrawal, A. K., Samali, B., and Wu, J.-C. (2004b). Benchmark problem for response control of wind-excited tall buildings. *Journal of Engineering Mechanics*, 130(4):437–446.
- Yu, E., Whang, D. H., Conte, J. P., Stewart, J. P., and Wallace, J. W. (2005). Forced vibration testing of buildings using the linear shaker seismic simulation (lsss) testing method. *Earthquake engineering & structural dynamics*, 34(7):737–761.
- Yu, J.-K., Wakahara, T., and Reed, D. A. (1999). A non-linear numerical model of the tuned liquid damper. *Earthquake Engineering and structural dynamics*, 28(6):671–686.
- ZHANG, Y. and ZHONG, T.-y. (2004). Equivalent damping ratio analysis of the high-rise buildings' rectangular mtld system. *Research & Application of Building Materials*, 1:001.

Curriculum Vitæ

Eunchurn Park

1980.07.05 Born in Iksan, Korea.

Contact Information

1103, 619-3 Gyeongin-ro
Guro-gu, Seoul, Korea, 08210 +82-10-4499-6420
eunchurn.park@gmail.com

Education

History

1996–1999	Bugil High School 69 Dandae Ro, Dongnam-gu, Cheonan City
1999–2005	Bachelor of science, dept. of architectural engineering School of Architecture, Dankook University, Republic of Korea
2005–2007	Master of science, dept. of architectural engineering School of Architecture, Dankook University, Republic of Korea
2007–2017	Ph.D. School of Architecture, Dankook University, Republic of Korea

Qualification

Dankook University,

Ph.D., Architectural Engineering, School of Architecture, Aug. 2017

- Topic: *Hybrid Experimental Method and Excitation System for Seismic and Wind-resistance Performance Evaluation of Building Structures with Nonlinear Dampers*
- Advisors: Kyung-Won Min, Ph.D

M.S., Architectural Engineering, School of Architecture, Feb. 2007

- Topic: *Design of Excitation Systems for Simulating Dynamic Loads and Real-Time Hybrid Test Method of Building Structures*
- Advisor: Kyung-Won Min, Ph.D

B.S., Architectural Engineering, School of Architecture, Feb. 2005

Work Experience

- 2009.04 - 2015.05 한국유지관리(주) 부설기업연구소 : R&D > U-biz,
DAQ개발, 토목/건축 계측/해석
- 2015.08 - 현재 (주)승화기술정책연구소 기술연구소 : R&D > 컴퓨
터비전/IoT, M2M 플랫폼개발/Full stack Engineer
ing/Deep Learning/철도과제

Awards

- 2007 Excellence Prize, The 3rd Excellent Graduation Theses
of The Architectural Institute of Korea
석사부문 우수상, 제3회 대한건축학회 우수졸업논문전
- 2007 2007 Beomjeong Academic Paper Prize of Dankook Uni
versity Graduate School
2007 범정학술논문상
- 2008 2008 Beomjeong Academic Paper Prize of Dankook Uni
versity Graduate School
2008 범정학술논문상
- 2012 The 19th Science and Technology Best Paper Award
제19회 과학기술우수논문상 (한국소음진동공학회)

Publications

Papers in international journal (SCI)

Eunchurn Park, Kyung-Won Min, Sung-Kyung Lee, Sang-Hyun Lee, Heon-Jae Lee, Seok-Jun Moon, Hyung-Jo Jung, “Real-time Hybrid Test on a Semi-actively Controlled Building Structure Equipped with Full-scale MR Dampers”, *Journal of Intelligent Material Systems and Structures* 12/2010; 21(18):1831-1850. DOI:10.1177/1045389X10390253

Heon-Jae Lee, Hyung-Jo Jung, Seok-Jun Moon, Sung-Kyung Lee, **Eun
Churn Park**, Kyung-Won Min, “Experimental Investigation of MR Damper-based Semiactive Control Algorithms for Full-scale Five-story Steel Frame Building”, *Journal of Intelligent Material Systems and Structures* 06/2010; 21(10):1025-1037. DOI:10.1177/1045389X10374162

Jae-Sung Heo, Sung-Kyung Lee, **Eunchurn Park**, Sang-Hyun Lee, Kyung-Won Min, Hongjin Kim, Jiseong Jo, Bong-Ho Cho, “Performance test of a tuned liquid mass damper for reducing bidirectional responses of building structures”, *The Structural Design of Tall and Special Buildings* 11/2009; 18(7):789 - 805. DOI:10.1002/tal.486

Eun-Churn Park, Sang-Hyun Lee, Kyung-Won Min, Lan Chung, Sung-Kyung Lee, Seung-Ho Cho, Eunjong Yu, Kyung-Soo Kang, “Design of an actuator for simulating wind-induced response of a building structure”, *SMART STRUCTURES AND SYSTEMS* 01/2008; 4(1). DOI:10.12989/sss.2008.4.1.085

Sung-Kyung Lee, **Eun Churn Park**, Kyung-Won Min, Ji-Hun Park, “Real-time substructuring technique for the shaking table test of upper substructures”, *Engineering Structures* 09/2007; 29(9):2219-2232. DOI:10.1016/j.engstruct.2006.11.013

Sung-Kyung Lee, **Eun Churn Park**, Kyung-Won Min, Sang-Hyun Lee, Ji-Hun Park, “Experimental implementation of a building structure with a tuned liquid column damper based on the real-time hybrid testing method”, *Journal of Mechanical Science and Technology* 06/2007; 21(6):885-890. DOI:10.1007/BF03027063

Sung-Kyung Lee, **Eun Churn Park**, Kyung-Won Min, Sang-Hyun Lee, Lan Chung, Ji-Hun Park, ” Real-time hybrid shaking table testing method for the performance evaluation of a tuned liquid damper controlling seismic response of building structures“, *Journal of Sound and Vibration* 05/2007; DOI:10.1016/j.jsv.2006.12.006

Papers in Korean journal (KCI)

민경원, 이성경, 박은천, “진동대실험에 의한 동조액체기동감쇠기의 동적특성”, *한국소음진동공학회논문집 (Transactions of the Korean society for noise and vibration engineering)* v.19 no.6 = no.147, pp.620 - 627, 2009, 1598-2785

윤경조, 박은천, 이현재, 문석준, 민경원, 정형조, 이상현, ‘준능동 MR 감쇠기가 설치된 실물크기 구조물의 분산제어 알고리즘 성능평가”, *한국소음진동공학회논문집 (Transactions of the Korean society for noise and vibration engineering)* v.18 no.2, pp.255 - 262, 2008,

박은천, 이성경, 이현재, 문석준, 정형조, 민경원, “대형 MR감쇠기가 설치된 건축구조물의 실시간 하이브리드 실험 및 준능동 알고리즘 적용”, *한국전산구조공학회논문집 (Journal of the computational structural engineering institute of Korea)* v.21 no.5, pp.465 - 474, 2008, 1229-3059

이성경, 민경원, 박은천, “TMD와 TLCD를 이용한 2방향 감쇠기의 동적특성”, *한국전산구조공학회논문집 (Journal of the computational structural engineering institute of Korea)* v.21 no.6, pp.589 - 596, 2008, 1229-3059

허재성, 이성경, 박은천, 이상현, 김홍진, 조지성, 조봉호, “실시간 하이브리드 진동대 실험법에 의한 양방향 TLMD의 진동제어 성능평가”, *한국소음진동공학회논문집 (Transactions of the Korean society for noise and vibration engineering)* v.18 no.5 = no.134, pp.485 - 495, 2008, 1598-2785

허재성, 박은천, 이상현, 이성경, 김홍진, 조봉호, 조지성, 김동영, 민경원, “건축구조물의 2방향 진동제어를 위한 동조액체질량감쇠기”, *한국소음진동공학회논문집 (Transactions of the Korean society for noise and vibration engineering)* v.18 no.3 = no.132, pp.345 - 355, 2008, 1598-2785

허재성, 박은천, 이성경, 이상현, 김홍진, 조지성, 조봉호, 주석준, 민경원, “실물크기 구조물에 설치된 동조액체질량감쇠기의 성능실험”, *한국전산구조공학회논문집 (Journal of the computational structural engineering institute of Korea)* v.21 no.2, pp.161 - 168, 2008, 1229-3059

윤경조, 박은천, 이현재, 문석준, 민경원, 정형조, 이상현, “준동MR감쇠기가 설치된 실물크기 구조물의 분산제어 알고리즘 성능평가”, *한국소음진동공학회논문집 (Transactions of the Korean society for noise and vibration engineering)* v.18 no.2 = no.131, pp.255 - 262, 2008, 1598-2785

박은천, 이성경, 윤경조, 정희산, 이현재, 최강민, 문석준, 정형조, 민경원, “실시간 하이브리드 실험법을 이용한 대형 MR감쇠기의 제진 성능평가”, *한국소음진동공학회논문집 (Transactions of the Korean society for noise and vibration engineering)* v.18 no.1 = no.130, pp.131 - 138, 2008, 1598-2785

박은천, 민경원, 정란, 강경수, 이상현, “건축구조물의 풍하중 구현 및 풍특성 평가를 위한 가진시스템 설계”, *한국전산구조공학회논문집 (Journal of the computational structural engineering institute of Korea)* v.20 no.6, pp.769 - 778, 2007, 1229-3059

이성경, 민경원, 박은천, “진동대를 이용한 구조물의 하이브리드 실험”, *대한건축학회논문집大韓建築學會論文集 (Journal of the architectural institute of Korea : Structure & construction) / 構造系* v.22 no.5 = no.211, pp.57 - 63, 2006, 1226-9107

이상현, 박은천, 윤경조, 이성경, 유은종, 민경원, 정란, 민정기, 김영찬, “실물 크기 구조물의 강제진동실험 및 지진응답 모사를 위한 HMD 제어기 설계”, *한국지진공학회논문집 (Journal of the earthquake engineering society of Korea)* v.10 no.6 = no.52, pp.103 - 114, 2006, 1226-525x

이성경, 박은천, 이상현, 정란, 우성식, 민경원, “실시간 하이브리드 진동대 실험법을 이용한 TLD 제어성능의 실험적 검증”, 한국전산구조공학회논문집 (*Journal of the computational structural engineering institute of Korea*) v.19 no.4 = no.74, pp.419 - 427, 2006, 1229-3059

Papers in international proceedings

Eunchurn Park, Yu-Seung Kim, Joong-Yub Lee, Jun-Sung Choi, Yeon-Back Jung, Won-Kyun Seok, Kwang-Soo Jung, Soon-Jeon Park, Joo-Ho Lee, “Study on Vertical Alignment Maintenance Technique using GNSS in Skyscraper”, *2009 International Symposium on GPS/GNSS*; 11/2009

Eunchurn Park, Sung-Kyung Lee, Heon-Jae Lee, Seok-Joon Moon, Hyung-Jo Jung, Byoung-Wook Moon, Kyung-Won Min, “Real-Time Hybrid Testing of a Steel-Structure Equipped With Large-Scale Magneto-Rheological Dampers Applying Semi-Active Control Algorithms”, *ASME 2008 Conference on Smart Materials, Adaptive Structures and Intelligent Systems*; 01/2008

Eunchurn Park, Sang-Hyun Lee, Sung-Kyung Lee, Hee-San Chung, Kyung-Won Min, “System Identification and Pseudo-Earthquake Excitation of a Real-Scaled 5 Story Steel Frame Structure”, *ASME 2008 Conference on Smart Materials, Adaptive Structures and Intelligent Systems*; 01/2008

S. H. Lee, **E. C. Park**, K. J. Youn, K. W. Min, L. Chung, S. B. Choi, K. G. Sung, H. G. Lee, “RESPONSE CONTROL OF A REAL-SCALED FIVE-STORY STRUCTURE USING MAGNETO-RHEOLOGICAL DAMPER”, *Electrorheological Fluids and Magnetorheological Suspensions - 10th International Conference on ERMR 2006*; 01/2007

Papers in Korean conference proceedings

박은천, 강형구, 최준성, 김은성, 김만철, “고속열차의 주행 동적성능 평가시스템 개발”, 한국철도학회 2011년도 정기총회 및 추계학술대회 논문집 Oct. 20, pp.3226-3236 (2011)

박은천, 최준성, “전단파 속도계측에 의한 구조물 강도추정 실용화 연구”, 한국방재학회 2011년도 정기 학술발표대회 Feb. 24, pp.162-162. (2011)

김성용, 박은천, “차량의 가속도 진동계측 및 차량안정성 프로그램 개발에 대한 연구”, 한국철도학회 2010년도 춘계학술대회 논문집 June 10, pp.527-532. (2010)

김성용, 박은천, “차량의 동적 특성 분석을 통한 궤도틀림 식별”, 한국 철도학회 2010년도 춘계 학술대회 논문집 2010 June 10, pp.2095-2106. (2010)

민경원, 이성경, 박은천, “1 개의 TLD 를 이용한 건물의 양방향 진동제어”, 한국전산구조공학회 2009년도 정기 학술대회 2009 Apr. 16, pp.119 - 124, 2009

허재성, 이성경, 박은천, 이상현, 김홍진, 조지성, 조봉호, 민경원, “건축구조물의 2방향 진동제어를 위한 TLMD 제어 성능평가”, 한국소음 진동공학회 2008년도 춘계 학술대회 논문집 2008 Apr. 17, pp.432 - 441, 2008

허재성, 박은천, 이상현, 이성경, 민경원, 김홍진, 조지성, 조봉호, 주석준, “실물크기 구조물에 설치된 동조액체질량감쇠기의 성능시험”, 한국소음 진동공학회 2008년도 춘계 학술대회 논문집 2008 Apr. 17, pp.449 - 457, 2008

윤경조, 이상현, 박은천, 유은종, 민경원, “실물크기 구조물의 강제진동 실험을 통한 시스템 식별”, 한국소음진동공학회 2007년도 추계 학술대회 논문집 2007 Nov. 15, pp.195 - 200, 2007

허재성, 이성경, 이상현, 박은천, 김홍진, 조봉호, 조지성, 김동영, 민경원, “실시간 하이브리드 진동대 실험법에 의한 양방향 TLMD의 풍응답 제어 성능평가”, 한국소음진동공학회 2007년도 추계 학술대회 논문집 2007 Nov. 15, pp.189 - 194, 2007

허재성, 김홍진, 조봉호, 조지성, 박은천, 이상현, 이성경, 김동영, 민경원, “TLCD와 고무패드형 TMD를 이용한 2방향 TLMD의 성능평가 실험”, 한국소음진동공학회 2007년도 추계 학술대회 논문집 2007 Nov. 15, pp.465 - 470, 2007

박은천, 이상현, 민경원, 강경수, “ATMD를 이용한 건축 구조물의 풍응답 구현을 위한 가진시스템”, 한국소음진동공학회 2007년도 추계 학술대회 논문집 2007 Nov. 15, pp.210 - 215, 2007

박은천, 이상현, 민경원, 강경수, “풍하중 구현 및 내풍특성 평가를 위한 선형질량 가진시스템 설계”, 한국소음진동공학회 2007년도 추계 학술대회 논문집 2007 Nov. 15, pp.661 - 668, 2007

정희산, 이성경, 박은천, 민경원, “실시간 하이브리드 실험법을 이용한 동조액체기동감쇠기가 설치된 구조물의 지진응답 제어성능 평가”, 한국소음진동공학회 2007년도 추계 학술대회 논문집 2007 Nov. 15, pp.669 - 673, 2007

박은천, 이성경, 이현재, 최강민, 문석준, 정형조, 정희산, 민경원, “실시간 하이브리드 실험법을 이용한 대형 MR감쇠기의 준능동 제어 알고리즘”, 한국소음진동공학회 2007년도 추계 학술대회 논문집 2007 Nov. 15, pp.674 - 678, 2007

리즘 성능 비교”, 한국소음진동공학회 2007년도 추계학술대회논문집
2007 Nov. 15, pp.648 - 654, 2007

정희산, 이성경, 박은천, 민경원, 이현재, 최강민, 문석준, 정형조, “실시간 하이브리드 실험법을 이용한 대형 MR감쇠기의 제진 성능평가”, 한국소음진동공학회 2007년도 추계학술대회논문집 2007 Nov. 15, pp.655 - 660, 2007

이성경, 이상현, 민경원, 박은천, 우성식, 정란, 윤경조, “하이브리드 실험법을 이용한 TLD가 설치된 건물의 지진응답 제어”, 한국지진공학회 2006년도 학술발표회 논문집 제10권 2006 Mar. 17, pp.527 - 534, 2006

박지훈, 민경원, 문병욱, 박은천, “MR감쇠기가 설치된 구조물의 등가선형 시스템에 대한 가진 특성의 영향”, 한국지진공학회 2006년도 학술발표회 논문집 제10권 2006 Mar. 17, pp.503 - 510, 2006

이성경, 이상현, 민경원, 박은천, 우성식, 정란, “실시간 하이브리드 실험법을 이용한 동조액체댐퍼가 설치된 건물의 진동제어”, 한국전산구조공학회 2006년도 정기 학술대회 논문집 2006 Apr. 01, pp.256 - 263, 2006

이상현, 민경원, 이명규, 박은천, “복합모드형 소형 MR감쇠장치 성능에 관한 실험적 연구”, 한국지진공학회 2005년도 학술발표회 논문집 2005 Mar. 18, pp.461 - 468, 2005

Research projects

콘크리트궤도 도상/노반결함 상태평가 시스템 개발, 주관:한국철도공사 2016-2017

도시 인프라 자산관리 플랫폼과 서비스 모델 개발, 주관:(주)승화기술정책연구소 2015-2016

M2M 기반 지하공간(지하철) 재난대응 대화형 스마트 네트워크 시스템 개발, 주관:(주)승화기술정책연구소 2015-2017

진동특성을 이용한 LCD 생산로봇 및 부품 사전 진단 시스템 개발, 주관:한국유지관리(주) 2011-2012

감지형 앵커를 이용한 사면 보강 및 모니터링 기술 개발, 주관:한국유지관리(주) 2010-2011

교량 및 지반보강을 위한 스마트 텐던 기술의 사업화를 위한 추가기술개발 및 검증, 주관:한국유지관리(주) 2010

철골조 시설물의 붕괴를 방지하는 설치 용이한 경제적인 보강기구 개발, 주관:단국대학교 산학협력단 2006

다자유도 진동대 및 가력기를 이용한 2방향 동조식 액체형 댐퍼의 풍응답 저감 연구, 주관:단국대학교 20080901 ~ 20110831

대형 비탄성구조물 분산 제어시스템 설계기술 개발, 주관:단국대학교 20070301 ~ 20100228

모듈러 유닛 구조물 구조성능 평가 및 운송기술 개발, 주관:(사)대한건축학회 2006-2007

초대형 구조물의 내풍 및 내진성능향상을 위한 준동적 제어시스템 개발(The Development of a Semi-active Control System for Large-scale Structures under Wind and Seismic Loads), 주관:단국대학교 2005-2006

Lecture

2011.09.29	망조정과 외란보정기법의 RTK GNSS를 적용한 고층 구조물의 거푸집 연직도 관 리기술	서울시
2012.09.01– 2013.02.28	공학수치해석 (Numerical Analysis)	단국대학교 (Dankook Uni- versity)

Intellectual property

- NT

망조정과 외란보정기법의 RTK GNSS을 적용한 고층 구조물의 거푸집 연직도 관리기술

고시 : 국토해양부고시 제2011-313호

지정번호 : 제625호

명칭 : 망조정과 외란보정기법의 RTK GNSS을 적용한 고층 구조물의 거푸집 연직도 관리기술

기술분야 : 건축시공

개발법인 : 한국유지관리(주), 롯데건설(주)

개발참여자 : 박순진, 석원균, 정원백, 최준성, 김민수, 이중엽, 박은천

- Patents

철도차량의 승차감 분석 시스템(System for ride comfort analysis of Railway vehicle)

출원번호 : 1020100137577

등록번호 : 1012501040000

출원인 : 한국유지관리 주식회사, 코레일공항철도 주식회사

출원일자 : 2010.12.29

등록일자 : 2013.03.27

공개일자 : 2012.07.09

발명자 : 최준성, 박수열, 박은천, 김성용, 조한권

철도차량의 주행 안정성 분석 시스템(System for driving stability analysis of Railway vehicle)

출원번호 : 1020110068195

등록번호 : 1012590880000

출원인 : 한국유지관리 주식회사

출원일자 : 2011.07.11

등록일자 : 2013.04.23

공개일자 : 2013.01.21

발명자 : 최준성, 강형구, 박은천, 김만철, 유원희

이상진단 사전감시 방법(Method for preliminary surveillance of failure diagnosis)

출원번호 : 1020120138404

출원인 : 한국유지관리 주식회사

출원일자 : 2012.11.30

공개일자 : 2014.06.13

발명자 : 최준성, 임공철, 이은찬, 박은천

유에스엔 기반 지능형 교량 모니터링 및 안전성 평가 시스템(System for intelligent monitoring and safety evaluation of bridge based on USN)

출원번호 : 10-2011-0026810

출원인 : 한국유지관리 주식회사

출원일자 : 2011.03.25

공개일자 : 2012.10.17

발명자 : 최준성, 박은천, 윤종구

Relevant Skills

High Level

Dynamics of structure, Signal processing, Structural analysis, Data analytics, Algorithms, System Identification, Feed-back control system

Mid Level

Structural design, Adaptive control & filter design, Optimal control design, Neural network, Convolutional neural network, Recurrent neural network, Computer vision, Image processing

Computer Programming

Mathworks MATLAB, Mathworks Simulink, National Instruments LabVIEW, Visual Studio (C#, C++)

Python, Node.js, Javascript, SQL, NoSQL(MongoDB), Shell script of Linux(Debian)

Referees

Kyung-Won Min, Ph.D. : Professor, Advisor Phone :
+82-31-8005-3734

Dept. of Architectural Engineering of Dankook University E-mail :
kwmin@dankook.ac.kr

Sang-Hyun Lee, Ph.D. : Professor Phone : +82-31-8005-3735
Dept. of Architectural Engineering of Dankook University E-mail :
lshyun00@dankook.ac.kr